Design by Analysis Methods for Ductile Collapse Modes Under Static and Repeated Loading

Declan Gilmartin

Submitted for the Degree of Doctor of Philosophy in Mechanical Engineering

Department of Mechanical and Aerospace Engineering

University of Strathclyde

May 2024

This thesis is the result of the author's original research. It has been composed by the author and has not been previously submitted for examination which has led to the award of a degree.

Signed: 

Date: 01/05/2024

Acknowledgements

The research presented in this thesis is sponsored by Rolls-Royce plc and undertaken in collaboration with the University of Strathclyde. I would like to express my sincere thanks to my academic supervisor Prof. Donald Mackenzie and industrial supervisor Mr Chris Bell for the support and guidance they provided throughout. This would not have been possible without their technical expertise and willingness to help.

I would also like to acknowledge the rest of the Rolls-Royce Doctorate community, especially David Clarkson, Ed Williamson and Paul Wrigley who I wish all the best in their future endeavours.

Abstract

Pressurised components in civil nuclear power plants are required to operate under extreme thermal and mechanical loading conditions. There are many potential failure mechanisms and the consequences of a component failing could be disastrous. To help solve such a complex problem, dedicated Boiler and Pressure Vessel Design Codes exist to ensure the safe design of pressure vessels for Nuclear application. One widely recognised design code is ASME BPVC Section III Rules for Construction of Nuclear Facility Components.

ASME III allows the use of Design by Analysis (DBA) to prevent failure modes such as plastic collapse, ratcheting and fatigue from occurring by carrying out a detailed structural assessment using methods such as Finite Element Analysis (FEA). Linear elastic DBA is commonly used in industry due to the low computational cost compared to non-linear elastic-plastic DBA but requires extensive post-processing.

This thesis focuses on the use of elastic and elastic-plastic DBA to prevent failure due to plastic collapse and ratcheting. The advantages and disadvantages of various methods are discussed with an emphasis on the practicality for industrial application. An alternative stress linearisation approach is proposed and is investigated alongside established linearisation methods to determine how the stress distribution in thick components can be better represented using elastic DBA. This study highlights the sensitivity of such methods to complex geometry, loading conditions and code requirements, providing significant insight into the use of elastic DBA for industrial application. By validating the static and cyclic stresses against elastic-perfectly plastic limit load and cycle-by-cycle FEA, it is shown that linearising all 6 stress components proved to be the most reliable and consistent method for the cases studied.

A number of non-linear DBA methods are investigated using benchmark cases and the results analysed in detail. The ASME VIII Div 2 plastic analysis, twice elastic slope (TES), tangent intersection (TI), plastic work (PW) and plastic work curvature (PWC) methods are all investigated for the prediction of plastic collapse. In particular, the Plastic Work method is shown to provide a reliable method to determine the collapse load of complex nuclear structures whilst maintaining some conservatism. Also, the

ASME VIII monotonic stress-strain curve proved to be effective in predicting the structural response of a low carbon steel tubesheet. Combining the ASME VIII material model with the Plastic Work method and using it to assess thick walled nuclear components provides a novel application of both methods. Furthermore, the case studies provide significant evidence of how such an approach could be used to perform robust structural assessments that are complaint with ASME III.

Contents

Figures

Tables

Nomenclature

Abbreviations

ASME	American Society of Mechanical Engineers
BNL	Berkeley National Laboratory
BPVC	Boiler and Pressure Vessel Code
CORDEL	Cooperation in Reactor Design Evaluation and Licensing
DBA	Design by Analysis
DBA-L	Design by Analysis Limit Method
DBR	Design by Rule
DCA	Direct Cyclic Analysis
DSCA	Direct Steady Cycle Analysis
EMAP	Elastic Modulus Adaption Procedures
EP	Elastic Plastic
EPP	Elastic-perfectly plastic
ETT	Element Through Thickness
FE	Finite Element
FEA	Finite Element Analysis
GLOSS	Generalised Local Stress Strain
GPD	Gross Plastic Deformation
HCF	High Cycle Fatigue
HFEF	Hierarchical Finite Element Framework
IAEA	International Atomic Energy Agency
LAL	Limit Analysis Line
LB	Lower Bound
LCF	Low Cycle Fatigue
L-D Curve	Load vs Deformation Curve
LDYM	Load Dependent Yield Modification
LLA	Limit Load Analysis
LM	Linearisation Method
LMM	Linear Matching Method

LWR	Light water reactor
M+B	Membrane plus Bending
NCM	Noncyclic Method
NSM	Nonlinear Superposition Method
ONR	Office for Nuclear Regulation
PED	Pressure Equipment Directive
PEEQ	Equivalent Plastic Strain Abaqus Output
PEMAG	Plastic Strain Magnitude Abaqus Output
pLMM	Probabilistic Linear Matching Method
PW	Plastic Work
PWC	Plastic Work Curvature
R-Node	Redistributed Node
RPWC	Ratio of Plastic Work Curvature
SCL	Stress Classification Line
SCP	Stress Classification Plane
TES	Twice Elastic Slope
TI	Tangent Intersection
UB	Upper Bound
UK	United Kingdom
UKCA	United Kingdom Conformity Assessed
UMY	Uniform Modified Yield
UPFRA	Unified Procedure for Fatigue and Ratchet Analysis
UTS	Ultimate Tensile Strength
WNA	World Nuclear Association
WRC	Welding Research Council

Variables

A, B, C, D	Curve Fitting Parameters for Ricketts and Head Function
A, B	Lamé Equation Constants
A	Cross Section Area
E	Young's Modulus
E_i	Young's Modulus at Iteration i
F	Peak Stress
I	Second Moment of Area
K_e	Plasticity Correction Factor
M	Bending Moment
M_L	Bending Moment at Limit State
M_Y	Bending Moment at Yield
N	Axial Force
N_f	Number of Cycles to Failure
N_L	Axial Force at Limit State
N_Y	Axial Force at Yield
$P + Q$	Primary plus Secondary Stress
P_L	Limit Pressure
P_{SD}	Elastic Shakedown Limit Pressure
P_a	Allowable Pressure
P_b	Primary Bending Stress
P_{end}	End Cap Pressure
P_i	Applied Pressure
P_l	Local Primary Membrane Stress
P_m	General Primary Membrane Stress
P_{ref}	Reference Load
Q	Applied Load
R	$R = \sigma_Y/\sigma_{uts}$
R_i, R_o	Inner Radius, Outer Radius
R^2	Sum of the Square of the Difference
S_E	Von Mises Equivalent Stress

S_I	Tresca Stress Intensity
S_a	Alternating Stress
S_m	Design Stress Intensity
S_n^*	Stress Range Minus Thermal Bending Stress
S_t	Surface Area where Traction is Applied
T	Temperature Load
T_C	Cold Shock Temperature
U	Cumulative Usage Factor
V	Body Volume
W_e	Elastic Work
W_p	Plastic Work
a - i	Nozzle Dimensions
b	Beam Width; Fatigue Strength Exponent
c	Fatigue Ductility Exponent
dW	Work Done per Unit Volume
dx	Change in Position on SCL
$f(x)$	Ricketts and Head Curve Fitting Function
h	Half Beam Depth
m, n	Plasticity Correction Factor Material Parameters
$m_{L,a,U}$	Limit Load Multipliers
n_i	Number of Operational Cycles
n_j	Unit Vector Normal to Surface
q	EMAP Instability Factor
r	Radius
s_L	Static Multiplier
s_U	Kinematic Multiplier
t	Through Wall Thickness; Length of SCL
t_i	Surface Traction Load
x	Position on SCL; Normalised Membrane Stress; Scaling Factor
y'	Normalised Thermal Stress Range
z	Position Through Beam Thickness

Greek Letters and Symbols

v	Poisson's Ratio
α	Coefficient of Thermal Expansion
λ	Thermal Conductivity
θ	Angle of Elastic Region on L-D Curve
κ	Curvature
φ	Angle of TES Collapse Limit Line
η	Curve Fitting Parameter
χ	Curve Fitting Parameter
$\varepsilon - N$	Strain - Life
ε_a	Total Alternating Strain
ε_a^e	Elastic Strain Amplitude
ε_a^p	Plastic Strain Amplitude
ε_e	Equivalent Elastic Strain
ε_f'	Fatigue Ductility Coefficient
ε_{ij}	Strain Tensor
ε_{ij}^{pl}	Plastic Strain Field
$\bar{\varepsilon}^{pl}\big\vert_0$	Initial Equivalent Plastic Strain
$\dot{\bar{\varepsilon}}^{pl}$	Equivalent Plastic Strain Rate
ε_p	Equivalent Plastic Strain
$\Delta()$	Range
$\sigma_{1,2,3}$	Principal Stresses
σ_{const}	Constant Stress
σ_{cyclic}	Cyclic Stress
σ_{VM}	Von Mises Equivalent Stress
σ_Y	Yield Strength
σ_Y'	Modified Yield Strength
σ_a	Applied Alternating Stress; Arbitrary Stress
σ_b	Bending Stress
σ_e	Equivalent Stress

$\sigma_{e,i}$	Equivalent Stress at Iteration i
$\sigma_{e,ij}$	Cyclic Elastic Stress Field
$\sigma_{e,max}$	Maximum Equivalent Stress along SCL
σ_f'	Fatigue Strength Coefficient
σ_i	Maximum Equivalent Stress at Iteration i
σ_{ij}	Stress Tensor
$\sigma_{ij,b}$	Bending Stress Tensor
$\sigma_{ij,m}$	Membrane Stress Tensor
σ_m	Membrane Stress; Membrane Stress Tensor
σ_{m+b}	Membrane plus Bending Stress; M+B Stress Tensor
σ_n	Nominal Stress
$\sigma_{r,ij}$	Constant Residual Stress Field
σ_{uts}	Ultimate Tensile Strength
$\sigma_{uts,t}$	True Ultimate Tensile Strength
$\sigma_{x,y,z}$	Direct stress components
$\sigma_{xy,xz,yz}$	Shear Stress Components
σ_z	Total Stress at Position z Through Thickness

Chapter 1 Introduction

1.1 Design, Safety and Acceptance of Pressurised Nuclear Components

The nuclear industry has many unique challenges and safety criteria which make the design process for nuclear components especially challenging. Over the course of a nuclear power plants life, considerations must be taken for planning, siting, design, manufacture, construction, commissioning, operation and decommissioning. Along with the safe design of components for new plants, there is also increasing demand to prolong the life of existing plants. The International Atomic Energy Agency (IAEA) define five levels of defence [1] to ensure the safe design and operation of a nuclear power plant of which the selection and application of appropriate design codes and standards is a requirement.

The design and manufacture of pressurised equipment in the European Union must meet the requirements of the Pressure Equipment Directive (PED). The PED covers the design, manufacture and conformity assessment of pressure equipment and assemblies with an operating pressure above 0.5 bar [2]. Following the European Design Code EN 13445 would ensure compliance with the PED. The PED has not been applicable to new pressure equipment entering the UK market since 1 January 2021, instead a UK Conformity Assessed (UKCA) marking is required under new UK specific regulations.

The Office for Nuclear Regulation (ONR) is responsible regulating the nuclear industry in the UK. It is an independent body that ensures the safe design and operation of UK nuclear facilities. This includes enforcing the correct use and adherence to applicable pressure vessel regulations. As the failure of a nuclear pressure vessel could lead to the release of radioactive material, dedicated design codes and standards exist for nuclear components. The American Society of Mechanical Engineers (ASME) Boiler and Pressure Vessel Code (BPVC) Section III Rules for Construction of Nuclear Facility Components is an internationally recognised standard specifically for nuclear application. ASME III Division 1 Subsection NB covers the design requirements for Class 1 pressure vessels. The code contains guidance on the load case combinations, failure mechanisms and design criteria that must be adhered to. The use of codes and

standards such as ASME III and EN 13445 allow for the safe design and acceptance of pressurised structures and components.

1.2 Introduction to Pressure Vessel Design by Analysis

Design by Analysis (DBA) of nuclear pressure vessels has been an area of significant interest and investigation since it was introduced in ASME III in the 1960s. DBA was incorporated in ASME III to supplement the existing Design by Rule (DBR) methodology. Before the use of DBA was feasible, pressure vessels were designed by following a systematic procedure and set of rules to obtain permissible wall thicknesses. However, these rules were only applicable to standard components and included high margins of safety to ensure conservatism in the design.

DBA offers an alternative route, allowing complex components to be designed more accurately. By calculating the actual stress distributions, the analyst gains a better understanding of the structural response to defined loads and boundary conditions.

The Code now allows for linear elastic and non-linear elastic-plastic DBA. For the elastic route, if the stresses meet the allowable limits set out in ASME III, then the design is considered safe. The elastic stress limits imposed on the structure do not have to be met if plastic material properties are considered. Instead, allowable loads are calculated based on design margins specified in the Code.

The development of advanced finite element analysis (FEA) and the rapid increase in computing power since the introduction of DBA have made such methods more accessible, to the point where DBA is now a viable alternative to DBR for the design of Class 1 nuclear components. As such, there is a keen interest within industry to maximise the use of DBA to take advantage of the enhanced knowledge of the structural response and reduction in conservatism it offers over the use of DBR. If the wall thickness of a component can be reduced through use of DBA, significant cost savings may be achieved.

The use of DBA in the design of pressurised nuclear components to meet the requirements of ASME III specifically is still an area of interest. Much of the literature focuses on the science behind new methods without much consideration for the practical limitations that might exist. There are many considerations to take into

account when designing a nuclear component such as manufacturing capability and the resources available. Therefore, there is a need for efficient DBA methods which make the more detailed design process justifiable over simply using DBR. Any new design methods face a time consuming approval process to be included in nuclear design codes as code cases and to satisfy the nuclear regulatory body, it is important to use recognised design codes and methods. In the UK the nuclear industry is regulated by the ONR. Therefore, to ensure the regulatory body is satisfied and to minimise the time of the approval process, well-established DBA methods such as stress linearisation and classification are still of importance for companies designing pressurised components for use in the civil nuclear industry right now. Further development into current elastic DBA methods, along with continuing to demonstrate the possible advantages of non-linear DBA to increase confidence in their use, is therefore a useful area of research.

ASME III has not evolved at the same rate as stress analysis techniques, with one of the main issues in elastic DBA being that there is an incompatibility between the use of continuum FEA and the definitions of the ASME III stress categories. Although FEA is permitted within ASME III, there is an over reliance on analyst experience when carrying out many of the methods. This can lead to ambiguity and a lack of consistency in the results. Other pressure vessel design codes, such as ASME Section VIII Division 2, elaborate on some DBA methods in more detail and so there may be areas within the ASME III methodology where more guidance would be of benefit, especially when it comes to determining failure loads using elastic-plastic FEA. At the same time, the design Codes are not intended to be a step by step guide on how to perform stress analysis of pressure vessels. There has to be a balance between the instruction and specification provided by the Code and engineering judgement.

1.3 Project Aims and Objectives

This thesis aims to identify some of the issues associated with the use of DBA, especially in the relationship between the use of FEA and satisfying ASME III, to provide some clarity surrounding areas of ambiguity for the analyst. Areas of uncertainty and pessimism in various DBA methods are highlighted by analysing a selection of nuclear components incorporating 2D and 3D geometry, static and cyclic

loading conditions, non-linear material properties and non-linear geometry. An important part of this research was to consider design cases representative of those found in the nuclear industry. By carrying out the investigation in this way, this thesis aims to address the following objectives:

- Identify linear elastic and non-linear DBA methods which can be used to safely design nuclear pressure vessels to meet the requirements of ASME III
- Determine how the accuracy of elastic DBA can be enhanced for the prediction of plastic collapse loads by considering different stress linearisation methods
- Determine how influential the choice of linearisation method is in elastic DBA for predicting elastic shakedown limit loads of structures subject to cyclic loading
- Investigate the application of different non-linear elastic-plastic DBA methods for the prediction of plastic collapse loads
- Investigate how effective non-linear cycle-by-cycle FEA is for practical use in determining the structural response of components to cyclic loading conditions

1.4 Thesis Structure

This thesis consists of eight chapters, which demonstrate how the research was carried out and present the key findings. This introductory chapter concludes by providing background information into ductile failure mechanisms common to pressurised components and some theoretical insight into the plasticity theory from which many of the design methods originate. Chapter 2 then considers the actual DBA methods. To fulfil the first objective in section 1.3, a review of current methods and practices specified in ASME III is conducted. Alternative linear elastic and non-linear methods from the literature are also discussed.

To meet the aims and objectives, a clear research methodology was devised and followed. The main focus of this research is to explore DBA methods for use in the design of nuclear pressure vessels against failure due to plastic collapse and ratcheting. As such, various components exposed to different loading conditions and experiencing different failure modes are analysed. The aim of this research is not concerned with creating and applying a method specific to a single component, however, nozzle-vessel

configurations are used in the analysis frequently. Nozzles are complex components which can experience a variety of failure modes, so DBA of such components is favourable in the nuclear industry. Nozzle-vessel components are therefore appropriate for investigating the accuracy of linear elastic and non-linear DBA methods in predicting plastic collapse, alternating plasticity and ratcheting. Other components are also analysed to help determine if the methods in question can be applied universally. Most notably, a tubesheet is also used for the plastic collapse assessments. This allows a more comprehensive study into the DBA methods as the geometry is complex and the failure mechanism differs to the nozzle geometries.

The methodology involved following a logical path where linear elastic DBA methods are studied first before focussing on more complex non-linear methods. Within the linear elastic investigation, specific studies to determine the effectiveness of stress linearisation methods in designing for plastic collapse and then incremental plastic collapse are conducted. The same logic is applied to the investigation into non-linear DBA, with the focus initially on the plastic collapse failure mode and then on alternating plasticity and ratcheting. The complexity of the DBA methods increases as the study progresses.

As explained in detail in Chapter 3, Finite Element Analysis (FEA) was used extensively to carry out stress analysis in this research. FEA is a reliable tool for calculating stress results and deformations for pressurised components subject to specified loading and boundary conditions. Therefore, using FEA to calculate the raw data helped ensure that the investigation into the DBA methods is effective. To satisfy the aims and objectives for the linear elastic analysis, FEA was used to calculate elastic stress fields for each component being analysed. The six stress components could be easily extracted at the points of interest, ready for post-processing.

To calculate the linearised stress distributions for each linearisation method, programs in Matlab and Python were written. This allowed full control over how the stress components are treated during post-processing instead of relying on commercial stress linearisation tools built into the finite element (FE) software. By writing dedicated programs, calculating the linearised stress distributions was much faster. This was especially true for the cyclic analysis, where a Python script extracted the stress results

from Abaqus directly and automatically calculated linearised membrane plus bending stress ranges for each linearisation method. Automating the post-processing of the elastic stress results in this way greatly improved the efficiency of the research, allowing a greater number of methods to be investigated and more time for the results to be analysed.

FEA was also a key part of the research methodology for the investigation into non-linear DBA. Plastic collapse loads can be obtained directly from elastic-plastic FEA using limit analysis and the ASME VIII Div 2 plastic analysis methods. Other methods involved post-processing deformation, plastic strain and plastic work results, variables which are all calculated in elastic-plastic FEA. The results were used as inputs into Matlab scripts which calculate plastic collapse loads by carrying out the non-linear DBA methods, such as automatically plotting graphs and calculating intersection points as per the load-deformation DBA methods outlined in section 2.5. This allows plastic collapse loads for various methods to be calculated and analysed, meeting the aim of investigating non-linear DBA methods for plastic collapse.

Cycle-by-cycle FEA involves simulating multiple load cycles while incorporating non-linear material properties. While the analysis is not difficult to set up, the main concerns with this analysis are the computation time and interpretation of results to determine the structural response. Therefore, meeting the final objective requires the use of non-linear FEA in the research methodology.

FEA is not always necessary, as was the case for one component analysed in this thesis. Static analysis of a cylinder is carried out with elastic stress components and plastic collapse limit loads being calculated analytically. FEA is only used to calculate stress values for more complex design problems. Also, although a key part of the research methodology is to automate calculations where possible, Excel spreadsheets were used for basic calculations.

The pressurised nuclear components analysed in this research and the justifications for their use are presented in detail in Chapter 3.

The components are:

- Thick Walled Cylinder
- Light Water Reactor (LWR) Nozzle
- Tubesheet
- Oblique Nozzles
- Thermal Shock Nozzle

The cylinder is analysed with an internal pressure load only and with the addition of a cyclic thermal load during the linear elastic DBA study in Chapter 4. Due to its simplicity, elastic stress analysis of the cylinder provides an initial insight into possible issues that need to be addressed in the use of stress linearisation in elastic DBA of thick walled structures. The cyclic thermal analysis of the cylinder is similar to that of the Bree problem but with a thicker wall section.

The geometry definition for the LWR nozzle analysed in this thesis has been taken from a wider WNA research project investigating the use of DBA methods. It is typical of LWR component and provides a better insight into the use of elastic DBA for sizing components than the simple cylinder. The LWR nozzle is also analysed extensively in Chapter 5 alongside the tubesheet for the study on non-linear DBA methods for predicting plastic collapse.

The tubesheet was a useful component to analyse because experimental test results published by Jones and Gordon [3] allow the computational methods explored in this study to be validated. The ability to validate DBA results against real test data was the main reason the oblique nozzles were analysed in Chapter 4 and Chapter 5 for the prediction of elastic shakedown and alternating plasticity using linear elastic and non-linear DBA respectively. The location at which alternating plasticity was observed and the internal pressure loads leading to alternating plasticity were recorded experimentally by Procter and Flinders [4], allowing conclusions to be made on the accuracy of linearisation methods and cycle-by-cycle analysis in calculating allowable elastic shakedown loads. Validating the results obtained computationally in this research against test data published in the literature provides better evidence to justify the conclusions drawn on the use of each of the methods being investigated.

The final component is a nozzle in a spherical vessel subject to a pressure and temperature transient typical of a nuclear power plant. This component is used

extensively in the literature which helped validate the FE model setup and stress results.

Chapter 4 presents the linear elastic DBA investigation. The main aim of Chapter 4 is to identify a linearisation method which provides a robust solution for predicting failure due to plastic collapse by meeting the primary stress limit and ensuring shakedown to elastic action by satisfying the P+Q stress limits. A novel approach to stress linearisation is investigated alongside three more established methods. A key aspect of this thesis was to consider the industrial application as well as the theoretical accuracy of the methodologies and by analysing various components and failure mechanisms, various benefits and shortcomings of each linearisation method could be identified. The findings of this study are therefore significant when deciding on a suitable approach for elastic DBA for nuclear components in order to meet code requirements.

A study on the use of linearisation methods to prevent plastic collapse was conducted first. The research methodology was to begin by identifying any fundamental issues with elastic DBA and the linearisation methods of interest by analysing a simple component before identifying practical issues by applying each linearisation method to a design problem representative of the nuclear industry. Therefore, elastic analysis of the simple internally pressurised cylinder is conducted before analysing the LWR nozzle and tubesheet to determine which linearisation method is superior for the primary stress check, therefore meeting the second objective in section 1.3.

The second part of Chapter 4 then focusses on cyclic loading conditions leading to alternating plasticity and incremental plastic collapse. An analysis of how each linearisation method calculates P+Q stress distributions is conducted for the oblique nozzles, cylinder and thermal shock nozzle. To satisfy the third objective in section 1.3, the methodology is split into three distinct parts investigating the use of linearisation methods for:

1. Cyclic mechanical loads
2. Cyclic thermal loads
3. Combined cyclic mechanical and thermal loads

Each of the three loading conditions is specific to the components being analysed i.e. the oblique nozzles experience a cyclic internal pressure load, the cylinder has a static pressure and cyclic thermal load applied to the inside surface and the thermal shock nozzle is subject to a cyclic pressure load and cyclic thermal load in the form of a cold shock applied to the inside surface of the nozzle.

This methodology allows the effects of cyclic mechanical stresses and cyclic thermal stresses to be investigated separately for each linearisation method to determine how accurate each is at calculating the P+Q stress distribution. Final conclusions on the use of stress linearisation and the appropriateness of each LM can then be drawn from the combined cyclic analysis, where the loading conditions are more realistic of a typical nuclear power plant transient.

By analysing the results for the static and cyclic stress analysis together, an informed conclusion on the most appropriate linearisation method can be made. The methodology for the linear elastic analysis follows a logical path, leading to a final conclusion on the choice of linearisation method.

Following on from the detailed investigation into linear elastic DBA methods, Chapter 5 focusses on non-linear DBA. A similar format is followed as for the linear elastic analysis, with the study initially focussing on the plastic collapse failure mode. Various plastic collapse methods are investigated on the LWR nozzle and tubesheet. Limit analysis is explored in section 5.1 to validate the results from the linearisation methods study and identify any advantages and disadvantages with applying limit analysis using elastic-perfectly plastic FEA.

The methods investigated in section 5.2 incorporate material strain hardening into the FEA. The ASME VIII Div 2 material model is used to calculate true stress-strain curves for low alloy steels, allowing the material properties for the LWR nozzle and tubesheet to be defined in the FE model. Including material strain hardening in the analysis allows the actual structural response of the components to the applied loads to be determined and various DBA methods exist which allow plastic collapse limit loads to be calculated from the results of full plastic FEA. This research focussed on five such methods: ASME VIII Div 2 plastic method, twice elastic slope (TES), tangent intersection (TI), plastic work (PW) and plastic work curvature (PWC).

These methods have all seen extensive research previously, the novelty in this study is combining these post-processing methodologies with the ASME VIII Div 2 plasticity model and assessing two complex but very different components that are typical of the nuclear industry. This provides useful insight into the practical application of non-linear DBA methods and their potential for use in ASME III BPVC assessments. Stress-strain material data can be difficult to obtain and hence make full elastic-plastic non-linear DBA unachievable. This thesis provides evidence that the ASME VIII Div 2 material model for low carbon steel can be used with each of the non-linear DBA methods in question to determine reliable plastic collapse loads and is a noteworthy finding as it proves there is scope for full elastic-plastic DBA that is both robust and easy to implement. Published data for the tubesheet analysed in this study allows each method to be benchmarked against experimental test results. This is of particular significance as validation against experimental results is not particularly common for nuclear components in published works of academia.

The effectiveness of the ASME VII Div 2 material model in conjunction with graphical post-processing methods was investigated along with exploring the use of the ASME VIII Div 2 plastic method for the design of pressurised nuclear components. The study on non-linear analysis for protecting against plastic collapse is concluded by presenting the plastic collapse loads and allowable loads for each method and each component together, allowing any trends or advantages to be identified and thus satisfying the fourth objective in section 1.3.

Following the aims and objectives in section 1.3, cycle-by-cycle FEA for the prediction of elastic shakedown, alternating plasticity and ratcheting is the final non-linear analysis method researched in Chapter 5. The oblique nozzles and thermal shock nozzle are analysed using Abaqus FE models with the same mesh and boundary conditions as for their respective elastic analysis but with an elastic-perfectly plastic material model and different analysis settings to simulate multiple cycles. The oblique nozzles were analysed first and the results validated against published test results. This was an effective way to determine the accuracy of cycle-by-cycle analysis in calculating the internal pressure magnitude and location at which alternating plasticity occurs. Analysis of the thermal shock nozzle allowed the practical effectiveness of cycle-by-cycle FEA on a complex component subject to a typical nuclear power plant

transient to be investigated. Various thermal shock loads were analysed to induce different cyclic structural responses for the study. The aim of this analysis was to determine if cycle-by-cycle FEA, assuming elastic-perfectly plastic material properties, is an effective method for designing against the threat of ratcheting. Cycle-by-cycle analysis of the oblique nozzles and thermal shock nozzle also proves useful for validating the linear elastic results, further increasing the fidelity of the conclusions of the linearisation methods study.

A detailed discussion of the analysis conducted in Chapter 4 and Chapter 5 is given in Chapter 6. The discussion section considers the accuracy of the results, how the methods align with the requirements of ASME III, practical considerations with implementing DBA and highlights key findings through a detailed analysis of the linear elastic and non-linear DBA results.

The thesis is concluded in Chapter 7. General observations are discussed, the results are summarised and recommendations are provided based on the outcome of this research and any future work which could succeed it.

1.5 Ductile Failure Modes of Pressure Vessels

The Pressure Vessel Design Manual [5] outlines eight potential failures:

1. Elastic Deformation – buckling
2. Brittle Fracture
3. Gross Plastic Deformation (GPD)
4. Stress Rupture – creep deformation from cyclic loading
5. Plastic Instability – ratcheting
6. High Strain – Low Cycle Fatigue (LCF)
7. Stress Corrosion Cracking
8. Corrosion Fatigue – combination of fatigue and corrosion

This research will focus on design methods for the prediction and prevention of gross plastic deformation and ratcheting, caused due to static and cyclic loading conditions respectively. Failure due to low cycle fatigue is also discussed briefly. These particular failure modes are can be extremely dangerous, especially if they have a nuclear

application. Therefore, a detailed understanding of how such failure mechanisms form and how they can be prevented are vital.

GPD or plastic collapse is a ductile failure mode caused by a static load, such as a constant internal pressure. When the load is high enough, the material will yield, causing plastic deformation. For pressure vessels, the internal pressure at which the material yields and becomes plastic through the entire thickness is defined as the plastic collapse limit load. For an elastic-perfectly plastic material model, no further load can be supported, leading to structural instability and hence failure due to excessive plastic deformation.

Incremental plastic collapse occurs due to an accumulation of plastic strain during cyclic loading. This phenomenon, known as ratcheting, causes eventual failure due to excessive plastic deformation of the vessel and must be avoided. The Codes allow some plastic deformation of the vessel as long as it can be shown to exhibit shakedown, where there is no net plastic deformation over the load cycle. The most dangerous aspect of ratcheting is that failure of the vessel occurs at loads lower than the plastic collapse limit load. Failure caused by cyclic loading conditions must be considered, as nuclear pressure vessels experience a combination of cyclic loading histories during service, such as start-up and shutdown, pressure and temperature fluctuations due to load following or unexpected fault conditions.

There are three main structural responses to cyclic loading in the plastic regime of the material: elastic shakedown, alternating plasticity (or plastic shakedown) and ratcheting. If the cyclic load does not cause the material to yield, then no plastic deformation occurs and the material remains in the elastic regime. A common way of presenting the relationship between these is using the Bree diagram [6].

Bree analysed the structural response of a nuclear fuel casing component (i.e. a thin cylindrical section) subject to constant internal pressure and cyclic through-wall temperature distribution. The component was assumed to exhibit perfect plasticity and the problem was simplified to a 1-dimensional plane stress plate under a cyclic linear thermal gradient and constant axial tension. The Bree problem demonstrates that the cylinder exhibits five different responses which vary depending on the applied loading conditions. The shakedown and ratchet regimes can be visualised on the interaction

diagram in Figure 1, the Bree diagram, by plotting the constant mechanical load against the cyclic thermal load, both of which are normalised against the material yield strength.

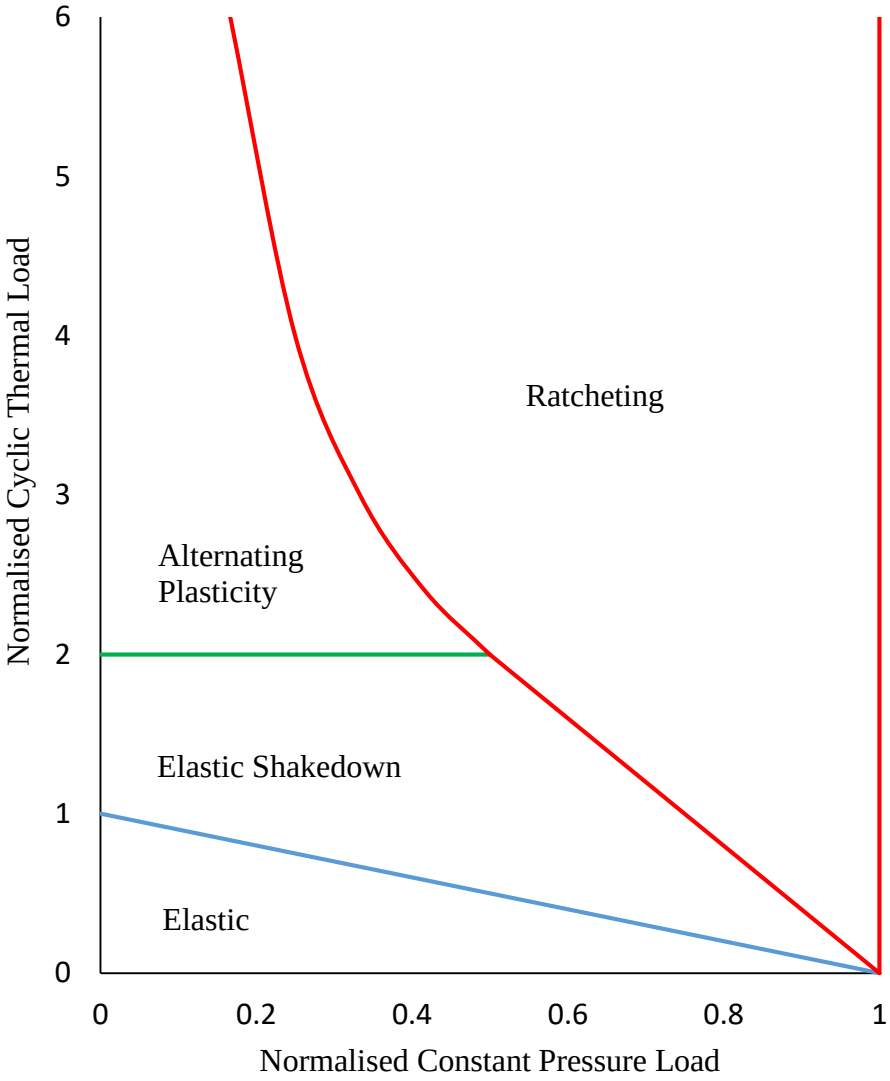

Figure 1: Bree Cylinder Interaction Diagram

Although the Bree diagram relates to a specific component under specific conditions, it highlights many features of shakedown behaviour which need to be considered for general shakedown and ratcheting analysis. It also forms the basis for the ASME III thermal stress ratcheting criteria [7]. Each of the five zones in Figure 1 relates to a

different structural response caused by the corresponding constant pressure and cyclic thermal loads.

The vertical line at the normalised constant load of 1 in Figure 1 represents the limit load for an elastic-perfectly plastic material. Therefore, cyclic loading is not even possible to the right of this line because when the load is applied during the first cycle, the structure experiences GPD.

If the loads are not sufficient to cause the material to yield, an elastic response as in Figure 2 is established. Only elastic stresses are present and therefore no plastic straining takes place. This means that the structure's geometry is identical at the start and end of the load cycle and remains so for subsequent load cycles.

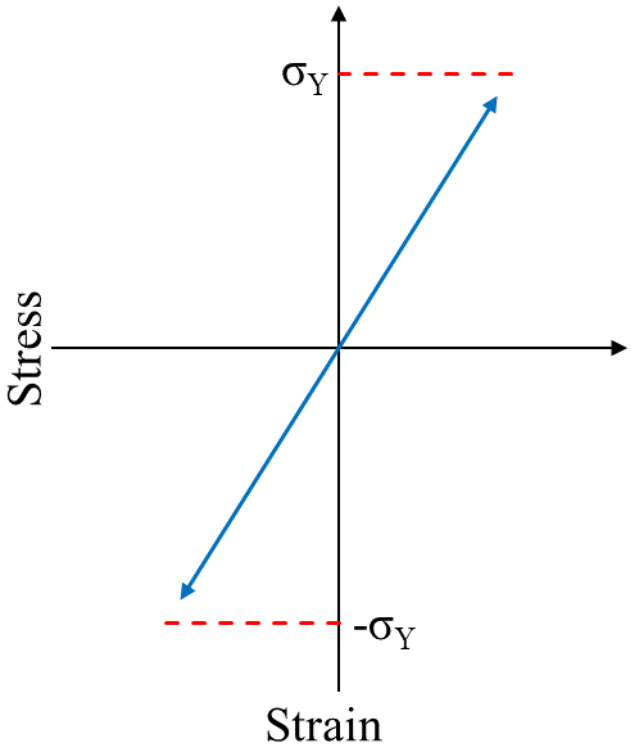

Figure 2: Fully elastic response to cyclic loading

If plastic deformation occurs during the early load cycles, but the structure then reaches a state where the response to future load cycles is elastic, it is said to experience elastic shakedown. This response is a result of the residual stress field created during initial loading. This has the effect of reducing the mean stress in future load cycles and as

long as the maximum stress does not exceed yield, no further plastic deformation will occur, i.e. the plastic strain remains constant over all future load cycles. This is demonstrated in Figure 3(a). The green line indicates initial load application and shows how some plastic deformation occurs before unloading the structure, denoted by the blue line. The blue, wholly elastic, cyclic load path is then followed on future loading and unloading of the structure.

If a steady cyclic state is reached whereby plastic deformation occurs at the start and end of each load cycle, alternating plasticity is said to occur. Also termed plastic shakedown or reverse plasticity, this response is similar to elastic shakedown in that a steady state is achieved over the cycle. The plastic strain at the start and end of the cycle is the same, however, the plastic strain does not remain constant. Plastic deformation occurs both on loading and on unloading of the structure but there is no net increase in plastic strain over numerous cycles. Figure 3(b) presents a typical alternating plasticity load path. As with the elastic shakedown behaviour, plastic straining occurs on loading the structure during the first cycle. In this case, the residual stress field does not ensure an elastic response to future loading. For successive load cycles, an equal magnitude of positive and negative plastic straining occurs on loading and unloading. This phenomenon may occur at highly localised regions, where the plastic strains are constrained by the elastic response of the rest of the structure. Distinguishing between elastic shakedown and alternating plasticity is important as this response can lead to failure due to low cycle fatigue.

Ratcheting is, unlike the previous responses, not permitted in any circumstance and will eventually lead to failure by incremental plastic collapse. This type of ductile failure occurs due to an accumulation of plastic strain over numerous load cycles. Figure 3(c) demonstrates what a hysteresis loop may look like for ratchet behaviour. The green line shows initial loading and the first load cycle. The residual stress field changes over the cycle however, causing the next cycle to follow the blue load path. This sequence of incremental plastic deformation will continue, growing the plastic region in the structure until a global plastic collapse mechanism forms.

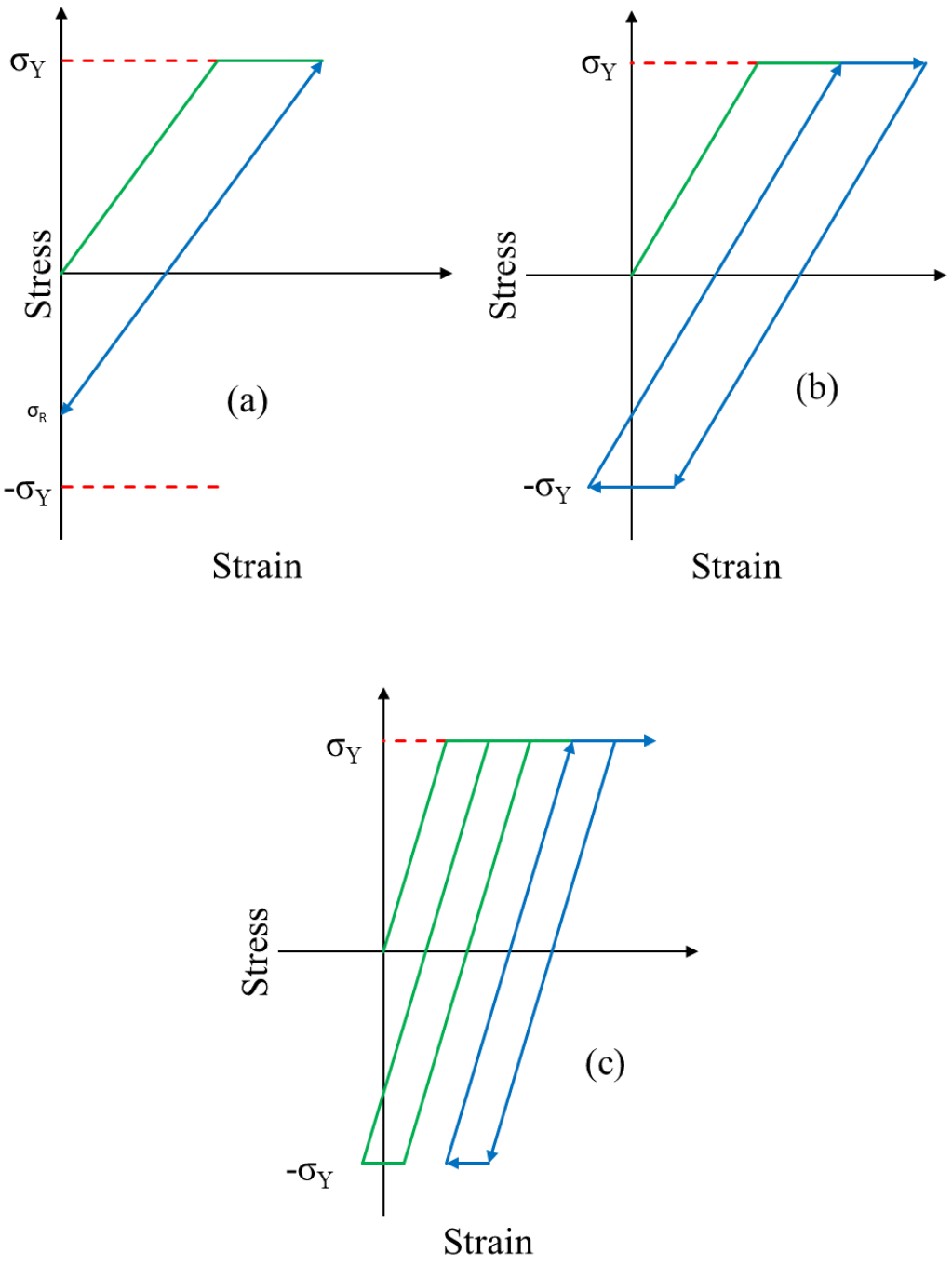

Figure 3: Elastic shakedown (a), alternating plasticity (b) and ratcheting (c) behaviour

1.6 Fatigue

Fatigue involves the formation and propagation of a crack in a structure under cyclic loading until eventual failure. Fatigue can be categorised under two main phenomena, high cycle and low cycle fatigue. From the Bree diagram in Figure 1, high cycle fatigue occurs in the elastic shakedown region. For nuclear pressure vessels however, low cycle fatigue is the main area of concern and can be an issue at sections experiencing alternating plasticity under a cyclic load. Typically, low cycle fatigue is said to occur when the number of cycles to failure is less than 10,000.

Fatigue failure generally occurs in three stages. Firstly, the cyclic stress induces a microscopic defect at a single point due to a local reduction in ductility over repeated cycles. Next, the crack will propagate slowly over a number of cycles, finally resulting in sudden failure due to fracture. A number of approaches can be taken when designing against fatigue and different pressure vessel Codes may adopt different philosophies. A safe life design approach ensures that the calculated life of the structure far exceeds the service requirements. A damage tolerant design is another approach, in which the structure should be capable of withstanding the loads, despite the existence of in-service fatigue cracks, until the damage is detected through routine inspection.

Classical stress-life approaches require a series of design factors, based on surface finish, size, load, temperature and other factors, to be calculated and applied to the mean endurance limit of a test specimen. The stress-life method is not always accurate in the low-cycle fatigue regime, where significant plastic straining occurs. To address this, strain-life methods exist which determine the life of a test specimen to crack initiation. This is discussed further in section 2.1.3.

1.7 Limit Analysis and Shakedown Theorems

Various design methods exist to preclude the ductile failure mechanisms described in section 1.5 from occurring. The majority of these methods find their roots in classical limit analysis and shakedown plasticity theorems.

A body is said to be in equilibrium with external forces if it follows the principle of virtual work. This states that the external work done on the body by the external loads must equal the internal work done by the strain energy [8]. The principle of virtual

work ensures both equilibrium and compatibility is maintained and forms the basis for deriving the classical limit analysis and shakedown theorems.

The lower and upper bound limit analysis theorems depend on finding statically admissible stress and kinematically admissible velocity fields. A number of boundary conditions must be satisfied in order for such conditions to arise. For static admissibility a stress field must exists that satisfies a prescribed yield condition, static equilibrium and displacement boundary conditions. A velocity field is said to be kinematically admissible if boundary conditions imposed on the velocity field, strain rate and work done are satisfied.

Theorems of limit analysis provide upper and lower bounds to the limit load of an elastic-perfectly plastic structure. Lubliner [8] summarises both classical theorems as:

> "The loads that are in equilibrium with a stress field that nowhere violates the yield criterion do not exceed the collapse loads, while the loads that do positive work on a kinematically admissible velocity field at a rate equal to the total plastic dissipation are at least equal to the collapse loads. If the loads produced by the application of the two theorems are equal to each other, then they equal the collapse loads."

The limit load is described as the load at which unrestricted plastic flow occurs [8] i.e. the structure experiences excessive plastic deformation for a small increase in load. Closed-form analytical solutions for simple structures such as beams in bending and pressurised cylinders exist but limit analysis bounding theorems can be used to find the limit load of non-standard components. A lower bound theorem is based on a statically admissible stress field with the upper bound solution derived from a kinematically admissible plastic strain rate field.

The lower bound limit load is of particular interest as there will always be some conservatism in the solution. This is displayed in Figure 4, showing how a lower bound solution converges on the exact solution from below. This makes analysis methods which employ lower bound theorems more desirable in actual pressure vessel design as they should produce safe results.

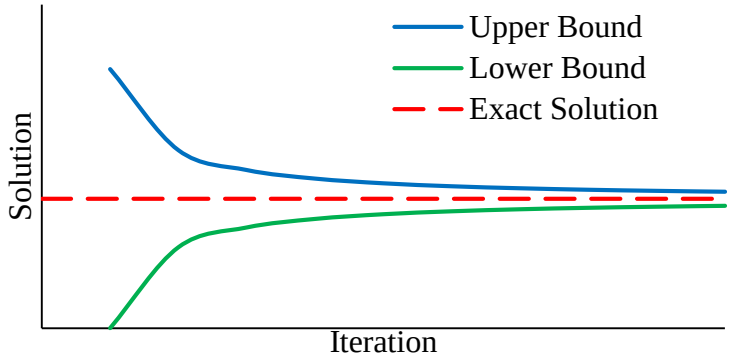

Figure 4: Lower and upper bound convergence

Classical limit analysis theorems are derived from the principle of maximum plastic dissipation [8], that is, for purely plastic strains the power of the stress per unit volume of material is dissipated as heat during plastic flow [9]. This is because, for unrestricted plastic flow, the elastic strain rate can be neglected, allowing the assumption for rigid-plastic behaviour to be made for elastic-plastic bodies. The rigid-plastic idealisation can be made since neither classical limit analysis theorem is influenced by the material behaviour prior to yielding, hence whether an elastic or rigid response is assumed prior to yielding has no bearing on the solution.

An elastic-perfectly plastic material model and small deformation theory are assumed. The structure is also subject to proportional loading, whereby the surface traction acting on the surface is increased monotonically via a load multiplier [10]. Lower and upper bound solutions are required to converge on the limit load multiplier due to the complexity and sometimes inability to calculate all of the governing equations of limit analysis. As such, classical lower and upper limit analysis theorems are widely used.

The lower bound limit analysis theorem can be expressed as the maximum load at which a statically admissible stress field is present that does not violate the yield condition anywhere i.e. external forces in static equilibrium with internal stresses.

Lubliner [8] provides a mathematical derivation based on the principle of virtual work originally presented by Drucker, Pager and Greenberg [11] for which a statically admissible stress field can never exceed the actual stress field at the limit state. It is common to see the lower bound limit analysis theorem given as in equations (1) and

(2). In this case, proportional loading is assumed such that a lower bound limit load multiplier m_L is applied to a single traction force t_i acting on the surface S_t of the body [10].

$$\sigma_{ij} n_j = m_L t_i \ \ on \ S_t \tag{1}$$

Where σ_{ij} is the stress tensor and n_j is a unit vector normal to the surface S_t.

By the lower bound limit analysis theorem, any statically admissible limit load multiplier, m_L, must be less than or equal to the actual limit load multiplier, m_a, to give a lower bound to the limit load.

$$m_L \leq m_a \tag{2}$$

The problem then lies in determining a statically admissible stress field in which m_L is maximised.

The upper bound theorem is derived from an energy balance between the work done by the external forces and the rate of internal dissipation. If the rate of external work is equal to or greater than the rate of internal dissipation, then the applied load will equal or exceed the limit load. This means that the kinematically admissible upper bound load multiplier m_U will be greater than or equal to the actual limit load multiplier [12], as shown in equation (3).

$$m_U \geq m_a \tag{3}$$

An upper bound on the limit load can therefore be obtained by finding a kinematically admissible velocity field which minimises m_U.

The proof presented by Lubliner [8] is similar to that of the lower bound, utilising the principle of virtual work, except that instead of considering a body with a stress field that's in equilibrium with the load set, it is assumed that a collapse mechanism has been established with a velocity field and strain rate. Lubliner shows that an upper

bound on the limit load exists because the energy transferred to the body is always going to exceed or be equal to the internal work done by plastic dissipation.

Shakedown and ratchet bounding theorems are based on two classical methods: Melan's lower bound theorem and Koiter's upper bound theorem. Over time, these two theorems have seen many extensions and have led to the development of more in-depth shakedown and ratcheting methods. The shakedown and ratcheting phenomena have been discussed in terms of the Bree cylinder problem, however, the Bree solution is an ideal case and does not necessarily provide accurate solutions to more complex geometries and loading conditions.

The classical methods reviewed in this section provide the basis for determining the strict elastic shakedown boundary for arbitrary problems, with Melan's theorem seeking a static equilibrium solution to provide a lower bound to the elastic shakedown load and Koiter's theorem providing an upper bound by minimising the strain energy to cause ratchet.

Melan's theorem is a lower bound quasi-static shakedown theorem [8] based on the premise that for shakedown to occur, there must be the presence of a time-independent residual stress field, i.e. constant plastic strain over each cycle. Applying Melan's theorem in equation (4), elastic shakedown is said to occur when a constant self-equilibrating stress field combined with a cyclic elastic stress field does not violate the yield condition at any location in the structure or at any time over the cycle [8,13,14] such that:

$$\left|\sigma_{e,ij} + \sigma_{r,ij}\right| \leq \sigma_Y \qquad (4)$$

Where $\sigma_{e,ij}$ is the cyclic stress field, $\sigma_{r,ij}$ is the constant residual stress and σ_Y is the yield stress.

Melan's theorem uses an elastic-perfectly plastic material model to find the load combination at which the structure will shake down to purely elastic action and is not load path-dependent. The self-equilibrated stress field could result from thermal stress or the difference between the elastic and elastic-plastic stress field for a specific load

combination. Obtaining the optimal self-equilibrating stress field is often where most issues arise [14]. As such, Melan's theorem works well for proportional loading cases but may be problematic when non-proportional loading is considered as the self-equilibrating stress field required for Melan's theorem is obtained when all external loads are removed [15]. Also, secondary stresses are by nature self-equilibrating and so must be cyclic to have an effect. As such, Reinhardt [16] discusses how this is not the case for constant primary stress, as this cannot be equilibrated by a residual stress. A stabilised cycle requires the load to be reversed and, as a result, ratcheting is regularly caused by constant primary stress.

Koiter proposed an upper bound kinematic shakedown theorem [8]. Koiter's theorem states that elastic shakedown will not occur if any kinematically admissible plastic strain rate and displacement field exist such that the work done on the structure exceeds that of the plastic strain. It is not the plastic strain rate at each point in time but the accumulation of plastic strain that must be compatible with the displacement field [8,17].

Effectively, what Koiter's theorem does is perform an energy balance of internal and external work done over the cycle. The shakedown limits calculated using Koiter's theorem will always be greater than or equal to the strict shakedown limit, hence it is described as the upper bound theorem [18]. As such, Melan's theorem is more commonly used to develop direct shakedown methods due to its inherent conservatism. Due to the classical methods reliance on linear kinematics and perfect plasticity, they are not always effective in predicting shakedown limits when other factors such as large deformations, strain softening, non-proportional loading and alternating plasticity are considered [19]. Melan and Koiter's theorems have seen many extensions to provide more comprehensive solutions and address such issues, however, the basis for the advanced limit and shakedown analysis methods stems from the classical theorems.

Chapter 2 Design by Analysis Methods

2.1 ASME III Elastic DBA

The ASME BPVC Section III Rules for Construction of Nuclear Facility Components [7] is widely used in the design of pressurised nuclear components. The following section considers the ASME III design philosophy, before introducing the concept of stress classification in elastic DBA. The actual elastic DBA procedure is then discussed in detail. A review of previous research into the use of elastic DBA is presented, identifying the mathematical procedures, assumptions and justification for the use of elastic DBA. An in-depth review of the elastic methods specified in ASME III to prevent failure due to plastic collapse, ratcheting and fatigue is then presented.

ASME III specifies a set of stress limits to be followed to prevent ductile failure of pressurised nuclear components. The failure criteria set out in the ASME BPVC developed from beam-shell theory, where membrane and bending stresses act on a single plane [20], are encapsulated by the stress limits. If a rectangular beam of width b and depth $2h$ experiences an axial force N and in-plane moment M, the elastic behaviour of the beam can be found through equilibrium of the applied forces and internal stresses. The membrane stress $\sigma_{m(z)}$, resulting from N and uniform through the thickness of the beam, can be calculated from equation (5).

$$\sigma_{m(z)} = \frac{N}{A} \tag{5}$$

The linear bending stress distribution, $\sigma_{b(z)}$, through thickness z of the beam is caused from the external moment M and is calculated from equation (6).

$$\sigma_{b(z)} = \frac{Mz}{I} \tag{6}$$

Where z is the location through thickness and I is the second moment of area.

In the linear elastic region, the total stress at any position z through the thickness of the beam is derived by simple stress superposition by taking sum of the membrane and bending action stress as shown in equation (7).

$$\sigma_{(z)} = \frac{N}{A} + \frac{Mz}{I} \tag{7}$$

For a tensile axial force, the material will yield at the outer surface first. Therefore, by substituting $z = h$, the cross-sectional area $A = 2bh$ and second moment of area $I = \frac{2}{3}bh^3$ into equation (7), the membrane and bending stress distribution at first yield, σ_Y, is given by equation (8).

$$\sigma_Y = \frac{N}{2bh} + \frac{3}{2}\frac{M}{bh^2} \tag{8}$$

Where h is the half beam depth and b is the width.

The stress limits are derived from the limit state of the beam, which is assumed to be made from an elastic-perfectly plastic material, so the maximum possible stress in the material must not exceed yield. This results in a plastic zone growing though the thickness of the beam, starting at the outer surface where yield first occurred, as stress redistribution is required to maintain equilibrium with the external forces. The beam is said to be fully plastic when the plastic zone has spread through the entire thickness, at which point the stress is unable to redistribute. The limit condition defined in equation (9) is derived by applying equilibrium between the applied forces and internal limit-state stress distribution.

$$\frac{M}{bh^2\sigma_Y} + \left(\frac{N}{2bh\sigma_Y}\right)^2 = 1 \tag{9}$$

The limit loads associated with membrane and bending loads respectively are $N_L = 2bh\sigma_Y$ and $M_L = bh^2\sigma_Y$. The interaction diagram in Figure 5 of the normalised

membrane and normalised bending loads gives a visual representation of the membrane plus bending limit condition of the beam.

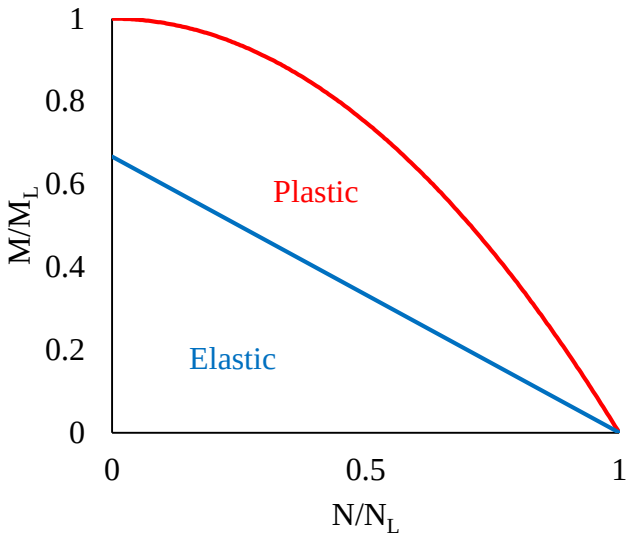

Figure 5: Interaction diagram

As the axial force required to cause first yield is equal to the force at the limit state, for a beam subject to pure membrane action only, there is no safety margin between first yield and plastic collapse, so $N_Y = N_L = 2bh\sigma_Y$. This is not the case when the beam is under a bending load only. There is actually a considerable margin of safety, as defined by the shape factor of the beam $M_Y/M_{\mathrm{L}} = \frac{2}{3}$.

This relationship between the elastic stress and limit state for a beam under combined bending and membrane action is used to define the limit for all pressure vessel structures, regardless of the geometry. The interaction diagram expressing the yield and limit surfaces in Figure 5 can be recreated in terms of membrane and bending stress. The ASME III [7] description for membrane stress in XIII-1300(p):

> "Membrane stress is the component of normal stress that is uniformly distributed and equal to the average stress across the thickness of the section under consideration."

Bending stress is defined in XIII-1300(a) as follows:

> "Bending stress is the component of normal stress that varies across the thickness. The variation may or may not be linear."

The limit surface can be presented in equation (10) as a function of membrane and bending stress.

$$\frac{2}{3}\left(\frac{\sigma_b}{\sigma_Y}\right) + \left(\frac{\sigma_m}{\sigma_Y}\right)^2 = 1 \qquad (10)$$

The maximum stress is the sum of membrane plus bending stress and yielding in the beam occurs when this value has reached the yield stress and can be written as equation (11), which describes the initial yield condition.

$$\frac{\sigma_m + \sigma_b}{\sigma_Y} = 1 \qquad (11)$$

By plotting equations (10) and (11), the interaction diagram in Figure 6 defining the initial yield and limit surfaces in terms of membrane and membrane plus bending stress is obtained. The ASME design stress limits used in elastic DBA are based on this. It can be seen that different limits are required depending on whether the vessel contains pure membrane or membrane plus bending stress and as such, the ASME BPVC imposes different design factors. The permissible design region within the ASME criteria is also shown in Figure 6. It is clear that the design region is well within the structural limit.

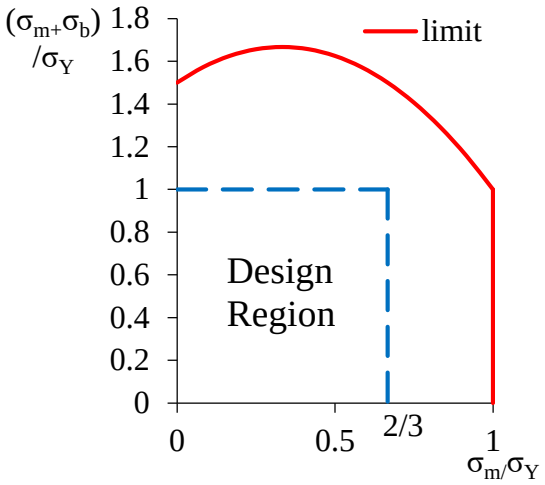

Figure 6: ASME interaction diagram in terms of membrane and bending stress

The membrane and bending stresses are meaningless with regard to the stress limits until they have been properly classified, a process which is subjective and requires the designer to have extensive experience and knowledge. The limits are defined in terms of primary membrane, local primary membrane, primary bending, secondary and peak stress.

The definition for primary stress is outlined in ASME III Article XIII-1300 as:

> **"**Primary stress is any normal stress or shear stress developed by an imposed loading that is necessary to satisfy the laws of equilibrium of external and internal forces and moments. The basic characteristic of a primary stress is that it is not self-limiting. Primary stresses that considerably exceed the yield strength will result in failure or, at least, in gross distortion. Primary membrane stress is divided into general and local categories. A general primary membrane stress is one that is so distributed in the structure that no redistribution of load occurs as a result of yielding. Examples of primary stress are: (1) general membrane stress in a circular cylindrical shell or a spherical shell due to internal pressure or to distributed loads; (2) bending stress in the central portion of a flat head due to pressure."

The definition for secondary stress in ASME III Article XIII-1300:

> **“**Secondary stress is a normal stress or a shear stress developed by the constraint of adjacent material or by self-constraint of the structure. The basic characteristic of a secondary stress is that it is self-limiting. Local yielding and minor distortions can satisfy the conditions that cause the stress to occur and failure from one application of the stress is not to be expected. Examples of secondary stress are: (1) general thermal stress; (2) bending stress at a gross structural discontinuity.”

It is vitally important that stresses are classified properly to ensure the safe and efficient design of a pressure vessel. The ASME III Code provides a hopper diagram which presents the stress categories and stress intensity limits. The hopper diagram can be used to classify the stresses in a vessel and identify the appropriate limits. While being straightforward for common geometries, it becomes more difficult as the complexity of the design increases. As such, ASME III also provides tables with guidance on how to classify stresses for specific vessel geometries. The location of interest, loading case and stress type influence the stress classification. Categorising primary stress correctly is the most important, as mistaking it for a secondary stress could have serious consequences. Alternatively, mistakenly classifying a secondary stress as primary can lead to an overly conservative design, resulting in thicker sections. Most problems arise in the stress categorisation procedure at discontinuities, as the stress field may contain a combination of primary and secondary membrane and bending stresses. Therefore, assuming all stresses at discontinuities are primary membrane plus secondary bending could underestimate the influence of any primary bending stresses, resulting in a potentially non-conservative design.

Each limit placed on the subsequent stress category relates to a different failure mode. The failure modes associated with the membrane and bending stresses are:

- Primary membrane (P_m): plastic collapse or GPD which includes ductile rupture and tensile instability
- Primary Bending (P_b): same as Pm but the stress must exceed the yield stress for through thickness yielding
- Local primary membrane plus primary bending ($P_l + P_b$): GPD and plastic instability
- Primary plus secondary ($P + Q$): plastic strain ratcheting
- Primary plus secondary plus peak ($P + Q + F$): fatigue failure

ASME III defines stress limits with regards to stress intensity. Stress intensity is the largest difference between the principal stresses and the Tresca Maximum Shear Stress failure criteria in equation (12) is used to calculate this.

$$S_I = \max[|\sigma_1 - \sigma_2|, |\sigma_2 - \sigma_3|, |\sigma_3 - \sigma_1|] \quad (12)$$

Where S_I is the stress intensity and $\sigma_{1,2,3}$ are the principal stresses.

ASME III limits were first defined in terms of stress intensity due to the simplicity and resources available at the time but not all the design Codes implement the Tresca criterion. ASME VIII Div 2 and EN 13445 have adopted the von Mises failure criterion (or Maximum Distortion Energy), which provides a less conservative approach. For this case, limits apply to the equivalent von Mises stress, S_E, which can be calculated from equation (13).

$$S_E = \frac{1}{\sqrt{2}}\sqrt{(\sigma_1 - \sigma_2)^2 + (\sigma_2 - \sigma_3)^2 + (\sigma_3 - \sigma_1)^2} \quad (13)$$

The stress intensity limits for primary and secondary stress intensities are in Table 1. The design stress S_m can be obtained directly from ASME II part D and is usually defined as the lower of $S_m = \frac{2}{3}\sigma_Y$ or $S_m = \frac{1}{3}\sigma_{uts}$ for ferritic steels. Where σ_{uts} is the ultimate tensile strength.

Stress Category	Stress Intensity Limit	
P_m	S_m	$2/3\sigma_Y$
P_l	$1.5S_m$	σ_Y
$P_m + P_b$ or $P_l + P_b$	$1.5S_m$	σ_Y
$P_l + P_b + Q$	$3S_m$	$2\sigma_Y$

Table 1: ASME III stress intensity limits

The nature of primary and secondary stresses dictates the limits imposed on them. Primary stress is load controlled and as such, when the material exceeds yield, it will deform plastically without bound, regardless of whether any additional load is applied. Therefore, as can be seen from Table 1, primary stress can never be allowed to go beyond yield. The strictest limit is on primary membrane stress. This type of stress occurs away from discontinuities and causes GPD of a vessel. Primary local membrane plus primary bending stress initiates the same ductile failure mode as primary membrane stress but due to the shape factor effect, the Code allows a higher stress for the limit load and plastic collapse.

Secondary stress is deformation controlled and results from compatibility requirements, unlike primary stress which is caused by equilibrium. Therefore, following yielding, the material will plastically deform but will be limited by the amount of displacement. There will be no further deformation when compatibility has been achieved. The ASME III Code takes this into account by allowing secondary stresses to exceed yield, as shown in Table 1. The primary plus secondary limit to prevent through-thickness plastic strain cycling is an important prerequisite for fatigue analysis since the stresses can still be acceptable, despite going beyond twice yield [21]. Peak stresses are responsible for causing local plastic strain cycling.

Defining the stress limits in terms of membrane and bending stress poses some problems when implementing DBA, especially in relation to continuum FEA. There are issues regarding the validity of applying these rules to 3D structures as the limits were derived for 2D axisymmetric geometries and loads [20]. For a 3D analysis, with complex loads and geometries, there may not be a single bending plane and meeting the requirement that the plane remains planar may not be possible. Also, to obtain the

stress field, Finite Element Analysis (FEA) has become the most common approach. If shell elements are used in the analysis, the membrane and bending stresses can be obtained directly from the results. This is fine for basic, thin-walled structures but for complex components, modelling the structure with shell elements may be an oversimplification. This will result in a loss of accuracy, especially at geometric discontinuities.

Processing power has become, and will be increasingly, more powerful; so it is much more common to carry out FEA with solid elements, as these provide a far more representative model, especially for thick-walled structures. The problem with using solid elements in the simulation is that the stress results are not expressed in terms of membrane and bending stresses, as required by the design Codes. Therefore, post-processing is required to separate out the stress field. The most common technique in elastic analysis is stress linearisation. This allows the total stress field to be broken down into membrane and bending stress components, which can then be used with ASME III to categorise the stresses appropriately before checking them against the prescribed limits.

The most comprehensive study carried out on stress linearisation and classification was conducted by Hechmer and Hollinger [20–22], who defined linearised stress as "stresses represented by linear distributions which develop the same net forces and moments on a section as the total stress distribution.'' They released a series of research papers highlighting the issues with 3D elastic stress analysis of pressure vessels and provided recommendations of how to best overcome these. They first discussed how membrane and bending stresses should be calculated from 3D non-linear stress distributions, what defines a bending plane in this context, how bending stresses can be obtained from 3D stress distributions and whether von Mises or Tresca failure criteria is more applicable to 3D FEA.

Six categories which outline the possible conditions for 3D stress analysis were discussed [20], ordered from most simple to most difficult these were:

1. Asymmetric loads on axisymmetric geometries
2. Perforations in otherwise axisymmetric geometries
3. Cylinder-to-cylinder intersections
4. Noncircular attachments to cylindrical shells
5. Non-radial penetrations and attachments to shells
6. General three-dimensional geometries

This prompted Hechmer and Hollinger [20] to investigate how primary and secondary stress failure modes relate to 3D FEA and carried out an extensive comparison between stress-at-a-point, stress-along-a-line and stress-on-a-plane procedures. They found that the degree of conservatism decreased from stress-at-a-point, stress-along-a-line and stress-on-a-plane, which was to be expected as the stress-on-a-plane method was the most extensive analysis procedure of the three. The results, however, between the plane and line methods did not differ significantly. This highlighted the possible advantages of stress-along-a-line, as the stress-along-a-plane results are heavily dependent on which planes are chosen for the analysis. The location, size and orientation of the analysis planes all required consideration and an improper choice could produce non-conservative results.

They carried out a stress linearisation study on a cylinder-flat plate structure and found that, for this particular geometry, SCLs located at the junction between the head and cylinder produced promising results, despite the bending plane not being perfect. A discussion into the use of shear theory (Tresca) and distortion energy theory (von Mises) highlighted that although von Mises is less conservative, it can provide more accurate solutions and that the preferred use of Tresca, due to its ease and conservatism, was archaic.

2.1.1 Influence of WRC 429

Following on from their previous work in which recommendations included the requirement of stress linearisation to calculate membrane and bending stresses,

redefining the linear stress description in ASME Codes, what component stresses to linearise and confirmation that stress-along-a-line can be used in 2D axisymmetric and 3D models, Hechmer and Hollinger developed WRC 429: 3D Stress Criteria Guidelines for Application [21]. This was a comprehensive investigation into the use of 3D FEA in DBA of pressure vessels in correspondence with the stress limits outlined in ASME BPVC Section III and Section VIII Division 2. The report focused on four key research areas:

1. The relationship between failure mechanisms and ASME stress categories
2. Appropriate stresses for each category
3. Appropriate locations for assessing each category
4. Appropriate stresses for obtaining membrane plus bending stresses

The authors' aims were to influence Appendix A in ASME III to incorporate the use of FEA and help create a dedicated FEA appendix in both ASME III and VIII Div 2. It was intended to change the wording in Appendix A-1000 from “not intended to exclude” FEA to “the methods include FEA”. This was to correspond with the increasing popularity and practicality of FEA in stress analysis of pressure vessels [22]. As of the 2017 version of ASME III, this has still not been revised. However, ASME VIII Div 2 has been influenced by many of the ideas and recommendations published in WRC 429.

Hollinger and Hechmer [22] believed that “better guidance provided in the Code would improve the use of modern analytical tools” and produced ten guidelines to help achieve this. Advice is also provided on suitable locations for evaluating the stress limits. Membrane plus bending stresses are not required to be calculated across the whole structure and should only be computed in basic structural elements, those which are pressure containing shapes such as a cylindrical shell or spherical head. Elastic limits should not be calculated in areas which connect these sections, known as transition elements, as it would be over conservative. The elastic limits stated in the Code are derived from interaction analysis which requires internal forces and bending moments to be known and these are not fully representative in transition areas. These regions are important for fatigue analysis. When membrane and bending stresses are

required in transition elements, either a stress concentration factor must be applied for the evaluation of membrane and bending stresses at the juncture between structural and transition elements or, if the $P + Q$ limit is not satisfied, a penalty factor, K_e, is applied to the region.

Examples for 10 different geometries are presented in WRC 429 and the key research areas are discussed for each. This provides a useful benchmark on which to base any elastic FEA around when carrying out DBA.

2.1.2 Stress Linearisation Procedure

Membrane and bending stresses are located on stress classification planes (SCP) that cut through the section thickness and straight lines dissecting a section of planar geometry, known as stress classification lines (SCL). Stress linearisation involves placing SCLs through the thickness of the FE model at prescribed locations. An example is shown in Figure 7 for a 2D axisymmetric nozzle model.

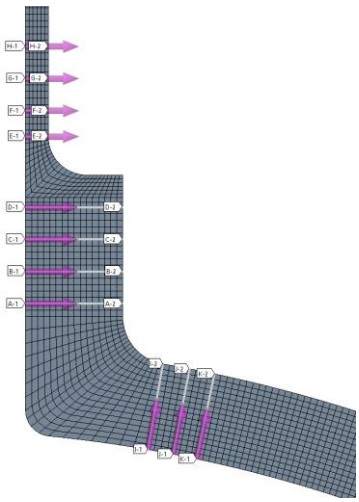

Figure 7: SCLs on 2D axisymmetric nozzle FEA model

As SCLs only provide membrane and bending results at localised regions, deciding where to locate the SCLs is important. If a SCL is not selected properly, the design could be incorrectly mistaken as being safe. There are guidelines in ASME VIII Div 2 to help determine the suitability of a SCL but ASME III provides no assistance.

The SCL is constructed from an infinitesimally small width and by extending one of these faces onto an axisymmetric plane, a SCP can be defined. The SCL should be normal to the contour of highest stress but for simplicity, orientating it normal to the mid-plane shell thickness produces adequate results [23]. The total stresses calculated in elastic FEA are then mapped onto points along the line to be used in the linearisation process for extracting membrane and bending stresses.

ASME III does not contain guidelines on how to obtain membrane and bending stresses but three methods are outlined in ASME VIII Div 2 for linearisation of FE results: stress integration method, structural stress method based on nodal forces and the structural stress method based on stress integration.

The linearised stresses are calculated explicitly using the internal forces and moments and integrated along the SCL. It is important that the membrane and bending stresses are calculated at component level before finding the principal membrane and bending stresses, as this eradicates any effect of rotating principal stresses. The membrane stress tensor is the average of each stress component and assuming a SCL of length t, it can be calculated from equation (14).

$$\sigma_{ij,m} = \frac{1}{t}\int_0^t \sigma_{ij}\, dx \tag{14}$$

The bending stress tensor, calculated using equation (15), is the linear varying portion.

$$\sigma_{ij,b} = \frac{6}{t^2}\int_0^t \sigma_{ij}\left(\frac{t}{2} - x\right) dx \tag{15}$$

Where σ_{ij} is the total stress tensor and x is the position on the SCL.

The ASME VIII Div 2 procedure does not use all of the stress components to calculate the linearised bending stress [23], stating that the through-thickness and in-plane shear stresses do not have linearised bending components. The reasoning for this is because

the radial stress in thin walled structures is negligible compared to the hoop and meridional stresses and there is no physical meaning to a shear bending stress. It is noted however, that shear stress distributions which cause torsion of the SCL, such as out of plane shear stress in the normal-hoop plane, do need consideration but are technically not bending stresses. The assumption that radial stress is irrelevant does not necessarily apply to thick walled structures and so there are concerns over the accuracy of this method for thick vessels.

The membrane and bending stress components can be used to calculate the equivalent and principal stresses. The stress intensities can then be checked against the limits to determine if the vessel design is safe. ASME III could benefit from including guidance on how to post-process continuum FEA stress results to calculate membrane and bending stresses to satisfy Code requirements.

Limits on primary membrane and primary membrane plus bending stresses are used in ASME III to protect against failure due to GPD. Upon calculation and classification of the membrane and bending stresses, the maximum allowable pressure can be obtained through proportionality of the primary membrane stress intensity limits in Table 1. The internal stress intensities are in proportion to the applied pressure load P_i, so the maximum allowable load P_a can be expressed as equation (16).

$$P_a = \frac{allowable\ stress}{actual\ stress} \times P_i \tag{16}$$

ASME III allows the use of DBA to prevent a vessel failing due to incremental plastic collapse. Adibi-Asl and Reinhardt [24] conducted a review of the elastic rules for shakedown and ratcheting in both ASME III and ASME VIII Div 2. ASME III permits the use of elastic, simplified elastic plastic and elastic plastic analysis to check for ratcheting. The elastic stress limit is defined in subsection XIII-3420 in terms of the primary-plus-secondary Tresca stress intensity range, $\Delta(P + Q)$, as equation (17).

$$\Delta(P+Q) \leq 3S_m \qquad (17)$$

It is highlighted by Adibi-Asl and Reinhardt [24] that it is not explicitly stated in ASME III that this limit is imposed to ensure elastic shakedown, however, it is confirmed in the ASME III companion guide [25] that one of the intentions of the $3S_m$ limit is to ensure elastic shakedown and XIII-2500 states that:

> "The limit on primary plus secondary stress intensity of $3S_m$ has been placed at a level that ensures shakedown to elastic action after a few repetitions of the stress cycle except in regions containing significant local structural discontinuities or local thermal stresses."

The $P+Q$ stress range can be thought of as the membrane-plus-bending stress range for all applied loads but does not include peak stresses. Theoretically, the $3S_m$ limit is a simplified way of expressing the twice yield stress $2\sigma_Y$ as the limit. This imposed limit guarantees an elastic response to a cyclic load. Elastic shakedown does not mean that no plastic deformation has occurred. Some permanent deformation is permitted so long as after a short number of cycles it can be shown that, due to stress redistribution, the structure will deform elastically for the duration of any further cycles.

The ASME III definition for shakedown is:

> "Shakedown of a structure occurs if, after a few cycles of load application, ratcheting ceases. The subsequent structural response is elastic, or elastic-plastic, and progressive incremental inelastic deformation is absent."

It is unclear as to what is meant by a "few cycles". Also, as the $3S_m$ limit is required for use with elastic analysis, stress redistribution is not considered. This tends to mean that the $P+Q$ stress limit is conservative as stress redistribution can move the ratchet boundary, reducing the size of the ratchet region on the Bree diagram.

ASME III Article XIII-3420 states that the stress limit is to be applied to stress at a point which includes primary membrane, primary bending and secondary stresses created from specified mechanical loads and thermal effects related to the Loadings. As the limit is based on the range of $P+Q$, the range is taken as the absolute value of

maximum difference in stress intensity over the life of the component due to Level A and B Service conditions. All relevant transient and service loadings must be included in the check as the limit does not just apply to the stress range from a single transient. If the secondary stress results from thermal or displacement constraints only, then S_m is taken as the average temperature dependent S_m value between the highest and lowest temperatures over the cycle. If, however, part or all secondary stresses arise due to mechanical loads, S_m is defined at the highest metal temperature.

The Thermal Stress Ratchet criteria are outlined in ASME III Article XIII-3430 and are required when the structure has a through wall thermal gradient [7]. Limits on the maximum cyclic thermal stress are based on the thermal stress range as a function of steady-state general primary membrane stress, calculated from elastic analysis. Taking $x = P_m\ from\ presure\ loading/\sigma_Y$ and $y' = max\ thermal\ stress\ range/\sigma_Y,$ the limits are defined in equations (18) and (19) for both a linear and parabolic variation of temperature through thickness, with the parabolic distribution being used when one surface is insulated. The thermal stress range should be linearised through the thickness to obtain the $M + B$ stress at the surface. It should be noted that if the temperature distribution is parabolic, the maximum thermal stress on the wall surface should be used, not the linearised stress. Also, if $1.5S_m > \sigma_Y$ then $1.5S_m$ should be used in place of σ_Y in the definitions of x and y'.

Linear variation:

$$y' = \begin{cases} \dfrac{1}{x}, & 0 < x < 0.5 \\ 4(1-x), & 0.5 < x < 1 \end{cases} \qquad (18)$$

Parabolic variation:

$$y' = \begin{cases} 4.65, & x = 0.3 \\ 3.55, & x = 0.4 \\ 2.7, & x = 0.5 \\ 5.2(1-x), & 0.615 < x < 1 \end{cases} \qquad (19)$$

It is highlighted by Adibi-Asl and Reinhardt [24] that unlike ASME VIII Div 2 and RCC-MRx, which require a separate assessment of thermal membrane stress, ASME III only considers the range of thermal membrane stress in combination with the primary membrane plus bending stress range. The thermal stress ratchet procedure is based on the classical Bree diagram [25] which leads to questions over the accuracy of the solution at discontinuities, as it may be over-conservative.

The Simplified Elastic-Plastic analysis in XIII-3450 must be carried out if the $3S_m$ limit on $\Delta(P+Q)$ is exceeded. In this event, shakedown will depend on the cyclic hardening of the material [25]. The structure will not experience elastic shakedown but may be subject to alternating plasticity over the cycle. This increases the chance of ratcheting and may have an impact on fatigue. Ratcheting is directly related to the number of cycles and so it may be shown that even with ratcheting, the number of cycles is so low that it may not be an issue. Low cycle fatigue is more likely to cause failure of the vessel in such a case. To account for the effect of cyclic plasticity, a fatigue penalty factor, known as a K_e factor, is applied in the fatigue procedure. Therefore, plastic shakedown is permitted within the context of ASME III so long as a thermal ratcheting and low cycle fatigue check are carried out.

To protect against ratcheting, it is stated in XIII-3450 that the primary plus secondary stress range, excluding thermal bending stress, must not exceed $3S_m$ and that the Thermal Stress Ratchet criteria in XIII-3430 must be met. The only difference between the elastic and simplified elastic-plastic Code requirements are that, unlike in equation (17), thermal bending stresses are not considered. The simplified elastic-plastic shakedown criterion is given in equation (20).

$$S_n^* \leq 3S_m \tag{20}$$

Where $S_n^* = \Delta(P+Q) - thermal\ bending\ stress$.

2.1.3 Fatigue Analysis

The ASME III fatigue procedure requires the alternating stress, S_a, for each cyclic condition to be calculated from the stress differences over the cycle as per XIII-2400.

The appropriate S-N design fatigue curve in Mandatory Appendix 1 is then consulted to obtain the maximum number of cycles to failure, N_f, for the calculated value of alternating stress. Cycle counting techniques may be required to identify individual cycles and their corresponding stress levels for complex cyclic loading. Nuclear pressure vessels will experience various cyclic conditions which may result in significant stress ranges and, as such, the cumulative fatigue damage must be calculated.

Miner's Cumulative Damage Rule is a simple way of performing a cumulative fatigue assessment by assuming each load cycle will generate a proportional level of damage, which will accumulate until failure. The ratio of required cycles to cycles to failure defines the usage factor for that load cycle and the cumulative usage factor, U, can be calculated using equation (21). In order to satisfy ASME III, the cumulative usage factor must not exceed 1.

$$U = \sum \frac{n_i}{N_f} < 1 \qquad (21)$$

Where for a certain alternating stress intensity level, n_i is the number of actual cycles and N_f is the number of cycles to failure.

If the stress intensity range exceeds $3S_m$, alternating plasticity is said to occur. In such a case, the simplified elastic-plastic analysis in XIII-3450 can be used to calculate a plasticity correction factor K_e to be applied to the alternating stress S_a prior to the fatigue calculation. The values of K_e are detailed in equation (22).

$$K_e = \begin{cases} 1, & S_n \leq 3S_m \\ 1 + \dfrac{1-n}{n(m-1)}\left(\dfrac{S_n}{3S_m} - 1\right), & 3S_m < S_n < 3mS_m \\ \dfrac{1}{n}, & S_n \geq 3mS_m \end{cases} \qquad (22)$$

Values for the material parameters m and n in equation (22) are given in Table XIII-3450-1 in ASME III for permitted materials.

Stress-life methods are effective at predicting high cycle fatigue failures, where the stress and strain field are primarily elastic. For low cycle fatigue however, where the failure mechanism is dictated by plastic strain, strain-life (ε-N) methods should be used.

Equation (23) was formulated by Basquin [26] and defines the relationship between alternating stress and the number of cycles to failure. This is a commonly accepted method for determining the high cycle fatigue life of metallic components.

$$\sigma_a = \sigma_f'\left(2N_f\right)^b \tag{23}$$

Where $2N_f$ is the number of reversals to failure for an applied alternating stress σ_a, the fatigue strength coefficient is σ_f' and b is the fatigue strength exponent.

To predict the low cycle fatigue life for metallic parts based on plastic strain, as opposed to alternating stress as in equation (23), Manson [27] originally proposed the plastic strain based relationship given in equation (24) with Coffin [28] proposing a generalised version of the same formula, as discussed in Tavernelli [29].

$$\varepsilon_a^p = \varepsilon_f'\left(2N_f\right)^c \tag{24}$$

Where $2N_f$ is the number of reversals to failure for an applied plastic strain amplitude ε_a^p, with ε_f' defined as the fatigue ductility coefficient and c as the fatigue ductility exponent.

Applying Hooke's law to equation (23) to express it in terms of the elastic strain amplitude ε_a^e and combining it with equation (24), the Coffin-Manson [30] formula can therefore be expressed in equation (25).

$$\varepsilon_a = \varepsilon_a^e + \varepsilon_a^p = \frac{\sigma_f'}{E}\left(2N_f\right)^b + \varepsilon_f'\left(2N_f\right)^c \tag{25}$$

Where ε_a is the total alternating strain and E is the Young's Modulus.

A number of other formulations exist to predict fatigue life based on stress and strain amplitude. Clarkson [31] provides a comprehensive review of such methods and proposes original plasticity correction factor methodologies which are ASME III code complaint.

2.2 Alternative Elastic DBA Methods

In order to overcome some of the problems associated with the stress linearisation and classification techniques, research into different approaches has been vast. This was a popular research topic in the mid-2000s and is still an area of interest. Especially as stress classification remains to be a challenge for analysts, with no clear consensus on the best solution.

Kalnins [32] investigated the meaningfulness of linearised stress through singularities, such as stress concentrations at sharp corners and structural discontinuities. It was shown that membrane plus bending stresses do not diverge at singularities on a welded joint. A "Stress Intensity Edit" was conducted to find the effect on the primary plus secondary stress calculation by placing a SCL through a singularity in a cylindrical vessel. This acknowledged that there was an 'invalid' SCL zone around the joint. The through-thickness radial stress was affected by the singularity and when included in the linearised stress calculation, non-conservative results were observed.

It was then shown by Strzelczyk and Stojakovic [33] that the stress linearisation results for axisymmetric and 3D Abaqus FEA models of the same cylindrical vessel did not match. For the 3D model, all stress components were linearised but for an axisymmetric model, Abaqus automatically assumed that that the through-thickness membrane plus bending stresses were equal to the total stress at the start and end points of the SCL. This was not representative of the actual stress field and as a result, over predicted the membrane plus bending stress, even though the total stress field matched for both models. ASME VIII Div 2 requires linearisation of the radial membrane stress and exclusion of the radial bending stress in the membrane plus bending stress check. The effect of the singularity will be almost eradicated in the stress integration procedure as the stress along the line is averaged. Therefore, the invalid zone discussed by Kalnins could be reduced significantly and almost eradicated with increased mesh density, indicating that SCLs could be placed at stress concentrations.

Strzelczyk and Stojakovic [33] made reference to a modified solid-element approach to stress linearisation proposed by Strzelczyk and Ho [34]. It was found that by modelling the vessel with a single quadratic element through thickness (1ETT), membrane and bending stresses could be taken directly from the analysis solution, so there was no need to carry out the stress linearisation post-processing procedure. The reason for this is that stress components vary linearly in FEA quadratic displacement elements; this is equivalent to finding the linear distribution through the thickness of the vessel. As it was only one element thick, this represented a linearised stress.

There was a difference in the maximum stress location for 1ETT and 4ETT. When a SCL was placed on the 4ETT model in the location predicted by the 1ETT model, it showed that the maximum linearised stress did not actually occur at the stress concentration in the 4ETT FEA. This highlighted that the maximum linearised stress does not necessarily occur at the location of the maximum total stress.

Lu et al [35] introduced a two-step primary structure method for stress classification. The first step was to identify whether the stress is primary or self-limiting. In the second step, the stress distribution is considered in order to classify primary stresses into general primary membrane, local primary membrane or primary bending stress. As stated in the Codes, all local membrane stresses are classified as local primary membrane to remain conservative; however, defining such stresses in certain cases can be difficult as local membrane stress can exhibit similar characteristics to secondary stress. The two-step method requires constraints to be identified as one of the following:

- Essential Constraint: constraints required to equilibrate external imposed loading, which if removed prevent the structure from being capable of carrying the load. The reactions cause primary stress.
- Redundant Constraint: all non-essential constraints. They are not required to take the external load and so stresses are secondary, however, some of these stresses help when carrying the load and so redundant constraints can be separated into favourable and unfavourable.
- Favourable Redundant Constraint: when removed, the maximum linearised membrane and bending stress of the reduced structure is larger than the

original. These constraints should be maintained and the stress classified as primary.

- Unfavourable Redundant Constraint: when removed, the maximum linearised membrane and bending stress of the reduced structure is less than the original. These should be removed and the stress classified as secondary.

A primary structure is defined as a reduced structure constructed by the removal of "unfavourable redundant constraints" [35]. These are constraints which have no bearing on the structures ability to withstand the applied external load and when removed, the maximum linearised stress is less. Any stress caused by unfavourable redundant constraints can be considered as secondary stress with all other equivalent linearised stresses classified as primary. Therefore, if there are no unfavourable redundant constraints on the original vessel, the primary structure is the original structure and all equivalent linearised stresses are classified as primary. By constructing a primary structure, it can be determined if the maximum membrane plus bending stress in the whole structure is in fact primary or if there are also secondary stresses to consider, which can then be found through FEA and stress linearisation of the primary structure.

There has been further research into the use of the two step stress classification and primary structure method [36,37] to evaluate the effectiveness of this method when analysing a cylindrical vessel with a nozzle. Reduced finite element shell models for both the cylinder and nozzle were created with three different boundary conditions for the cylinder and five for the nozzle. The membrane and bending stresses at the vessel-nozzle intersection were compared for each reduced model and the results were used to determine basic characteristic of each stress.

One of the main issues with the primary structure method is the difficulty in applying this procedure to continuum FEA with solid elements. Unlike shell elements, standard 3D solid elements do not possess rotational degrees of freedom. Instead, rotation is simulated through translation of the nodes only, meaning removing specific DOFs becomes difficult. Work has been carried out to investigate the use of the primary structure method in conjunction with FEA [38] and more recently applying the technique to a 3D nozzle structure [39].

Gao et al. [40,41] recognised the importance of decomposing the stress field obtained by FEA to carry out a pressure vessel DBA but believed the primary structure method demonstrated some problems with the need to remove unfavourable constraints. As such, Gao developed a process established on the principle of superposition which allows the primary bending stress to be found. The idea behind this method is that different load combinations can be used as a parameter in FEA to calculate the primary bending stress in a structural element. Then, a standard FEA can be carried out with all loads applied to find the membrane stress and this can be superposed with the calculated bending stress. The procedure is outlined in the following steps:

1. Apply SCLs on FEA model
2. Find loads which cause P_b, calculate stress field for these loads, linearise the stresses on the set SCLs and determine bending stresses required for stress superposition
3. Calculate overall stress field with all loads applied and find membrane stresses from linearisation results
4. Superpose bending stress from 2 and membrane stress from 3 and determine $P_l + P_b$. Add membrane stress from 3 and bending stress from 3 to get $P + Q$

The four structures Gao analysed were a flat-head cylinder, nozzle in a conical shell, sphere-nozzle intersection and a flange-cylinder connection. The aim was to define a set of load and boundary conditions for each which would allow the primary bending stress to be identified. This was achieved by discovering if the load caused bending stress without self-limitation and if displacement agreement was satisfied.

Mackenzie [42] proposed relating the stress linearisation procedure to that of a lower bound limit load analysis. In order to relate the linearisation procedure to that of a limit analysis, the correct boundary conditions would have to be established. For a limit analysis of a cylindrical vessel, the forces acting on the inside surface must be equal in magnitude to the internal pressure and zero at the outside surface. The lower bound limit load theorem requires that the stress field is in equilibrium with the section forces and tractions. As such, to satisfy these boundary conditions, the through-thickness normal stress must be considered in the analysis. This is contradictory to what is

defined in the ASME VIII Div 2 guidelines, which as stated previously, do not consider a linear bending stress in the radial direction. For this case, it is needed for equilibrium with the applied load and will bound the normal through thickness stress so that it is contained within the yield criteria. The stress distribution along a specified SCL can then be calculated in the same manner as for the standard stress linearisation method.

As with the standard linearisation procedure, this method does not differentiate between primary and secondary stresses, assuming all stress components are primary. The lower bound limit load P_L is calculated from proportionality, by finding the ratio of the yield stress to the maximum equivalent stress along the SCL and multiplying it by the external load as in equation (26).

$$P_L = P_i \frac{\sigma_Y}{\sigma_{e,max}} \tag{26}$$

Where, P_i is applied load, σ_Y is yield stress and $\sigma_{e,max}$ is maximum equivalent stress.

Although in this instance, the SCL stress distribution is defined in terms of a lower bound limit load analysis, the internal stresses are still calculated using the linear elastic distribution. Mackenzie suggests an alternative to the standard stress categorisation method by defining a limit state stress distribution along the SCL, rather than a linear stress distribution, to more accurately represent the actual stress distribution experienced during plastic deformation. Figure 8 illustrates the two-parameter candidate functions for the plastic limit stress distribution for bending.

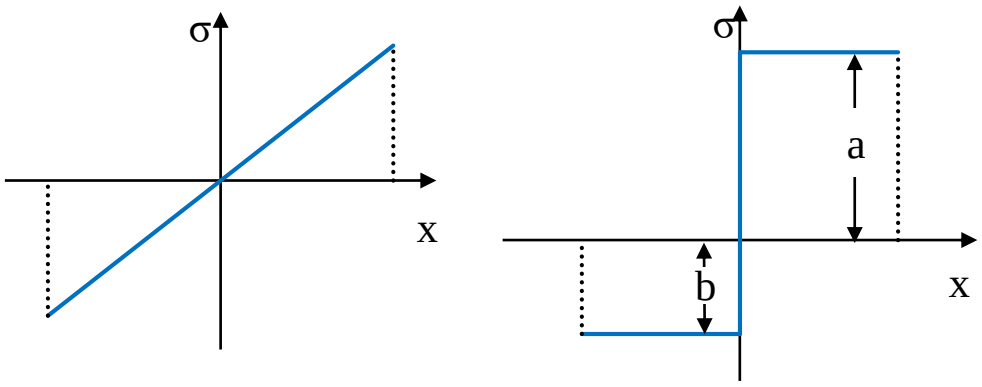

Figure 8: Linear and limit state stress distributions through thickness

Li et al. [43,44] looked into a similar idea and proposed the DBA-L method, which considered stress classification of primary stress as a lower bound limit load analysis. In the same way that membrane and bending stresses are calculated on a SCL, they renamed the path through-thickness as the Limit Analysis Line (LAL). The through-thickness limit state stress was based on a beam under bending, similar to how the elastic stress limits were derived, and the distribution defined in terms of two new parameters for the position and assumed stress amplitude respectively. The authors recommended calculating the stress distributions for all stress components.

The DBA-L method was demonstrated on various components [44] and more recently on a vessel with a hemispherical head [45]. Results were compared to the ASME stress linearisation and classification procedure and to an elastic-plastic analysis, which considered non-linear geometry effects. For a nozzle on a spherical head, it was found that the DBA-L result was lower than that calculated using ASME stress linearisation. It did, however, agree more closely with the elastic-plastic analysis. One issue, as highlighted by Mackenzie [42], is that a distribution derived from a beam under bending would not offer an accurate model for the behaviour of thick cylinders and spheres experiencing internal pressure. In this case, from continuum mechanics, a logarithmic variation function would be more applicable when calculating the limit load.

As previously mentioned, the Thermal Stress Ratchet criteria outlined in XIII-3430 is based on the Bree cylinder problem and as such, contains an element of conservatism and lack of accuracy when applied to real problems. McKillop et al [46] aimed to highlight how the Code deals with high thermal membrane stresses as the $3S_m$ limit can be non-conservative at high temperatures.

A thermal stress ratchet analysis was conducted on a nozzle attached to a vessel head subject to an extreme thermal and pressure cycle and McKillop proposed incorporating a new factor for thermal membrane stress range to add conservatism to the elastic thermal stress ratchet criteria. A modified simplified elastic-plastic procedure was also proposed, recommending that the $\Delta(P+Q)$ check should be based on primary plus non-thermal secondary stress only.

2.3 Elastic Modulus Modification and Stress Redistribution Methods

A number of methods have been developed to remove the subjective nature of stress classification that involve pseudo-plastic analysis techniques in which the elastic modulus of the structure's material is altered iteratively to simulate stress redistribution.

Dhalla [47] classified primary and secondary stresses using the reduced elastic modulus method. This involved performing a series of elastic analyses with the material elastic modulus and an assumed secant modulus to identify a trend of stress relaxation with respect to the reduction in secant modulus. A generalised stress-strain plot can be used to determine if the response was predominantly load or deformation controlled. This is based on the theory that if the stress in a structure was primary, the elastic stress generated from constrained loading would be the same in a subsequent analysis with a reduced modulus but the strain would be greater. Conversely, the opposite is true for secondary stress. Altering the elastic modulus would have no effect on the strain but would result in a different stress.

By reducing the elastic modulus systematically to allow stress redistribution, the inelastic response is simulated through iterative elastic FEA. This allows the elastic stress results to be separated into primary and secondary components.

Seshadri and Fernando [48] developed the Generalised Local Stress Strain (GLOSS) and Redistributed Node (R-Node) method. It's application within stress classification was investigated by Seshadri [49] and Fanous and Seshadri [50]. It is an elastic analysis technique in which the elastic modulus is modified at every Guassian integration point using the elastic modulus adjustment procedure (EMAP), shown in equation (27).

$$E_{i+1} = \left(\frac{\sigma_a}{\sigma_{e,i}}\right)^q E_i \qquad (27)$$

Where σ_a is an arbitrary stress, $\sigma_{e,i}$ is the equivalent stress at iteration i, q is an instability factor and E_i is the Young's modulus at iteration i.

This allows the stress redistribution to be analysed and r-nodes to be identified. R-Nodes are points at which stress remains constant after comparing the stress

distribution of an initial elastic analysis to the redistributed stress. These are of interest because at the location of a plastic hinge, the r-node stress value will be very high and failure can be predicted when the r-node stress reaches yield. This only applies to structures which experience a single plastic hinge. For a structure that fails due to numerous plastic hinges forming, plastic collapse is said to occur when the average of the r-node peak stresses reaches yield. As the number of iterations increases, the r-node peak stresses will all tend to the same value, indicating the stress at plastic collapse.

The r-node stress is load controlled, and therefore for pure membrane stress, there will be no stress redistribution, making the r-node stress comparable to membrane stress. In the case of pure bending, the shape factor of 2/3 dictates that the r-node stress will be less than the maximum elastic value for bending stress. The equivalent primary membrane plus bending stress can be defined by combining the membrane and bending components. As the r-nodes are in equilibrium with the applied load, the stress identified by them is always going to be classed as a primary stress. In order to satisfy both the primary membrane and primary membrane plus bending stress limits, the maximum r-node equivalent stress is limited to the design stress.

Mackenzie and Boyle [51] proposed the elastic compensation method to calculate primary stresses. Iterative elastic FEA, where the elastic modulus is modified using equation (28), simulates stress redistribution by stiffening low stress regions and softening high stress regions. The resulting stress fields are used to obtain a lower-bound limit load. The stress field obtained from elastic compensation is an equilibrium stress field and as such, can be classified as primary stress.

$$E_i = E_{i-1}\frac{\sigma_n}{\sigma_{i-1}} \qquad (28)$$

Where σ_n is the nominal stress, σ_{i-1} is the equivalent stress at iteration $i-1$ and E_{i-1} is the Young's modulus at iteration $i-1$.

The elastic compensation method has been developed to calculate lower and upper bound limit loads of structures as well as lower and upper bound shakedown loads by employing Melan and Koiter's classical shakedown theorems [52].

2.4 Limit Analysis

A common theme running through the literature on elastic DBA methods is that in general, elastic stress linearisation and classification techniques are being superseded by inelastic methods. Limit load analysis (LLA) is a non-linear method used to predict the pressure at which a vessel will experience GPD. The classical lower bound theorem was discussed in section 1.7 but this section discusses how that theory can be applied to practical design applications.

LLA is a useful technique as it can be carried out using FEA, identifies the maximum pressure a vessel can withhold and removes the need for stress classification. Limit analysis is permitted within ASME III as long as a lower bound theorem is employed and, for standard structures, the tentative pressure thickness requirement in NB-3324 is satisfied. The ASME III definition for limit analysis is:

> "a special case of plastic analysis in which the material is assumed to be ideally plastic (nonstrain-hardening). In limit analysis, the equilibrium and flow characteristics at the limit state are used to calculate the collapse load"

ASME III states that primary stress intensity limits need not be met if LLA proves that the maximum pressure does not exceed 2/3 of the lower bound collapse load. This means that stress classification can be avoided in the plastic collapse check when LLA is used. When used in conjunction with FEA, it is slightly more complex than elastic analysis and simulations take longer to run. However, for 2D axisymmetric models the difference in computing time is insignificant when compared to the advantages. No post processing is required, the global response is observed so the failure location can be easily identified and, by considering material non-linearity, the behaviour of the actual structure is more closely represented.

The defining aspect of limit load analysis is the application of an elastic-perfectly plastic material model. To define the material properties all that is required is the material yield strength and elastic modulus as the tangent modulus is set to zero, as

shown in Figure 9. ASME III defines a value of $1.5S_m$ is to be used as the flow stress in the analysis and the limit load is multiplied by 2/3 to give the maximum operational load.

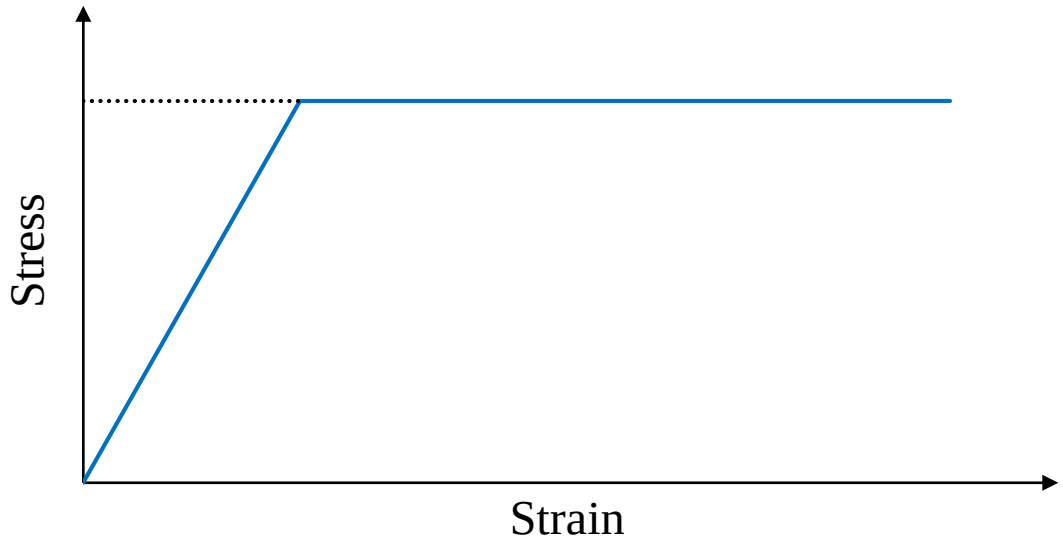

Figure 9: Elastic-perfectly plastic material model

If a load is applied to a component, as the load is increased beyond the elastic limit, the structure will experience plastic deformation. The load is increased until the plastic region has spread through the thickness of the structure and equilibrium can no longer be achieved. Figure 10 represents the spread of the plastic region through the thickness of a spherical vessel with increasing internal pressure. Due to the EPP material model, the stress in the material cannot exceed yield. At this point, it loses any load carrying capabilities and will deform without bound. Stress redistribution allows the structure to continue carrying the load until the plastic region spreads throughout the shell thickness and equilibrium can no longer be achieved. In FEA, this loss of equilibrium will result in a loss of convergence and as such, the limit load is taken as the last converged solution. This satisfies the classical lower bound limit analysis theorem, as the load is ramped up from zero to find the maximum load at which equilibrium is still maintained.

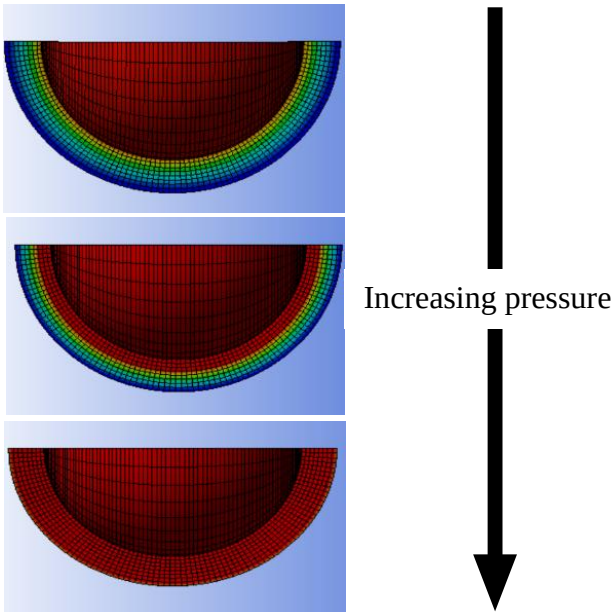

Figure 10: Spread of plastic region

As part of the wider Hierarchical Finite Element Framework (HFEF) produced by Martin et al. [53], an ASME III Code case aimed at providing comprehensive guidance on the use of LLA in the design of nuclear pressure vessels was developed. A Code case would be beneficial because although ASME III specifies the use of limit load analysis, there is no guidance on the best practices for use of LLA with FEA.

In a review of the Code case [54], some limitations were highlighted. It was recommended that LLA is not suitable where large geometric weakening is observed. LLA is typically performed using small displacement linear geometry, which is a good assumption for thick walled structures. In slender structures, however, a non-linear response is possible where there is an area of reduced load capacity or geometric weakening. By not considering large deformations and changing load direction, LLA could over predict the limit load resulting in non-conservative results.

Small displacement could be compared to large deformation analysis to investigate any geometrical effects. Geometric weakening is caused from changes in load-bearing cross-section, second moment of area and direction of load paths and can be determined to have occurred if the linear geometry solution exceeds that of the non-linear geometry analysis. Therefore, if the non-linear geometry solution is greater than

the linear geometry solution, geometric hardening is present and the LLA is conservative. In this case, the LLA solution should be used. If the design loads are not satisfied by the LLA, a full plastic analysis involving a strain hardening material model is required. For an elastic-perfectly plastic material the strains do not demonstrate the true deflection of the structure. In reality, strain hardening will occur and a full plastic analysis would give a more representative solution.

Towse and Martin [55] expanded on this work by applying the LLA methodology to more complex structures. It was demonstrated that the use of elastic material regions to inhibit the first failure mode of a pipe-nozzle component can allow the next failure mode to be identified and the margin between each to be calculated. By doing this repeatedly, successive failure mode locations can be found. When dealing with multiple load cases, it was highlighted that relative proportions of each load should be altered. This was to prevent the loads from counteracting and resulting in a higher limit load than if they were applied separately. Alexander and Biel [56] investigated the effect of multiple loads in LLA, commenting on the effectiveness of LLA in the analysis of complex structures as models which represent the actual component can be constructed, preventing oversimplification and overly conservative solutions.

An area of contention surrounding the use of LLA with FEA is that commercial FE packages, including ANSYS and Abaqus, use the von Mises failure criterion in plastic analysis. Therefore it is not clear whether the FEA results can be accurately related to Code limits, as the elastic limits are still defined in terms of Tresca stress intensity [25]. This has also been raised as a potential issue in a WNA report on non-linear analysis [57]. Hechmer and Hollinger [20] suggested that the design Codes for plastic analysis should adopt the von Mises criteria to define the onset of plasticity to coincide with FEA software.

Jones and Gordon [3] highlight the effectiveness of FEA limit analysis in predicting the limit load of a perforated test plate tubesheet, concluding that the results satisfy ASME III. The failure mode and location were correctly identified, whilst maintaining a factor of safety of 3 with respect to the actual failure load obtained from the experimental data.

2.5 Plastic Analysis for Gross Plastic Deformation

Unlike LLA, where an elastic-perfectly plastic material model is used, plastic analysis can be used to find the collapse load whilst considering material strain hardening and geometric non-linearities. ASME III defines plastic analysis as:

> "that method which computes the structural behaviour under given loads considering the plasticity characteristics of the materials including strain hardening and the stress redistribution occurring in the structure."

Elastic plastic (EP) FEA requires specifying a strain hardening material model so the load-deformation structural response can be measured. Plastic collapse loads are then typically obtained through the use of load and deformation parameters to define a characteristic curve.

There are several methods for calculating the plastic load using load and deformation parameters. Townley et al [58] suggested the simple 1% plastic strain method. The twice elastic slope (TES) and tangent intersection (TI) methods provided inspiration for more modern procedures such as the plastic work (PW) criterion [59], plastic work curvature (PWC) [60], ratio of plastic work curvature (RPWC) method [61,62] and rate of change of relative plastic work [63,64].

ASME III specifies the use of the TES method for the calculation of the collapse load in Mandatory Appendix II-1430. Elastic-plastic FEA can be used to plot a characteristic curve with load as the ordinate and either deflection or strain as the abscissa. The angle θ is measured between the linear part of the curve and the vertical axis. A straight line, known as the "collapse limit line", can then be drawn which intersects the origin and is at an angle of $\varphi = \tan^{-1}(2\tan\theta)$ with the vertical axis. This corresponds to a slope of half the stiffness of the elastic region. The plastic collapse load is determined from the point of intersection between the load-deformation curve and the collapse limit line. A design factor of 2/3 is then applied to the plastic collapse load. Figure 11 illustrates the TES method graphically.

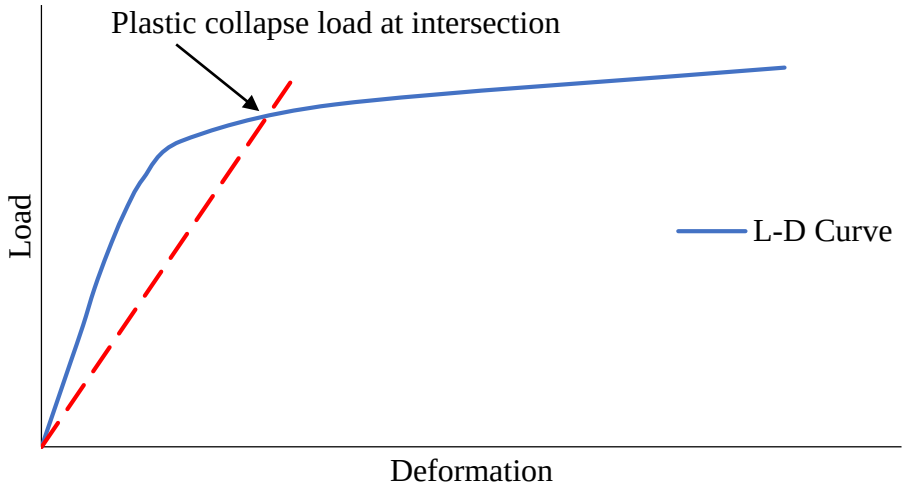

Figure 11: TES method

The analyst must decide between maximum principal total strain and deflection as the deformation parameter to be used, however, it is noted that the selected deformation parameter should be indicative of the load-carrying capacity of the structure. Choice of load and deformation parameters is one of the main issues with the TES [59] and can lead to inaccurate plastic collapse loads. The results can be sensitive to the deformation parameter and for multiple load cases, the choice of a suitable load parameter is not always obvious [63]. As it relies on the local load-deformation (L-D) curve, identifying the plastic collapse load can be challenging and does not always give a unique solution. It was shown by Moffat et al. [65] that the response in elastic regions can impact the TES plastic collapse load, despite being remote from the failure location. Cases were also observed where the L-D curve and collapse limit line failed to intersect, making it impossible to quantify the plastic collapse load.

Another common graphical technique is the TI method. Similar to the TES, it relies upon the use of a characteristic L-D curve but the plastic load is calculated differently. Tangents are drawn from the elastic and from the plastic part of the L-D curve. The point at which they intersect is taken as the plastic collapse load, as demonstrated in Figure 12.

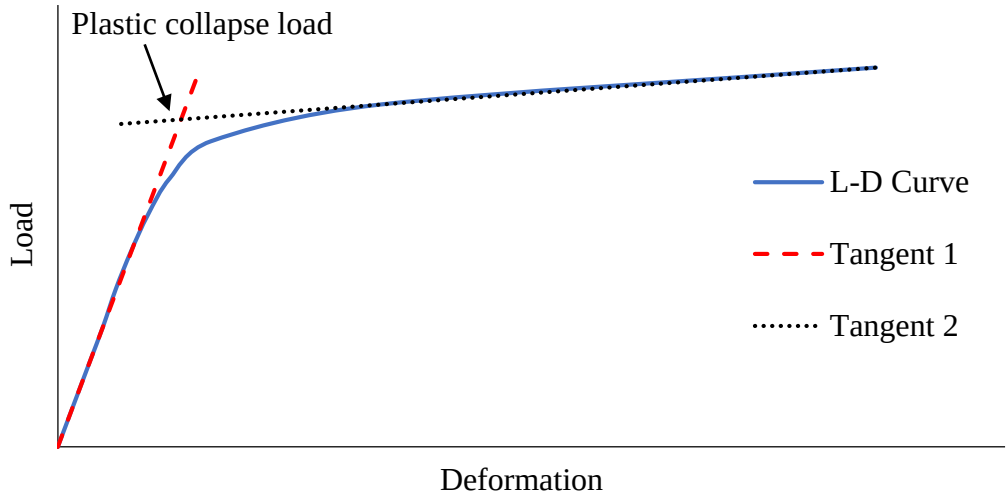

Figure 12: TI method

It suffers from many of the same problems as TES but the most common issue is determining from where the tangent to the plastic part of the L-D curve should be taken [59]. Assuming a steady-state is achieved, this is not difficult and the TI method should produce a unique solution. However, if there is no plateau, EN 13445 states that the tangent should go through 5% maximum strain [59,65] but results have been inconsistent when applying this.

In an effort to eliminate some of the problems associated with the TES and TI methods, Muscat et al [59] developed the PW criterion. This is based on forming the characteristic curve using plastic work as the deformation parameter, shown in Figure 13. Plastic collapse is said to occur when PW becomes "excessive" and the plastic collapse load is calculated by finding the intersection point between a tangent to the curve and the vertical axis. Muscat recommended taking the tangent from 5% PW if no steady state is achieved. The load parameter, plotted as the ordinate, was characterised as a proportional load multiplier λ. Assuming a load set P comprising of different loads applied proportionally, if the load is ramped up from zero to P_{max} then the applied load can be defined as $P = \lambda P_{max}$. This allowed the plastic collapse load to be calculated with all loads considered when multiple loads are acting on the structure.

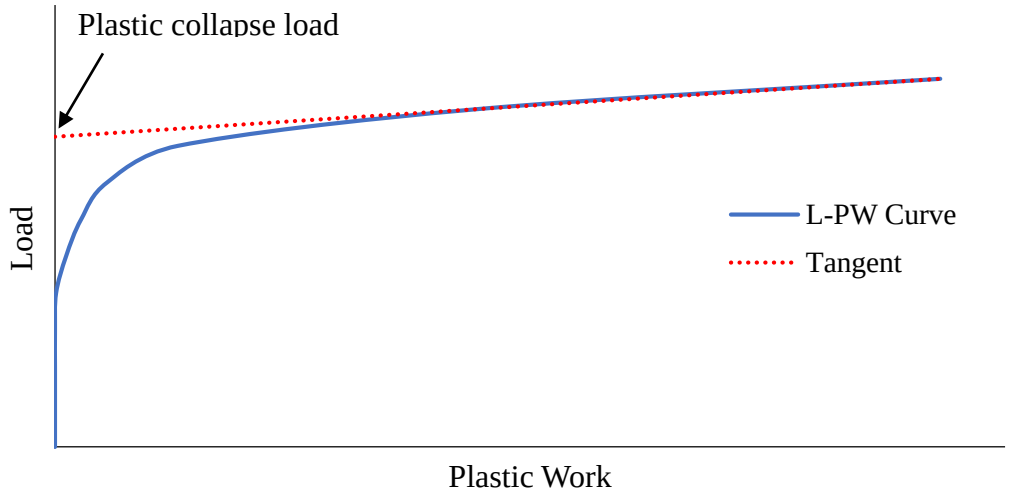

Figure 13: PW Criterion

The load and deformation parameters should be chosen so that the product of the two has units of work (Nm) to ensure the area under the characteristic curve represents total work done. Total work is a combination of the elastic work (EW) and PW and plastic collapse occurs when the PW becomes dominant. The work done per unit volume, dW, is given in equation (29).

$$dW = dW_e + dW_p \tag{29}$$

Where dW_e and dW_p are the elastic and plastic work done per unit volume.

Integrating through the volume of the structure, the elastic and plastic work terms can be expressed in terms of elastic stress (σ_e) elastic strain (ε_e) and plastic strain (ε_p) in equations (30) and (31).

$$W_e = \int \sigma_e d\varepsilon_e \tag{30}$$

$$W_p = \int \sigma_e d\varepsilon_p \tag{31}$$

When in the elastic region, there is no PW. Seal et al [66] defined PW as the ability of the structure to redistribute stress through increasing volume of material that is

plastically deforming and that GPD occurs when the volume of material ceases to increase and instead, the PW changes solely due to strain hardening behaviour. This is because as the load increases, the plastic zones grow and PW increases until small additions of load result in large increases in PW, indicating that a plastic failure mechanism has formed as more of the work done is dissipated as plastic action.

The PW criterion defines the global response of the structure, which is a significant advantage over the TES and TI methods, as they require local load and deformation parameters to be defined. Also, another advantage of a global deformation parameter is that it always increases and the characteristic curve is monotonic.

From a practical sense, the PW criterion is useful as PW is a standard output in most FE software, including ANSYS. It is simple to implement and the plastic collapse load is not affected by the elastic response, as was found with the TES.

More recently, focus has been on the rate of change of PW. Li and Mackenzie [60] developed the plastic work curvature (PWC) method which defines the plastic load in terms of the curvature of the load-PW curve and can be calculated using equation (32).

$$\kappa = \frac{\frac{d^2 W_p}{dQ^2}}{\left[1 + \left(\frac{dW_p}{dQ}\right)^2\right]^{3/2}} \qquad (32)$$

Where: κ is the curvature, $Q$is the load and W_p is the plastic work.

The change in the curvature could be used to characterise the structural response. The onset of curvature represented initial yield, maximum curvature indicated the change from elastic to plastic dominated response and GPD was defined as the point of constant or zero curvature. This identified where the plastic collapse load was to be taken from. However, this was for very simple structures and defining a value of curvature that represents plastic collapse for every scenario would be less straight forward. Figure 14 presents an example plot of the PWC criterion for a rectangular beam under an end moment load.

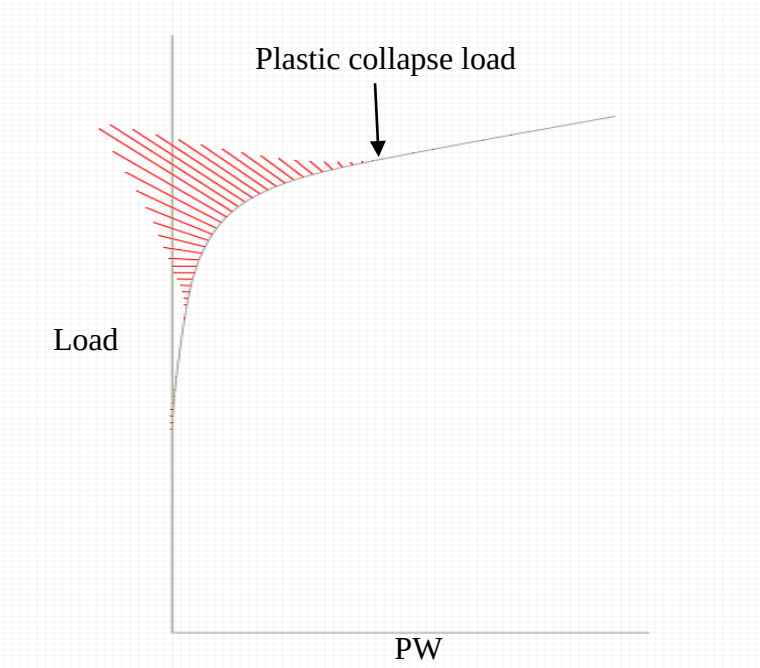

Figure 14: PWC Criterion

Seal et al. [66,67] compared methods to calculate plastic collapse and indicated that use of the first local maximum in the curvature plot to define the plastic load was conservative as the PW continues to increase at an increasing rate beyond this point. This implies that the volume of material experiencing plastic deformation is expanding as the plastic region spreads due to stress redistribution and as such indicates that plastic collapse has not occurred at the local maximum of curvature.

Research has been conducted to look at alternative ways to calculate the curvature to try and negate the problem of multiple peaks in the curvature plot. Seal et al. [66,67] recommended using a curve fitting method to calculate the curvature as, for the example problems they investigated, this produced a smooth normalised load vs curvature plot with a distinct peak. The method used to calculate the single parameterised curve fitting function was a modified Ricketts and Head [68] function. By specifying that the $W_P \geq 0$, Seal et al [66] were able to define equation (33).

$$f(x) = \frac{A}{1 + \chi + \eta} \tag{33}$$

Where χ and η are defined in equations (34) and (35).

$$\chi = \frac{e^{B(C-x)}}{1 + e^{\left(\frac{2BD(C-X)}{|B+D|}\right)}} \tag{34}$$

$$\eta = e^{D(C-x)}\left(1 - \frac{1}{1 + e^{\left(\frac{2BD(C-X)}{|B+D|}\right)}}\right) \tag{35}$$

A, B, C and D are curve fitting parameters which must be optimised to define the function which best fits the plastic work vs pressure curve obtained from elastic-plastic FEA. Upon calculating the curve fit function, equation (32) is used once again to calculate the curvature.

Seal et al also investigated plastic work normalisation, comparing normalising to the max PW and the RPWC method developed by Camilleri et al [61]. The RPWC method plots a characteristic curve of the ratio of plastic work to total work on the abscissa against the load on the ordinate, as per equation (36).

$$Ratio = \frac{W_p}{W_e + W_p} \tag{36}$$

Camilleri suggested the use of the circumradius method to obtain the curvature, which in the plastic region, defined the rate of change from plastic deformation to GPD and eventually global plastic collapse at "near zero" curvature. The onset of GPD was taken as the load corresponding to the point of maximum curvature. When compared to the TES for a torispherical head, the plastic loads were found to be conservative but had a more distinct point of excessive plastic deformation compared to other methods. The use of the circumradius method with RPWC sometimes resulted in multiple local maximums [66] and so engineering judgement was required, highlighting the degree of subjectivity still associated with such methods.

Skopinsky and Berkov [63] proposed the rate of change of relative plastic work and demonstrated the method to analyse a nozzle-vessel [64]. This was based on the PW, PWC and RPWC method. It is proposed that the "maximum criterion of the rate of change of relative plastic work" can be used to determine the plastic load.

2.6 ASME VIII Div 2 Elastic-Plastic Analysis Method

The non-nuclear ASME VIII Div 2 [23] covers elastic-plastic stress analysis more comprehensively. Full plastic analysis utilising strain hardening material properties is prescribed to prevent failure due to plastic collapse of a pressurised structure under a static load. The criteria for use and applicable design factors are outlined but what sets the ASME VIII Div 2 procedure apart from ASME III, is that Annex 3-D contains a set of equations to derive material strength parameters to define a true stress-strain curve. The stress-strain data can then be used as an input to the FEA to simulate the actual structural response, improving on the accuracy of the linear elastic and elastic-perfectly plastic FEA. Plastic analysis of the LWR nozzles to the ASME VIII Div 2 procedure was therefore investigated.

The ASME VIII Div 2 material model in Annex 3-D [23] can be formulated with material property data easily obtained from ASME II. The true stress-strain data to define the curve can be calculated using equations (37) to (49), taken from Annex 3-D. Please see Table 2 for variable definitions.

$$\varepsilon_t = \frac{\sigma_t}{E_y} + \gamma_1 + \gamma_2 \tag{37}$$

$$\gamma_1 = \frac{\varepsilon_1}{2}(1.0 - \tanh H) \tag{38}$$

$$\gamma_2 = \frac{\varepsilon_2}{2}(1.0 + \tanh H) \tag{39}$$

$$\varepsilon_1 = \left(\frac{\sigma_t}{A_1}\right)^{\frac{1}{m_1}} \tag{40}$$

$$A_1 = \frac{\sigma_{ys}(1+\varepsilon_{ys})}{\left(\ln(1+\varepsilon_{ys})\right)^{m_1}} \tag{41}$$

$$m_1 = \frac{\ln R + \left(\varepsilon_p - \varepsilon_{ys}\right)}{\ln\left(\frac{\ln(1+\varepsilon_p)}{\ln(1+\varepsilon_{ys})}\right)} \tag{42}$$

$$\varepsilon_2 = \left(\frac{\sigma_t}{A_2}\right)^{\frac{1}{m_2}} \tag{43}$$

$$A_2 = \frac{\sigma_{uts} e^{m_2}}{m_2^{m_2}} \tag{44}$$

$$H = \frac{2\left[\sigma_t - \left(\sigma_{ys} + K(\sigma_{uts} - \sigma_{ys})\right)\right]}{K(\sigma_{uts} - \sigma_{ys})} \tag{45}$$

$$R = \frac{\sigma_{ys}}{\sigma_{uts}} \tag{46}$$

$$\varepsilon_{ys} = 0.002 \tag{47}$$

$$K = 1.5R^{1.5} - 0.5R^{2.5} - R^{3.5} \tag{48}$$

$$\sigma_{uts,t} = \sigma_{uts} e^{m_2} \tag{49}$$

With the stress-strain curve parameters from Table 3-D.1 in ASME VIII Div 2 Annex 3-D given in equations (50) and (51).

$$m_2 = 0.60(1.00 - R) \tag{50}$$

$$\varepsilon_p = 2.0e^{-5} \tag{51}$$

A_1	Curve fitting constant for the elastic region of the stress-strain curve
A_2	Curve fitting constant for the plastic region of the stress-strain curve
ε_p	Stress-strain curve fitting parameter
ε_t	Total true strain
ε_{ys}	0.2% engineering offset strain
ε_1	True plastic strain in the micro-strain region of the stress-strain curve
ε_2	True plastic strain in the macro-strain region of the stress-strain curve
E_y	Modulus of elasticity evaluated at temperature of interest
γ_1	True strain in the micro-strain region of the stress-strain curve
γ_2	True strain in the macro-strain region of the stress-strain curve
H	Stress-strain curve fitting parameter
K	Material parameter for stress-strain curve model
m_1	Curve fitting exponent for the stress-strain curve equal to the true strain at the proportional limit and the strain hardening coefficient in the large strain region
m_2	Curve fitting exponent for the stress-strain curve equal to the true strain at the true ultimate stress
σ_t	True stress at which the true strain will be evaluated, may be a membrane, membrane plus bending or membrane plus bending plus peak stress
σ_{ys}	Engineering yield stress evaluated at the temperature of interest
σ_{uts}	Engineering ultimate tensile stress evaluated at the temperature of interest
$\sigma_{uts,t}$	True ultimate tensile stress evaluated at the true ultimate tensile strain
R	Engineering yield to engineering tensile ratio

Table 2: Parameters for ASME VIII Div 2 Elastic-Plastic Material Model

The material model defined in equations (37) to (49) can be used in conjunction with ASME VIII Div 2 Article 5.2.4, which specifies that FEA with an elastic-plastic material model and non-linear large deformation effects can be used to find the plastic collapse load [23]. Similar to limit analysis, plastic collapse is determined by a loss of equilibrium. Therefore, the solution will not converge if the plastic collapse load is exceeded as this indicates structural instability. The plastic collapse load can be identified as the last converged solution and the allowable load is calculated by applying a specified design factor.

To determine if elastic-plastic analysis is suitable, ASME VIII Div 2 states that both global and service criteria are met. The global criteria require load and resistance factor design methodologies to be employed with elastic-plastic analysis to find the collapse load pertaining to overall structural instability. The service criteria ensure that, even if the global criteria are met, the deformation in the structure is not so excessive as to

negatively impact the performance of the component. If excessive deformation occurs, a reduction in the design loads may be necessary.

The actual assessment procedure is laid out in 5 steps in ASME VIII Div 2 Article 5.2.4.4. The first step is to create a numerical model, i.e. FEA model, which accurately represents the geometry, boundary conditions and loading conditions. The second step is to define the load cases under investigation. Step 3 contains details of the material definition. The von Mises yield function and associated flow rule are to be used and the elastic-plastic material model may include strain hardening or softening or simply perfect plasticity. Hardening is only considered up to the true ultimate tensile strength of the material, after which, perfect plasticity is assumed. Also, large deformation should be taken into account in the numerical model to incorporate the effects of geometric hardening or softening. The next step uses the information from the second step to determine the global, local and serviceability load case combinations which must be evaluated. The final step involves performing the elastic-plastic analysis to determine if, for each given load case, convergence is achieved. If the solution fails to converge, the load case or wall thickness must be modified and the analysis repeated.

2.7 Elastic-Plastic Shakedown and Ratcheting Analysis

ASME III allows the use of elastic-plastic analysis to calculate the cyclic response of a component. Not much guidance is provided other than in ASME III Article XIII-3440 which specifies that the local membrane stress intensity limit in XIII-3120, $\Delta(P+Q)$ stress limit in XIII-3420, thermal stress ratchet in XIII-3430 and progressive distortion of non-integral connections in XIII-3730 are not required to be satisfied if plastic analysis is used. This involves modelling the plastic material properties and simulating the actual load cycle using FEA. The plastic strain history can be used to determine whether elastic shakedown, alternating plasticity or ratcheting occurs, although this is dependent on the number of load cycles that are simulated. The only Code requirement is that elastic shakedown or alternating plasticity is demonstrated and the accumulated plastic strain does not exceed 5%, for materials where $\sigma_Y/\sigma_{uts} < 0.7$.

Molitoris et al [69] carried out an elastic-plastic shakedown analysis of a nozzle using ASME III and ASME VIII Div 2 procedures and commented on the uncertainty over

the definition of “accumulated strain” not exceeding 5%. Basing their interpretation on the intent of ASME III to limit plastic growth, Molitoris et al measured the cumulative growth of plastic strain in a certain direction at a single point at the end of a load cycle. The main area of uncertainty, however, was the choice of strain to be used in this measurement as ASME III Article XIII-3440 does not define this. The paper also commented on the vagueness of the Code procedure and that Code interpretation and analyst experience could influence the analysis method. Also, a lack of consistency was discovered between the ASME III and ASME VIII Div 2 allowable loads as a result.

To avoid the computational cost associated with full cycle-by-cycle elastic-plastic analysis of a component, a number of shakedown screening and ratchet boundary prediction methods have been proposed and it remains an active area of research. Although prediction of the ratchet boundary is useful, in terms of satisfying ASME III, shakedown must be proven for the specified loading conditions but the proximity to the ratchet boundary is not a requirement. Therefore, there is no real necessity to calculate the full ratchet boundary interaction diagram for all cases, as a shakedown screening procedure will fulfil the ASME III Code requirements. Many of the direct shakedown methods rely upon similar concepts to those in section 2.3 on elastic modulus adjustment procedures.

Abaqus direct cyclic analysis (DCA) can be used to produce a stabilised cyclic stress-strain hysteresis loop of a structure under cyclic loading. It is a quasi-static analysis which employs Fourier series and time integration of the material behaviour to determine the stabilised response. Originally developed to determine the cyclic response of an engine cylinder head [70], DCA has also been shown to have the potential for application in the nuclear industry [71]. It can be a useful tool in shakedown prediction, as an instability causing the simulation to fail to converge after a predefined number of iterations indicates the accumulation of plastic strain.

The numerical procedure employed by the direct cyclic algorithm is covered in detail by Nguyen et al. [70]. DCA combines a modified Newton method with Fourier series representation of the solution and residual vector. This allows a stabilised cyclic response to be calculated directly. A plug-in was developed for use with Abaqus CAE

and the Abaqus documentation provides a detailed description of the procedure [72]. The Abaqus solver assumes convergence when the residual vector coefficients and the corrections to the displacement Fourier coefficients are sufficiently small when compared to time-averaged force and displacement Fourier coefficients respectively. The default tolerances for the ratio of the maximum residual coefficient to the time-averaged force and the ratio of the maximum correction to displacement coefficients to the largest displacement coefficient are 0.005. Failure to converge indicates that a stabilised response is not achieved within the specified number of iterations. This instability may be due to ratcheting and can be identified since the displacement and residual coefficients of the periodic terms all converge but the constant terms diverge with each iteration and these are used to detect ratcheting. The default tolerance set by Abaqus are 0.005 for both constant terms but can be modified by the user.

The accuracy of DCA is determined by both the number of Fourier terms and the number of iterations. The variation of the cyclic load and structural response will influence the number of Fourier terms required to find a solution. Increasing the number of Fourier terms does, however, impact the computation time.

Muscat, Mackenzie and Hamilton [73] developed a nonlinear superposition method (NSM) which invokes Melan's lower bound shakedown theorem to give a conservative limit to the shakedown load. Adaptions of the NSM have been applied to hillside nozzles [74] and validated against experimental results for elastic shakedown [75] in more recent times.

NSM is used in conjunction with FEA to find the shakedown limit load [76]. NSM requires two separate FEA to be performed: a linear elastic analysis followed by an elastic-plastic analysis. The linear elastic FEA requires the cyclic load to be applied monotonically, neglecting the constant load, to obtain a reference load, P_{ref}. The EP FEA considers both the cyclic and constant loads, with the constant load ramped up in the first analysis step and the cyclic load applied in a second step, causing the structure to exceed yield. The residual stress field is calculated at every integration point by scaling the elastic stress field at each increment and subtracting it from the stress results of the EP analysis.

The residual stress components are used to calculate the equivalent stress in the structure at each increment. The minimum load increment at which the yield criterion is violated is identified and the previous load increment can therefore be taken as a lower bound elastic shakedown load. This satisfies Melan's theorem since the equivalent stress nowhere exceeds yield in the structure. This has been tested to validate the use of NSM in predicting elastic shakedown in pressurised nozzles [75].

NSM can also be used to identify alternating plasticity and ratcheting [77]. The alternating plasticity and ratcheting check using NSM consists of two stages. Firstly, the load increment at which the residual equivalent stress just exceeds the yield strength must be identified. Then, the corresponding equivalent stress at the same load increment and integration point in the EP analysis is compared to the yield strength. Alternating plasticity is said to occur if the corresponding equivalent stress from the EP FEA is equal to the yield strength. If, however, the equivalent stress is less than the yield strength, a ratchet mechanism is observed if for any other integration points in other elements in the model, the equivalent stress is equal to the yield strength i.e. the stricture is yielding at points other than that identified in the first stage.

Reinhardt [78] proposed the non-cyclic method (NCM) for shakedown analysis and it has seen extensive development by Adibi-Asl and Reinhardt [79–82]. This method relies upon the use of limit load analysis in conjunction with elastic modulus adaption procedures (EMAP) [83] to find a shakedown limit load. A basic outline of the method is given in the following steps [80]:

1. Decompose the load into proportional cyclic and constant parts
2. Develop an EPP FEA model with a yield strength of $2\sigma_Y$
3. Calculate the cyclic stress distribution by applying the cyclic load range only
4. Calculate a modified yield strength for each element by subtracting half of the cyclic equivalent stress range from the original yield strength
5. Replace the yield strength in the FEA model with the modified yield strength for all elements and apply the constant load only
6. Use EMAP to find the limit load multiplier

In more recent studies, Adibi-Asl and Reinhardt have used NCM to derive the ratchet boundary for beams under primary and secondary bending loads [84] and showed that the NCM can be used to predict ratcheting in a section with a non-monotonic temperature distribution [85], where the extreme temperatures are not on the surface but midway through the thickness. If a case such as this were to arise, the linearised thermal bending stresses would be very small (approximately zero). The results would satisfy the thermal ratchet criteria in ASME III, but in reality, ratcheting could still occur.

As part of the Rolls-Royce HFEF [53], Martin and Rice developed the hybrid method [86] for predicting shakedown and ratcheting. This builds upon the use of DCA as a shakedown screening tool to develop a method capable of determining the boundary between shakedown and ratcheting directly. The hybrid method involves separating the load history into cyclic and constant components to determine the additional yield capacity of the static load following the determination of the yield capacity from the cyclic component. This is achieved by carrying out a cyclic analysis, then modifying the yield strength at each integration point before performing a limit analysis. This allows the ratchet limit to be identified for an arbitrary number of cyclic loads.

Upon decomposing the load history, the next step in the hybrid method is to determine the direction of the stress vector caused by the constant load. This is done by carrying out an elastic analysis where the applied load is a unit load in the direction of the constant load. This does not consider any changes in the limit load vector as plasticity develops but is a suitable assumption if there is not considerable redistribution of plastic strains in the structure. The cyclic load is then considered by carrying out a cyclic analysis using a suitable procedure, such as DCA or full cycle-by-cycle analysis, to find the cyclic stress state. The initial yield strength can be defined in terms of the cyclic stress state and constant stress state using equation (52). The scaling factor x applied to the constant state of stress can be found for each integration point through vector summation as the cyclic and constant stress states have already been determined. The modified yield strength can then be calculated and is defined in equation (53) as the von Mises equivalent stress of the scaled unit vector in the constant

stress direction. The ratchet boundary can then be found by carrying out a limit load analysis using the modified yield strength distribution.

$$\sigma_{VM}\left([\sigma]_{cyclic} + x[\sigma]_{const}\right) = \sigma_Y \quad (52)$$

$$\sigma'_Y = \sigma_{VM}(x[\sigma]_{const}) \quad (53)$$

Where x is a scaling factor, $[\sigma]_{const}$ is the constant stress, $[\sigma]_{cyclic}$ is the cyclic stress, σ_{VM} is the equivalent von Mises stress, σ_Y is yield strength and σ'_Y is the modified yield strength.

The main difference between the hybrid method and pure DCA is that the hybrid method detects the ratchet boundary directly and only requires the cyclic analysis to be conducted once for each cyclic load component whereas pure DCA relies upon the bisection method search algorithm to narrow down on the ratchet boundary iteratively using a series of DCA steps at various cyclic and constant loads.

Abou-Hanna and McGreevy [87] introduced the Uniform Modified Yield Surface (UMY) and Anisotropic Load Dependent Yield Modification Method (LDYM) for calculating the ratchet boundary of a component. Based on Koiter's kinematic theorem, the methods are based on determining the ratchet boundary by modifying the yield strength and carrying out limit analysis of a component. The basic procedure consisted of the following stages:

1. Elastic analysis at cyclic load amplitude to calculate von Mises stresses
2. Modification of the material yield strength using UMY or LDYM
3. Limit analysis to predict load at which ratcheting occurs

Two yield surface modification techniques were discussed by Abou-Hanna and McGreevy [87]. UMY involved shrinking the entire yield surface by an equal amount, thus maintaining an isotropic yield surface. The cyclic von Mises stress from the initial elastic analysis was used to shrink the yield surface at each integration point and therefore determine the modified yield strength at each integration point.

LDYM is a more advanced version of UMY. LDYM takes into account the direction of both the cyclic and constant loads to shift the yield surface as opposed to simply shrinking it. The yield surface is modified by shifting the yield surface in the direction of the cyclic stress vector by a magnitude determined by the cyclic von Mises stress. This results in an anisotropic yield surface, bounded by the points where the original and new yield surfaces intersect. Therefore, the constant load to cause ratcheting, calculated using limit analysis, will depend on the direction of the constant load vector. Abou-Hanna and Michael Paluszkiewicz [88] developed the method further to use FEA to apply LDYM in the determination of elastic shakedown, alternating plasticity and ratcheting.

An early version of the Linear Matching Method (LMM) was first introduced by Ponter and Carter [89]. It involves the use of an elastic modulus modification procedure to calculate the residual stress field without using elastic-plastic analysis. Procedures based on Koiter's upper and Melan's lower bound theorems were presented by Chen [90]. It has been demonstrated that the LMM is capable of determining the ratchet boundary of various structures for a number of cyclic loading problems [91,92] and has been adopted by the R5 high temperature assessment procedure [18].

The LMM framework has seen extensive research and continuous development [93]. An Abaqus plug-in was developed by Ure and Chen [94,95] making the LMM more accessible to analysts with no knowledge of the underlying procedures. The plug-in is an intuitive tool for engineers to use in industry for the structural assessment of components under cyclic thermal and mechanical loads.

Direct methods typically rely on the total cyclic load history being split into cyclic and constant components, which allows the ratchet limit to be defined by the addition of a constant load. The direct method proposed by Chen [96], known as the direct steady cycle analysis (DSCA), was expanded on by Lytwyn et al. [97,98] to develop a generalised LMM which allows efficient ratchet analysis for proportional cyclic thermo-mechanical loads. Lytwyn [99] provides a direct comparison between the generalised LMM and Rolls-Royce HFEF for shakedown and ratcheting assessments.

More recent developments have seen the implementation of a limited kinematic hardening material model and temperature dependent material properties, with the method being demonstrated through shakedown analysis of an aero-engine turbine disk [100] and printed circuit heat exchanger [101]. Ma et al. [102] proposed the Unified Procedure for Fatigue and Ratchet Analysis (UPFRA), which utilises the LMM to perform a ratcheting and LCF assessment for arbitrary cyclic loads. This allows shakedown limit, ratchet limit and constant life curves to be generated. Other recent developments include the proposal of the probabilistic Linear Matching Method (pLMM) framework [103,104]. The pLMM combines the deterministic LMM with reliability methods to allow for an efficient probabilistic shakedown analysis procedure. This allows the impact of load fluctuation and design parameter uncertainties to be included in the shakedown assessment. The pLMM framework has been extended to probabilistic creep-fatigue [105] and LCF assessments [106].

Chapter 3 Methodology and Finite Element Modelling

3.1 FEA for Design by Analysis

To calculate the stress and strain fields required to investigate the DBA methods, finite element analysis (FEA) was used extensively. Ansys Workbench and Abaqus FE software packages were both used. Ansys was typically used for the linear elastic and non-linear plastic collapse cases investigated, while Abaqus was predominantly used in the assessment of cyclic loads. This was due to ease of post-processing linearised M+B stress results from Abaqus with a dedicated python script, as discussed in section 1.4. A number of example problems are considered, focussing on typical nuclear power plant components. Nozzle-vessel geometries were of particular interest, as they are susceptible to several failure modes and the complexity of the geometry means that for sizing them, DBA provides significant advantages to standard DBR techniques.

This section provides details of each FEA model set up. There are a combination of 3D and 2D axisymmetric models and the dimensions, material properties, boundary conditions and mesh settings are all provided. Each FEA model is set up to investigate a particular failure mode and the loading conditions defined for each reflect this, with some FEA models focussing on plastic collapse caused by static loads and others concentrating on incremental plastic collapse due to cyclic loading.

Details for an internally pressurised cylinder with thick walls are given first. The aim of this model is to study how accurate linearised elastic stress distributions are at representing the structural response to loads which cause plastic deformation. Dimensions and material properties for the simple component are given, however; a FEA model was not created for the elastic static analysis of the cylindrical vessel, as the elastic stresses in the cylinder wall can be calculated analytically.

The next two models focus on using linear elastic and non-linear plastic stress analysis to investigate plastic collapse of nuclear components due to static pressure loads. Details are provided for a light water reactor (LWR) nozzle-vessel intersection subject to a static internal pressure load as this is representative of design problems faced in industry for the sizing of vessels. Following this, FEA model specifications for a

tubesheet are presented to simulate test conditions leading to failure of the component due to excessive plastic deformation.

The focus of the investigation then moves onto mechanical and thermal cyclic loading, beginning with an investigation into the use of elastic and elastic-plastic FEA for the determination of elastic shakedown limit loads. Initially, cyclic mechanical loads and cyclic thermal loads are examined separately. FEA models for two oblique nozzle configurations are detailed and the cyclic internal pressure load is defined. The same pressurised cylindrical vessel detailed in section 3.2 and studied as part of the investigation into elastic stress distributions due to static pressure loading is also investigated when subject to cyclic thermal loads. For the cyclic analysis, a FEA model for the thick pressurised cylinder is created and details for the cyclic thermal loading conditions are provided.

The final FEA model involves a more in depth analysis of a nozzle in a spherical vessel. It is subject to a pressure and thermal transient more typical of an actual nuclear power plant to investigate methods for the prediction of elastic shakedown, alternating plasticity and ratcheting.

3.2 Thick Walled Cylindrical Vessel

Static analysis of an internally pressurised thick cylinder was investigated first as its simplicity allowed some basic principles to be explored and potential issues which may arise in the analysis of more complex components to be highlighted. In section 4.1.1, a thick cylinder with an outer radius of $R_o = 300\ mm$ and inner radius of $R_i = 200\ mm$, to give a wall thickness of $100\ mm$, is investigated under a static internal pressure load. The yield stress is specified as $\sigma_Y = 240\ MPa$ allowing the plastic collapse limit load of the component to be calculated analytically. Through thickness elastic stress intensity distributions are also calculated analytically and analysed in more detail, along with linearised stress distributions for various linearisation methods.

The structural response to a cyclic thermal load was also investigated for a cylindrical vessel. For this study however, FEA was used to calculate the elastic stress history of the cylinder when subject to constant internal pressure and cyclic temperature distribution. Analysis of this simple component allowed some initial results to be

gathered and possible trends in the data to be identified before looking at more representative nuclear components under transient loading conditions. The main focus of this analysis was to identify how much of an impact cyclic thermal stresses had on the effectiveness of each linearisation method in determining the temperature at which alternating plasticity is observed in the component.

The thick cylindrical vessel was modelled in Abaqus CAE as a 2D axisymmetric section with the dimensions consisting of: $R_o = 300\,mm$ and $R_i = 200\,mm$. This closed-end cylinder is similar to that of the Bree problem [6] but with a thicker wall section. The material properties for the thermo-mechanical FEA are presented in Table 3 and taken from a Bree cylinder analysis by Martin [71].

$\boldsymbol{\lambda}$ $(\mathbf{W/mm°C})$	$\boldsymbol{\alpha}$ $(°C^{-1})$	$\boldsymbol{E}$ $(\boldsymbol{GPa})$	$\boldsymbol{\sigma_Y}$ $(\boldsymbol{MPa})$	$\boldsymbol{v}$
0.035	$1.335e^{-5}$	185	402.7	0.3

Table 3: Cylinder material properties[71]

Sequentially coupled thermal and structural analysis was conducted, with the thermal analysis run first to obtain the through-thickness temperature distribution. The thermal results are then included in the mechanical analysis which followed to calculate the thermal stresses. For the heat transfer analysis, the whole cylinder was specified to be at an initial temperature of $20°C$ and a cyclic temperature distribution was applied to the inside surface. A range of maximum inside temperatures were investigated, from $100℃$ to $700℃$. The outside surface was insulated, creating a temperature difference between the inside and outside surfaces of the cylindrical vessel and hence a temperature distribution through the thickness.

The boundary conditions for the structural analysis were such that the bottom edge was constrained in the axial direction and an end-cap pressure load using equation (54) was applied to the top edge to simulate the closed-end, as shown in Figure 16. A constant internal pressure of $100\ MPa$ was applied to the inside surface of the vessel. Also, a constraint equation was applied to couple the nodes in the vertical direction on the top edge to ensure that the surface remains planar. The temperature distribution results from the thermal analysis of the cylinder were included in the structural analysis

as a predefined field in Abaqus CAE. This allowed the thermo-mechanical stress history to be calculated over the cycle. As this was a linear elastic analysis, only a single cycle was simulated. A load cycle is shown in Figure 15.

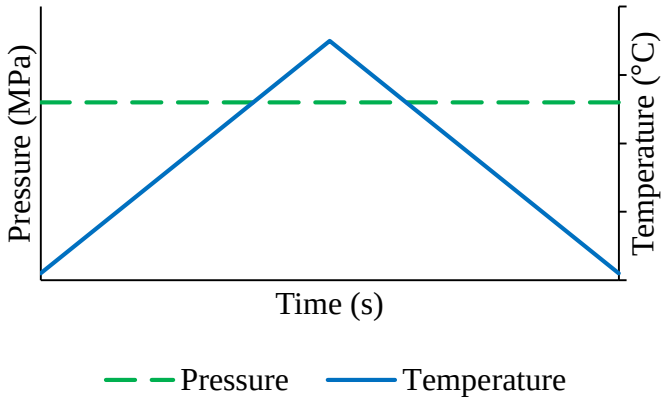

Figure 15: Thick cylinder model loading transient for cyclic thermal analysis

The meshed component is also shown in Figure 16. The mesh consisted of 200 elements with 10 through thickness. DCAX4 linear elements were used to discretise the model for the thermal analysis, with CAX4R linear 4 node quadrilateral elements used for the structural analysis. Both element types were axisymmetric. The mesh settings were based on published FEA of a Bree cylinder [71].

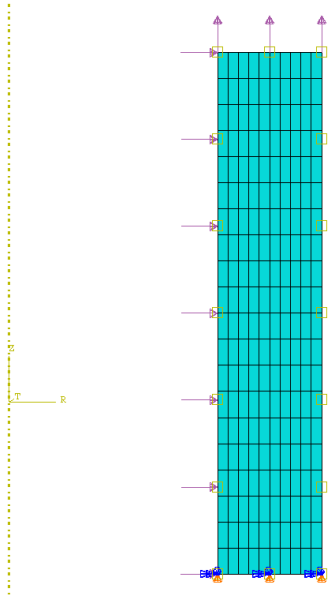

Figure 16: Meshed 2D axisymmetric cylinder with boundary and loading conditions

3.3 Light Water Reactor Nozzle

A non-linear analysis benchmarking project by the World Nuclear Association (WNA) Cooperation in Reactor Design Evaluation and Licensing (CORDEL) Working Group is currently investigating the divergence between Code assessment of nuclear components [107]. The CORDEL non-linear analysis benchmark aims to investigate the effectiveness of different DBA methods in characterising the structural response of nuclear components. This is achieved by inspecting the difference between allowable loads calculated using linear elastic DBA and non-linear elastic-plastic DBA approaches and will identify current Code procedures and processes which require updating and further guidance. One component being analysed in the CORDEL benchmark is a thick-walled light water reactor (LWR) nozzle-vessel intersection [108].

The LWR nozzle structure was chosen as part of the current study to investigate elastic and elastic-plastic DBA methods in the computation of maximum allowable static pressure loads, ensuring the component does not fail due to plastic collapse. The CORDEL benchmark is very much focussed on performing elastic DBA and limit analysis that strictly meet the requirements of ASME III. This thesis expands on this, utilising the same component to investigate the actual stress linearisation process and individual stress component distributions in more detail. This thesis utilises the nozzle-vessel geometry to investigate various stress linearisation methods as well as more advanced elastic-plastic methods. These were not in the scope of the CORDEL benchmark study. The same nozzle geometry and material is used as it is typical of a LWR component.

The nozzle-vessel intersection was modelled in Ansys Workbench. The actual component consists of a cylindrical vessel and reinforced nozzle. The dimensions, taken from the CORDEL Benchmark [107], are detailed in Figure 17.

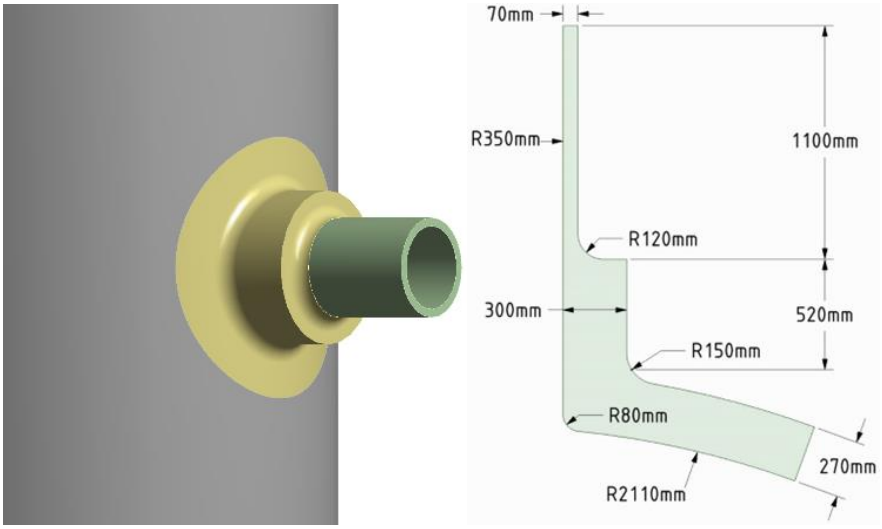

Figure 17: LWR Nozzle model and cross-sectional dimensions

The material properties specified in the CORDEL benchmark are for 16MND5 low alloy steel, which is the RCC-M equivalent of SA-508 Grade 3 Class 1 low alloy steel in ASME II. The published material properties for each grade are slightly different but for the purposes of this study and to keep strictly to ASME III, the material properties from ASME II Part D were used at the design temperature of 300℃.

The material properties in Table 4 allow linear elastic FEA and non-linear limit analysis to be carried out to find the plastic collapse load. For the limit analysis, an elastic perfectly-plastic material model was specified in Ansys. As per ASME III, the onset of plasticity was defined as $1.5S_m$ and the tangent modulus set to zero.

Material	$\boldsymbol{E}$ $(\boldsymbol{GPa})$	$\boldsymbol{\upsilon}$	$\boldsymbol{\sigma_Y}$ $(\boldsymbol{MPa})$	$\boldsymbol{\sigma_{uts}}$ $(\boldsymbol{MPa})$	$\boldsymbol{S_m}$ $(\boldsymbol{MPa})$	$\boldsymbol{1.5S_m}$ $(\boldsymbol{MPa})$
SA508 Gr3 Cl1	174	0.3	292	552	184	276

Table 4: LWR nozzle material properties for SA508 Gr3 Cl1[109]

To perform plastic analysis with material strain hardening, a bilinear or multilinear stress-strain curve is required. ASME III contains no stress-strain curve data and relies upon the analyst conducting their own material testing.

Here, the ASME VIII Div 2 elastic-plastic material model described in section 2.6 was used to calculate the true stress-strain curve for SA508 Gr3 Cl1. The true plastic strain component of the total strain was used to generate the curve shown in Figure 18. This defined the multilinear material model for the plastic analysis of the LWR nozzle. Ansys software automatically assumes perfect plasticity beyond the maximum stress defined in the model, which in this case corresponds to $\sigma_{uts,t}$.

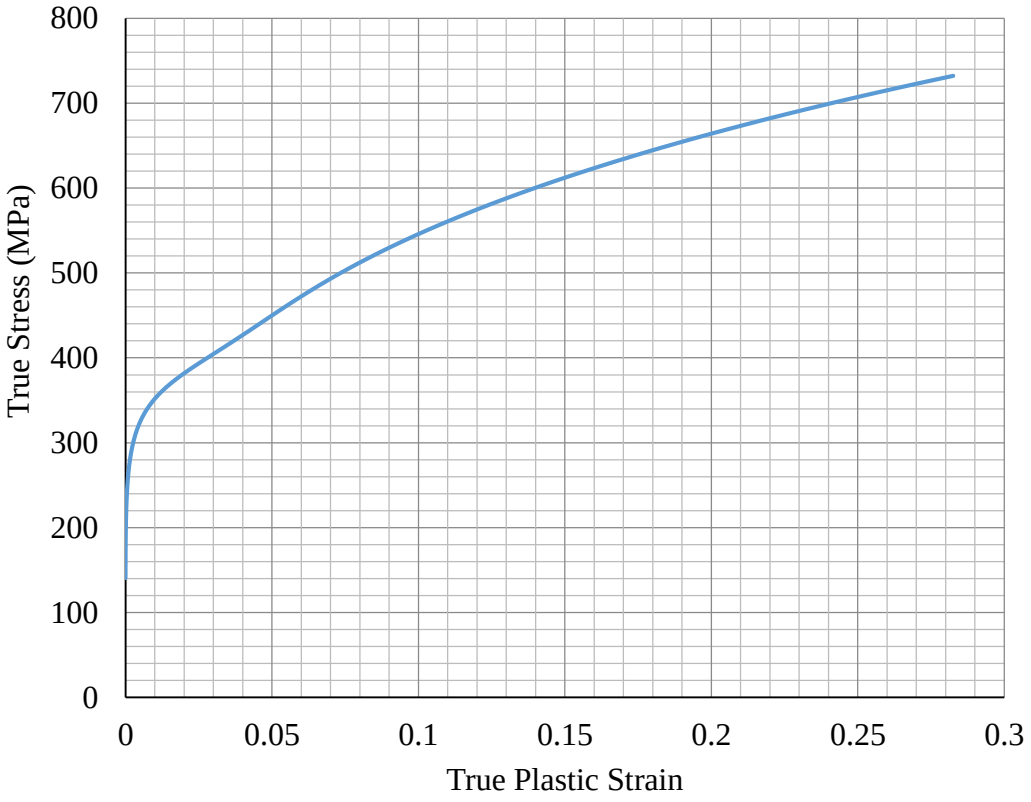

Figure 18: ASME VIII Div 2 true stress-plastic strain curve for SA508 Gr3 Cl1

For the 3D model, symmetry was used to model a quarter section of the nozzle only. Symmetry boundary conditions in Ansys were applied to the cut faces. An internal pressure was applied to the inside surface of the vessel and nozzle and an end-cap pressure load was applied to the top surface of the nozzle. An end pressure load was also applied to the cross-section of the cut cylindrical vessel, which was also constrained from being able to rotate around the z axis (i.e. the cylindrical vessel longitudinal axis). The end-cap pressure loads were calculated using equation (54).

$$P_{end} = \frac{P_i R_i^2}{R_o^2 - R_i^2} \tag{54}$$

Where P_i is the internal pressure, R_i is the internal radius and R_o is the external radius.

The load and boundary conditions are displayed in Figure 19. For the linear elastic FEA of the LWR Nozzle model, the pressure load is applied in a single step. For the elastic-plastic analysis, the internal and end-cap pressures were ramped up in proportion incrementally. A suitably small minimum load step was chosen to allow plasticity to develop and spread.

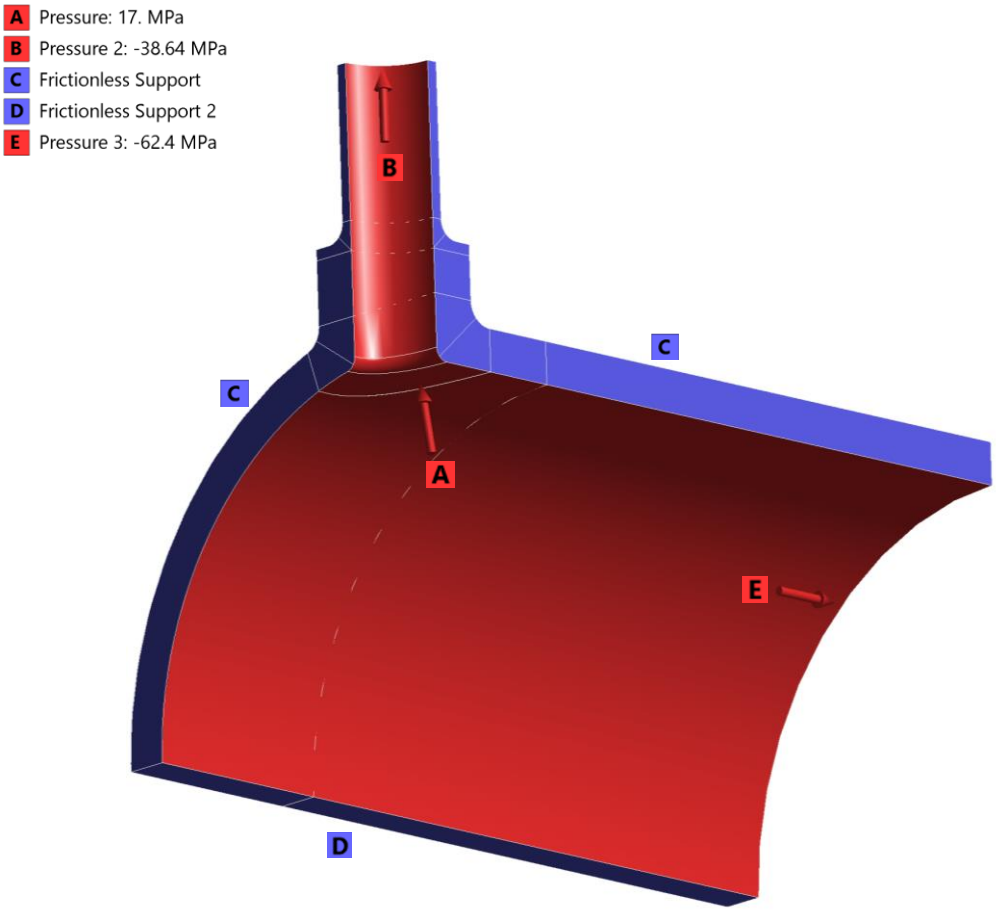

Figure 19: LWR nozzle applied load and symmetry boundary conditions

The mesh for the 3D model is shown in Figure 20. The nozzle was meshed with 20 node hexahedral SOLID186 elements in Ansys Workbench. A mesh sensitivity study was performed by altering the number of elements, primarily though thickness and at the nozzle junction, to determine a suitable mesh resolution. The final mesh in Figure 20 consisted of 26455 elements.

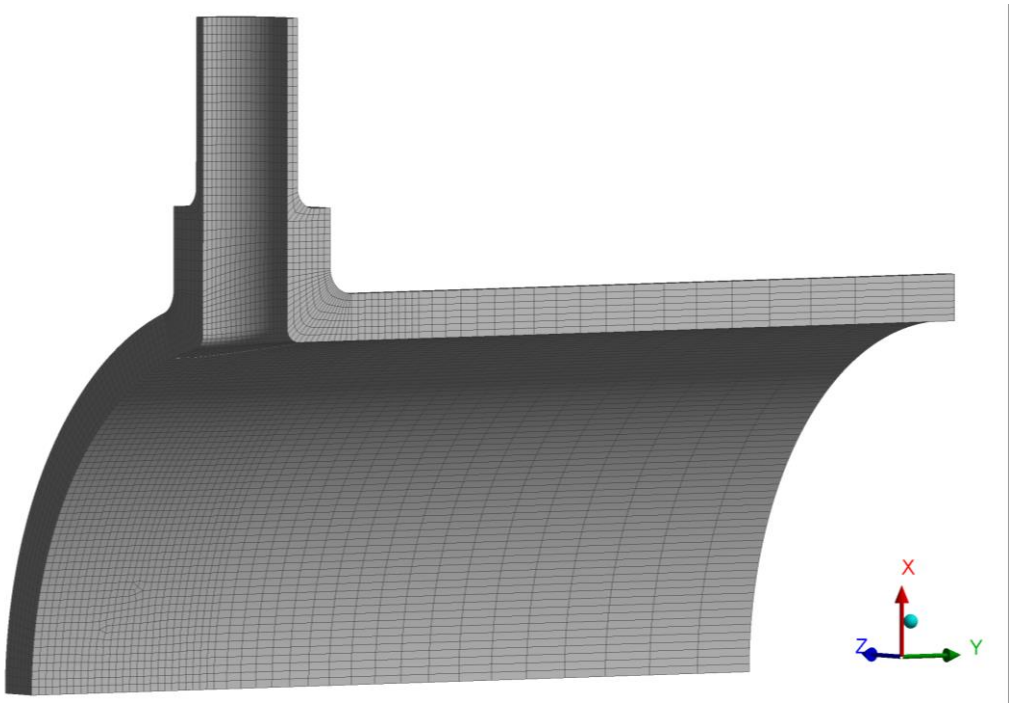

Figure 20: LWR nozzle mesh

The results from the sensitivity study are presented in Figure 21. The maximum stress intensity had reached a converged value for these mesh settings and this was deemed to provide accurate results for the elastic stress analysis and not require excessive computing power for the elastic-plastic nonlinear analysis. For the nonlinear analysis, the mesh may not need to be as refined, as long as the onset and spread of plasticity is captured properly.

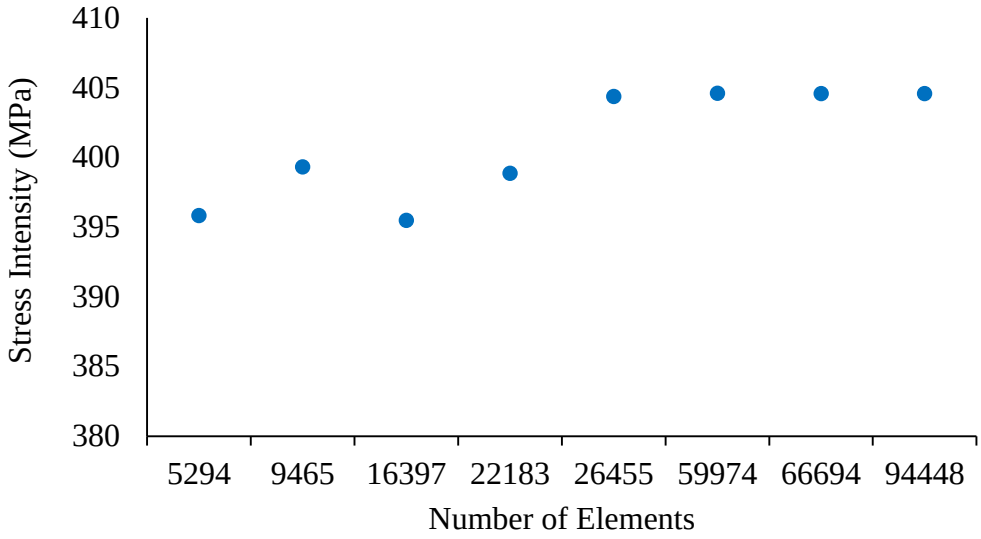

Figure 21: LWR nozzle mesh sensitivity study

3.4 Tubesheet

Jones and Gordon [3] conducted experimental tests on a tubesheet made from low alloy steel to determine how the structure deforms when subject to a load acting at the centre of the plate parallel to the axis of the penetrations. Two tests were conducted measuring the load vs deformation of the test plates until eventual plastic collapse. These test results were then used to provide validation for the use of computational limit analysis.

It was found that the deformed structures from experimental tests and 3D FEA resembled very similar shapes, demonstrating the accuracy of the elastic-perfectly plastic FEA in predicting the structural response of the tubesheet. The plastic collapse load calculated using limit analysis was conservative with respect to the measured collapse loads and failure was found to occur at the inner most row of penetrations in both the FE limit analysis and experimental tests.

Jones and Gordon [3] explain that the test was set up to gather data which can be used to assess the applicability of analytical methods used in the design of a steam generator tubesheet. The boundary between the solid and perforated material in the tubesheet is often the most susceptible to failure. As such, it is important to be able to accurately

determine the loads at which the outer/inner most row of perforations lead to plastic collapse. The in-plane bending and out-of-plane shear stresses which are typically experienced at the penetrations were induced by loading the tubesheet in a hydraulic press. A force was applied to the inner hub, which is so thick that it acts as a rigid body, transferring the load to the perforations. The maximum transverse displacement was able to be measured using linear displacement sensors located on the inner hub.

The tubesheet problem is expanded upon in this thesis as part of the investigation into the use of non-linear DBA methods in protecting against plastic collapse. Published plastic collapse loads for actual components are uncommon, so the data provided by Jones and Gordon is useful for validating DBA methods for the prediction of plastic collapse. By comparing the published results to those of the limit analysis using Ansys Workbench, evidence is gathered to show that the same procedure can be carried out to calculate the collapse load of the LWR nozzle.

Also, as the load-deflection curves from both tests are presented, an investigation into ASME VIII Div 2 strain hardening material model can be carried out. The material properties required to define the material model are given, so the material model can be easily constructed. The load-deflection data from the tests can therefore be compared to that of the elastic-plastic FEA to determine how accurate the material model really is. Plastic collapse loads can also be calculated using various elastic-plastic DBA methods and compared to the actual collapse load of the component. This means that the plastic DBA methods can be compared to real test data, not just other computational methods.

The tubesheet of interest is shown in Figure 22, along with the cross-sectional dimensions in mm. There are a total of 414 penetrations ordered in five rows and in a triangular arrangement. Each penetration has a ligament efficiency of 0.32 and pitch of 19.05 mm [3]. The geometry definition and material properties were defined in terms of metric units converted from the imperial units provided by Jones and Gordon [3].

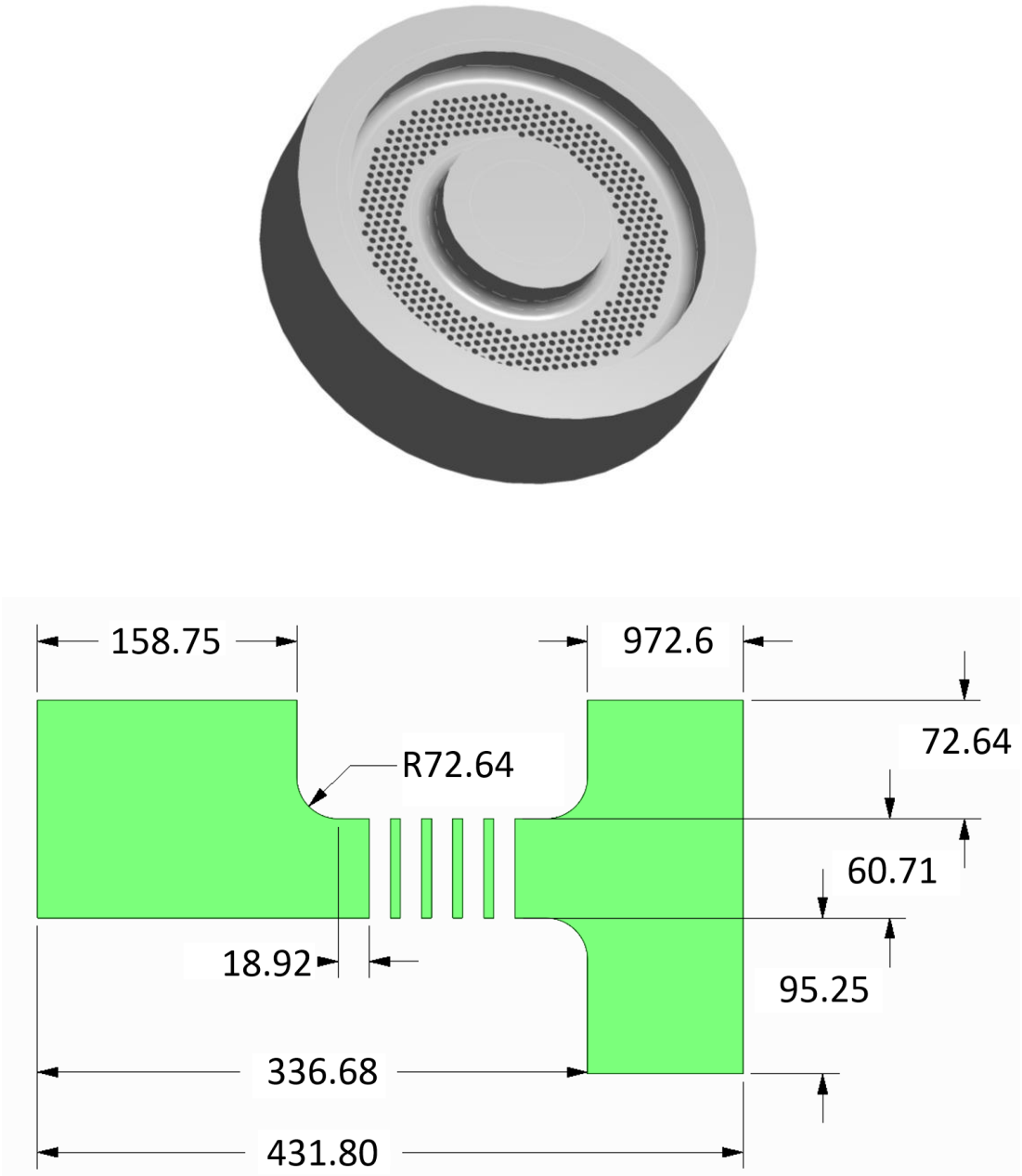

Figure 22: Full tubesheet geometry and cross section dimensions

The low-alloy steel elastic material properties presented in Table 5 were taken as the average of nine tensile tests of the material [3]. For the limit analysis, a bilinear kinematic hardening material model with a tangent modulus of zero was used to model the EPP material behaviour. The design stress was taken as one-third of the ultimate tensile strength as this was lower than two-thirds of the yield strength [3].

E (GPa)	υ	σ_Y (MPa)	σ_{uts} (MPa)	S_m (MPa)
190.98	0.3	655.56	786.63	262.21

Table 5: Tubesheet material properties

As with the LWR nozzle, the ASME VIII Div 2 elastic-plastic material model was used to calculate a true stress-strain curve for full plastic analysis. The true plastic stress-strain curve in Figure 23 was generated based on the material properties for the low alloy steel in Table 5. Again, perfect plasticity was assumed beyond $\sigma_{uts,t}$.

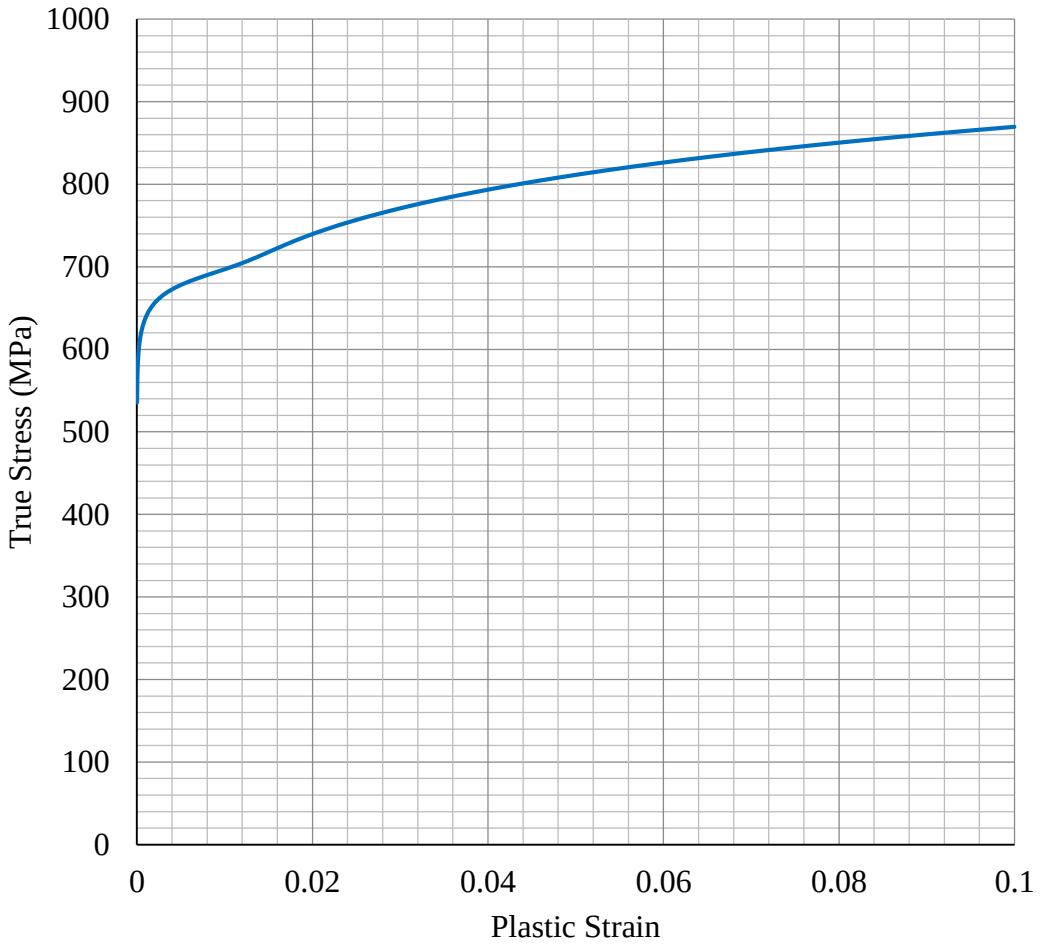

Figure 23: ASME VIII Div 2 true plastic stress-strain curve for the tubesheet low alloy steel

FEA was carried out on a 30° section of the tubesheet to take advantage of symmetry (as performed by Jones and Gordon [3]). Figure 24 displays the section to be analysed with regards to the full geometry, showing how this reduces the size of the model and hence should reduce the computation time of the simulation.

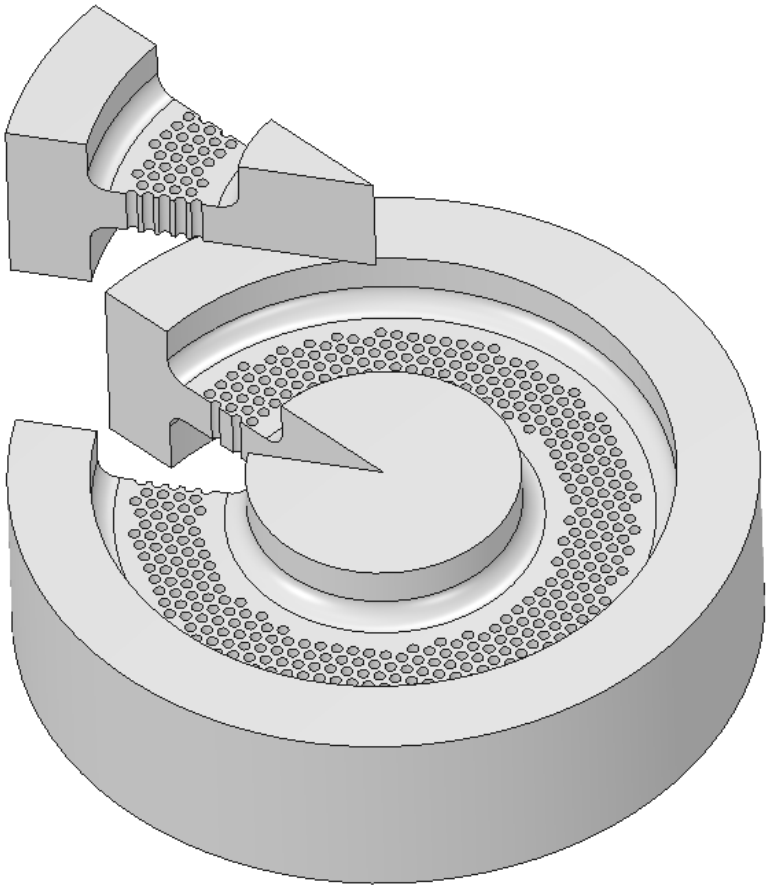

Figure 24: 30° section modelled to represent full tubesheet

To ensure the cut section is an accurate representation of the full structure, appropriate boundary conditions were specified in Figure 25. A pressure load was applied to a 50.8mm annulus region on the upper surface of the inner hub and frictionless boundary conditions on the cut faces were applied to model the symmetry of the 30° wedge. The model constraints were completed by a fully fixed support on a 1in annulus region on the lower surface of the outer hub.

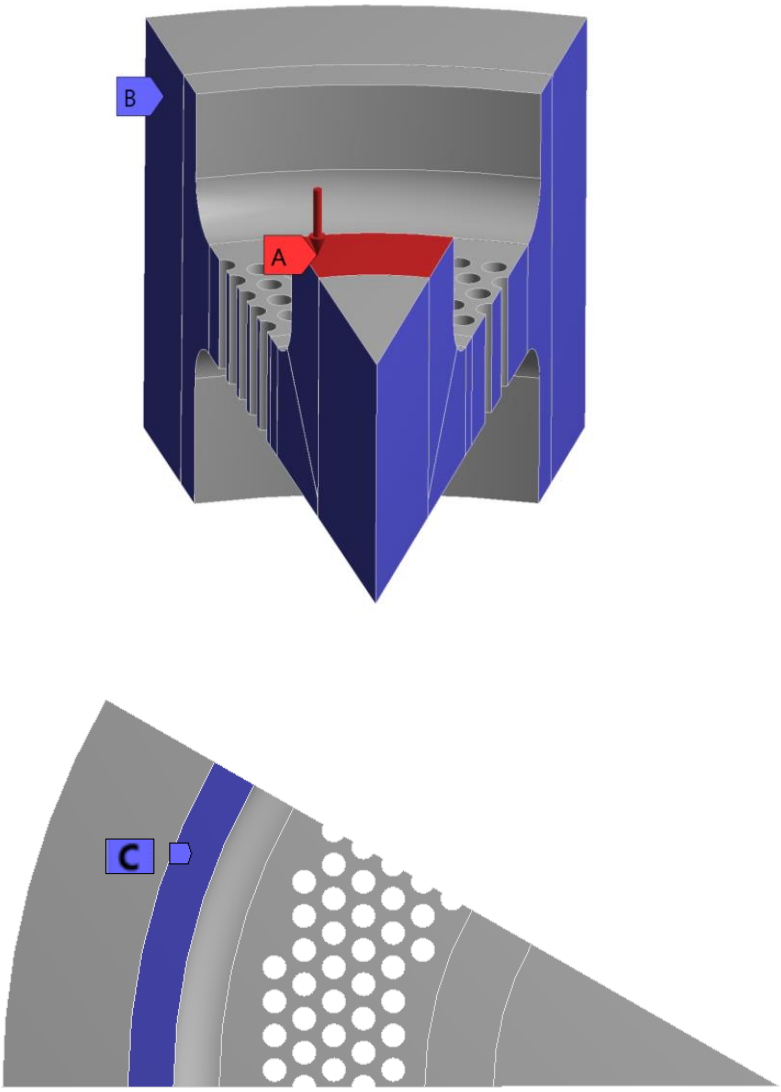

Figure 25: Applied pressure (A), frictionless (B) and fixed (C) boundary conditions on tubesheet

The mesh for the tubesheet FE model is shown in Figure 26. As with the LWR nozzle, Ansys SOLID186 elements were used and a mesh sensitivity study was carried out to check the suitability of the mesh density, with the final mesh consisting of 39494 elements and 192872 nodes. The majority of the elements were concentrated on the penetrations as this is where the high stress regions were expected to be and the plate was modelled with 10 elements through thickness. This allowed the mesh to be kept fairly coarse in other regions remote from the penetrations.

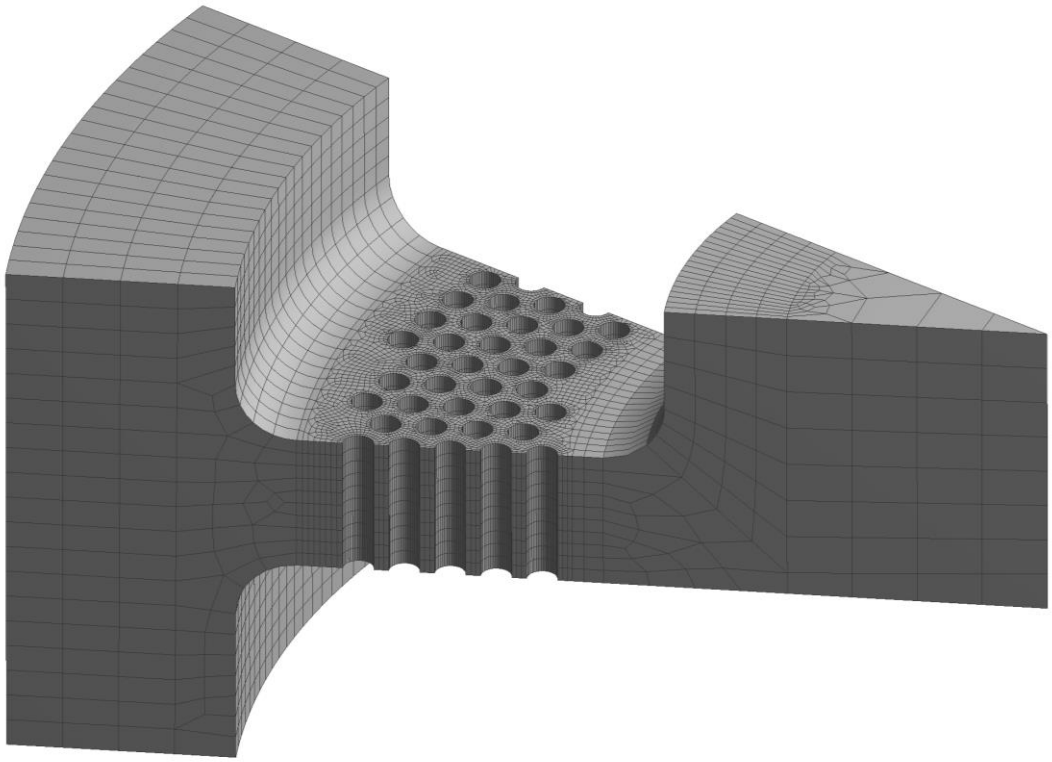

Figure 26: Tubesheet mesh

3.5 Oblique Nozzle

Experiments were conducted by Procter and Flinders [4,110] in 1968 at Berkeley National Laboratory (BNL) to investigate the cyclic behaviour of radial and oblique nozzles on spherical vessels. They published elastic shakedown limits for three radial and three oblique nozzle configurations. These were representative of those found on a nuclear reactor pressure vessel. The results have been used in other studies [75,111] to validate the use of the linear matching method and nonlinear superposition method in predicting elastic shakedown.

The first report [110] focussed on the elastic response of the radial and oblique nozzles under an internal pressure at ambient temperature by measuring the stress distribution in the shell plate adjacent to the nozzle. Their aim was to provide test results for verification of theoretical solutions and to give plant designers and operators an indication of the behaviour of typical plant components which, at the time, could not be theoretically analysed. Despite being conducted in the 1960s, these test results are still useful to help validate analysis methods and in particular the second report [4] can be used in this case to validate elastic shakedown limit pressures.

Procter and Flinders [4] go into detail about the setup of the test vessel for the experimental shakedown investigation. The experimental results would be heavily dependent on the positioning of the strain gauges and to ensure the most accurate recordings, 400 strain gauges were attached to the structure, with particular consideration for areas where high strain gradients were expected, such as the inside surface of the nozzles.

In the shakedown tests, the vessel was pressure cycled at $50\,psi$ $(0.345\,MPa)$ increments between internal pressures of $450\,psig$ $(3.1\,MPa)$ and $700\,psig$ $(4.83MPa)$. Over the course of a cycle, strains were recorded at zero, mid pressure and test pressure at the positions of maximum equivalent stress and plotted against the number of cycles. The criteria used to determine shakedown was that if the strain measure was identical for three consecutive cycles, the structure was said to have shaken down.

Procter and Flinders calculated shakedown loads of 4.82 MPa for nozzle 5 and 4.48 MPa for nozzle 6 [4]. Ure and Chen [111] calculated lower and upper bound shakedown loads of 4.53 MPa and 4.58 MPa for nozzle 5 and 4.12 MPa and 4.16 MPa for nozzle 6 using the LMM. These results can be used in this thesis to help validate the use of different linearisation methods in predicting elastic shakedown and preventing failure due to incremental plastic collapse. FE models were setup in Abaqus for oblique nozzles 5 and 6 to determine the elastic and elastic-plastic response to a simple cyclic pressure load.

The generic nozzle geometry is shown in Figure 27, with the dimensions in Table 6 and Table 7 for oblique nozzles 5 and 6. Oblique nozzle 4 was not modelled due to inaccuracies in the experimental results caused by misplacement of some of the strain gauges reported by Procter and Flinders [4]. The general shape of both nozzles is similar, with the main difference being in the nozzle wall thickness, denoted dimension 'e' in Figure 27 and Table 6, which show nozzle 5 is thicker than nozzle 6.

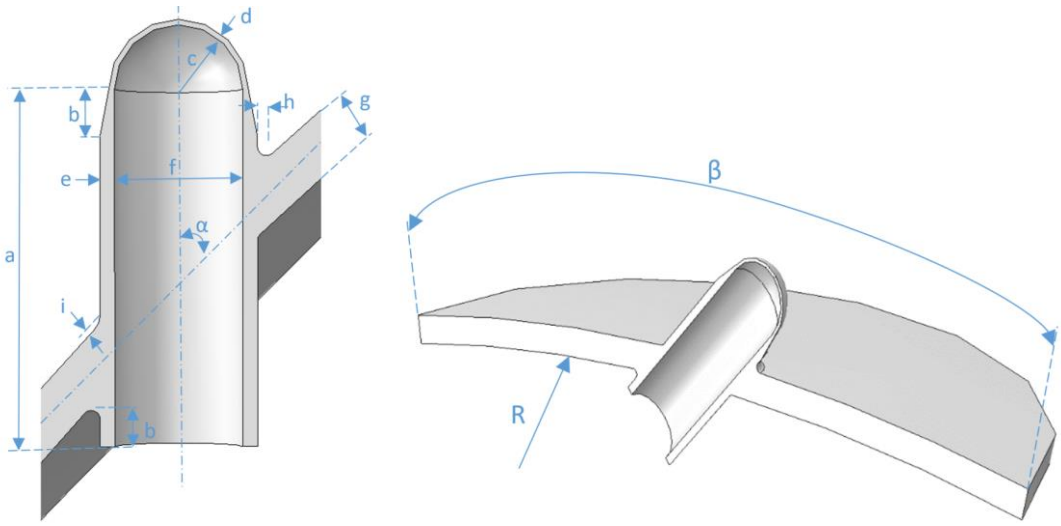

Figure 27: Generic oblique nozzle geometry definition

Nozzle	**Dimension (mm)**								
	a	**b**	**c**	**d**	**e**	**f**	**g**	**h**	**i**
5	203.2	26.93	36.513	3.175	8.33	73.025	28.575	5.08	3.175
6	228.6	25.4	36.513	3.175	3.175	73.025	28.575	6.35	3.175

Table 6: Oblique nozzle dimensions

Nozzle	Dimension		
	Radius, R (mm)	$\boldsymbol{\alpha}$ (°)	$\boldsymbol{\beta}$ (°)
5	2467.05	45	20
6	2467.05	45	20

Table 7: Oblique nozzle dimensions continued

Nozzles 5 and 6 were made from the same low carbon steel, with material properties given in Table 8. These allowed an isotropic elastic material model to be defined for the linear elastic analysis and an elastic-perfectly plastic material model for the cycle-by-cycle analysis. An EPP material model was sufficient as Procter and Flinders note that for the low carbon steel, hardening only occurs at plastic strains greater than those observed at the maximum shakedown conditions.

The weld between the nozzle and shell was not modelled. It was assumed that the weld had the same material properties as the nozzle, as this was conservative. It was also assumed that there would be no residual stress at the welds, due to the use of weld stress relief, and they were considered to be free from flaws.

Section	Material Property			
	$\boldsymbol{E\ (GPa)}$	$\boldsymbol{v}$	$\boldsymbol{\sigma_Y\ (MPa)}$	$\boldsymbol{3S_m\ (MPa)}$
Nozzle	200	0.3	265	530
Vessel	200	0.3	273	546

Table 8: Oblique nozzle material properties

3D FEA was required, as the oblique nozzle does not exhibit axisymmetric geometry. However, they are symmetrical about the mid-section, so a half section of each nozzle was modelled. To constrain the model, the cross sectional area cut by the symmetry plane had a symmetry boundary condition applied to it. Also, only part of the spherical vessel, local to the nozzle, was modelled. A local spherical coordinate system was defined and the nodes on the cut surface of the spherical vessel were constrained in the

meridional and circumferential directions, allowing the vessel freedom to expand or contract in the radial direction only, whilst preventing the vessel from rotating or experiencing rigid body motion.

The nozzles were subjected to a cyclic pressure load only with no thermal loads. The internal pressure was applied to all internal surfaces of the structure and was increased from zero to the test pressure and then back to zero over the course of a cycle. For the elastic analysis, only a single cycle was simulated. For the elastic-plastic cycle-by-cycle analysis, 25 cycles were simulated and the results history stored for each.

Both nozzles 5 and 6 were meshed with C3D10 elements in Abaqus CAE. These ten node solid tetrahedral elements were used as they allowed the complex geometry to be modelled accurately and with relative ease. Ure and Chen [111] modelled the nozzle with hexahedral elements. Typically, hexahedral elements provide a more accurate solution at a lower computational cost. In industry, the ability to obtain comparable results with a tetrahedral mesh could be advantageous where analyst time may be more valuable than computational cost. One thing that needs more consideration when dealing with tetrahedral elements is to ensure that volumetric locking does not occur. The mesh density for each nozzle can be seen in Table 9, with the actual meshes displayed in Figure 28 and Figure 29 for nozzles 5 and 6 respectively.

Oblique Nozzle	**Element Type**	**Number of Elements**
Nozzle 5	C3D10	29631
Nozzle 6	C3D10	18579

Table 9: Oblique nozzle mesh settings

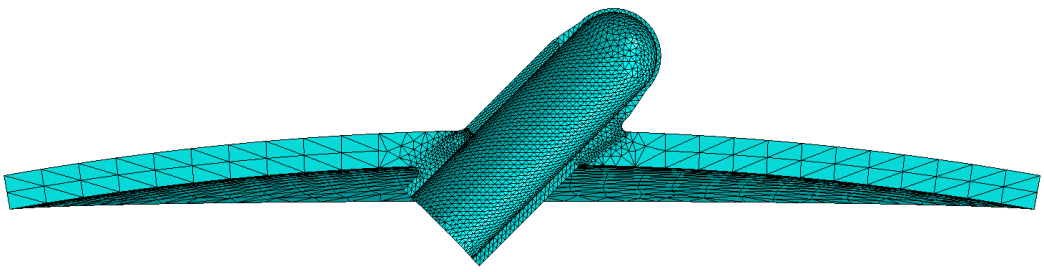

Figure 28: Nozzle 5 mesh

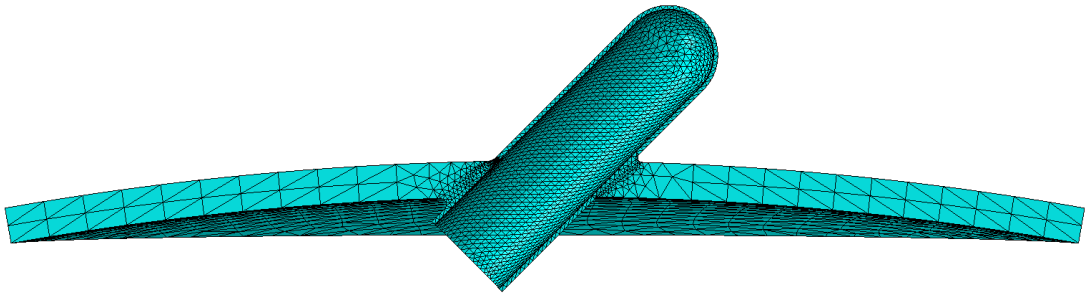

Figure 29: Nozzle 6 mesh

Local mesh refinement was used to ensure the peak stresses were captured in the areas of interest such as at the nozzle junction, fillet radius and inside surface of the nozzle. The stress in the main shell away from the nozzle was of little interest, this allowed the main vessel to be assigned a coarse mesh to maximise the efficiency of the analysis.

3.6 Thermal Shock Nozzle

A typical plant transient on a nozzle in a spherical vessel was the final component to be analysed. The structure, shown in Figure 30, has been commonly used to investigate computational shakedown and ratcheting methods [53,71,99,112] having originally been used in the DBA Manual as a benchmark problem [14]. The structure and loading conditions are included in this thesis as part of an investigation into the use of elastic and elastic-plastic DBA for combined thermal and mechanical cyclic loading. The main aim of the thermal shock nozzle study is to investigate how efficient elastic DBA is for complex design problems and, by simulating the actual cyclic response, if cycle-by-cycle elastic-plastic FEA can be used as a viable alternative to detect ratcheting in nuclear components and ensure elastic shakedown or alternating plasticity.

The nozzle-spherical vessel component used in the thermal shock analysis is shown in Figure 30 and was modelled in Abaqus CAE. As this is an axisymmetric component, a full 3D model was not required.

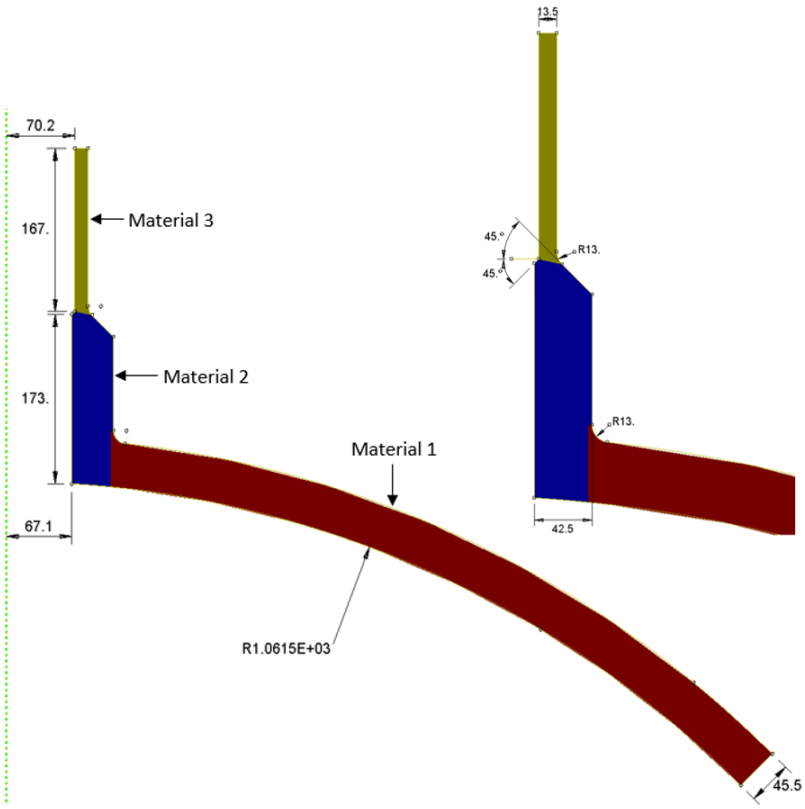

Figure 30: Nozzle geometry

The structure comprises of three different materials, given in Table 10. The material definitions were taken from the European standards for three grades of low alloy steel, originally specified for use by Rauscher[112] and also employed by Martin[71].

Material	**Grade**	**European Standard**
1	10CrMo9-10+NT	EN 10028-2
2	11CrMo9-10+QT	EN 10216-2
3	P265GH	EN 10216-2

Table 10: Thermal shock nozzle materials

Temperature dependent material properties are presented in Table 11 and the corresponding yield strengths are in Table 12.

Property	**Material**	**Temperature (°C)**			
		20	**100**	**200**	**300**
Conductivity (W/mm°C)	1,2	0.0349	0.0373	0.0382	0.0378
	3	0.051	0.0508	0.0487	0.0458
$E\ (GPa)$	1,2,3	212	207	199	192
v	1,2,3	0.3	0.3	0.3	0.3
Thermal Expansion(°C^{-1})	1,2	1.15e-5	1.21e-5	1.27e-5	1.32e-5
	3	1.19e-5	1.25e-5	1.30e-5	1.36e-5
Specific Heat (J/kg°C)	1,2,3	461	479	499	517

Table 11: Thermal shock nozzle material properties [71,112]

Property	**Material**	**Temperature (°C)**					
		20	**100**	**150**	**200**	**250**	**300**
$\sigma_Y\ (MPa)$	1	290	249	238	232	227	221
	2	355	323	312	304	296	289
	3	265	226	213	192	171	154

Table 12: Thermal shock nozzle yield strength [71,112]

A sequentially coupled thermal and structural analysis was performed. The thermal transient simulates start-up, cold shock, steady operation and shutdown. As shown in Figure 31, the entire load cycle lasted 3900s.

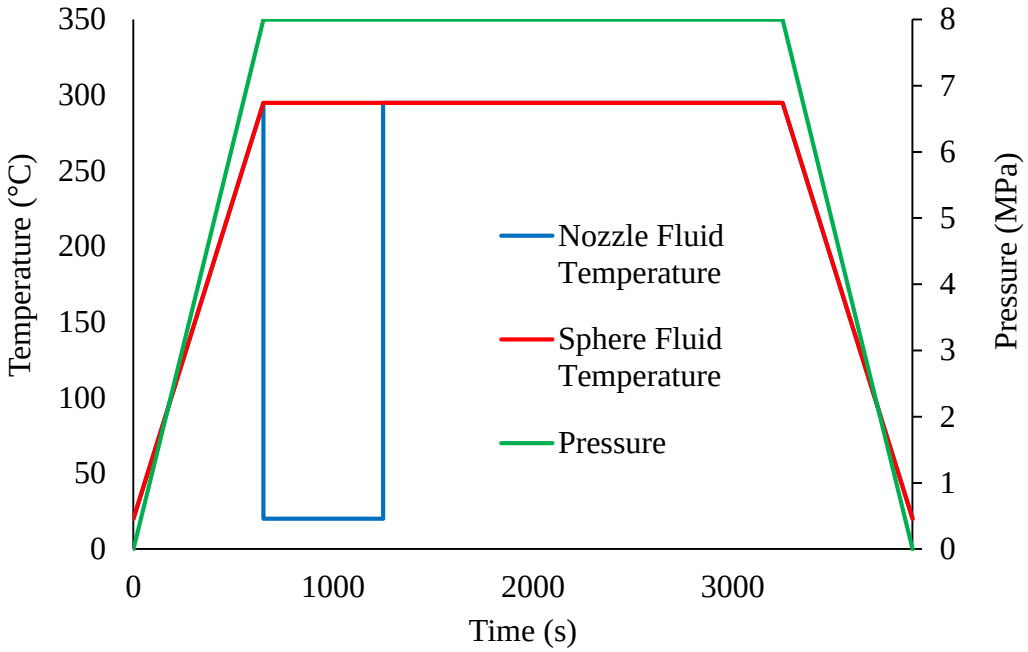

Figure 31: Nozzle transient loading

The thermal boundary conditions were defined using heat transfer coefficients applied to the inner surface of the shell and nozzle. The initial temperature of the component was set to $20℃$ and the start-up condition was simulated through a steady-state heat transfer analysis, so that the whole structure was at a temperature of $295℃$ after $650s$. The nozzle then experienced a cold shock. This was modelled as a transient heat transfer through a step change of the bulk fluid temperature and heat transfer coefficient to $0.0108\ W/mm℃$ at the inner surface of the nozzle only. The cold shock lasted for $600s$, at which point, the bulk fluid temperature was raised back to $295℃$ by changing the heat transfer coefficient back to the original value of $0.00116\ W/mm℃$. The heat transfer coefficient remained constant in the sphere at $0.00116\ W/mm℃$ for the entire duration of the simulation and the bulk fluid temperature was assumed to remain at $295℃$ in the sphere during the nozzle cold shock. Following the cold shock, the temperature was held constant for $2000s$ before simulating shutdown through a steady-state heat transfer analysis, reducing the temperature from $295℃$ to $20℃$ in the whole structure.

For the structural analysis, a displacement boundary condition was applied to the cut end of the spherical shell constraining it in the direction normal to the surface to prevent rigid body motion. The vessel was cut at an angle of 45° as the rest of the vessel was not of any interest. The pressure load was applied to the internal surfaces of the nozzle and spherical vessel with an end pressure load, once again calculated using equation (54), applied to the top face of the nozzle. The internal pressure and end pressure were ramped up in proportion from zero during start-up, held constant during the operation phase and then reduced back down to zero for shut-down. One full cycle was simulated for the elastic analysis and for the nonlinear analysis, 10 cycles were simulated. The temperature distribution obtained from the thermal analysis was used as input to both the linear elastic and non-linear analysis.

The nozzle-vessel mesh shown in Figure 32 consists of 7336 quadratic 2D axisymmetric elements with 22751 nodes. The 8 node axisymmetric element types for the thermal and structural analysis were DCAX8 and CAX8R respectively. The mesh was assumed to be of suitable quality as it is more refined than meshes used in other publications which have analysed this component [99]. A refined mesh was used to capture the maximum thermal stresses on the inside surface of the nozzle and the nozzle wall is 15 elements thick in the reinforced area.

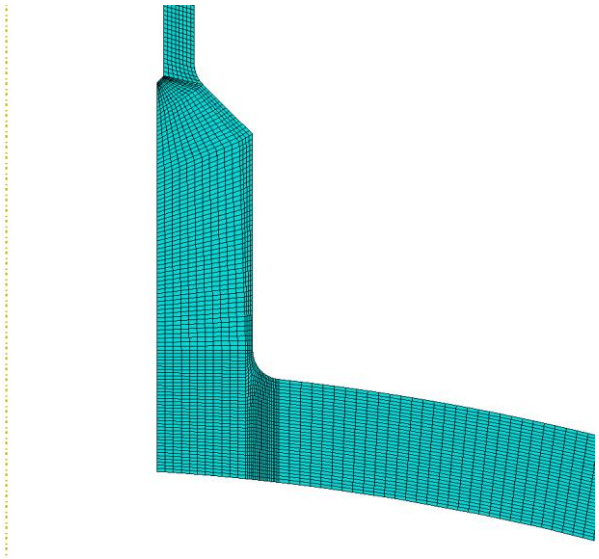

Figure 32: Thermal shock nozzle mesh

Chapter 4 Linear Elastic Analysis

Linear elastic DBA is still widely used in industry and is an ongoing topic of discussion. Although recent literature has focussed more on non-linear methods, practical issues still persist within elastic DBA and limitations exist that may not be immediately evident to the analyst.

This chapter considers application of linear elastic DBA to structural analysis of nuclear components to satisfy ASME III. The aim is to investigate design methodologies which may have become outdated or for which there is a general lack of guidance. This is of practical importance when performing analysis of nuclear components in industry.

FEA is used to calculate the elastic stress field and static and cyclic load limits are investigated for four stress linearisation methods. The theoretical basis behind the choice of linearisation method is discussed, with a detailed investigation into the individual stress component distributions which form the total linearised stress tensors.

While WRC 429 [21] provided a detailed insight into the use of stress linearisation, this investigation aims to identify how the individual stress component distributions relate to the actual stress distributions at the limit state of a structure under static or repeated loading. By considering limit state boundary conditions, one aim is to identify if the linearised stress tensor can better represent the non-linear stress distribution in thick components. Also, determining when elastic DBA is feasible and removing some ambiguity in the ASME III procedure would aid future analysts.

ASME III does not contain specific guidance on how to calculate the linearised membrane and membrane plus bending (M+B) stresses. While this allows analysts more freedom, it relies on them having experience in carrying out elastic DBA of structures. Furthermore, different analysts may have different interpretations and preferences with regards to the linearisation process, which could lead to inconsistent results for the same problem. While the linearisation procedure should not have a significant influence on the results for thin-walled components, this may not be the case for thick components. While other Codes provide more detail than ASME III, there is a general lack of consistency between them, with different Codes prescribing different methodologies. The lack of agreement between various Codes also means

that the analyst should be careful not to simply depend on integrated stress linearisation modules in commercial FE packages. Without a clear understanding of how the individual stress components are treated in the linearisation process, uncritically relying on the linearisation tools in FE packages could result in the calculation of allowable loads which do not actually satisfy the design Code they are working to.

The four linearisation methods (LMs) presented in Table 13 are investigated in this thesis. Each method is described in terms of the stress components used to construct the linearised membrane and membrane plus bending stress tensors. Linearisation of the total stress component vectors is calculated using equation (14) for membrane stress (σ_m) and equation (15) for bending stress (σ_b) for all methods in Table 13. Membrane plus bending stress components (σ_{m+b}) are calculated by summating the membrane and bending stresses at component level. It can be seen in Table 12 that some components of the stress tensors may not be linearised, in such cases the total stress component is used directly.

The LMs in Table 13 were discussed in previous work looking at the plastic collapse load of a nozzle [113]. The study begins by summarising the results from the linearisation methods for the primary stress check, then considers the individual stress component distributions in more detail and investigates the influence of elastic DBA methods on the $3S_m$ check on primary plus secondary stress for cyclic loading.

Method	Membrane Stress Tensor	M+B Stress Tensor
ASME VIII	$\boldsymbol{\sigma}_m = \begin{bmatrix} \sigma_{x,m} & \sigma_{xy,m} & \sigma_{xz,m} \\ \sigma_{xy,m} & \sigma_{y,m} & \sigma_{yz,m} \\ \sigma_{xz,m} & \sigma_{yz,m} & \sigma_{z,m} \end{bmatrix}$	$\boldsymbol{\sigma}_{m+b} = \begin{bmatrix} \sigma_{x,m} & \sigma_{xy,m} & \sigma_{xz,m} \\ \sigma_{xy,m} & \sigma_{y,m+b} & \sigma_{yz,m+b} \\ \sigma_{xz,m} & \sigma_{yz,m+b} & \sigma_{z,m+b} \end{bmatrix}$
LM 1	$\boldsymbol{\sigma}_m = \begin{bmatrix} \sigma_{x,m} & \sigma_{xy,m} & \sigma_{xz,m} \\ \sigma_{xy,m} & \sigma_{y,m} & \sigma_{yz,m} \\ \sigma_{xz,m} & \sigma_{yz,m} & \sigma_{z,m} \end{bmatrix}$	$\boldsymbol{\sigma}_{m+b} = \begin{bmatrix} \sigma_{x,m+b} & \sigma_{xy,m+b} & \sigma_{xz,m+b} \\ \sigma_{xy,m+b} & \sigma_{y,m+b} & \sigma_{yz,m+b} \\ \sigma_{xz,m+b} & \sigma_{yz,m+b} & \sigma_{z,m+b} \end{bmatrix}$
LM 2	$\boldsymbol{\sigma}_m = \begin{bmatrix} \sigma_{x} & \sigma_{xy} & \sigma_{xz} \\ \sigma_{xy} & \sigma_{y,m} & \sigma_{yz,m} \\ \sigma_{xz} & \sigma_{yz,m} & \sigma_{z,m} \end{bmatrix}$	$\boldsymbol{\sigma}_{m+b} = \begin{bmatrix} \sigma_{x} & \sigma_{xy} & \sigma_{xz} \\ \sigma_{xy} & \sigma_{y,m+b} & \sigma_{yz,m+b} \\ \sigma_{xz} & \sigma_{yz,m+b} & \sigma_{z,m+b} \end{bmatrix}$
LM 3	$\boldsymbol{\sigma}_m = \begin{bmatrix} \sigma_{x,m} & \sigma_{xy,m} & \sigma_{xz,m} \\ \sigma_{xy,m} & \sigma_{y,m} & \sigma_{yz,m} \\ \sigma_{xz,m} & \sigma_{yz,m} & \sigma_{z,m} \end{bmatrix}$	$\boldsymbol{\sigma}_{m+b} = \begin{bmatrix} \sigma_{x} & \sigma_{xy,m+b} & \sigma_{xz,m+b} \\ \sigma_{xy,m+b} & \sigma_{y,m+b} & \sigma_{yz,m+b} \\ \sigma_{xz,m+b} & \sigma_{yz,m+b} & \sigma_{z,m+b} \end{bmatrix}$

Table 13: Stress linearisation methods

Where $\boldsymbol{\sigma_m}$ is the membrane stress tensor and $\boldsymbol{\sigma_{m+b}}$ is the membrane plus bending stress tensor. Stress component, σ, subscripts are: m for membrane, $m+b$ for membrane plus bending, x, y, x for direct stresses and xy, yz, xz for shear stresses.

The ASME VIII Div 2 stress linearisation procedure states that the radial bending and in-plane shear stress components should be neglected in the bending stress tensor [21]. As the stress linearisation procedure is based on shell theory, the concepts of radial bending stress and in-plane shear bending stress have no physical meaning. However, radial and in-plane shear stress components in 3D components do exhibit non-linear distribution and this will impact the structural response, so it may be unreasonable to discount them. Therefore, part of this study is to investigate how these stress components can be integrated into the linearisation process effectively.

Out-of-plane shear stresses acting in the normal-hoop plane are also not strictly speaking bending stresses. They cause the SCL to experience torsion but ASME VIII Div 2 specifies that these torsional stresses do require consideration when calculating the bending stress tensor. It has been shown [113] that using ASME VIII Div 2 stress linearisation can actually result in a non-conservative limit pressure calculation for pressurised cylinders where $radius/thickness < 4$.This is discussed in more detail in section 4.1.1.

The procedure employed by the European Code EN 13445 involves linearising all 6 stress components. While the simplicity of this approach is an advantage in terms of practical application, apart from the work published in WRC 429, the technical basis for this has not been investigated in detail. The stress tensors for linearising all stress components are included in Table 13 and is referred to as LM 1 (i.e. Linearisation Method 1).

LM 2 is defined from work published by Li [114], which stated that only hoop, axial and out-of-plane shear stresses are valid for linearisation, to satisfy limit state surface traction boundary conditions. Li suggested in-plane shear stress should not be linearised due to the parabolic distribution it exhibits through the thickness of a structure, where the stress is actually zero at the inner and outer surfaces. Instead, the total stress in-plane shear components should be used. The radial component of the membrane and M+B stress tensors is also just the total stress component taken directly

from the FEA, as can be seen in Table 13. The reason for not linearising the radial stress is to meet the condition of $-P_i$ and 0 at the inner and outer surfaces respectively. Defining the membrane stress tensor in this manner results in a non-uniform "membrane" stress distribution through-thickness, which means that it is not strictly a membrane stress [113].

LM 3 is a combination of LM 1 and LM 2, whereby the membrane stress tensor is calculated as per LM 1 to ensure that the membrane stress is indeed the average stress through-thickness but the radial component of the M+B stress tensor is defined as per LM 2. This means that the radial surface traction boundary condition discussed by Li is still incorporated in the linearisation process but through the M+B stress tensor.

The methods in Table 13 are investigated using a custom program to calculate the linearised stress components, however, in industry it would be more practical to utilise built-in tools in commercial FE software packages such as Ansys and Abaqus. Both Ansys and Abaqus use equations (14) and (15) to calculate linearised membrane and bending stresses respectively but it is not always obvious what stress components the built-in tools are linearising by default. The stress linearisation tool in Ansys Workbench generates linearised stress results identical to that of LM 1. There is an option to disable through-thickness bending stress, similar to the ASME VIII method but there is no immediately obvious way for the analyst to disable the linearised bending stress component for in-plane shear stress. Abaqus is more comprehensive, allowing individual stress components to be selected for linearisation [72] but as discussed in section 2.2 and observed by Strzelczyk and Stojakovic [33] care must be taken as the default settings for 3D models differs to that for 2D axisymmetric models.

4.1 Stress Linearisation Methods for Plastic Collapse

4.1.1 Thick Pressurised Cylinder Elastic DBA

To highlight some of the issues with stress linearisation in the primary stress check, a thick cylinder of the same dimensions to that detailed in section 3.2 was analysed. The differences being that the stresses were calculated analytically, not using FEA, and the yield strength was specified as $\sigma_Y = 240\ MPa$.

This structure was chosen due to its simplicity and lack of complex geometrical features which could influence the stress analysis. Plastic collapse limit pressures for the pressurised cylinder were calculated analytically and then compared to the result obtained using the ASME VIII Div 2 stress linearisation method.

Lower bound limit solutions exist for thick cylinders under an internal pressure load. These are given in equations (55) and (56) and allow analytical solutions to be calculated. Both equations are derived using the Tresca failure criterion with elastic-perfectly plastic material behaviour assumed. The exact limit solution is given by equation (55), which adopts a logarithmic distribution through-thickness, whereas equation (56) assumes a linear distribution.

$$P_{L,exact} = \sigma_Y \ln\left(\frac{R_o}{R_i}\right) \tag{55}$$

$$P_{L,linear} = \sigma_Y \left(1 - \frac{R_i}{R_o}\right) \tag{56}$$

Figure 33 plots the exact and linear analytical solutions and the ASME VIII Div 2 linearised stress solution for cylinders of increasing thickness. It can be seen clearly that the results calculated using ASME VIII Div 2 linearisation diverge from the exact solution as the thickness is increased.

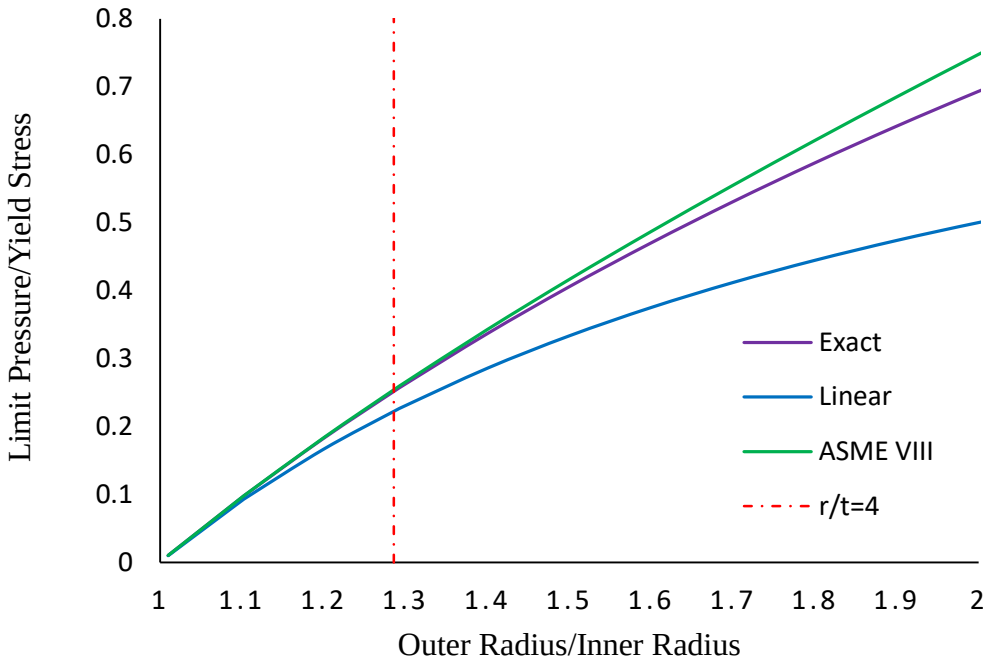

Figure 33: Pressurised cylinder limit solutions

To identify why this occurs, the elastic and plastic stress distributions through thickness were investigated. A 100 mm thick cylinder vessel with a radius to thickness ratio $r/t = 2.5$ was subject to a constant internal pressure of $P_i = 97.3\ MPa$. This value for P_i was determined using equation (55) as the limit pressure for a cylinder of these dimensions and is used as the load in this case because it is the limit state that is of most interest.

The through-thickness elastic and plastic stress distributions were calculated analytically for a cylinder with radius r, using equations derived from the Lamé equations in (57) and (58) and applying suitable limit state boundary conditions to find constants A and B.

$$\sigma_x = A - \frac{B}{r^2} \tag{57}$$

$$\sigma_z = A + \frac{B}{r^2} \tag{58}$$

The radial (σ_x), axial (σ_y) and hoop (σ_z) stress distributions were plotted in Figure 34 for both elastic and elastic-perfectly plastic material properties, showing how the distributions vary.

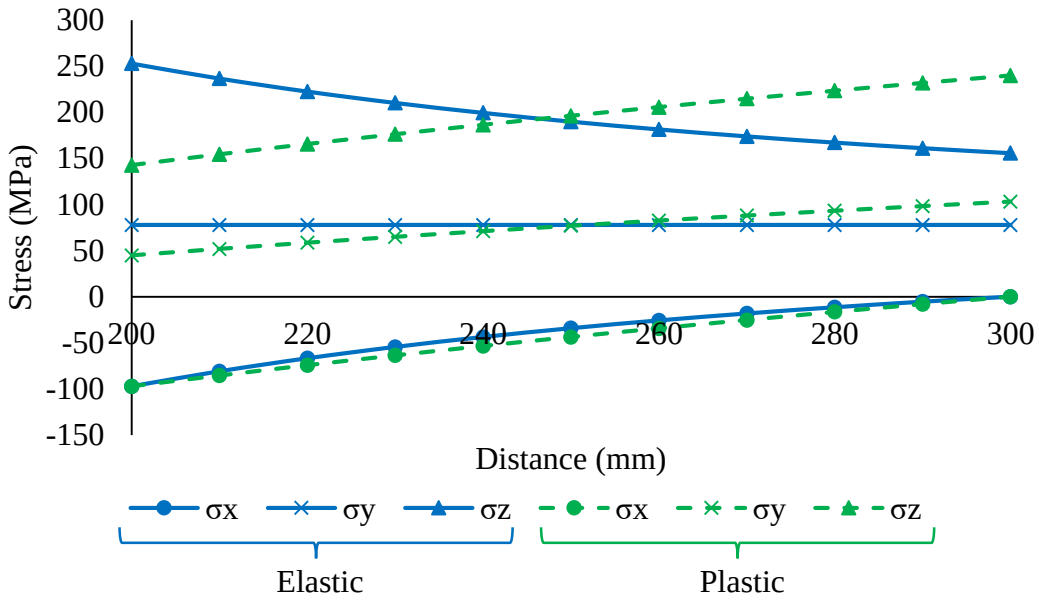

Figure 34: Elastic and plastic stress distributions in a pressurised cylinder

Performing ASME VIII Div 2 stress linearisation on the $100mm$ thick cylinder, the allowable pressure is calculated as $P_a = 66.67\ MPa$. The total and linearised stress intensity distributions along a SCL dissecting the wall of the cylinder are shown in Figure 35. Linearised stress intensity plots for each LM in Table 13 are presented to give a clear visualisation that there are noticeable differences in the stress results obtained from each method.

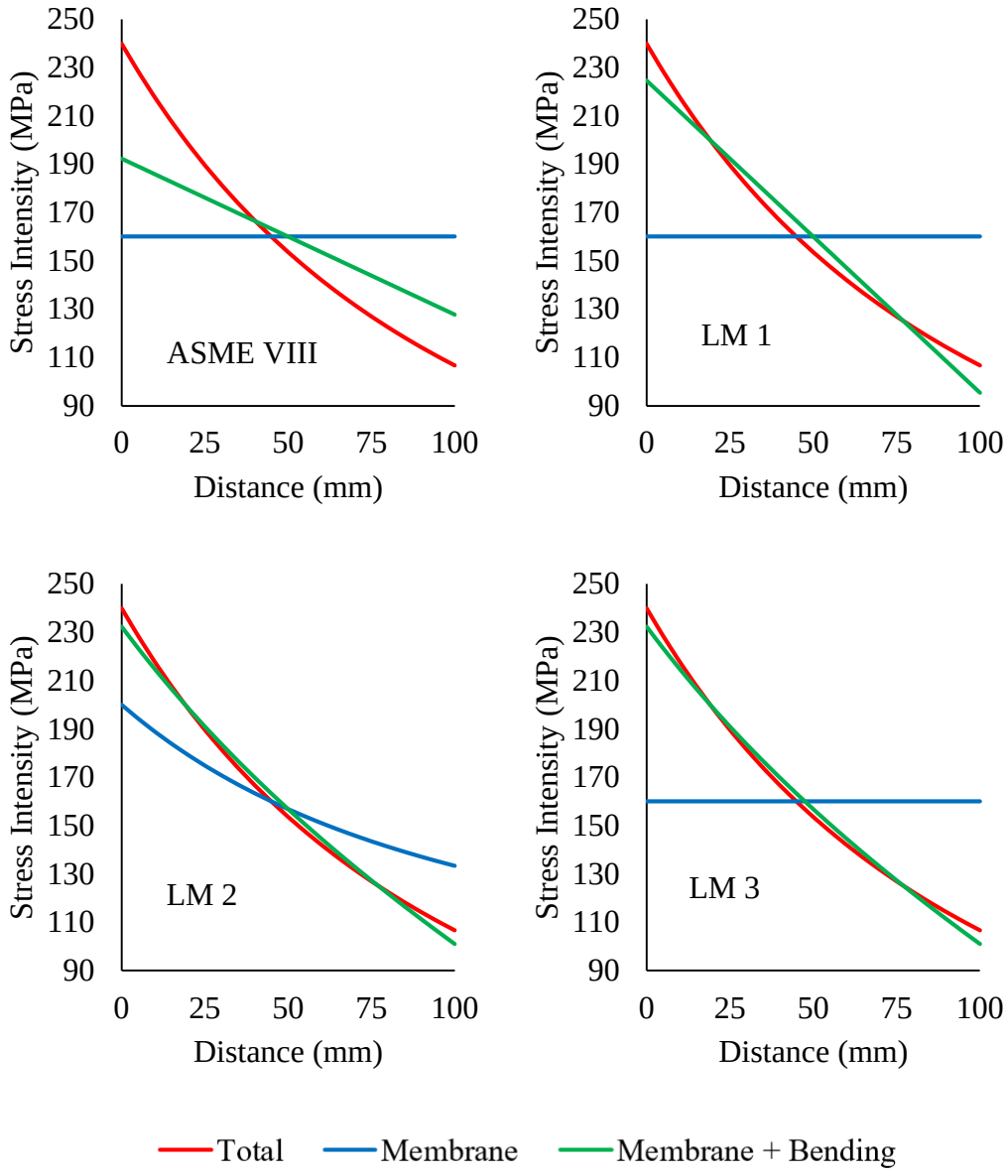

Figure 35: Linearised stress intensity distributions for pressurised cylinder

The hoop, radial and axial membrane stress component distributions plotted along the SCL are shown in Figure 36, highlighting that there is a difference in the LM 2 membrane stress in the radial direction.

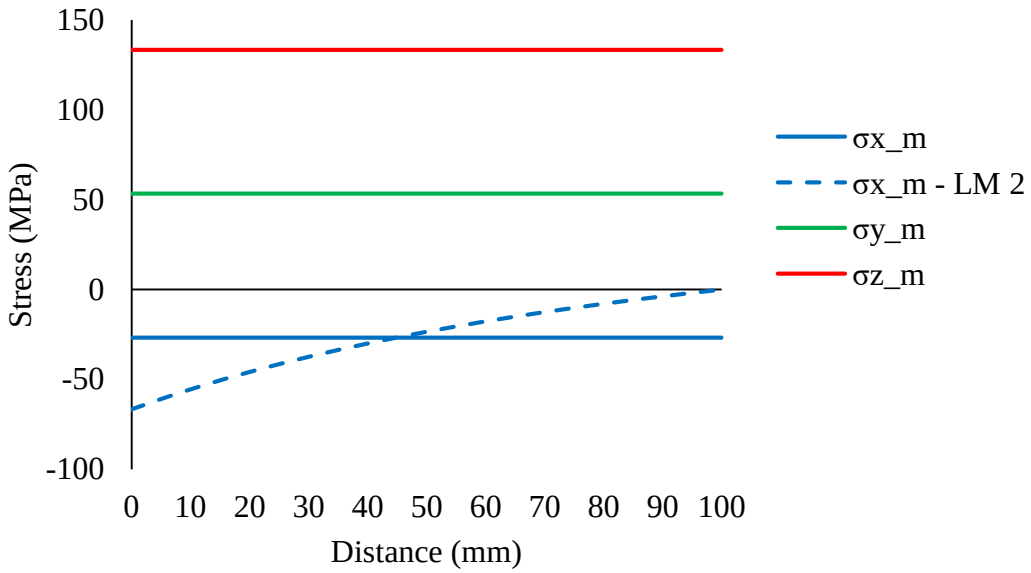

Figure 36: Linearised stress components for pressurised cylinder

The hoop, radial and axial M+B stress component distributions through thickness calculated using each LM are displayed in Figure 37.

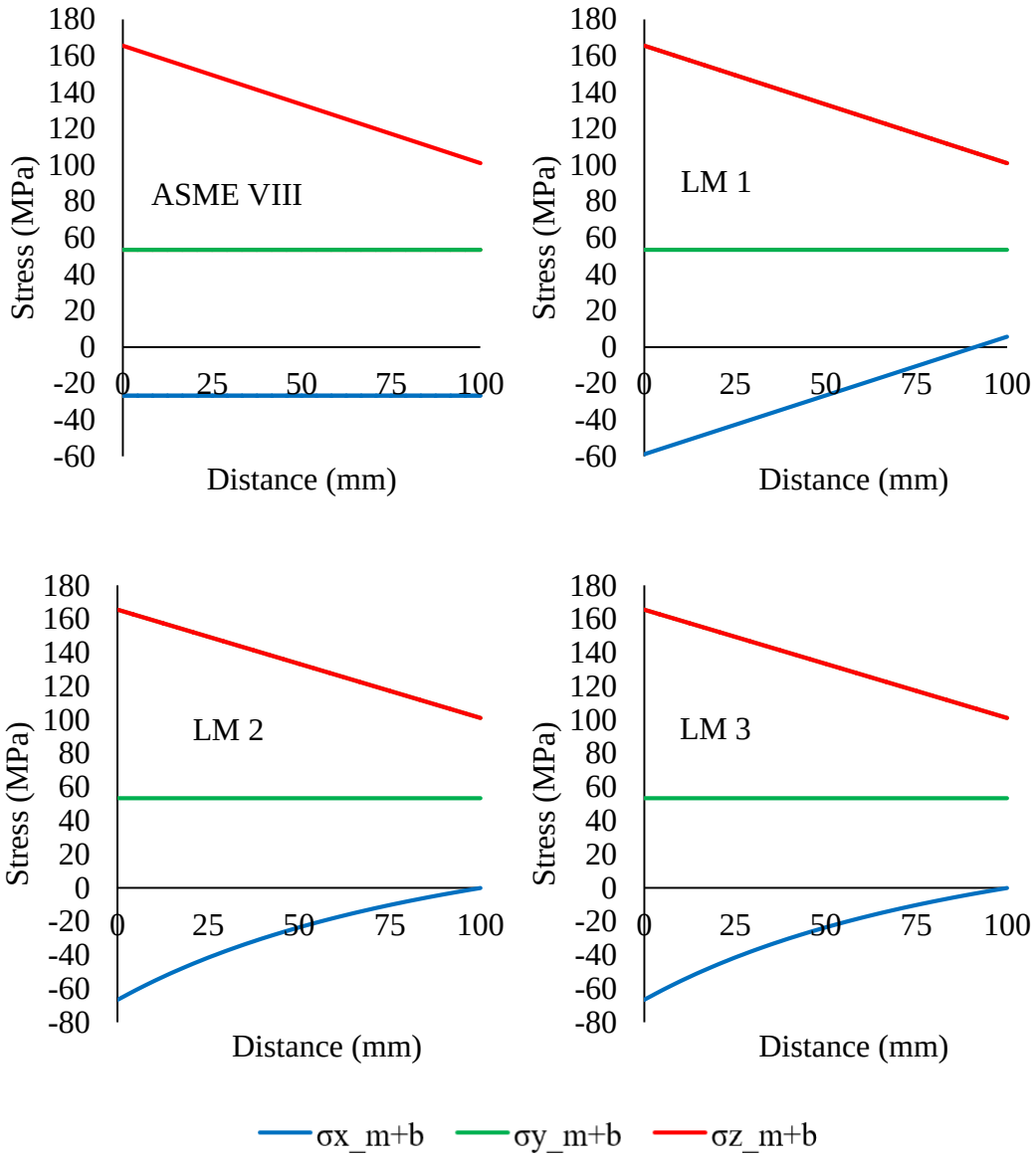

Figure 37: M+B stress components for pressurised cylinder

4.1.2 Light Water Reactor Nozzle DBA

Elastic FEA of the LWR nozzle detailed in section 3.2 was conducted using Ansys Workbench. The design pressure of the component was specified as 17 MPa and Figure 38 displays the elastic Tresca stress intensity contour plot at this design pressure for the full 3D nozzle.

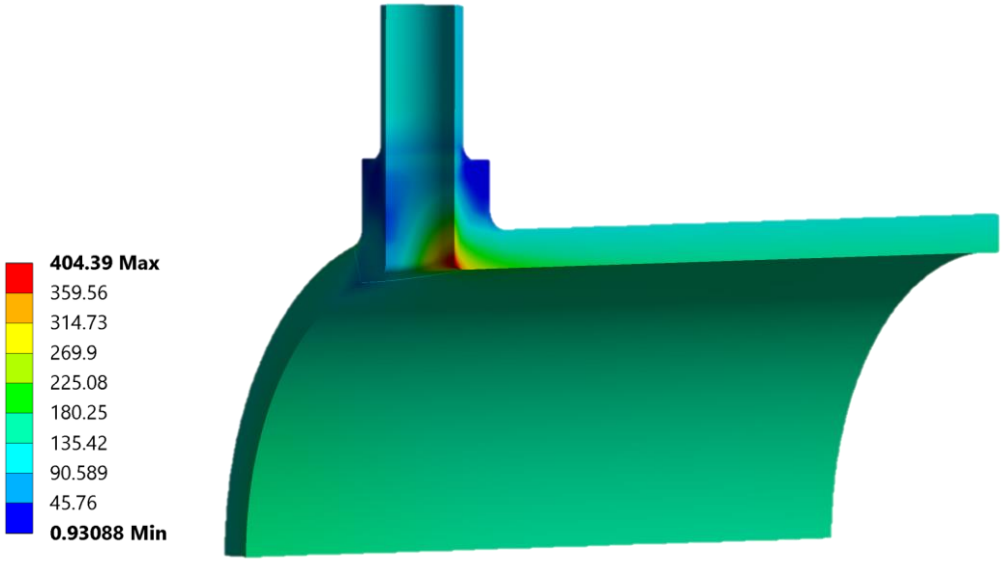

Figure 38: Elastic stress intensity contour plot of LWR nozzle

The CORDEL Benchmark [107] specifies several SCLs to be considered. Here, the SCLs in the vessel and pipe regions remote from the nozzle opening are not considered. Instead, linearised stress results at SCLs concentrated around the ring juncture region have been investigated because this is where the critical location in nozzle-vessel intersections tends to be. However, in practice for a full DBA assessment, more SCLs should be considered. The SCL placement in the nozzle model is shown in Figure 39. The tags indicate the start and endpoint of each SCL and the arrow indicates the direction of the local coordinate system parallel to the line.

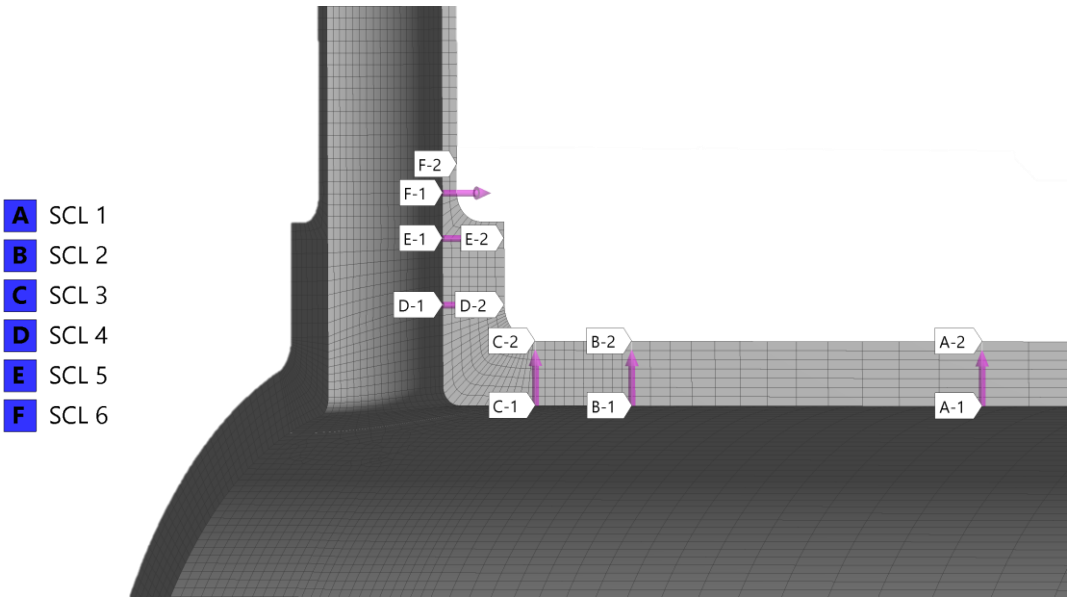

Figure 39: SCL locations on LWR nozzle model

Linearised membrane and M+B stress results for the 3D nozzle were calculated at each SCL for each LM in Table 13. The stresses were then classified appropriately as per ASME III. The linearised membrane stress in the shell, just outside the transition region, was the greatest for each LM. This meant SCL 3 is taken as the point where plastic collapse will occur first. The linearised Tresca stress intensity distributions at SCL 3 for each linearisation method are displayed in Figure 40 and the allowable pressures are shown in Table 14.

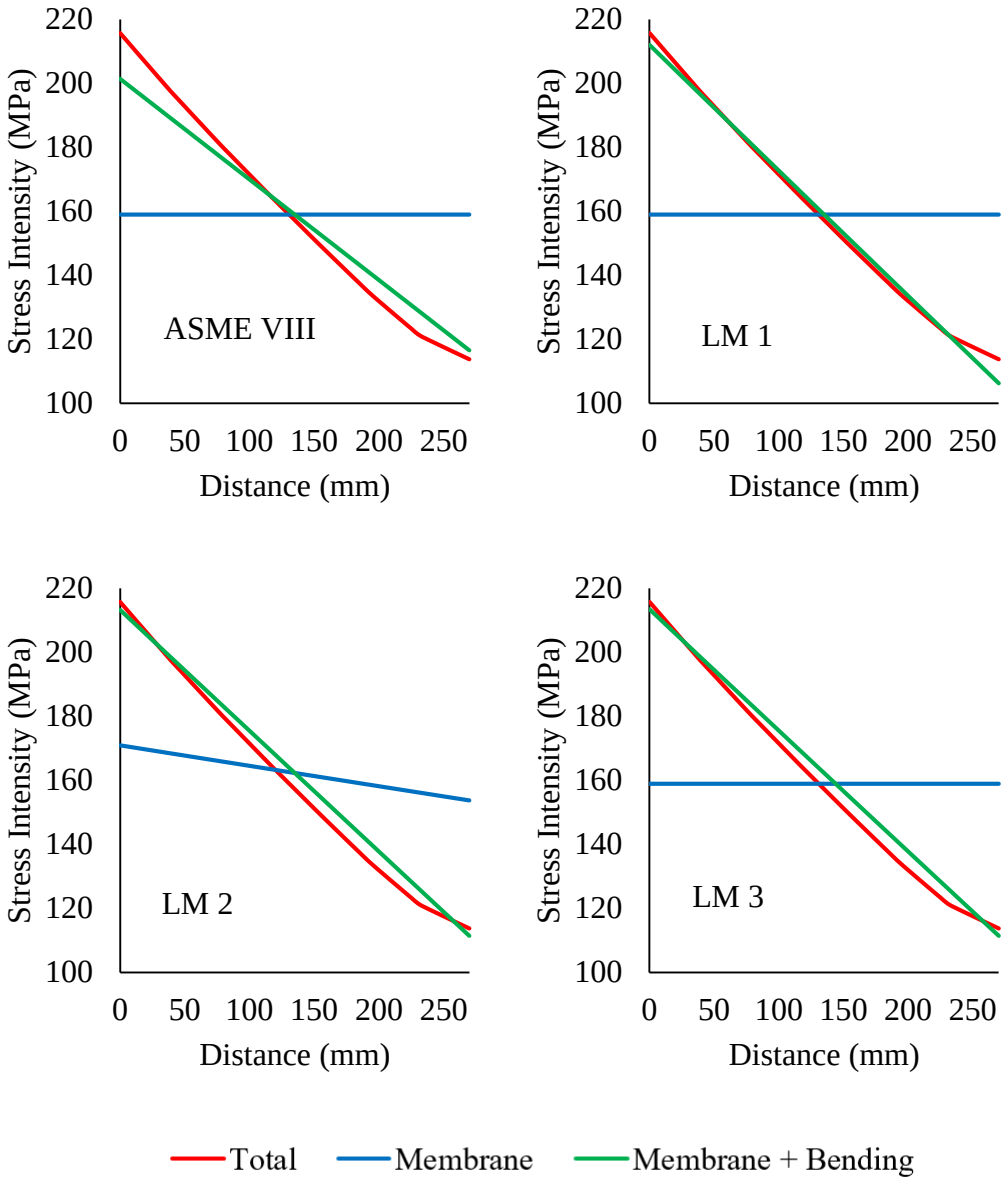

Figure 40: Linearised stress intensity distributions for LWR nozzle

Method	**P_m (MPa)**	**SCL**	**P_a (MPa)**	**P_L (MPa)**
ASME VIII	158.99	3	19.67	31.22
LM 1	158.99	3	19.67	31.22
LM 2	170.90	3	18.30	29.05
LM 3	158.99	3	19.67	31.22

Table 14: 3D LWR Elastic DBA allowable pressure results

4.1.3 Tubesheet Elastic DBA

Elastic FEA of the tubesheet described in section 3.4 was carried out in Ansys Workbench. A pressure load of 68.95 MPa (10,000 psi) was applied to the inner annulus as shown in Figure 25 and the Tresca stress intensity plot at this load is shown in Figure 41.

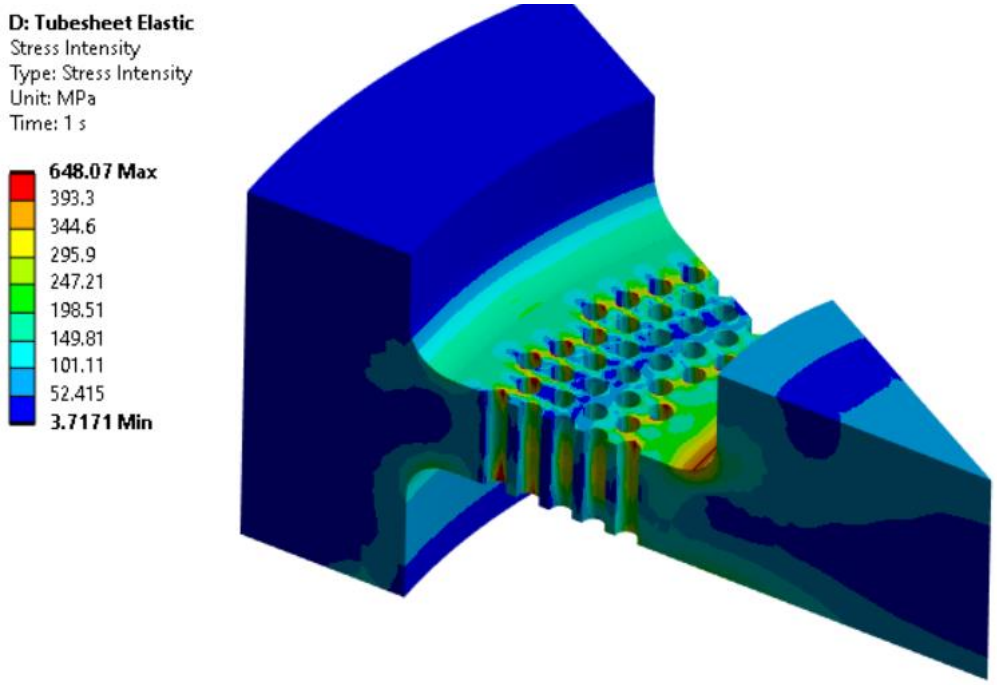

Figure 41: Elastic stress intensity plot for tubesheet

SCLs were placed through the thickness of the tubesheet on the inner row of penetrations as shown in Figure 42. Three locations across the ligament were assessed as the ASME stress classification guidelines for perforated shells specify that primary bending stress be taken as the gradient through the thickness of the tubesheet but averaged along the width of the ligament [7,23].

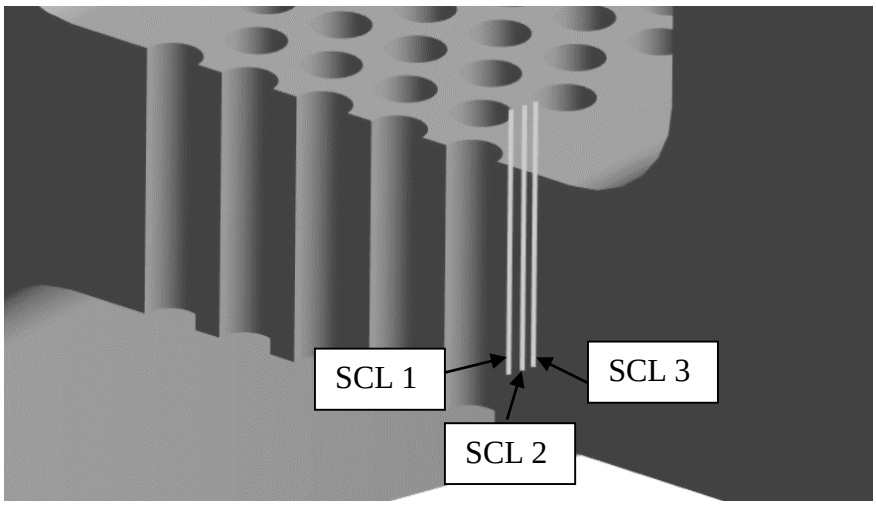

Figure 42: SCL locations for tubesheet model

Defining the allowable M+B stress as $1.5S_m = 393.3\ MPa$, tubesheet collapse loads are calculated for each LM and presented as a pressure (P_L) and force in Table 15, where $P_m + P_b$ is the linearised primary membrane plus bending stress.

Method	**P_m+P_b (MPa)**	**P_L (MPa)**	**Collapse Force (kN)**
ASME VIII	385.87	70.27	2991.22
LM 1	376.67	71.99	3064.26
LM 2	328.93	82.44	3509.02
LM 3	387.90	69.91	2975.61

Table 15: Tubesheet elastic DBA results

4.2 Stress Linearisation Methods for the Prediction of Shakedown

To expand on the findings of section 4.1, the impact each LM has on the $3Sm$ primary plus secondary stress check for determining the onset of alternating plasticity was investigated. The effects of cyclic loading to determine which linearisation method predicts the elastic shakedown load with greatest accuracy is studied for the oblique nozzles, thick cylinder and thermal-shock nozzle. Elastic DBA results for cyclic pressure loading of oblique nozzles are validated against published experimental results and elastic-plastic FEA before finding the effects of a cyclic temperature distribution on a pressured cylindrical vessel. Finally, the accuracy of each linearisation method in finding the elastic shakedown limits of the thermal-shock nozzle, subject to a transient load representative of nuclear power plant conditions, is investigated.

4.2.1 Oblique Nozzle Elastic DBA

The geometry definition, material properties, boundary and loading conditions for the FEA of oblique nozzles 5 and 6 are presented in section 3.5. The elastic Tresca stress intensity contour plots for each nozzle at an internal test pressure $P_i = 4\ MPa$ are shown in Figure 43 and Figure 44 respectively. This corresponds to the maximum stress state over the cycle and highlights the regions experiencing high stress. Elastic FEA is required to obtain the stresses prior to post-processing but the contour plots also provide an indication as to where SCLs should be located to capture the required stress components. It should be noted that the maximum linearised stress range is not necessarily located at the exact location on the structure as the highest total stress, hence why multiple SCLs are required. Also, Abaqus FE Code was used to obtain the stress results for the oblique nozzle investigation.

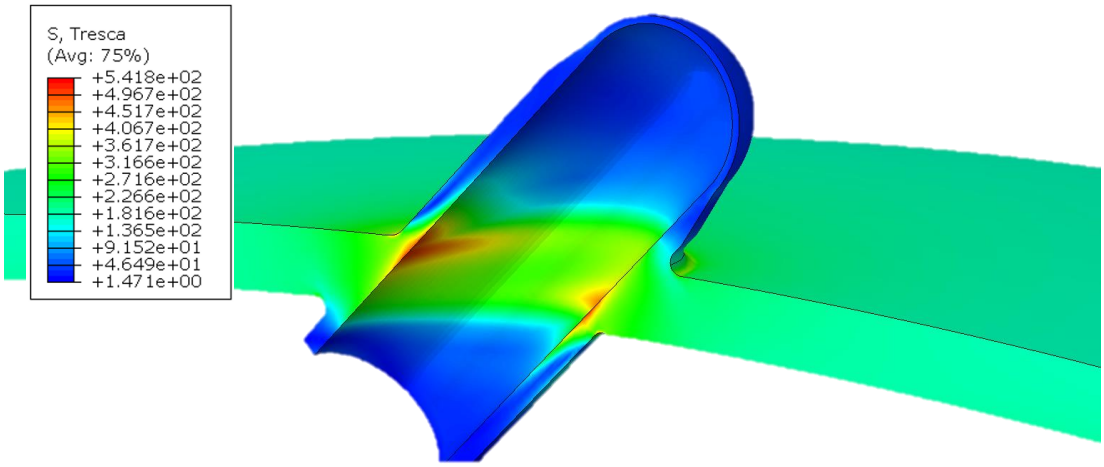

Figure 43: Elastic stress intensity distribution in nozzle 5

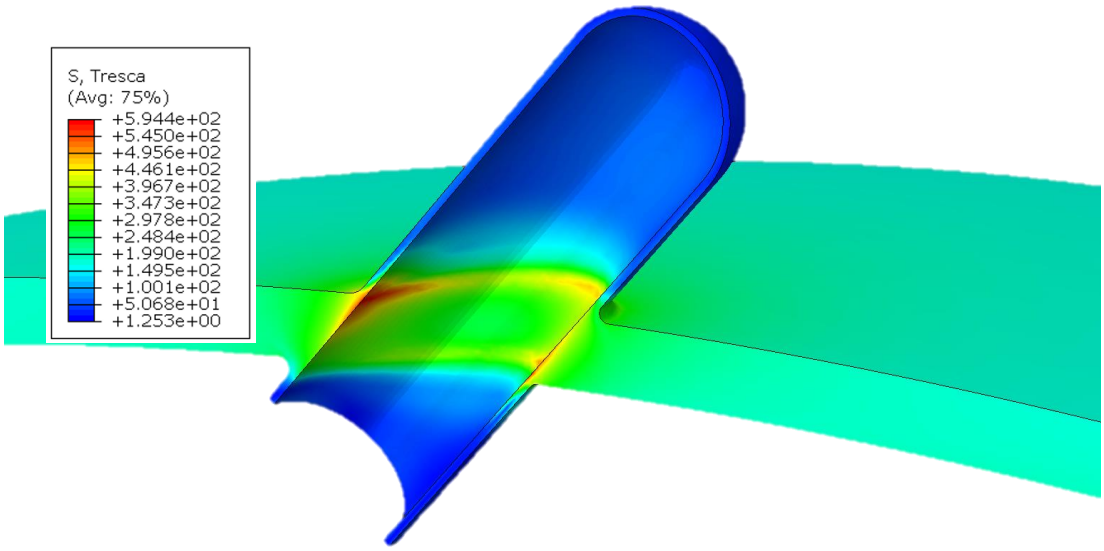

Figure 44: Elastic stress intensity distribution in nozzle 6

To satisfy the requirements of ASME III, $\Delta(P+Q)$ was calculated for a number of SCLs in each nozzle. The edge of the ring juncture was defined as being at the end of the blend radius and so SCL 1 is located in this location for both nozzles, as shown in Figure 45.

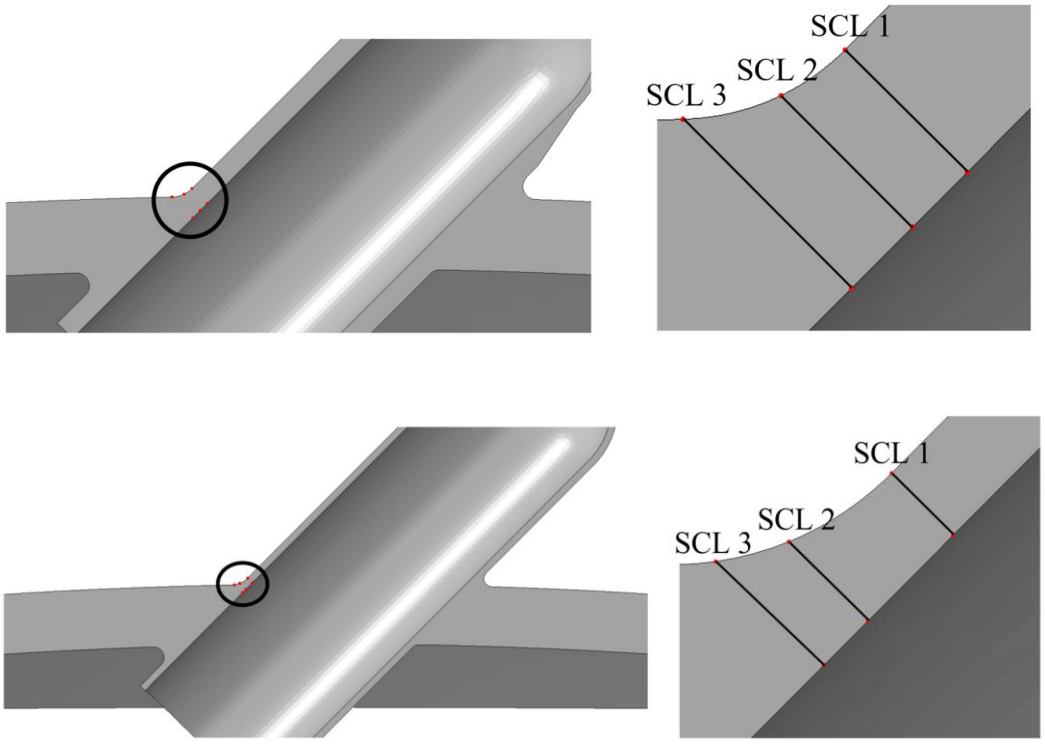

Figure 45: SCL placement in nozzles 5 and 6

The maximum values for $\Delta(P+Q)$ and the elastic shakedown limit pressure, P_{SD}, calculated using each LM are shown in Table 16 to Table 19 for both nozzles. Only results for SCL 1 and SCL 2 are presented as the stresses at SCL 3 were not as high as SCL 2 for any LM.

The shakedown limit for each method is calculated using the twice yield criteria. This is equal to using $3S_m$ in this case as $S_m = \frac{2}{3}\sigma_Y$.

$3S_m$ can be taken from the material properties presented in Table 8 for the oblique nozzles. The shakedown limit (P_{SD}) is then calculated using equation (59).

$$P_{SD} = P_i \times \frac{3S_m}{\Delta(P+Q)} \tag{59}$$

Method	**SCL**	$\Delta(\boldsymbol{P+Q})$ $(\boldsymbol{MPa})$	$\boldsymbol{P_{SD}}$ $(\boldsymbol{MPa})$	**Error to BNL (%)**
ASME VIII	1	507.78	4.18	13.38
LM 1	1	497.93	4.26	11.67
LM 2	1	485.04	4.37	9.32
LM 3	1	512.22	4.14	14.13

Table 16: Nozzle 5 linearised stress results at SCL 1

Method	**SCL**	$\Delta(\boldsymbol{P+Q})$ $(\boldsymbol{MPa})$	$\boldsymbol{P_{SD}}$ $(\boldsymbol{MPa})$	**Error to BNL (%)**
ASME VIII	2	539.98	3.93	18.55
LM 1	2	500.98	4.23	12.20
LM 2	2	497.05	4.27	11.51
LM 3	2	502.27	4.22	12.43

Table 17: Nozzle 5 linearised stress results at SCL 2

Method	**SCL**	$\Delta(\boldsymbol{P+Q})$ $(\boldsymbol{MPa})$	$\boldsymbol{P_{SD}}$ $(\boldsymbol{MPa})$	**Error to BNL (%)**
ASME VIII	1	535.88	3.96	11.69
LM 1	1	547.80	3.87	13.62
LM 2	1	536.38	3.95	11.78
LM 3	1	548.20	3.87	13.68

Table 18: Nozzle 6 linearised stress results at SCL 1

Method	**SCL**	$\Delta(\boldsymbol{P+Q})$ $(\boldsymbol{MPa})$	$\boldsymbol{P_{SD}}$ $(\boldsymbol{MPa})$	**Error to BNL (%)**
ASME VIII	2	613.38	3.46	22.85
LM 1	2	583.63	3.63	18.92
LM 2	2	580.91	3.65	18.54
LM 3	2	583.67	3.63	18.93

Table 19: Nozzle 6 linearised stress results at SCL 2

The allowable elastic shakedown pressures for each method are plotted in Figure 46 and Figure 47 for nozzles 5 and 6 respectively. The BNL experimental result [4] is included in the figures as the solid red line. The lower bound (LB) and upper bound (UB) results from Ure and Chen [111] are plotted as the dashed purple and solid orange lines respectively.

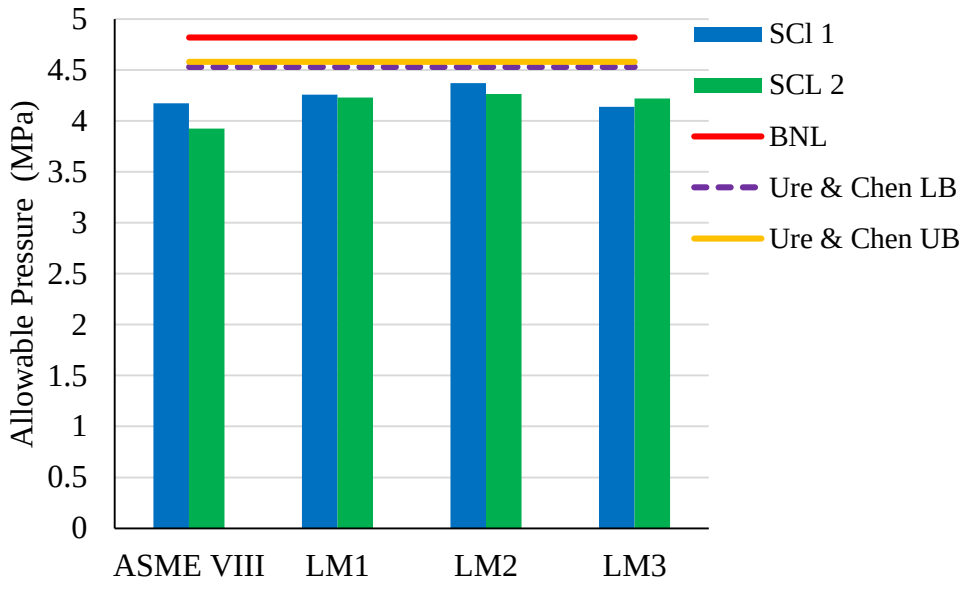

Figure 46: Allowable pressure loads for nozzle 5

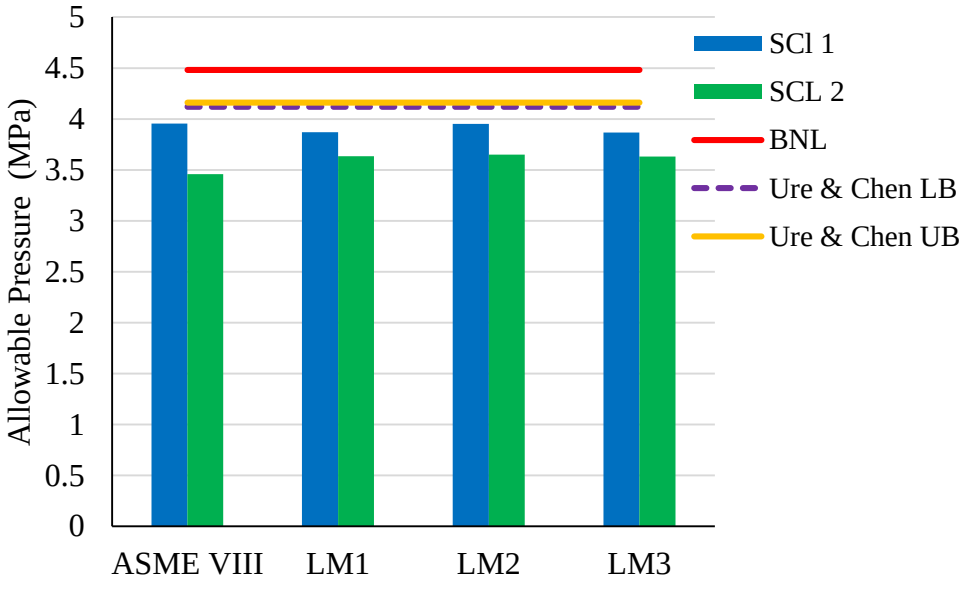

Figure 47: Allowable pressure loads for nozzle 6

4.2.2 Thick Cylinder Under Cyclic Thermal Loading DBA

To determine how the $3Sm$ design limit on $\Delta(P+Q)$ for nuclear components under combined pressure and thermal loading can be represented most accurately using stress linearisation methods, a problem similar to that of the Bree cylinder [6] was investigated. The $100mm$ thick cylinder detailed in section 3.2 was analysed when subject to a cyclic thermal load and constant pressure. This meant a sequentially coupled thermal-stress analysis was required. The heat transfer was simulated first, with results stored for inner wall temperatures of 100℃, 250℃, 400℃, 550℃, and 700℃. The temperature distribution at 700℃ is presented in Figure 48.

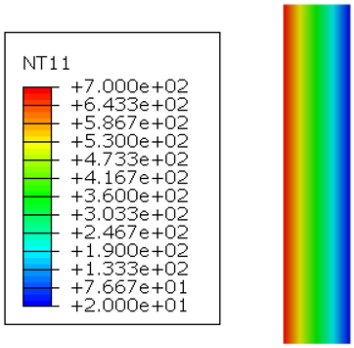

Figure 48: Temperature distribution in thick cylinder

Thermal analysis results were used to create predefined field boundary conditions for the structural analyses. An internal pressure of $100\,MPa$ is applied and the temperature cycled between 20℃ and 700℃ on the inside surface. The elastic Tresca stress intensity at the start and at the peak of the thermal cycle is shown in Figure 49.

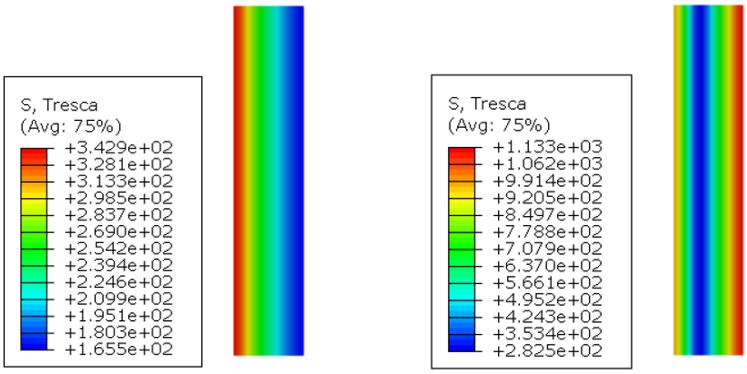

Figure 49: Elastic stress intensity contour plots of thick cylinder

A SCL was defined through-thickness and the stress components were extracted. The linearised primary plus secondary stress range values were calculated as per ASME III and for each LM. The plot in Figure 50 shows, for a fixed internal pressure of 100 MPa, the cyclic thermal load and corresponding stress range, with the horizontal line denoting the allowable stress intensity range calculated as $3Sm$.

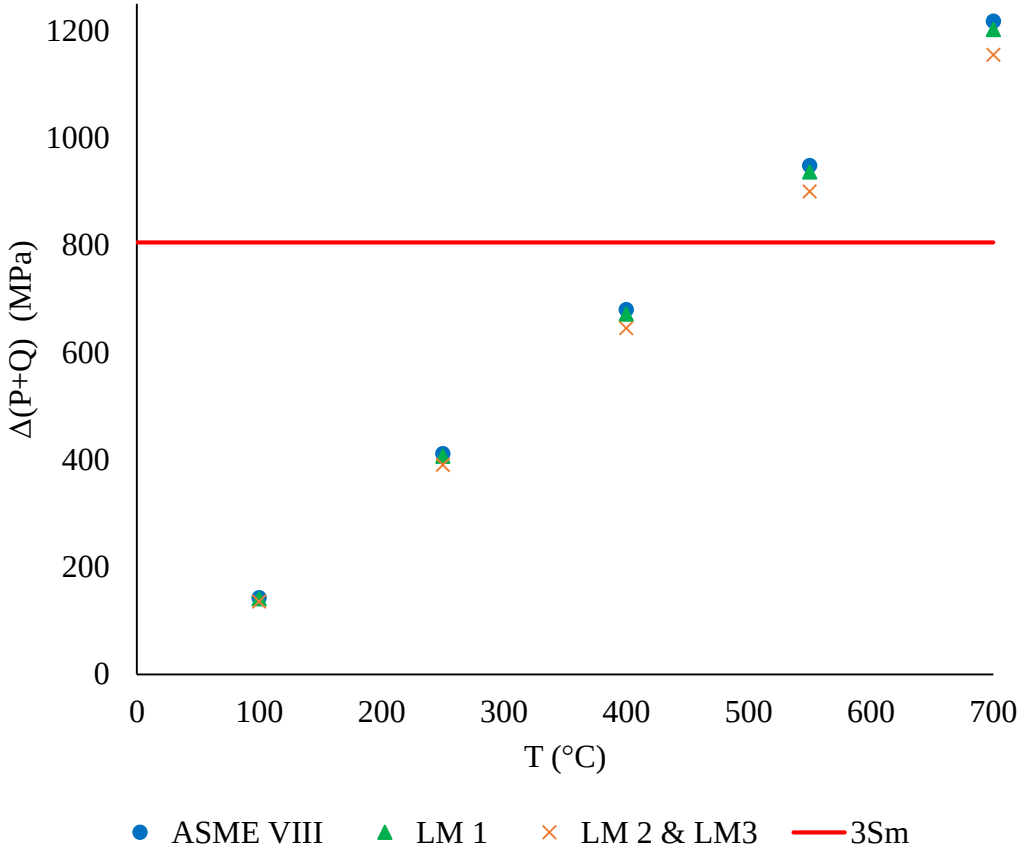

Figure 50: Elastic stress intensity range vs max temperature plot for the thick cylinder

The primary and secondary stress intensity results were normalised against the yield strength of the material and plotted on the Bree diagram in Figure 51. Each marker shape indicates the thermal load and the linearisation method is depicted using the following colour coded key:

- Blue – ASME VIII
- Green – LM 1
- Orange – LM2 & LM 3

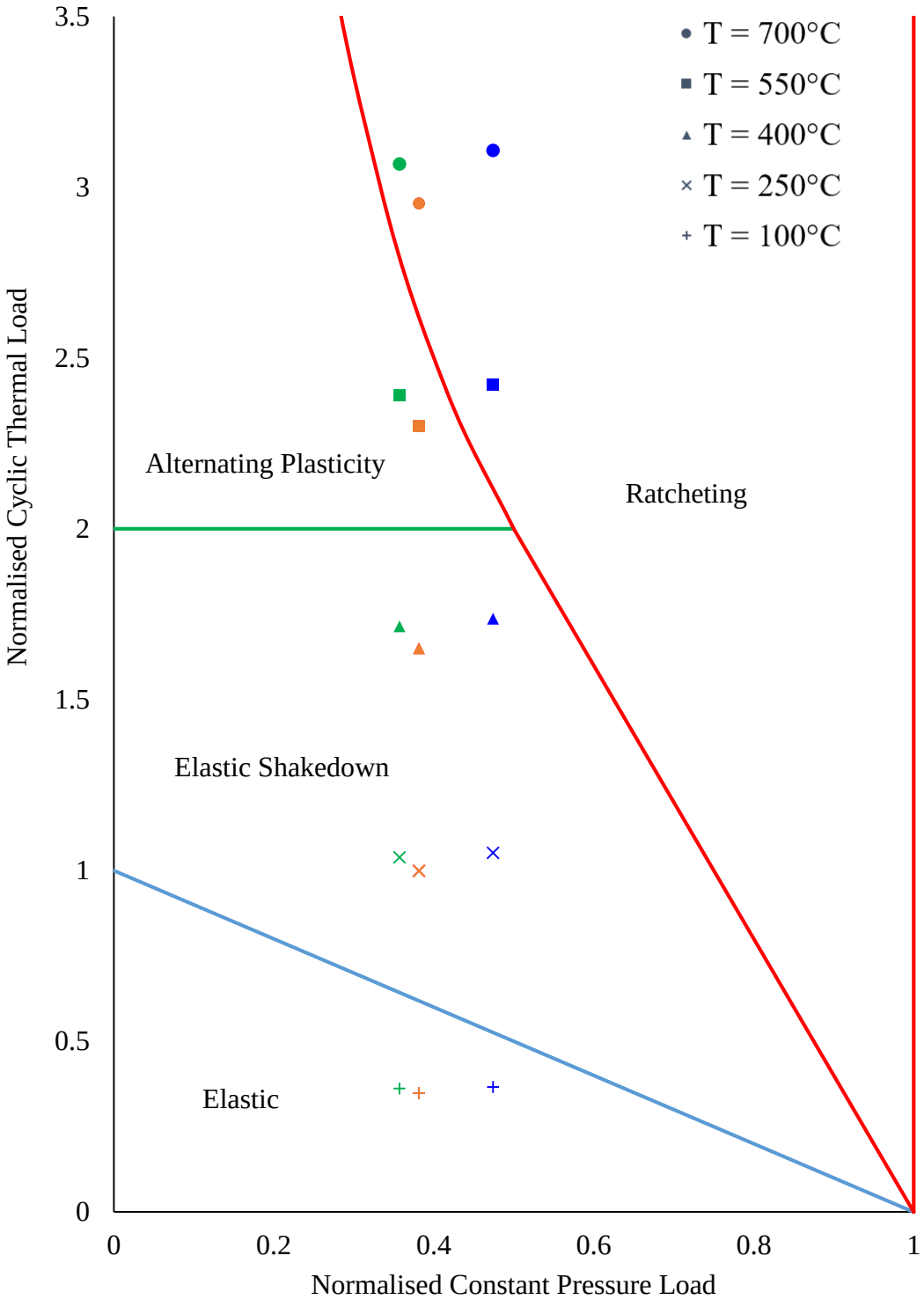

Figure 51: Thick cylinder elastic stress results plotted on a Bree diagram

4.2.3 Thermal-Shock Nozzle Elastic DBA

The final elastic analysis investigated the stress intensity ranges for the nozzle in a spherical vessel detailed in section 3.6. It was subject to a cyclic thermal and mechanical transient typical of nuclear power plant conditions and, as with the analysis of the cylinder, this was simulated using a sequentially coupled thermal and structural FEA. The nodal temperature distributions for a cold fluid injection of 20℃ are shown in Figure 52 and are consistent with the results found by Martin [71].

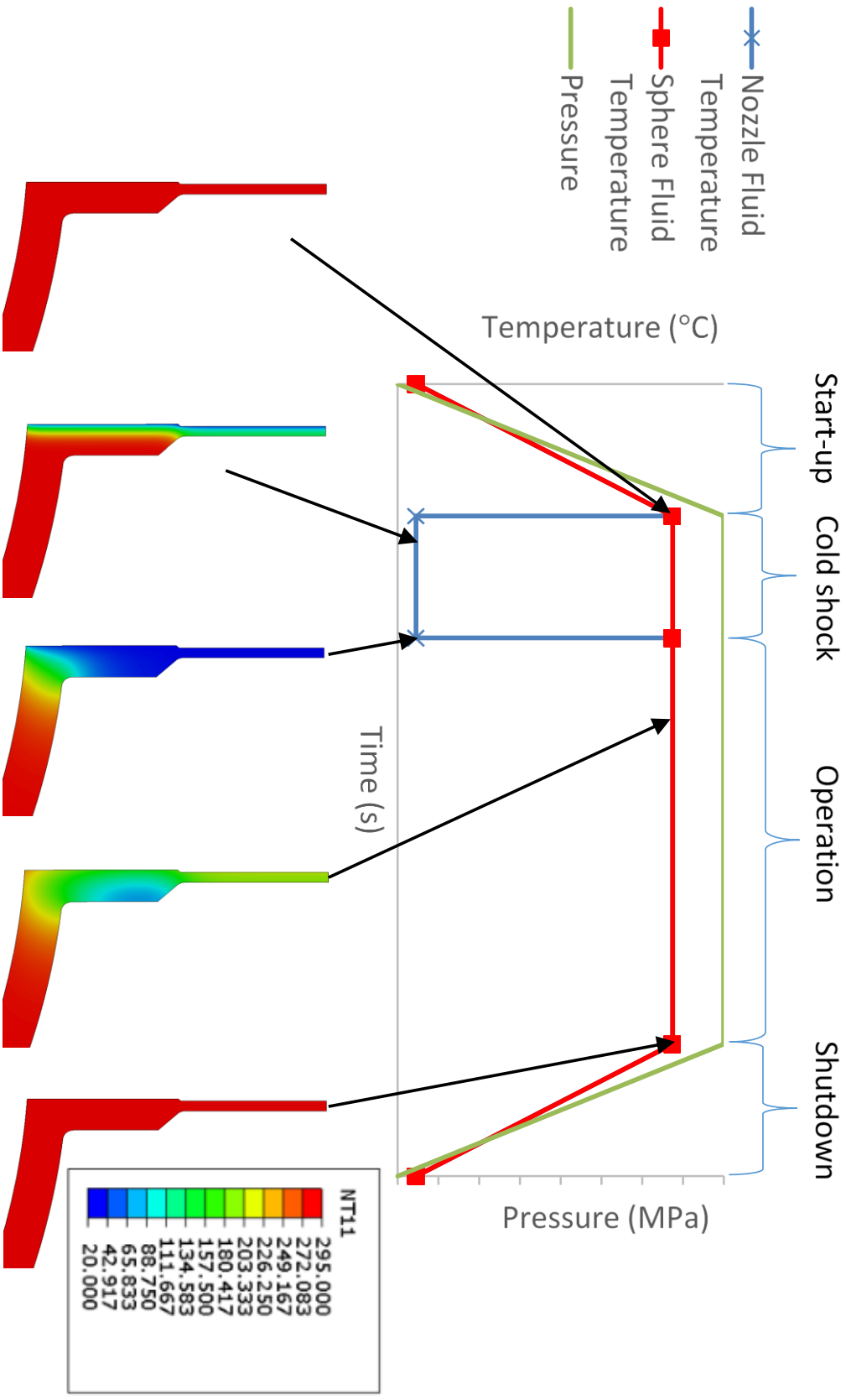

Figure 52: Nodal temperature distribution in the nozzle over one thermal cycle

The pressure load was applied and the temperature distribution was superposed onto the model during the structural analysis. The elastic stress intensity was stored at a number of points over the cycle and the maximum primary plus secondary stress range was calculated as per ASME III Article XIII-2420 along predefined SCLs in Figure 53.

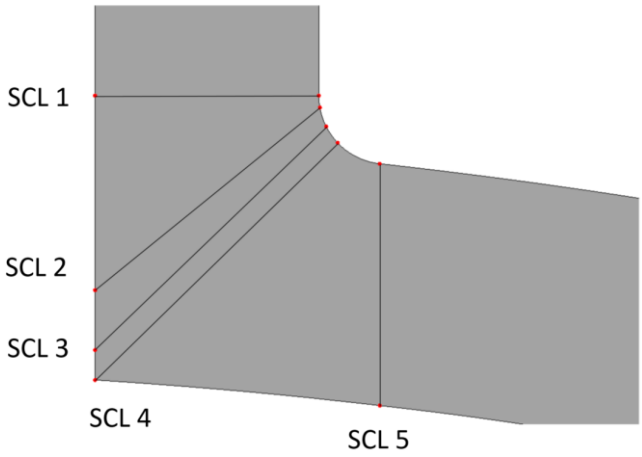

Figure 53: SCL placement in thermal-shock nozzle

A parametric study was conducted and results were gathered for a range of thermo-mechanical load combinations. For an internal pressure (P_i) of 8MPa, the allowable cold shock temperatures (T_c) calculated for each linearisation method are presented in Table 20. T_c is the temperature of the fluid entering the hot nozzle.

Method	**SCL**	$\boldsymbol{P_i}$ $(\boldsymbol{MPa})$	$\boldsymbol{T_c}$ (℃)
ASME VIII	2	8	107.85
LM 1	3	8	79.06
LM 2	3	8	90.15
LM 3	3	8	91.65

Table 20: Allowable thermal shock loads (T_c) for each linearisation method

The primary plus secondary stress ranges for different cold shock temperatures for each LM at SCL 3 is presented in Figure 54. These results are for an internal pressure load of 8 MPa.

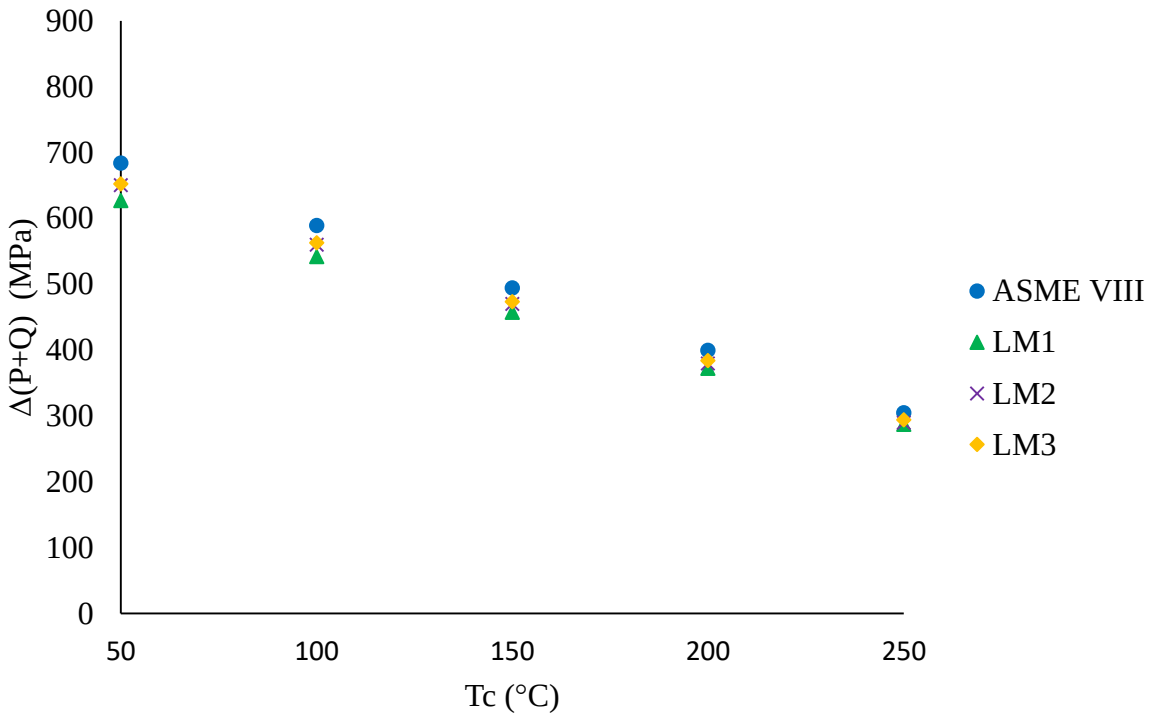

Figure 54: Calculated $\Delta(P+Q)$ when $P_i = 8\ MPa$ at SCL 3

Figure 55 to Figure 57 shows the internal pressure (P_i) and corresponding cold shock temperature (T_c) resulting in $(\Delta P + Q) = 3S_m$ for each linearisation method at SCLs 1, 2 and 3. Each point indicates the load combination at which elastic shakedown will cease and alternating plasticity or ratcheting will occur i.e. the lowest possible T_c for each P_i to satisfy $3Sm$. Results at SCLs 4 and 5 are not presented as the stress ranges were not as extreme.

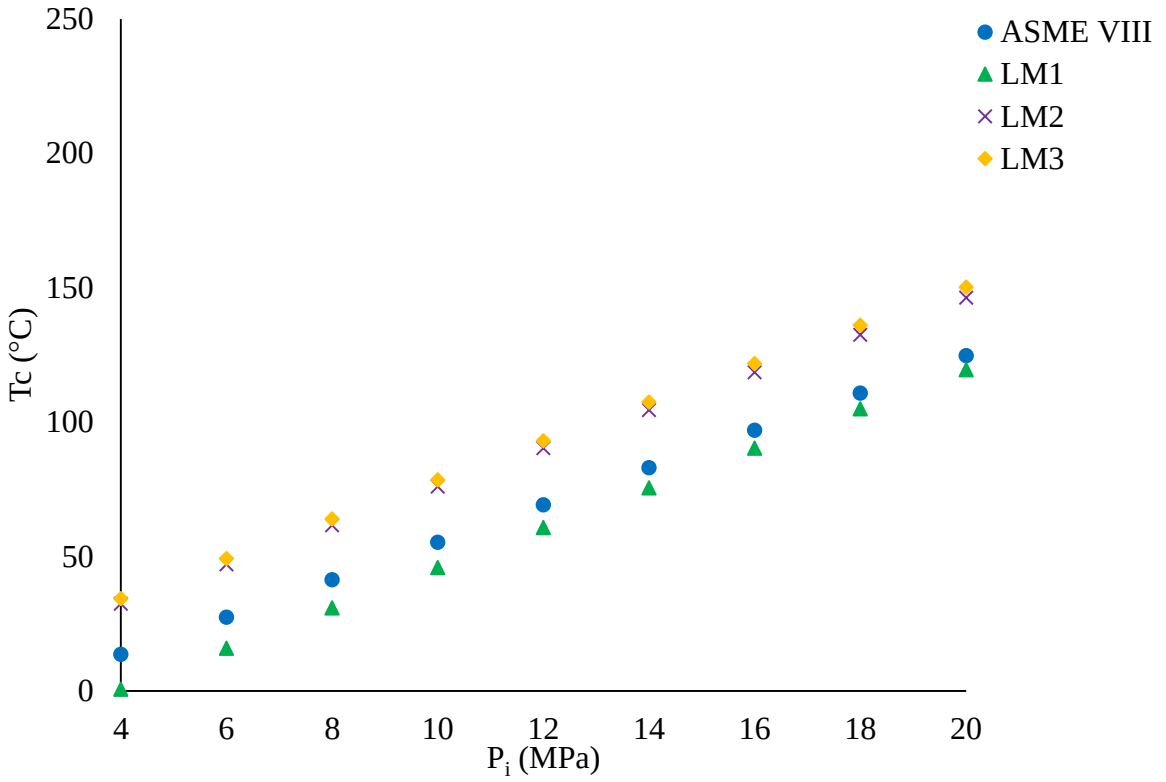

Figure 55: Allowable loads at SCL 1

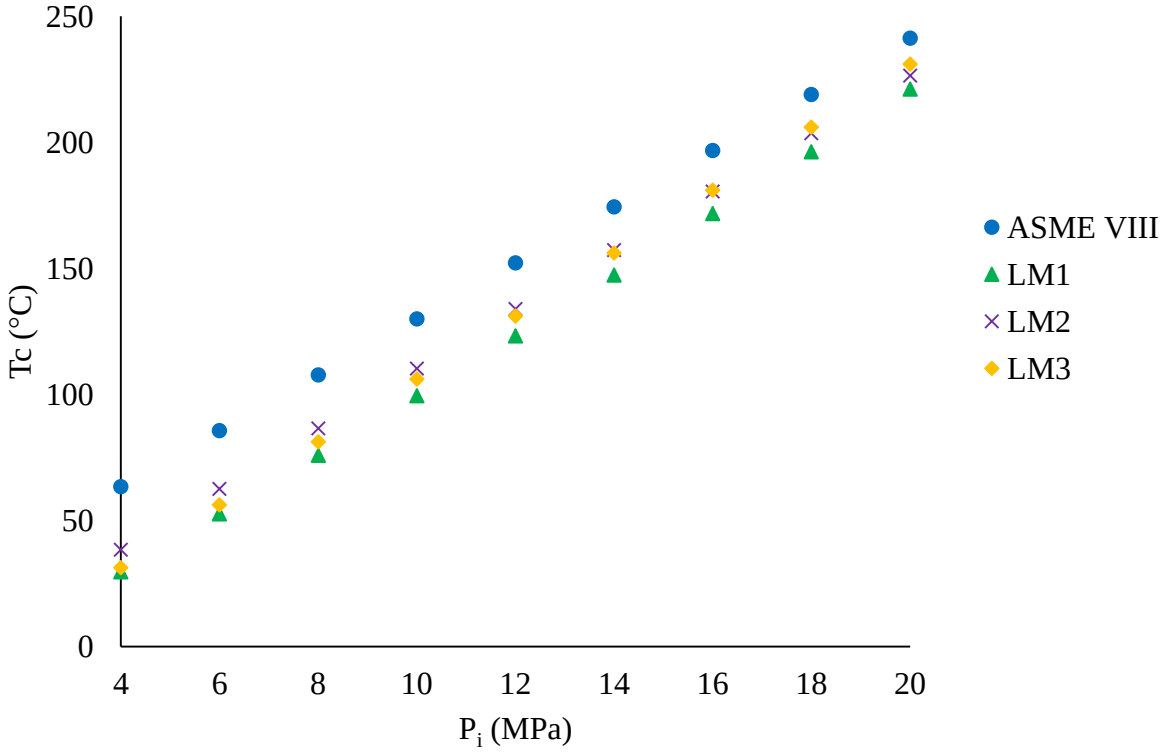

Figure 56: Allowable loads at SCL 2

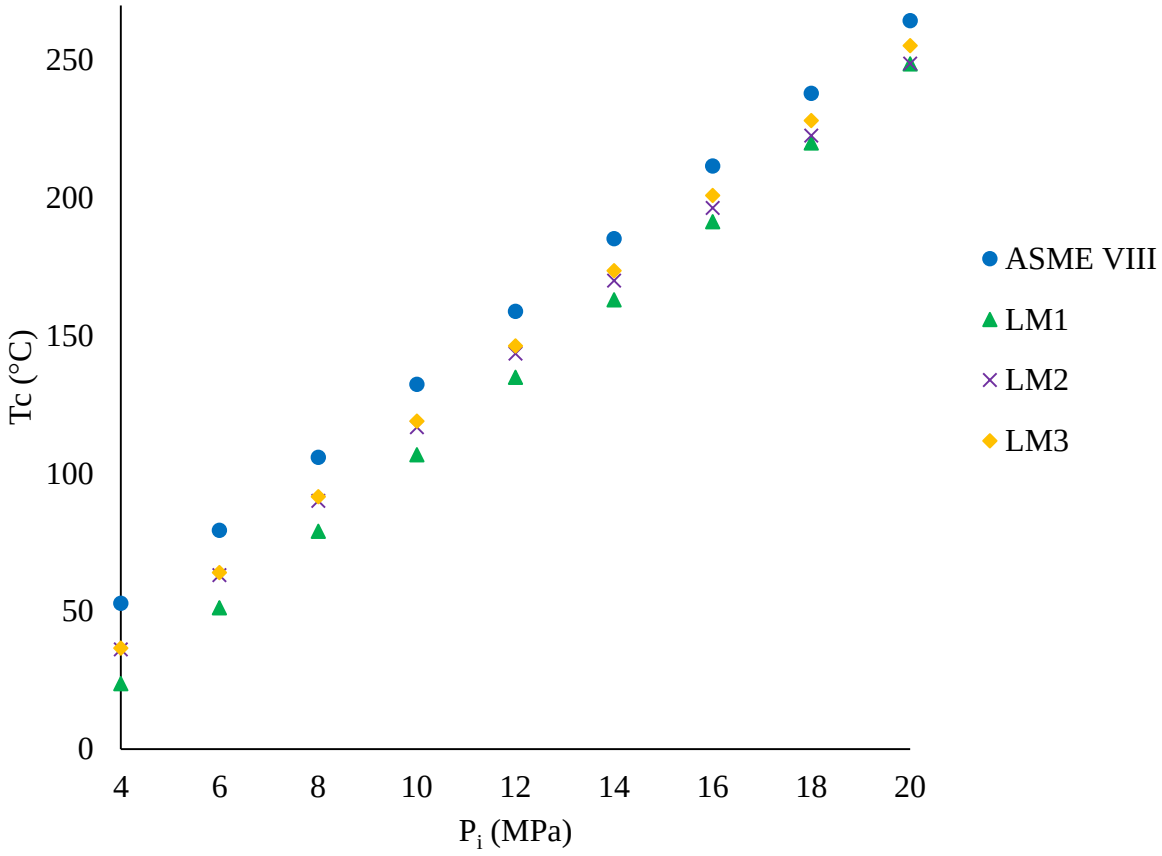

Figure 57: Allowable loads at SCL 3

Chapter 5 Non-Linear Analysis

Following the study on the use of elastic DBA to calculate plastic collapse and elastic shakedown limits, an investigation into the use of non-linear methods was conducted. By incorporating plastic material properties into the analysis, more detailed FEA could be used to validate the elastic results and help determine which linearisation methods are most effective. Also, it could help determine if the extra cost in computing power and analysis complexity proves to be more effective than the use of elastic DBA.

Of the many plastic analysis methods discussed in Chapter 2, limit analysis, plastic analysis for plastic collapse and cycle-by-cycle analysis for the prediction of shakedown and ratcheting are explored in more detail in this Chapter.

The initial focus is on the LWR nozzle from section 3.3 and tubesheet from section 3.4. Limit analysis results are presented first, before investigating the use of a strain hardening material model, with plastic collapse loads being calculated for a range of elastic-plastic DBA methods.

Following the same format as the linear elastic analysis chapter, focus then moves on to the effects of cyclic analysis. The elastic results for the oblique nozzles and thermal-shock nozzle are validated through use of full cycle-by-cycle FEA. The plastic strain histories and residual strain plots are presented, providing an insight into the actual cyclic response of the structures and how accurately the elastic DBA represented this.

5.1 LWR Nozzle and Tubesheet Limit Analysis

Using an elastic-perfectly plastic material model, small deformation theory and the von Mises yield criterion, limit analysis of the 3D LWR nozzle model was carried out in Ansys Workbench to provide a more accurate calculation of the limit pressure to plastic collapse. As previously mentioned, this is permitted within ASME III and the only additional material property requirement is the design stress from ASME II. The plastic collapse loads are given in Table 21 along with the ASME III allowable pressure loads, which are calculated by applying a design margin of 1.5 on the plastic collapse load. As the elastic results are all in terms of Tresca stress intensity but the plasticity solver in Ansys uses the von Mises Yield criterion, for consistency the results have also been factored by $\sqrt{3}/2$. The reasoning behind this is elaborated in more

detail in section 6.2. These results helped to validate the elastic DBA results whilst providing information on the actual failure location.

Component	**Failure Criterion**	$\boldsymbol{P_L}$ $\boldsymbol{(MPa)}$	$\boldsymbol{P_a(MPa)}$
LWR Nozzle	von Mises	37.05	24.70
LWR Nozzle	Tresca	32.09	21.39

Table 21: Limit and allowable pressures for the LWR nozzle

The equivalent plastic strain contour plot for 3D simulation at the von Mises limit load is presented in Figure 58.

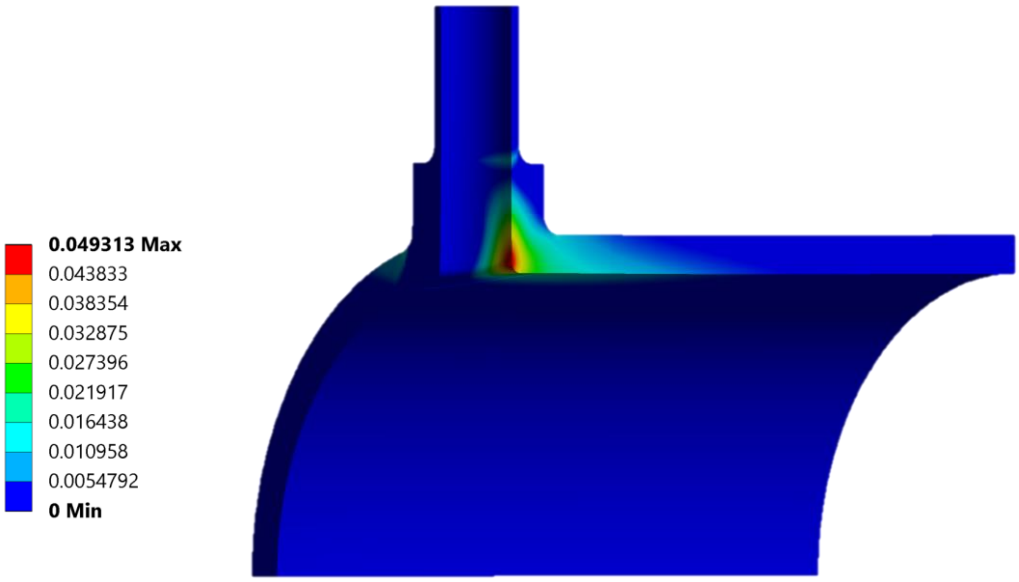

Figure 58: Equivalent plastic strain contour plot of LWR nozzle at the limit pressure

Limit analysis of the tubesheet detailed in section 3.4 was also carried out. As the structure approached failure, the load was ramped up at $0.689\,MPa$ $(100\,psi)$ increments to mimic the analysis of Jones and Gordon [3], which presented results in terms of the maximum allowable force, in US customary units, applied to the annulus region on the inner hub. Therefore, the limit pressure calculated from FEA was divided

by 1.5 to give the allowable pressure and multiplied by the area of the annulus region to give the allowable load as a force. Assuming the von Mises failure criterion, the collapse force is displayed next to that of the explicit FEA conducted by Jones and Gordon (converted to kN) in Table 22. This equates to a pressure of 87.44 MPa.

Component	**Collapse Force from FEA Limit Analysis (kN)**	**Collapse Force - Jones and Gordon (kN)**
Tubesheet	3721.83	3749.84

Table 22: Tubesheet limit analysis results comparison

The equivalent plastic strain at the limit load is shown in Figure 59 for the plastically deformed tubesheet.

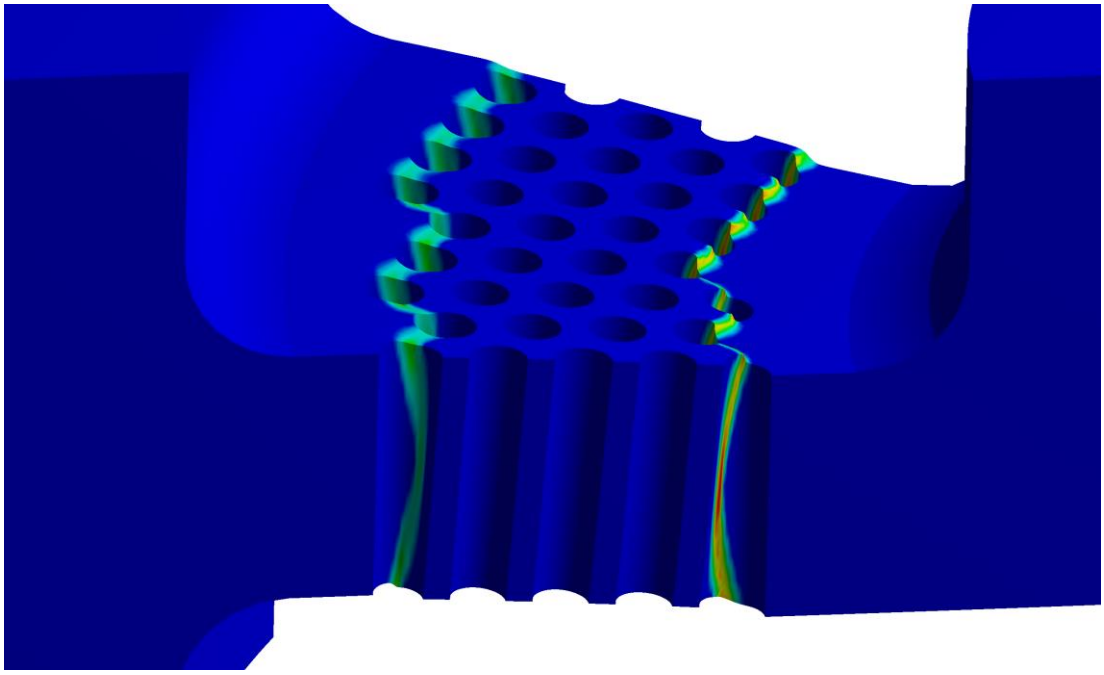

Figure 59: Equivalent plastic strain at tubesheet limit load

5.2 Plastic Analysis for the Prediction of Plastic Collapse Loads

Limit analysis is a very useful way to obtain the plastic collapse load of a pressure vessel, however, neglecting the strain hardening properties of the material means that there is still scope to improve the accuracy of the analysis to match real-world conditions. Therefore, this section investigates the use of plastic DBA methods, utilising strain hardening material properties and non-linear geometry in the FEA to determine the structural response even more precisely. The LWR nozzle and tubesheet are analysed once again but with their respective material definitions updated to include strain hardening.

Non-linear FEA of each component was carried out using Ansys Workbench. The stress and strain outputs were then used to investigate various techniques to determine the plastic collapse load. Most plastic DBA methods require post-processing of the non-linear FEA results. This is because the load at which plastic collapse occurs is not always obvious directly from the plastic FEA and so the methods described in section 2.5 were devised to determine collapse loads based on load and deformation parameters. Plastic collapse loads calculated using the ASME VIII Div 2 method, twice elastic slope (TES), tangent intersection (TI), plastic work (PW) and plastic work curvature (PWC) methods, are presented in this section.

5.2.1 ASME VIII Div 2 Plastic Analysis

The material model for the LWR nozzle FE model was updated to include the true stress-strain curve in Figure 18 derived using the ASME VIII Div 2 strength parameter equations. Elastic-plastic non-linear FEA was then carried out in Ansys Workbench, following the criteria set out in section 2.6.

As with the limit analysis, structural instability of the LWR nozzle was found by running the analysis until it failed to converge. The plastic collapse load was calculated as $64.45\,MPa$ and the allowable load as $26.85\,MPa$. The allowable load was calculated by dividing the collapse load by a design factor of 2.4 as required for the design condition [23]. The equivalent plastic strain at the last converged solution is shown in Figure 60.

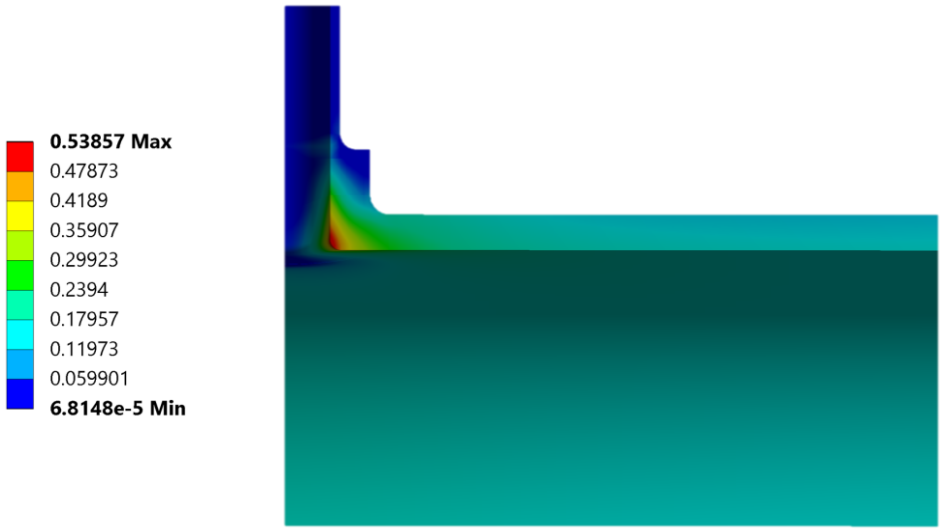

Figure 60: Equivalent plastic strain of the LWR nozzle with strain hardening

The stress-strain curve in Figure 23 was applied to the tubesheet FE model and elastic-plastic FEA of the component was carried out until loss of convergence. The plastic collapse load was calculated as 276.45 MPa (40096 psi) and factored by 2.4 to give the allowable pressure as 115.19 MPa (16706.67 psi). This corresponds to a limit force of 18.24 kN (2645.27 $kips$) and allowable force of 7.60 kN (1102.20 $kips$). The equivalent plastic strain at the collapse load is shown in Figure 61.

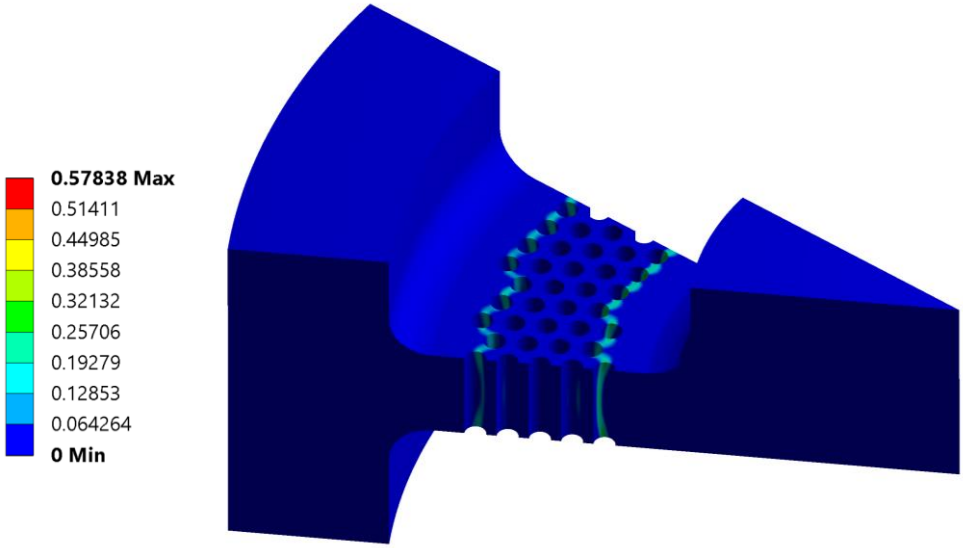

Figure 61: Equivalent plastic strain in tubesheet at ASME VIII Div 2 plastic collapse load

Elastic-plastic FEA of the tubesheet showed how accurate the ASME VIII Div 2 material model was at predicting the structural behaviour. The experimental data for Test 1 conducted by Jones and Gordon [3] was not provided in tabulated form, however, estimated values of the data points were obtained from the curve they published. This allowed the FEA load-deflection results to be plotted against the approximated test results in Figure 62. The load is normalised against the shear out load at the failure location [3] to allow a direct comparison with the published curve for test 1.

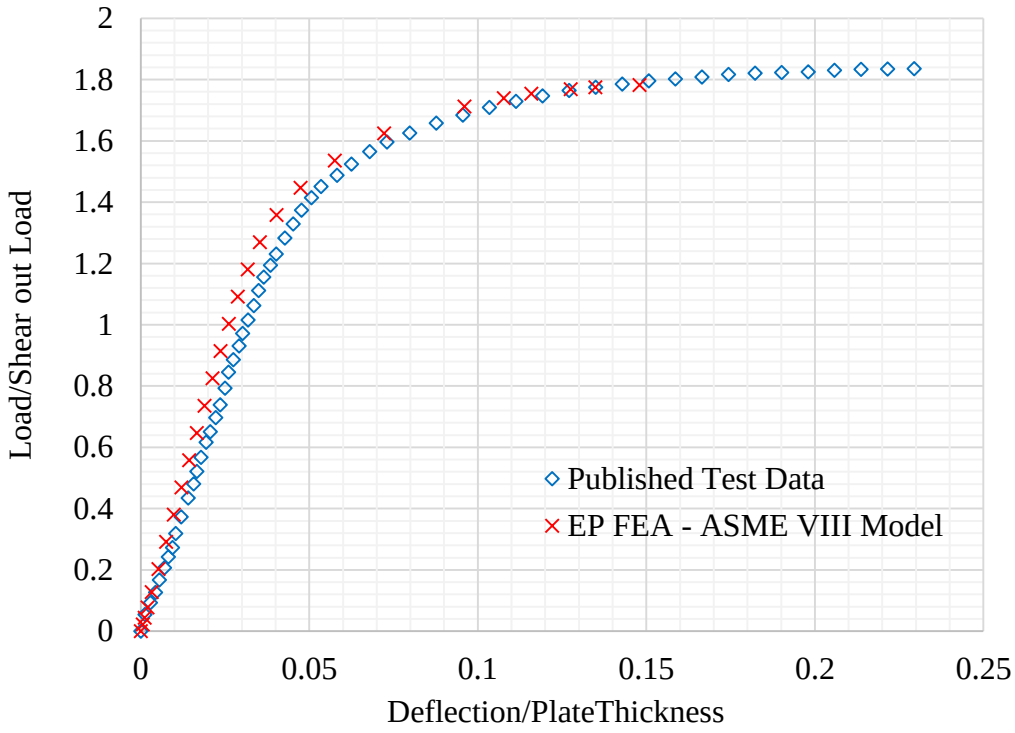

Figure 62: Normalised load vs deflection curves for the tubesheet [3]

5.2.2 Twice Elastic Slope

To find the TES plastic collapse load, the pressure vs maximum principal total strain curve was obtained from plastic FEA. The TES tangent line or plastic collapse line was then calculated, as per section 2.5. Figure 63 shows where the plastic collapse line and characteristic strain vs load curve intersect, hence defining the load at which

plastic collapse occurs. A TES plastic collapse load was also calculated based on the maximum deformation for comparison.

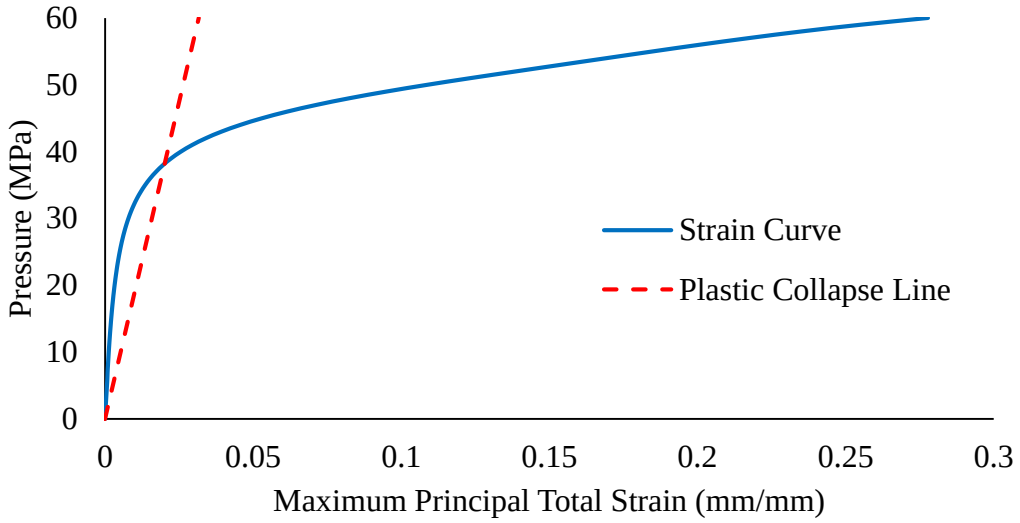

Figure 63: TES maximum principal total strain vs pressure load curve for the LWR nozzle

The plastic collapse load was calculated as $P_{L,TES} = 33.78\,MPa$ using maximum principal total strain as per ASME III. Using max deformation as the deformation parameter, $P_{L,TES} = 36.73\,MPa$. The maximum principal total strain and maximum deformation are shown in Figure 64 at each of their corresponding TES collapse loads.

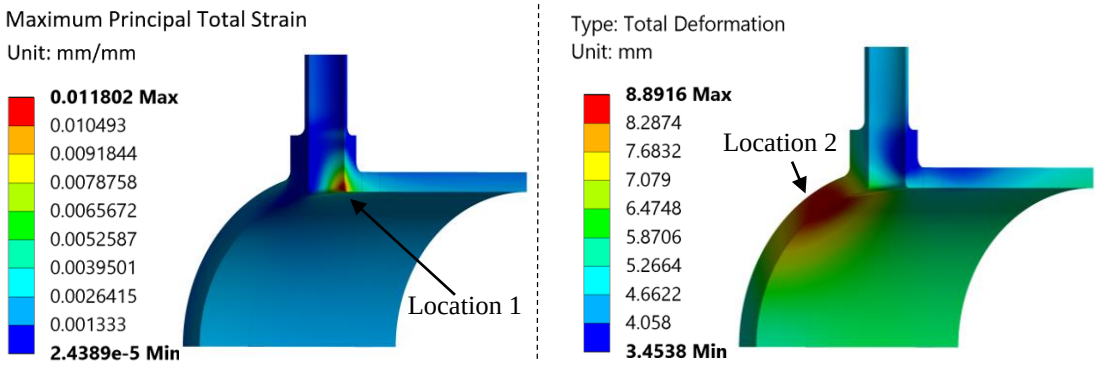

Figure 64: LWR nozzle maximum principal total strain and deformation after plastic FEA

TES collapse loads were calculated by probing the maximum principal total strain and deformation at both the max strain and max deformation locations, labelled as locations 1 and 2 in Figure 64. These are summarised in Table 23.

Location	**Deformation Parameter**	$P_{L,TES}$ **[MPa]**
1	Maximum Principal Total Strain	33.78
2	Maximum Principal Total Strain	---
1	Deflection	37.00
2	Deflection	36.73

Table 23: LWR Nozzle TES Collapse Loads

TES plastic collapse loads were found based on the max principal total strain and deflection of the tubesheet. Using the max principal total strain was more conservative. The plastic collapse line intersects the curve in Figure 65 at $P_{L,TES} = 187.00\ MPa$.

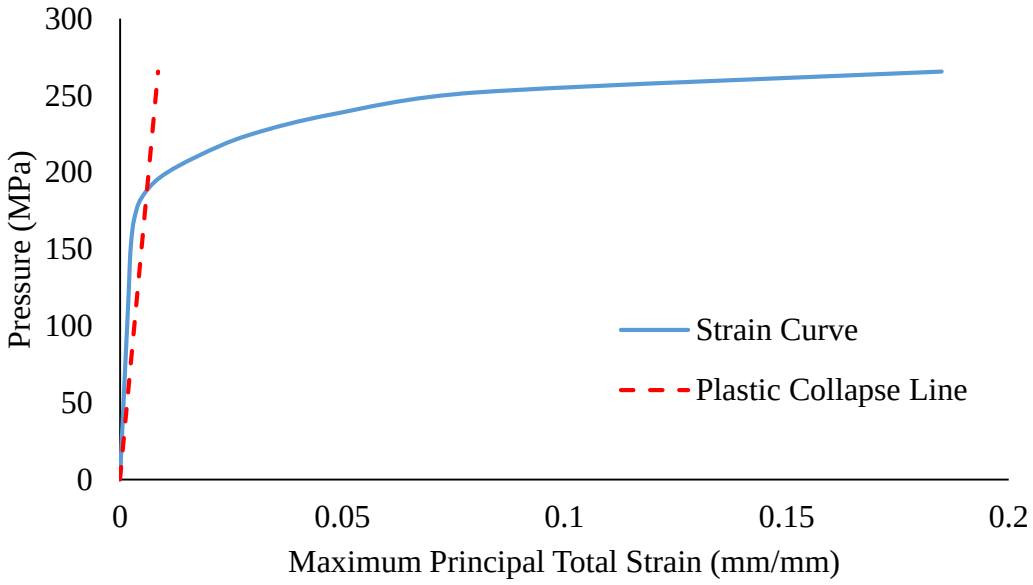

Figure 65: Tubesheet TES using max principal total strain curve

Figure 66 highlights that the maximum principal total strain occurs on the inside surface of one of the inner penetrations; this is the location from which the strain curve in Figure 65 was generated.

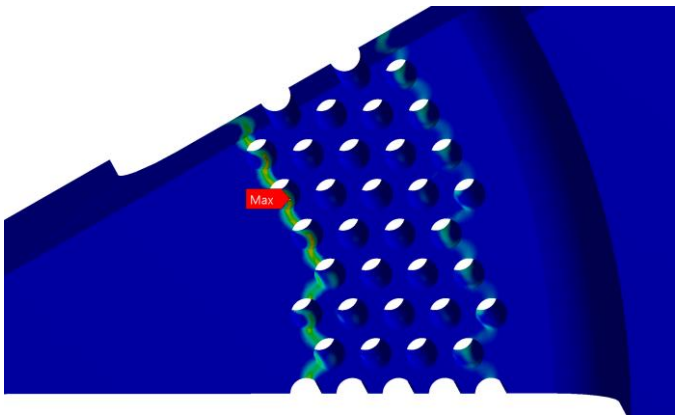

Figure 66: Maximum principal total strain in tubesheet

As with the LWR nozzle, TES collapse loads were generated at both locations for both deformation parameters. These are presented in Table 24, with locations 1 and 2 shown in Figure 67. Location 1 is in the perforated region where the max principal total strain occurs (shown in Figure 66) and location 2 is at the edge of the inner hub, where max transverse deflection occurs.

Location	**Deformation Parameter**	$P_{L,TES}$ **[MPa]**
1	Maximum Principal Total Strain	187.00
2	Maximum Principal Total Strain	---
1	Deflection	270.00
2	Deflection	259.96

Table 24: Tubesheet TES Collapse Loads

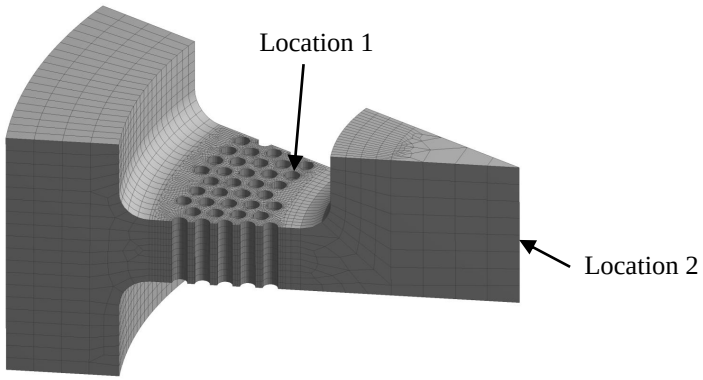

Figure 67: Tubesheet Locations for Deformation Parameters

5.2.3 Tangent Intersection

The TI, PW and PWC methods were also utilised to calculate plastic collapse loads for the actual 3D nozzle. The procedure for the TI method is outlined in section 2.5. Using the maximum principal total strain as the deformation parameter, the plastic collapse load obtained using the TI method was found to be 47.92 MPa. Figure 68 shows the TI method being implemented using the max principal total strain vs pressure curve, with the point at which the elastic and plastic tangents intersect denoting the collapse load. Table 25 presents TI collapse loads at locations 1 and 2 from Figure 64.

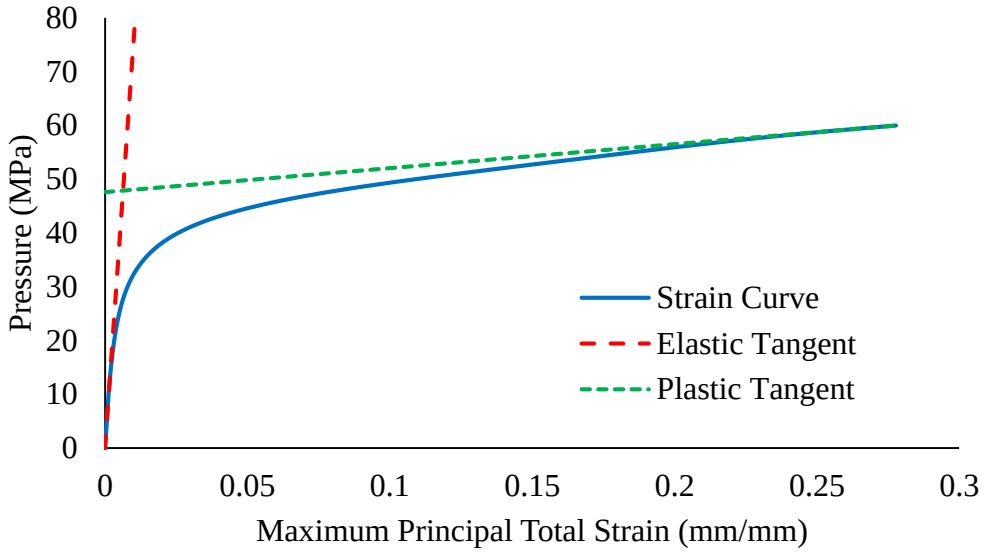

Figure 68: TI method for LWR nozzle

Location	**Deformation Parameter**	**$P_{L,TI}$ [MPa]**
1	Maximum Principal Total Strain	47.92
2	Maximum Principal Total Strain	---
1	Deflection	51.54
2	Deflection	49.73

Table 25: LWR Nozzle TI Collapse Loads

Plastic collapse loads for the tubesheet were also found using the TI method, with deflection as the deformation parameter giving the more conservative result of $P_{L,TI} = 232.85\ MPa$. The deformation parameter was taken from a node at the edge of the inner hub, as this is where the transverse deflection was greatest. The intersection point of the two tangent lines on the load vs deflection curve in Figure 69 presents how the collapse load was obtained. This procedure was repeated at both locations in Figure 67 with the results presented in Table 26.

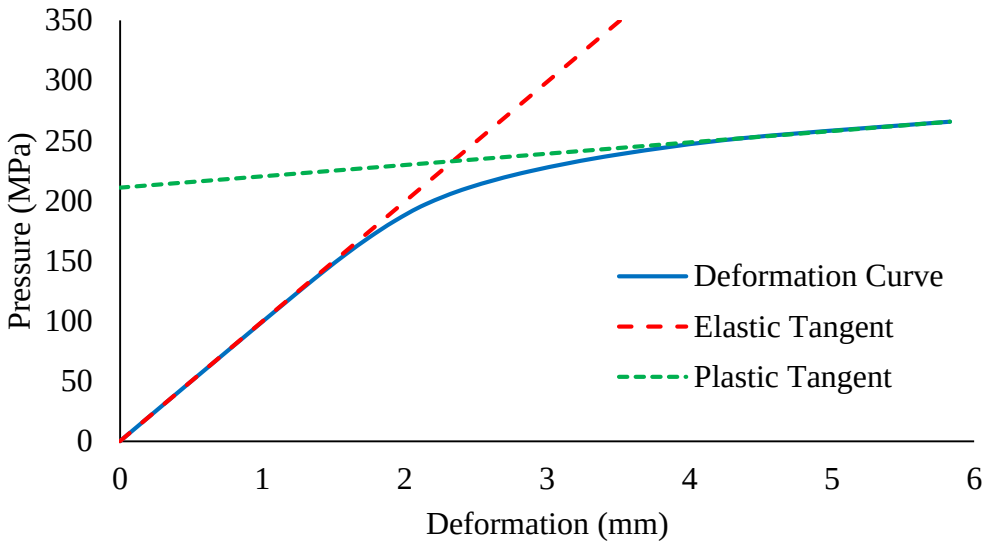

Figure 69: Tubesheet TI using deformation curve

Location	**Deformation Parameter**	**$P_{L,TI}$ [MPa]**
1	Maximum Principal Total Strain	242.18
2	Maximum Principal Total Strain	243.39
1	Deflection	256.90
2	Deflection	232.85

Table 26: Tubesheet TI Collapse Loads

5.2.4 Plastic Work

The plastic work criterion was then implemented on the LWR nozzle. This method, as outlined in section 2.5, relies upon the relationship between the applied pressure load and the plastic work done in the structure. A load vs plastic work curve can be plotted and the plastic collapse load is taken as the point at which a tangent from the curve meets the vertical (load) axis. The pressure load and plastic work were normalised against their maximum respective values. Figure 70 shows the normalised curve for the LWR nozzle, with, the plastic collapse load calculated as $50.24\ MPa$.

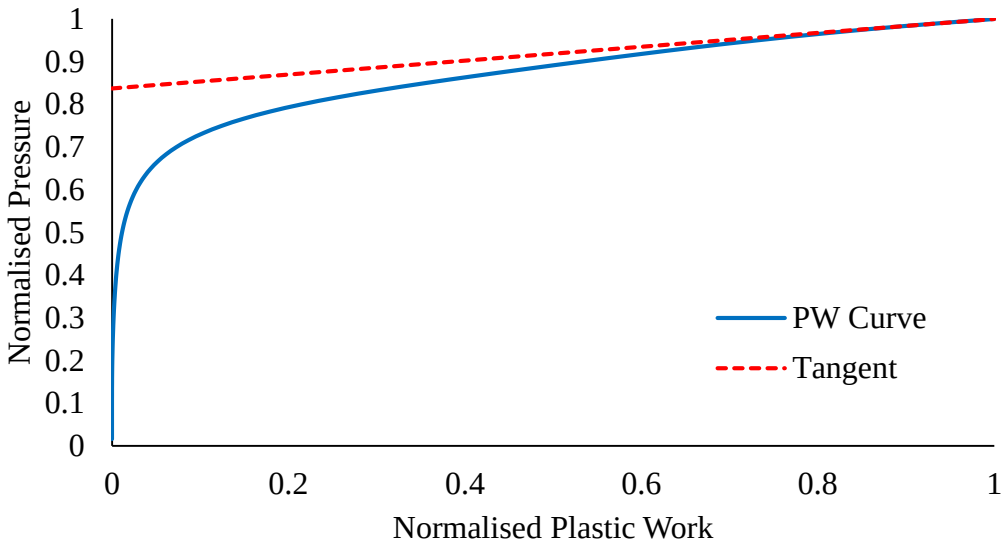

Figure 70: PW method for LWR nozzle

The normalised curve in Figure 71 displays how the plastic work increases as the pressure load applied to the tubesheet inner hub is increased. Where the tangent intersects the vertical axis corresponds to a collapse pressure of $P_{L,PW} = 243.78\ MPa$.

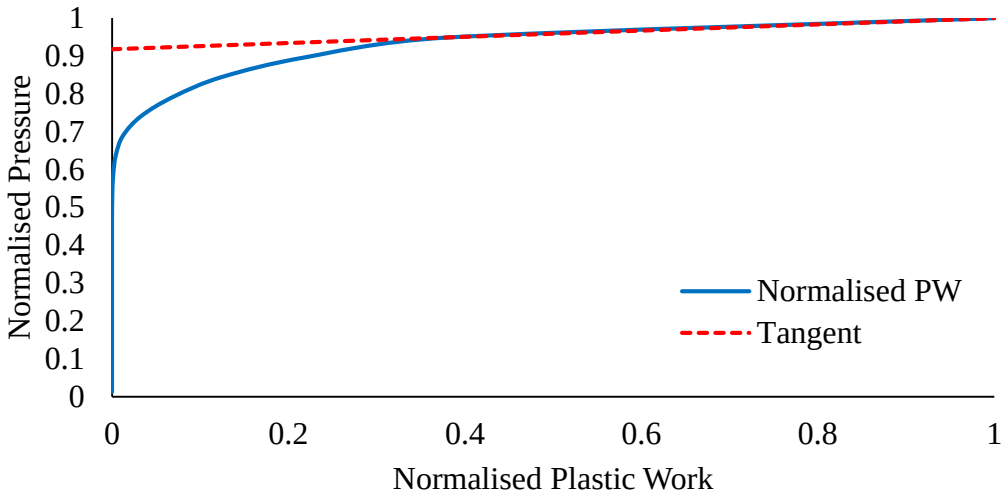

Figure 71: PW method for tubesheet

5.2.5 Plastic Work Curvature

The plastic collapse load was then found using the PWC method. Two different methods of calculating the curvature were investigated. The first involved fitting a cubic spline to the normalised plastic work vs load FEA output data and then applying equation (32) at each value to find the curvature. A plot of the normalised load vs curvature for the LWR nozzle is shown in Figure 72. The peak corresponds to a limit pressure of $P_{L,PWC} = 41.62\ MPa$.

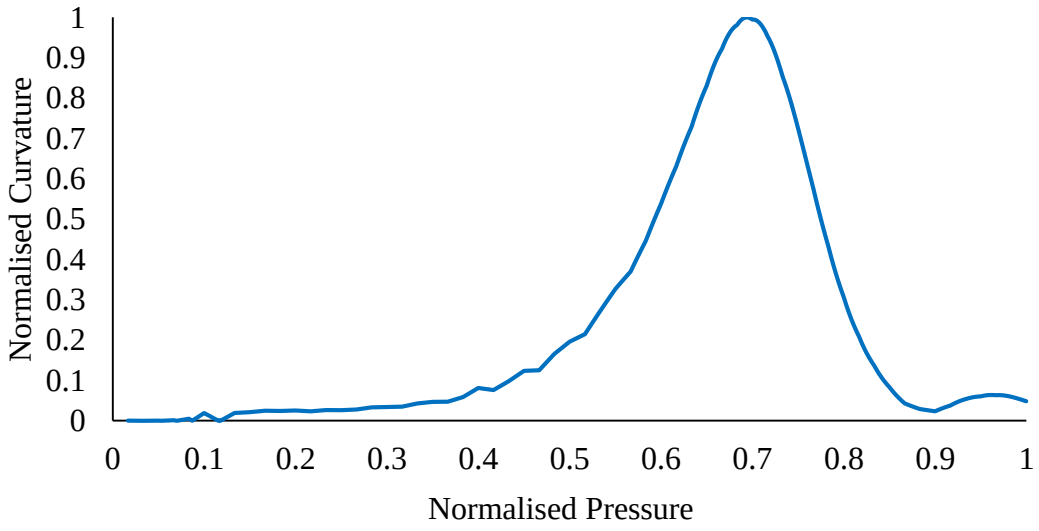

Figure 72: Load vs curvature plot for the LWR nozzle using PWC-Cubic Spline method

Next, the curve fit method proposed by Seal [67] and described in detail in section 2.5 was implemented. The load-plastic work curve in Figure 73 is made up of a number of data points which define the amount of plastic work done for a specific internal pressure load and plotted using a cubic spline. Parameters A, B, C and D were optimised to define a function which best fits this plastic work vs pressure data. The optimised parameters in Table 27 can be applied to equations (33), (34) and (35) to define a curve which fits the data points. The normalised curve is also shown in Figure 73 along with the cubic spline curve using the actual data points from the FEA.

A	**B**	**C**	**D**
1.784011	10.19386	0.98111	11.02679

Table 27: Curve fitting parameters for LWR nozzle PWC-curve fit method

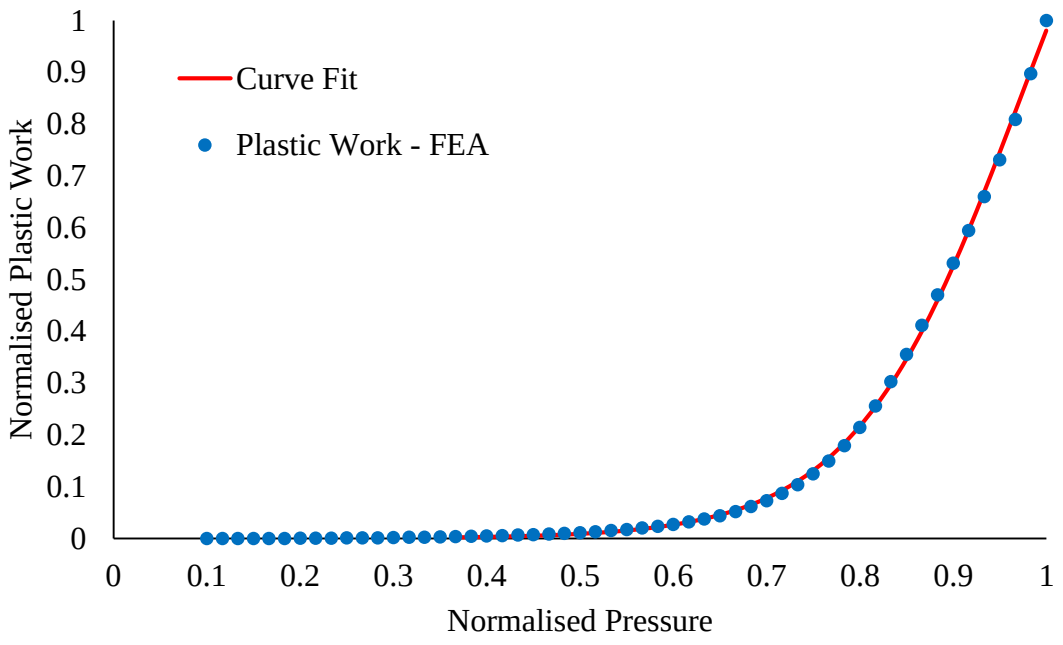

Figure 73: Normalised plastic work vs load curves – LWR nozzle FEA data points and fitted curve

Upon calculating the curve fit function, equation (32) was used once again to calculate the curvature. The curvature of the normalised load vs plastic work curve in Figure 73 is plotted in Figure 74 to show how the rate of plastic work done changes as the load is increased. The maximum curvature equated to a limit pressure of $40.78\ MPa$.

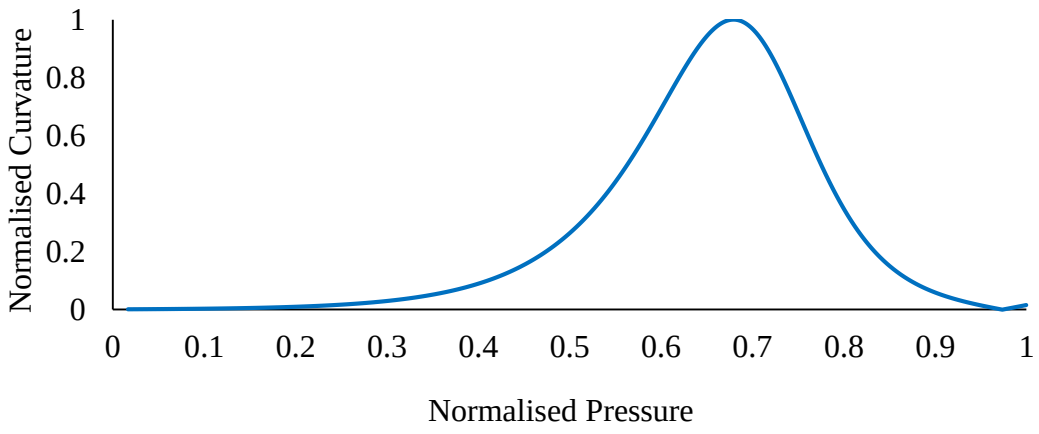

Figure 74: Load vs curvature plot for the LWR nozzle using PWC-curve fit method

Collapse loads for the tubesheet were then found by applying the PWC method. As with the LWR nozzle, a cubic spline was fitted to the load vs plastic work FEA output data and equation (32) was used to find the curvature. Figure 75 displays the normalised curvature with respect to pressure load. If the collapse load is said to occur at the maximum curvature, then $P_{L,PWC} = 193.68\ MPa$.

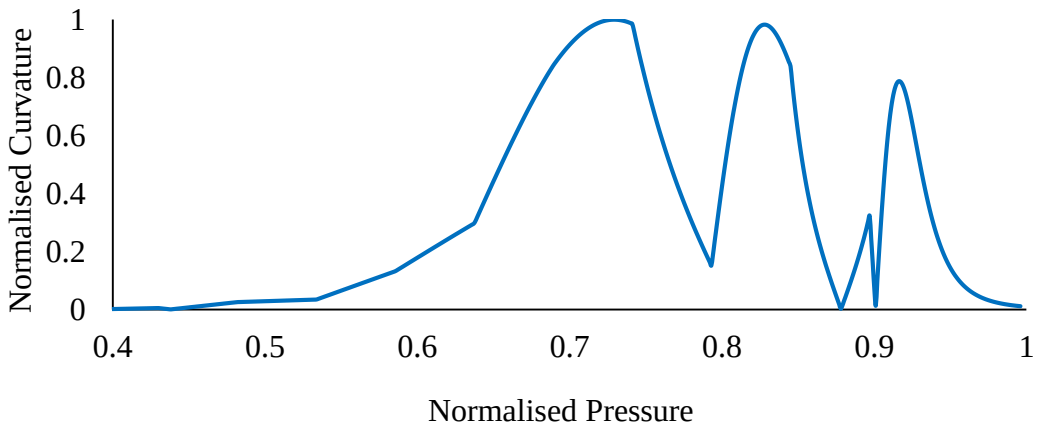

Figure 75: Load vs curvature plot for the tubesheet using PWC-Cubic Spline method

The PWC curve fit method used when analysing the LWR nozzle was also investigated on the tubesheet. The curve fitting parameters in Table 28 provide a good fit to the FEA data, as shown in Figure 76.

A	B	C	D
86.43361	4.554328	1.299374	15.28301

Table 28: Curve fitting parameters for tubesheet PWC-curve fit method

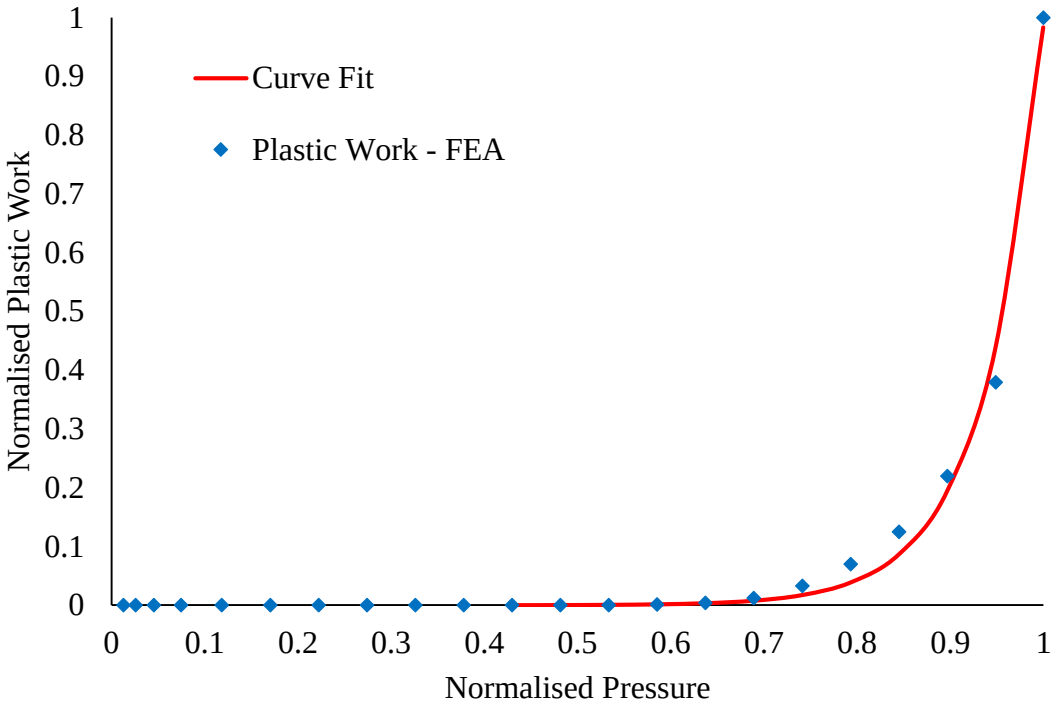

Figure 76: Normalised load vs plastic work curves – tubesheet FEA data points and fitted curve

The normalised load vs curvature plot is Figure 77 has a maximum turning point corresponding to a plastic collapse load of $P_{L,PWC} = 213.60\ MPa$.

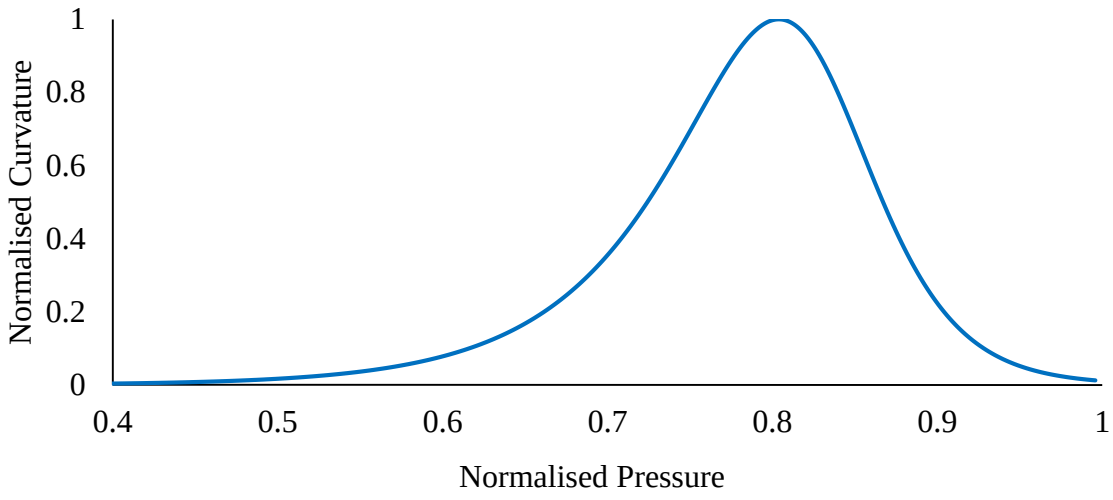

Figure 77: Load vs curvature plot for the tubesheet using PWC-curve fit method

5.3 Summary of Plastic Collapse Load Results

All of the plastic collapse loads for the LWR nozzle model calculated using each non-linear analysis method are summarised in Table 29. The plastic collapse loads are derived from stress results calculated using the von Mises plastic failure criterion within the Ansys Workbench FEA software.

Component	Elastic-Plastic Design Method	Plastic Collapse Load (MPa)	Allowable Load (MPa)
LWR Nozzle	LLA	37.05	24.70
	ASME VIII	64.45	26.85
	TES	33.78	22.52
	TI	47.92	31.95
	PW	50.24	33.49
	PWC – Cubic Spline	41.62	27.75
	PWC – Curve Fit	40.78	26.95

Table 29: Summary of plastic collapse and allowable loads for LWR nozzle

The loads calculated using each method are shown graphically in Figure 78, ordered from most to least pessimistic. Appropriate design factors were applied to the limit pressure loads predicted by each method to give the allowable loads.

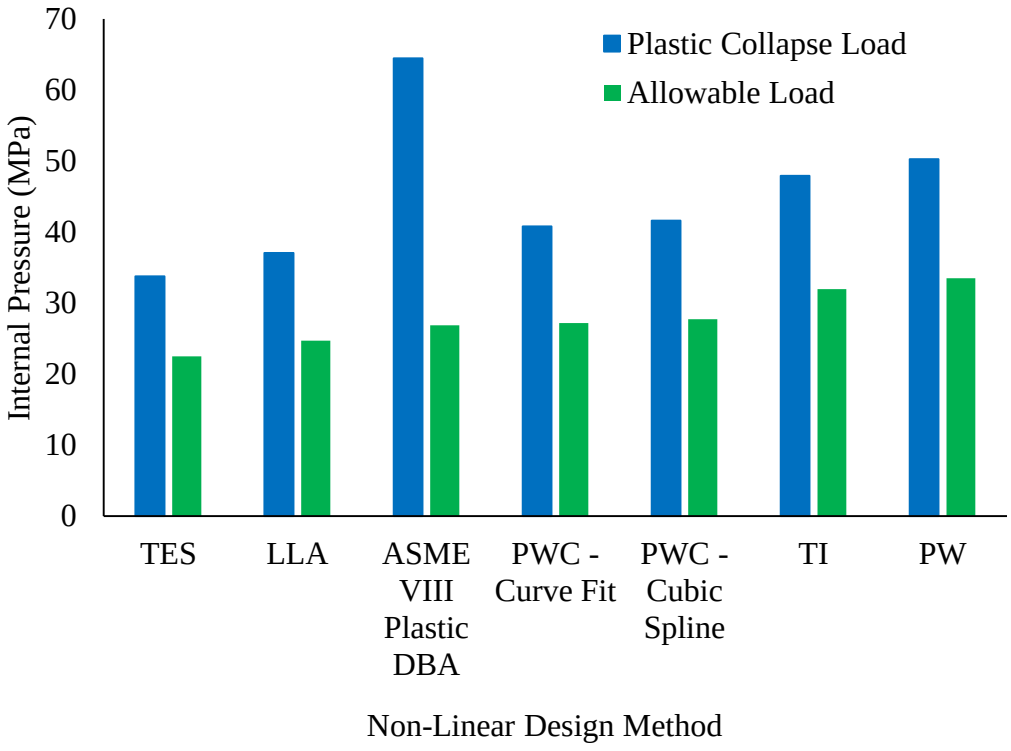

Figure 78: Plastic collapse loads and allowable loads calculated for the LWR nozzle

A summary of the plastic collapse and allowable pressure loads in SI units for the tubesheet case study are presented in Table 30.

Component	Elastic-Plastic Design Method	Plastic Collapse Load (MPa)	Allowable Load (MPa)
Tubesheet	LLA	131.16	87.44
	ASME VIII	276.45	115.19
	TES	187.00	124.67
	TI	232.85	155.23
	PW	243.78	162.52
	PWC – Cubic Spline	193.68	129.12
	PWC – Curve Fit	213.60	142.40

Table 30: Summary of plastic collapse and allowable loads for tubesheet

Figure 79 presents the tubesheet results for each method in order from the least to most pessimistic allowable load.

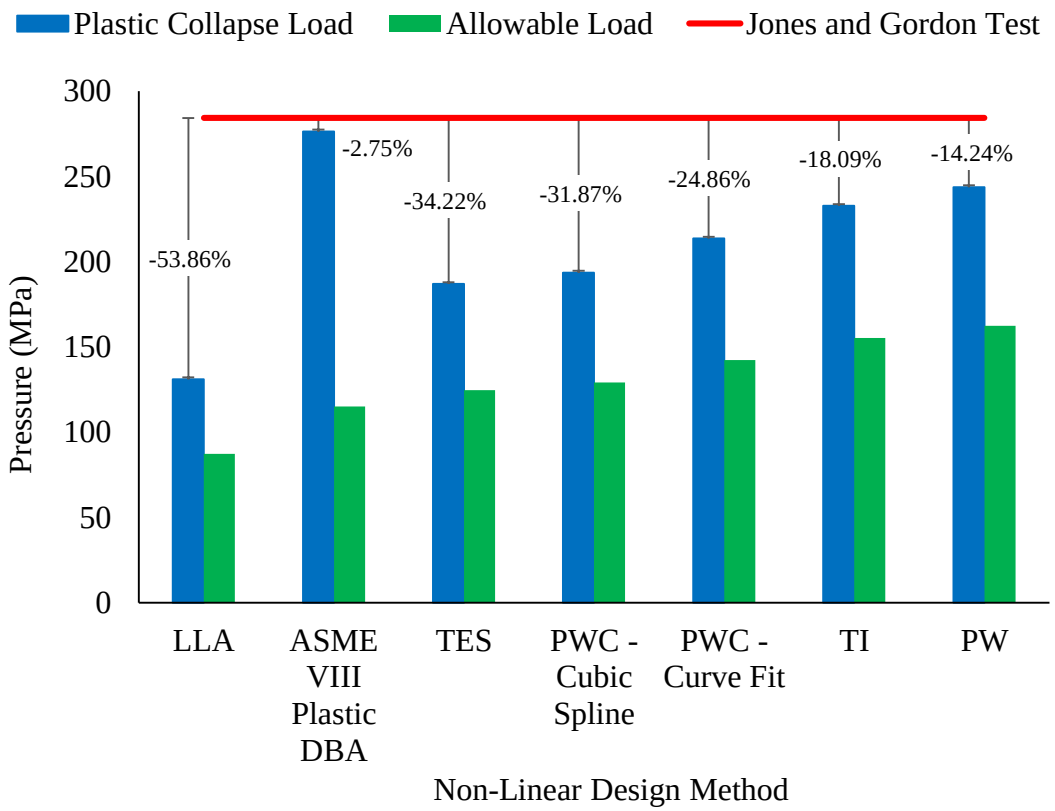

Figure 79: Plastic collapse loads and allowable loads calculated for the tubesheet

The two collapse loads found experimentally by Jones and Gordon [3] were $2734\ kips$ for Test 1 and $2706\ kips$ for Test 2, These give an average of $2720\ kips$ or $284.26\ MPa$. The percentage difference between the experimental test average and each plastic DBA collapse load is also displayed in Figure 79.

5.4 Plastic Analysis for the Prediction of Shakedown and Ratcheting

Non-linear DBA can also be used to provide validation of the elastic stress analysis for cyclic loading. The actual structural response can be simulated by performing cycle-by-cycle FEA and in this case, elastic-perfectly plastic material properties were utilised. The results presented in this section will be used to help determine which linearisation methods can be used to best represent the real structural behaviour of components under cyclic loading by determining if the allowable loads do indeed ensure elastic shakedown. The plastic cyclic response of each oblique nozzle was investigated first, followed by cycle-by-cycle analysis of the thermal-shock nozzle.

To determine if the allowable pressures calculated using the elastic route do guarantee elastic shakedown of oblique nozzles 5 and 6, cycle-by-cycle analysis, taking the result from the LM with the least conservative pressure load, was conducted for each nozzle. For nozzle 5, using $P_i = 4.37\ MPa$ as the peak cyclic pressure, elastic shakedown was observed, as the plastic strain became constant after a few cycles. Elastic shakedown was also demonstrated through use of cycle-by-cycle analysis of nozzle 6 at $P_i = 3.96\ MPa$.

Alternating plasticity does develop in the nozzles at a high enough pressure. Figure 80 displays the plastic strain history for nozzle 6 over 10 simulated cycles where $P_i = 5\ MPa$ at the peak of each cycle.

Nozzle	**Cyclic Pressure, P_i (MPa)**	**Cyclic Response**
5	4.37	Elastic shakedown
6	3.96	Elastic shakedown
5	5	Alternating plasticity
6	5	Alternating plasticity

Table 31: Summary of oblique nozzle cyclic response results

Both the equivalent plastic strain (PEEQ) and plastic strain magnitude (PEMAG) field outputs from Abaqus are presented and both indicate that alternating plasticity occurred in nozzle 6 for $P_i = 5\ MPa$. The simulation was left to run for a further 15 cycles but the trend shown in Figure 80 continued. The six plastic strain components over the full 25 cycles for nozzle 6 are displayed in Figure 81. Similar observations were made for nozzle 5.

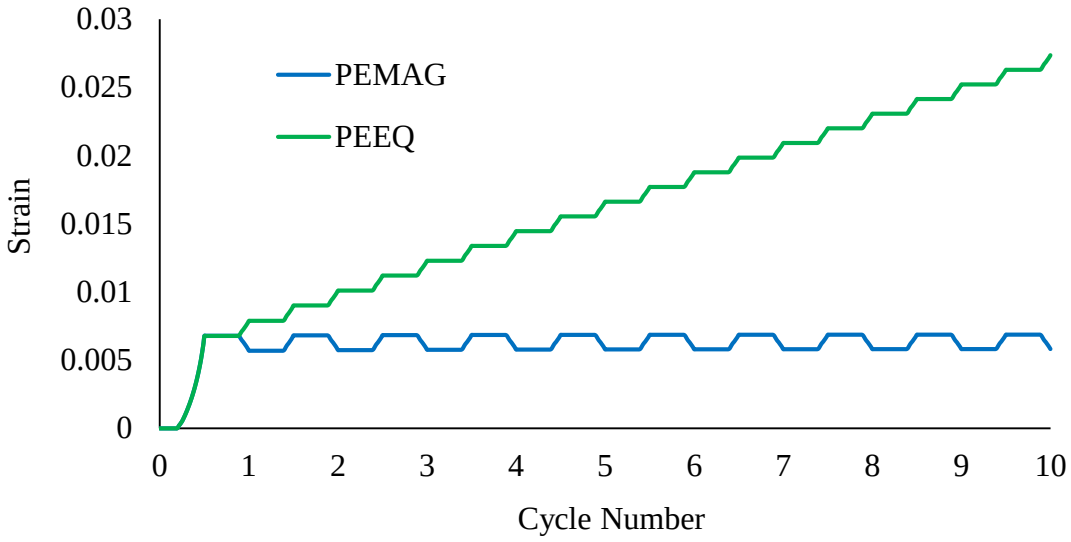

Figure 80: PEMAG and PEEQ history for nozzle 6 at $P_i = 5\ MPa$

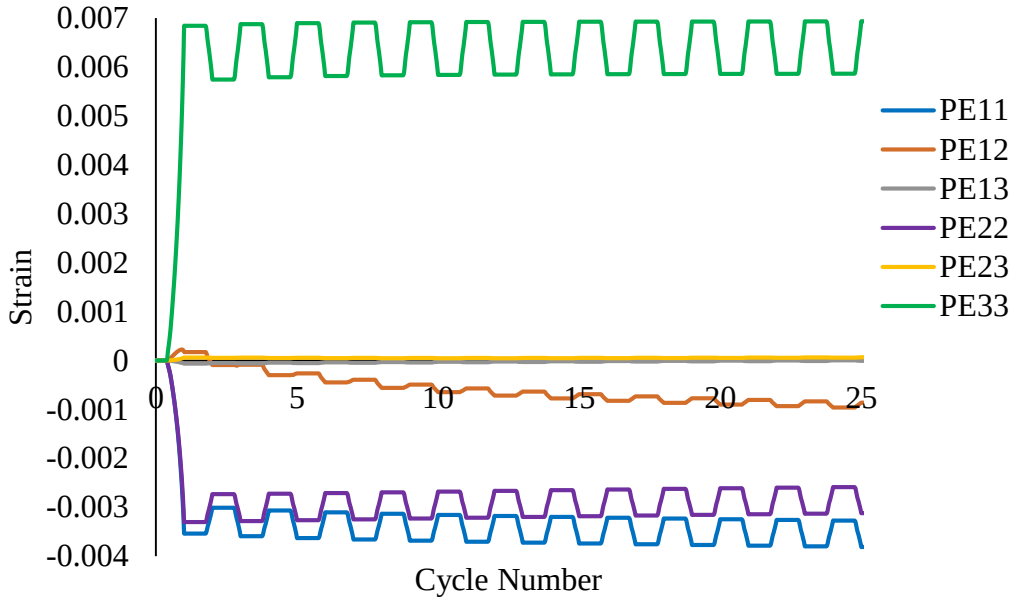

Figure 81: Plastic strain component history for nozzle 6 at $P_i = 5\ MPa$

For $P_i = 5\ Mpa$ (i.e.$P_i > P_{SD}$), the point at which alternating plasticity developed on the inside surface of nozzle 6 is highlighted in the residual PEEQ plot in Figure 82.

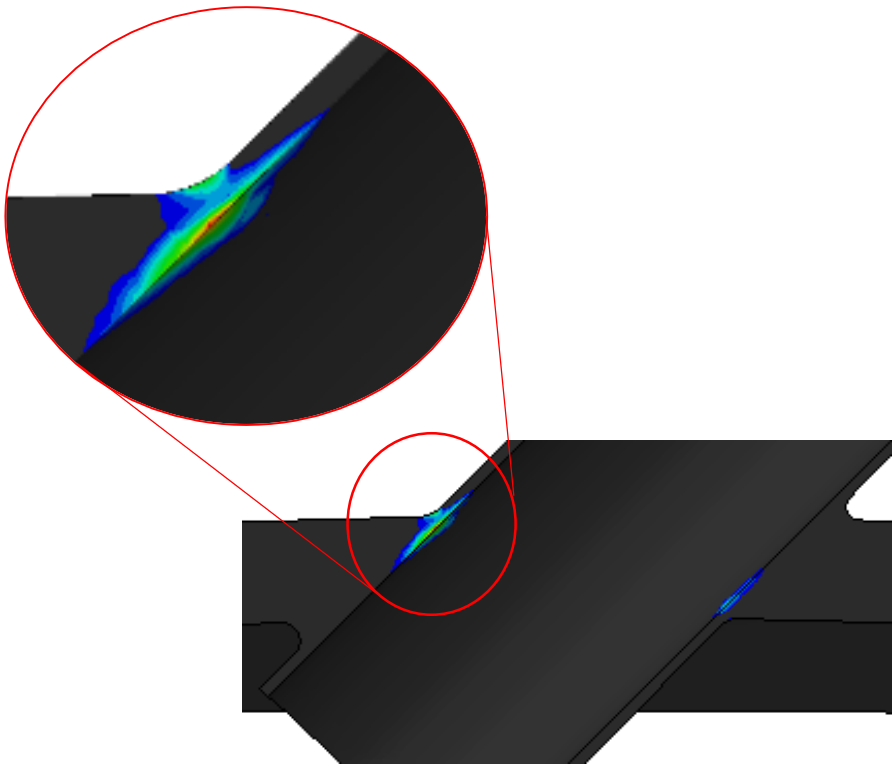

Figure 82: Residual equivalent plastic strain in nozzle 6 when $P_i = 5\ MP$

Elastic-plastic cycle-by-cycle analysis was also carried out on the thermal-shock nozzle. An elastic-perfectly plastic material model was used and 10 full cycles of the thermo-mechanical transient in Figure 31 were simulated. Two separate transient analyses were conducted, to investigate the structural response for two different cold shock temperatures to determine if elastic shakedown, alternating plasticity or ratcheting was occurring and to validate the elastic results from section 4.2.3 for each LM.

The residual plastic strain magnitude plots after 10 cycles for three different loading conditions are shown in Figure 83, highlighting that the inside surface of the nozzle near the junction with the vessel experiences significant plastic deformation.

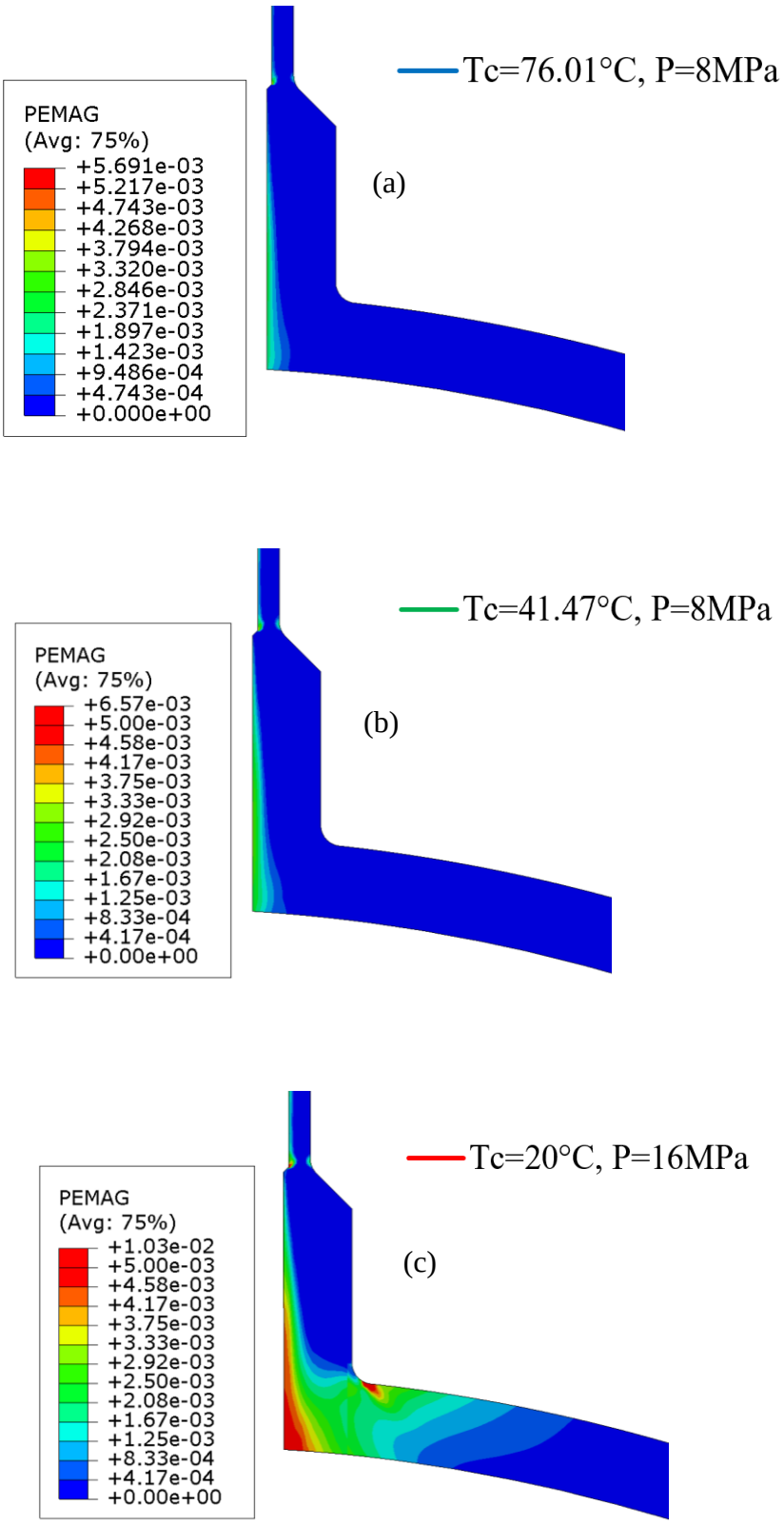

Figure 83: Residual plastic strain magnitude in nozzle showing elastic shakedown (a), alternating plasticity (b) and ratcheting (c) after 10 cycles

The plastic strain magnitude at the inside surface of the nozzle was plotted against time for $P_i = 8\,MPa$ and cold shock temperatures of $T_C = 41.47℃$ and $T_c = 76.01℃$. These relate to the allowable T_c at SCL 1 for the ASME VIII Div 2 method and at SCL 2 for LM 1. The allowable thermal shock loads at SCL 3 were slightly stricter than at SCL 2, however, as elastic shakedown was observed for the most extreme condition at SCL 2; the same behaviour will be exhibited for all LMs at SCL 3. The PEMAG strain history in Figure 84 shows the structural response to the two thermal shock loads along with the cyclic response for the more extreme conditions of $P_i = 16\,MPa$ and $T_c = 20℃$ to demonstrate ratchet behaviour.

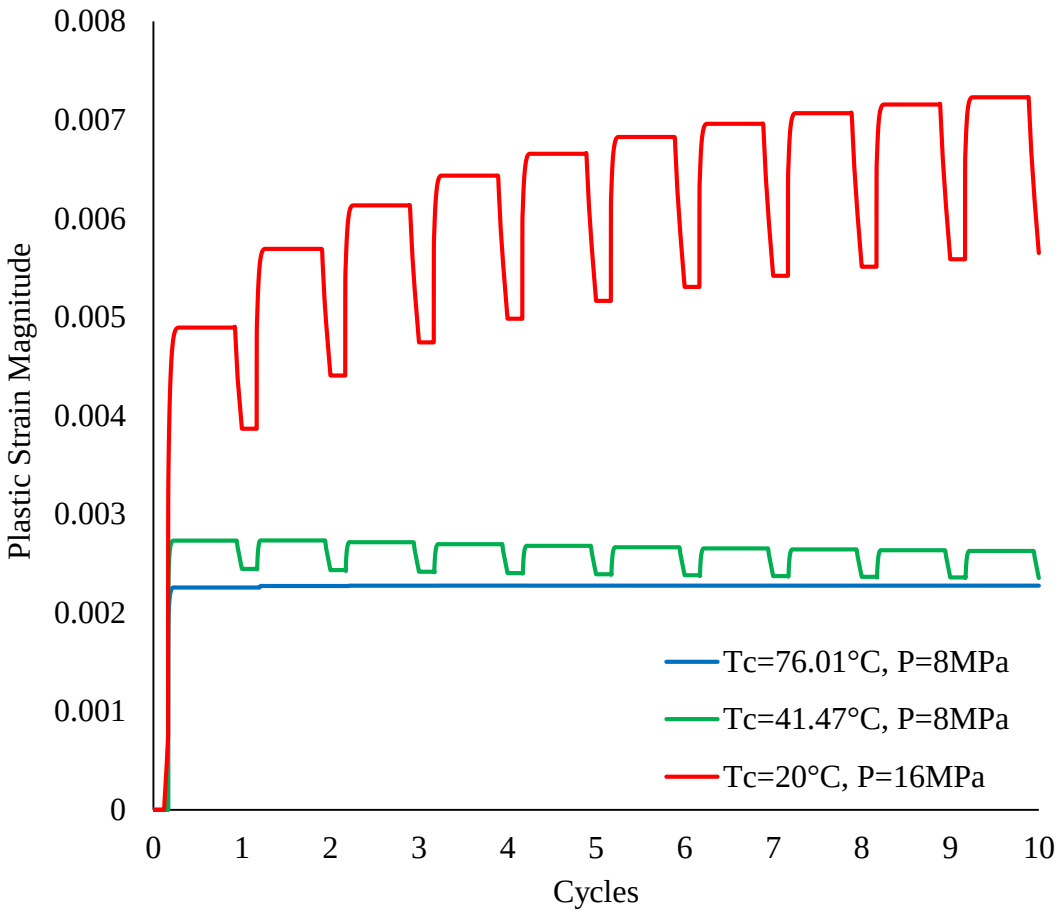

Figure 84: Plastic strain magnitude history

Chapter 6 Analysis of Results

The main aim of this analysis of the results is to support recommendations for the use of linearisation methods and to identify when plastic DBA is more effective.

The results presented in Chapter 4 and Chapter 5 for the linear elastic and non-linear DBA provide many useful insights into the use of different DBA methods for the safe design of pressurised nuclear components. The linear elastic DBA results are considered first. General limitations in the elastic DBA procedure are highlighted before focusing on the influence of the individual stress components. The linearised stress distributions obtained using each LM are discussed, along with the accuracy and validity of the calculated allowable loads to prevent GPD and incremental plastic collapse of the various components.

The plastic collapse and elastic shakedown limit loads obtained using plastic non-linear DBA methods are then considered. These are used to validate the elastic DBA and identify potential advantages and disadvantages of non-linear DBA. A discussion on the use of limit analysis is conducted before focussing on the plastic collapse loads obtained using the ASME VIII Div 2 elastic-plastic method. The discussion then focusses on results using post-processing techniques: twice elastic slope (TES), tangent intersection (TI), plastic work (PW) and plastic work curvature (PWC) to highlight the differences in the methods and justifications for their use. The analysis of results is concluded by discussing the accuracy and efficiency of cycle-by-cycle FEA in the prediction of shakedown and ratcheting.

6.1 Linear Elastic DBA Results Discussion

The plastic collapse loads of a thick, internally pressurised cylinder calculated analytically and using ASME VIII Div 2 stress linearisation were presented in section 4.1.1. The linear analytical model was found to give poor agreement with the exact solution for thick-wall cylinders, as shown in Figure 33. The results diverge rapidly as the thickness is increased, with the linear solution becoming overly conservative. The ASME VIII Div 2 limit pressure for the cylinder becomes non-conservative as it begins to diverge from the exact solution at an approximate radius ratio of $R_o/R_i = 1.3$,

which equates to $r/t = 4$. These findings agree with the recommendation in ASME VIII Div 2 that plastic analysis should be used for thick components where $r/t < 4$.

To determine why the ASME VIII Div 2 linearised results diverge from the exact solution, the elastic and plastic stress component distributions in the cylindrical vessel at the limit pressure were investigated in more detail. Figure 34 highlights the differences in the elastic and plastic stress distributions at the limit state of the cylindrical vessel.

The radial stress distributions are broadly similar. They exhibit the same trend, with the radial stress varying from $-P_i$ at the inner surface to $0\ MPa$ at the outer. There is a small difference in the axial stress distributions. Where the elastic axial stress remains constant, the plastic axial stress is lower than the corresponding elastic stress at the inside surface and increases gradually through-thickness but the difference is relatively low when compared to that for the hoop stress.

The elastic and plastic hoop stress distributions are entirely different. The elastic hoop stress is at its greatest on the inside surface of the cylinder and decreases towards the outside surface. The plastic hoop stress however, follows the opposite trend as it gradually increases through the thickness. This is caused by stress redistribution. As the pressure is increased and plasticity spreads, the hoop stress increases to accommodate the additional load until the stress intensity reaches yield, at which point no additional load can be carried if perfect plasticity is assumed. The stress intensity is then calculated as the difference between the maximum and minimum principal stresses. Therefore, if the principal stresses act in the same direction as the traction stress components, this becomes the difference between the hoop and radial stresses in this instance. As the traction boundary condition for radial stress dictates that the stress must be at $-P_i$ on the inside surface and zero on the outside, once the inside surface of the cylinder yields, the hoop stress cannot increase further, unlike in the elastic solution. Also, as plasticity spreads through the thickness as the load is increased to P_L, the hoop stress must also increase since the radial stress is increasing.

These differences bring into question the use of linearised elastic stress results to determine allowable loads when assessing a plastic failure mechanism. Also, in thick components such as this cylindrical vessel, the elastic hoop and radial components are

clearly non-linear, further indicating that linearised elastic stresses may not provide a sufficiently accurate representation of the stress distribution in thick components.

To investigate this further, stress linearisation of the cylindrical vessel was carried out using the ASME VIII Div 2 method and the three additional methods from Table 13. The linearised stress intensity plots in Figure 35 show that how the individual stress components are treated can have a significant impact.

One of the most notable differences is in the membrane stress of LM 2. Unlike the other three LMs, the membrane stress is not constant along the SCL. This is due to the radial membrane stress being defined as $\sigma_{x,m} = \sigma_x$. This effectively means that the surface traction boundary condition of $-P_i$ to 0 is applied to the radial component of linearised membrane stress. Figure 34 shows that the total elastic radial stress component follows this distribution. The primary membrane stress was taken as the maximum value, located on the inside surface, but as this is greater than the membrane stress for each of the other methods, the limit pressure calculated using LM 2 was lower.

The limit pressures using ASME VIII Div 2, LM 1 and LM 3 were equal, as the membrane stress tensors are constructed in the same manner. They exceeded the exact analytical solution by 2.7%. The higher membrane stress obtained using LM 2 meant it was the only method that did not over calculate the allowable load but went the opposite way, being a whole 19.5% less than the exact analytical solution.

The main reason for applying the limit state boundary condition to the radial component of membrane stress was to investigate if satisfying this condition would remove the non-conservatism observed in the ASME VIII Div 2 linearisation of thick walled components. It was found that for decreasing r/t, LM 2 followed the same trend as the linear analytical limit pressure plot in Figure 33. So although the LM 2 limit pressures never exceed the exact solution, they do quickly become over-conservative. Also, the LM 2 membrane stress is not a true membrane stress as the distribution varies through-thickness and does not represent an average stress.

Although the limit pressure of the cylinder is dictated by the primary membrane stress, there is a clear difference in the maximum M+B stress and the total Tresca stress

intensity at the inside surface of the cylinder when using the ASME VIII Div 2 LM. The difference in the total stress and M+B stress is the peak stress. The ASME III definition states that peak stresses occur: “by reason of local discontinuities or local thermal stress including the effects, if any, of stress concentrations”[7]. Some examples of the conditions giving rise to peak stresses are then given, including thermal stresses in austenitic steel cladding, thermal stresses leading to fatigue, stresses at local discontinuities and surface stresses resulting from a thermal shock. The example investigated here is of a simple cylindrical vessel subject to an internal pressure only, so by the ASME III definition, no peak stress should be present. Instead, the non-linearity stress predicted using the ASME VIII Div 2 LM must arise from a non-linear component of the true bending stress. The ASME VIII Div 2 recommendation is that plastic analysis be used when $r/t < 4$. The thick cylinder example deliberately violates this, with $r/t = 2.5$ to investigate the impact of LM 2 in particular to help determine if an alternative linearisation method could be used in lieu of plastic analysis in such cases. The results reinforce the need for the r/t ratio imposed by ASME VIII.

For thick components such as this cylinder, the bending stress normally follows a non-linear distribution through-thickness. ASME VIII Div 2 prescribes that the radial bending stress component is to be neglected in the linearised bending stress tensor as it has no physical meaning. However, a non-linear stress component acting along the SCL does exist and although it may not make sense to call this a “bending” stress with regards to the SCL, simply ignoring it may not be appropriate either. In the case of the pressurised cylinder, neglecting the radial bending stress component results in the prediction of false peak stresses and a non-conservative approximation of the M+B stress. During stress classification, this may have a significant bearing on the allowable design parameters, especially for the design check on the primary plus secondary stress.

The other three LMs under investigation all incorporate the radial bending stress into the analysis. It is immediately clear from Figure 35 that when LM 1 is used, where all stress components are linearised, the disparity in the maximum M+B stress and total stress on the inner wall surface is significantly reduced. That result is a consequence

of simply linearising the radial bending stress in the same manner as the other stress components.

The difference in the M+B and total stress intensity is reduced further when LM 2 is used. This indicates that by considering the limit state traction boundary condition during linearisation [114], the non-linearity stress is accounted for. A similar concept is applied in LM 3; however, the membrane stress tensor is calculated as per the ASME VIII Div 2 method. The non-linearity stress is included as part of the M+B stress tensor in LM 3 by applying the traction boundary condition to the radial M+B stress component, as opposed to the radial membrane stress component. This results in the M+B stress distribution of LM 2, while maintaining the less pessimistic membrane stress of ASME VIII Div 2 and LM 1.

Plots of linearised stress component distributions through-thickness highlight the dissimilarities in each LM. Figure 36 shows the hoop and axial membrane stress components are identical for each method. For the radial component in LM 2 however, instead of a constant through-thickness distribution, the limit state boundary condition for a pressurised cylinder is indeed satisfied.

For the M+B stress components in Figure 37, the radial limit state boundary condition is satisfied for LM 2 and LM 3. In fact, the normal M+B stress distribution is shown to be identical for LM 2 and LM 3. This result was to be expected, it can be seen in Table 13 that the radial, hoop and axial components of the M+B stress tensor are defined in the same way for LM 2 and LM 3. It is the linearisation of shear stress components that differ and, while inconsequential for this case, the tubesheet results were heavily dependent on the linearised shear stress. Figure 37 also shows that while the radial M+B stress in LM 1 does not quite vary from $-P_i$ to zero, it does follow a similar trend and approximates the limit state more effectively than the ASME VIII Div 2 distribution, for which the radial M+B stress component remains constant.

To determine more clearly which LM provides the most accurate assessment for the determination of plastic collapse loads, the same process was carried out on the LWR nozzle-vessel. As this geometry is typical of a nuclear component, these results allow the effectiveness of each LM for the practical assessment of a nuclear component to be investigated.

The elastic Tresca stress intensity plot in Figure 38 shows that the maximum stress occurs at the nozzle crotch corner. For the SCL placement, locations were chosen to try and capture the most damaging regions; however, Figure 39 shows no SCLs were placed diagonally at the corner as it is a transition region. If a SCL was placed here, the membrane stress would be classified as local primary, which has a lower design margin than general primary membrane stress. Therefore, the critical SCL is unlikely to be here.

Figure 39 shows a selection of SCLs were placed in the nozzle and vessel. For the 3D model, SCLs were placed in the straight section of the cylindrical vessel as this was expected to be the likely failure location. SCL 3 was placed at the boundary to the ring juncture, SCL 2 was at the 100% reinforcement limit and SCL 1 was in the vessel wall away from the nozzle opening. SCLs 4, 5 and 6 were in the nozzle section but the stresses at these regions were much lower.

The allowable pressure load for the 3D nozzle was calculated in Table 14 as $19.67\ MPa$ for ASME VIII Div 2, LM 1 and LM3 with the critical location being SCL 3. There are no primary bending stresses present and so the primary stress limit is calculated based on the membrane stress alone, hence why three of the LMs produce the same result. The LM 2 allowable pressure of $18.30\ MPa$ was more conservative and proved to be overly so, as it is shown in section 5.1 that limit analysis of the nozzle proves all the elastic results under predict the allowable pressure. This follows the same findings from the simple cylinder analysis, where the LM 2 primary membrane stress proved to be conservative. Figure 40 displays how the membrane stress for LM 2 is greater than for each of the other LMs on the inside surface.

Elastic DBA of the nozzle highlighted that limitations in the linearisation process are compounded by the importance and difficulty of SCL placement and stress classification in translating the raw stress data into meaningful results for component design. These practical design considerations were not apparent in the simple cylinder analysis.

The choice of LM did not have a significant impact on the plastic collapse loads for the LWR nozzle, as LM 2 is the only method which calculates the membrane stress

differently. There was a notable difference, however, when assessing the tubesheet using elastic DBA in section 4.1.3.

Bending stresses induced by a mechanical load on the tubesheet are classified as primary and therefore do impact the collapse load. The elastic stress intensity plot in Figure 41 highlights the inner and outer rows of penetrations as being high stress regions that are not just localised to the surface. This helped inform the location for the SCLs in Figure 42, where three SCLs extend through the thickness of the tubesheet at the edge of adjacent penetrations and at the midpoint between them. In order to properly capture the correct failure location, many SCLs may be required and correctly classifying the linearised stress is not obvious. ASME BPVCs define primary bending stress in a tubesheet as the average stress between perforations. The bending stress gradient through thickness is calculated at a number of SCLs along the ligament and then averaged. Primary membrane stress is averaged over the cross section of interest. This makes the stress linearisation and classification process even more convoluted, as multiple SCLs are required between ligaments for a single assessment.

Primary M+B stresses and corresponding collapse loads are presented in Table 15 for the tubesheet. From lowest to highest, the collapse loads calculated using LM 3 (2975.61 kN), ASME VIII (2991.22 kN) and LM 1 (3064.26 kN) were separated by 88.65 kN. The collapse load calculated using LM 2 (3509.02 kN) was the highest by some margin, with a 533.4 kN difference to LM 3.

The reason for such significant discrepancies in the collapse loads between each method for this problem compared to the LWR nozzle is due to the failure mechanism. Bending stress is classified as primary, meaning the collapse load is not dictated by the membrane stress tensor only. Also, the tubesheet experiences a substantial shear load at the inner row of penetrations. LM 2 is the only method which does not linearise the in-plane shear stress components at all, instead the total shear stress is used in the M+B tensor. The ASME VIII method only considers average in-plane shear stresses but predicts a much lower collapse load. This highlights that the collapse load of the tubesheet under such loading conditions is highly sensitive to the in-plane shear stress distribution along the SCL.

The in-plane shear stress components have a parabolic distribution through the tubesheet thickness with the maximum at the centre. By linearising these components, the contribution of the in-plane shear stress is inflated at the surface (ends of the SCL). This results in a significant under estimation of the collapse load when combined with the other membrane and bending stress components, where maximum values do occur at the extremities of the SCL. The results of the tubesheet elastic DBA expands on the research conducted by Li [114] by applying the methodology to a complex but common component and highlighting a problem area where this method could yield substantially improved results over established BPVC elastic DBA procedures.

A limit analysis of the tubesheet, conducted in section 5.1, gave a collapse load of 3721.83 kN which is 212.82 kN (6.1%) greater than that of LM 2. This suggests that ASME VIII, LM 1 and LM 3 are all overly conservative when assessing the collapse loads of a thick tubesheet and that using the total shear stress in the M+B stress tensor provides a more accurate approximation of the limit state for components subject to high shear loads.

The effect each LM had on the $\Delta(P+Q)$ check for elastic shakedown was also investigated. The results for the oblique nozzles under a cyclic pressure load presented in section 4.2.1 are discussed first.

The elastic Tresca stress intensity plots for nozzle 5 in Figure 43 and nozzle 6 in Figure 44 both indicate a region of high stress inside the nozzle on the oblique side. For both nozzles, this occurs near the junction with the vessel. Based on this, SCLs were located as shown in Figure 45, in an attempt to capture the highest linearised stresses.

At SCL 1, the greatest value of $\Delta(P+Q)$ in Table 16 for Nozzle 5 was calculated using LM 3, with the lowest value obtained using LM 2. Therefore, P_{SD} using LM 2 was the least pessimistic at 4.37MPa and only 9.32% lower than the equivalent BNL result of 4.82MPa.

There was far less variation in $\Delta(P+Q)$ between linearisation methods for Nozzle 6 at SCL 1. Table 18 shows that all the results lie within a 2% margin. This could be due to the thinner wall thickness, which highlights how the nonlinear radial bending stress component has more of an influence on the overall M+B stress tensor in the thicker

Nozzle 5. For Nozzle 6, ASME VIII Div 2 was 11.69% lower than BNL and, as such, closest to the experimental result. LM 2 was very similar at 11.78% and LM 3 was the most pessimistic at 13.68%. Realistically, the difference between them makes the choice of LM negligible, confirming that the linearisation process does not require as much consideration for thin-walled structures.

The results discussed above were taken at SCL 1, however, issues regarding SCL placement persist. SCL 1 does not actually capture the highest stresses in the section and so two extra SCLs were investigated, for which the highest linearised stresses were observed at SCL 2. When following the recommendations in WRC 429 and ASME VIII Div 2, the validity of SCL 2 is questionable. Although not easily identifiable for oblique nozzles, SCL 2 would be considered to be within the transition region. Static pressure limits calculated in transition regions tend to be overly conservative [21] and looking at the SCL 2 results for each nozzle in Table 17 and Table 19, this study shows that this is also the case for P_{SD} of the oblique nozzles.

SCL 2 is placed such that it captures the maximum stresses. The allowable pressures presented in Table 17 and Table 19 show a similar trend between the linearisation methods and corresponding P_{SD} for both nozzles. ASME VIII Div 2 is the most conservative, then LM 3 and LM 1, with LM 2 giving the highest allowable P_{SD}. The percentage error between the elastic DBA and the BNL experiments shows that ASME VIII Div 2 under predicts P_{SD} by 18.55% and 22.85% for nozzles 5 and 6 respectively. LM 2 actually calculated P_{SD} to within the closest margin of BNL but there was very little difference in the results for LM 1, LM 2 and LM 3 with the allowable pressure between 12.43% and 11.51% for Nozzle 5 and between 18.93% and 18.54% for Nozzle 6.

This shows that the ASME VIII Div 2 method is more sensitive to SCL placement than the other linearisation methods investigated. For nozzle 6, the ASME VIII Div 2 LM goes from producing the lowest $\Delta(P+Q)$ at SCL 1 to the highest at SCL 2. The other LMs all predict higher $\Delta(P+Q)$ but do not increase by as much as the ASME VIII Div 2 result did. As such, the recommendation that SCLs should not be placed in transition regions may be less applicable if the radial bending and in-plane shear stresses are included in the linearisation procedure. A similar trend was seen in Nozzle

5, whereby the difference in $\Delta(P+Q)$ between SCL 1 and SCL 2 was much greater for ASME VIII Div 2 than the other LMs.

Despite the allowable cyclic loads being safe at SCL 1, there is only a slight decrease in the allowable cyclic load at SCL 2 for LM 1, LM 2 and LM 3 and they are being calculated based on higher M+B stresses. The ASME VIII Div 2 result is the only one that is severely affected by the use of SCL 2, indicating that perhaps SCLs in transition regions may be used with other LMs. The same conclusion is observed in the results of the thermal shock nozzle in section 4.2.3, which are discussed further down.

The solid red line in Figure 46 and Figure 47 for nozzles 5 and 6 indicate the BNL experimental values [4] for the onset of alternating plasticity. It is clear that all four linearisation methods maintain some conservatism, thus demonstrating that all the calculated elastic shakedown loads are safe. Some linearisation methods are less pessimistic than others. ASME VIII Div 2 is the most pessimistic at SCL 2 for both nozzles and LM 2 is the least, albeit by only a slight margin over LM 1 and LM 3. It is also clear that all four methods are conservative relative to both the upper bound and lower bound results calculated by Ure and Chen [111], highlighting the accuracy of the LMM in calculating the shakedown limit.

There were no clear trends in the results for nozzles 5 and 6 to base a recommendation for one of the four LMs as being superior. Further investigation was therefore conducted to identify the effectiveness of the elastic DBA methods in predicting elastic shakedown when components are subject to cyclic thermal loads.

The results for the pressurised cylinder under a cyclic temperature distribution are presented in section 4.2.2. The nodal temperature distribution, at $T = 700℃$, is shown in Figure 48. The temperature distribution was calculated by separate thermal analysis before being imported into the structural model.

Stress distributions in Figure 49 display how the thermal stress evolves over the cycle. The maximum Tresca stress intensity rises from $349.2\ MPa$ to $1133\ MPa$ at the peak of the cycle. High stresses occur at the inside and outside surfaces, with a low stress region in the centre. It is also clear that the axial position of the SCL has no bearing on the result, as the axial stress is constant.

Figure 50 presents linearised stress results for $\Delta(P+Q)$ over the cycle for different thermal loads. It is clear that at low cyclic temperatures, where the thermal stress is low, the difference in $\Delta(P+Q)$ is negligible (<1% difference in the results). The results for each method start to diverge slightly as the thermal load, and hence stress, increases. This suggests that under more extreme thermal transients, the choice of linearisation method could have an impact. At 700°C there is a difference of $62.2\ MPa$ between the ASME VIII Div 2 and LM 2&3 max stress range over the cycle.

The ASME VIII Div 2 procedure was the most conservative. This must be due to neglecting the radial bending stress component in the M+B stress tensor as the in-plane shear stress component is approximately $0\ MPa$ at the inside surface and so has no bearing on the final results. LM 1 includes the radial bending stress component but the result is only 1.3% lower, suggesting that linearising the radial stress component causes an overestimation. LM 2 and LM 3 gave identical results for $\Delta(P+Q)$ because the shear stresses are negligible. This means there was no difference between the M+B stress tensors for each in this case. Therefore, using the total radial stress in the M+B tensor as per LM 2 and LM 3 gives the least pessimistic value for P_{SD} for a thick cylinder under a constant pressure and cyclic temperature load.

Similar observations are shown when the results are plotted on the Bree diagram in Figure 51. The interesting observation with the Bree diagram is that it shows how different failure mechanisms may be predicted with different linearisation methods. At 550°C, all four methods exceed the $3S_m$ elastic shakedown limit, however, ASME VIII is more conservative as it predicts failure due to ratcheting. Linearised thermal and primary stress intensities calculated using the other three methods at 550°C lie within the alternating plasticity region. This is mainly due to the impact of the primary load. It was shown in Figure 35 that the linearised M+B stress intensity for an internally pressurised thick cylinder is greater on the inside surface for LM 1 compared to ASME VIII but is lower on the outside surface. This is what is observed in Figure 51. The maximum combined P+Q stress occurs on the outer diameter of the cylinder and is dominated by the secondary thermal stress. The linearised primary stress in this case is higher for ASME VIII compared to LM 1 despite neglecting the through thickness bending stress component. This results in LM 1 predicting alternating

plasticity while ASME VIII predicts ratcheting for the same loading conditions. LM 2 and LM 3 lie between LM 1 and ASME VIII on the Bree diagram for the primary load but give the least conservative linearised thermal stress results.

The previous two examples investigating the applicability of various LMs for the $\Delta(P+Q)$ design check have considered cyclic mechanical and cyclic thermal loads separately. The results in section 4.2.3 provide a more realistic insight, demonstrating which stress linearisation methods are most effective when analysing a typical plant transient on a component.

Figure 52 shows how the inside surface of the nozzle is cooled rapidly by the thermal shock, T_c. To capture the changes in stress caused by this over the cycle, five SCLs were placed as shown in Figure 53. Only SCL 1 and SCL 5 are technically valid in the context of WRC 429, as the other SCLs are within the nozzle transition region. However, as discussed with the oblique nozzles, SCL 1 in this case does not properly capture the high stress region. At SCL 1, Figure 55 shows that the ASME VIII Div 2 method allows a more severe T_c than LM 2 and LM 3.

For the oblique nozzles, the results at the "valid" SCL maintained some conservatism to the actual elastic shakedown limit. In the case of the thermal shock nozzle, SCL 1 fails to capture the high M+B stresses caused by the sudden drop in fluid temperature. Therefore, it is likely that alternating plasticity will not be predicted at SCL 1 first.

The most damaging stress ranges occur at SCL 3 and Table 20 shows that the ASME VIII Div 2 procedure is the most conservative LM when determining the allowable thermal shock load in this region. This is also shown in Figure 56 and Figure 57, as the ASME VIII Div 2 method becomes very conservative at SCL 2 and SCL 3. Once again it is far more sensitive to SCL placement than the other LMs and is the only method to predict higher linearised stresses at SCL 2 as opposed to SCL 3.

Focusing on the results at SCL 3, at low thermal shocks, there is very little difference in the results and as the thermal shock becomes more extreme, the results do diverge somewhat, as indicated in Figure 54. At $P_i = 8\ MPa$ there is a difference of $12.59℃$ in T_c between LM 1 and LM 3, equating to a difference of 13.7%. The thermal shock load difference between ASME VIII Div 2 and LM 1 was far greater at 25.4%, with

the ASME VIII Div 2 $\Delta(P+Q)$ value being calculated as $56.78\ MPa$ higher than that using LM 1.

Altering the internal pressure had less influence on the spread of results between each method, with the choice of linearisation method being more sensitive to the thermal shock load. This must be due to the presence of high thermal bending stresses, of which the component parallel to the SCL is not counted in the ASME VIII Div 2 M+B stress tensor. It has been shown that LM 1 gives the least conservative result.

6.2 Non-Linear DBA Results Discussion

Limit analysis of the LWR nozzle was carried out primarily to validate the elastic DBA results. The Tresca stress intensity allowable pressure for the 3D nozzle shown in Table 21 is $21.39\ MPa$, which indicates that the allowable pressures for each LM in Table 14 did maintain some conservatism. It also highlights the over conservatism of LM 2.

The equivalent plastic strain contour plot in Figure 58 shows that excessive deformation occurs around the nozzle junction with the straight part of the cylindrical vessel. This verifies the choice of SCL 3 as the critical location in the elastic DBA as it can be seen that in this region, plasticity has spread through the entire thickness of the vessel. The elastic DBA limit pressures at SCL 3 are still conservative with respect to the limit analysis. This is not just due to linearisation but also stress classification. There will be some discontinuity stresses acting, as SCL 3 lies within the reinforcement limit. Therefore, classifying the membrane stress as completely P_m may be conservative.

Limit analysis of the nozzle provides the global failure mechanism, negating the use of SCLs. Setting up the FEA model requires more experience than for the elastic FEA, however, it is still relatively straight forward and no post-processing of the results is required. The failure location can be easily identified from the plastic strain contour plot and the limit load is simply taken as the load at which the solution last converged. If following ASME III and the onset of plasticity is set to $1.5S_m$ in the FE software, the allowable load is calculated by dividing the limit load by 1.5.

To ensure that the limit load is found accurately, the minimum load step needs to be suitably small. If the load step is too large, then the last converged solution may be lower than the actual limit load. Reducing the load step will reduce conservatism; however, it will also increase the required computational time, as many more iterations may be required. The cost of computational time must be weighed up against solution accuracy. A load step sensitivity study for a 2D axisymmetric model with the same nozzle dimensions but for a spherical vessel was conducted to ensure that any further changes to the load stepping settings do not influence the final result [54]. There was only a 1.7% difference in the results between using a minimum load step of $0.1\ MPa$ to $0.0005\ MPa$, however, there was a 398% increase in computing time. Therefore, a minimum load increment of $0.01\ MPa$ was used in the 3D analysis as this represented a good compromise between accuracy in the solution and computational efficiency.

Table 21 presents limit pressures using the von Mises and Tresca failure criteria. The reason being that for elastic DBA, ASME III stress limits are all specified in terms of Tresca stress intensity. Other design Codes, such as ASME VIII Div 2, have precluded the use of Tresca stress intensity for elastic DBA by allowing the limits to be based on linearised von Mises equivalent stress. To keep the results coherent, the allowable pressures in Table 14 from the LM study are compared to the Tresca allowable pressure in Table 21 for the limit analysis. Most FE Codes, including Ansys Workbench, employ the von Mises failure criteria for non-linear plastic FEA. Utilising a Tresca failure criterion in plastic FEA can lead to convergence issues due to the sharp corners that define the yield surface.

A conservative approach to dealing with this is to scale the limit load obtained from EPP FEA by a factor of $\sqrt{3}/2$ (approximately 15%) as this will always be less than the Tresca equivalent limit load. This is shown in Figure 85, with the largest difference between the Tresca yield surface and von Mises yield surface being $\sqrt{3}/2$.

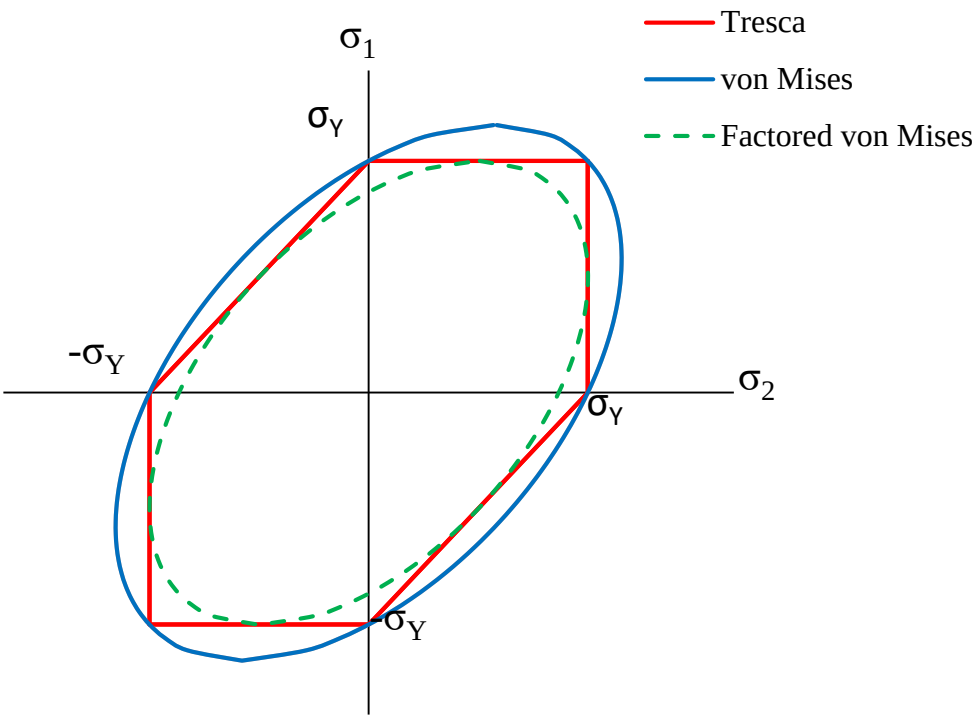

Figure 85: von Mises and Tresca yield surfaces

By scaling the limit load by $\sqrt{3}/2$, it will always fall within the Tresca failure criterion. It is not explicitly stated in ASME III that the von Mises failure criterion is prohibited for plastic analysis, only that it must not be used for the elastic analysis, so it can be assumed that this scaling factor is not necessarily required to satisfy the Code. It has been used in this case to maintain some consistency with the elastic results. This highlights that the use of finite element limit analysis within ASME III still requires more clarification and guidance.

Limit analysis of the tubesheet showed that use of the von Mises failure criterion is acceptable, as the limit analysis collapse load was 53.86% less than the average collapse load from two tests conducted by Jones and Gordon [3]. Table 22 shows that the allowable load found in this thesis is only $28.02\ kN$ (or $0.6\ MPa$) less than that of Jones and Gordon, who also conducted 3D FE limit analysis of the tubesheet. This provides validation that the procedure employed in this thesis is correct and that limit

analysis can be used to benchmark the elastic DBA results of the LWR nozzle and tubesheet.

As previously discussed in section 6.1, the LMs investigated under predict the tubesheet collapse load. Elastic FEA of the tubesheet was less computationally expensive but required substantial post processing of stress results. Elastic DBA is sensitive to the placement of SCLs and on components such as this, multiple SCLs are needed to carry out a robust analysis. The analyst needs to consider this at an early stage in the modelling process to make sure the mesh allows for easy and appropriate placement of SCLs. This all relies on analyst judgement and experience and as such, can be highly subjective and lacks repeatability. This highlights the relative ease with which limit analysis can be employed to achieve a better solution, assuming the computational resources are available.

The limit analysis failure location, shown as being at the innermost row of penetrations in Figure 59, and shape of the deformed structure also match the findings of Jones and Gordon. They highlighted how accurately the non-linear FEA approximated the deformed shape of the test specimen. As limit analysis can accurately predict the failure location, this indicates that the LWR nozzle is indeed likely to experience initial failure in the region of SCL 3 and validates the use of SCLs at the inner penetrations in elastic DBA of the tubesheet.

To carry out the elastic-plastic analysis, the same models were used as for the limit analysis, however, multilinear isotropic material hardening models were defined and non-linear geometry was assumed in the FEA. A discussion of the collapse loads in section 5.2.1 using the ASME VIII Div 2 elastic-plastic method, implementing the ASME VIII Div 2 stress-strain curve in the FEA, is conducted next.

The equivalent plastic strain plot in Figure 60 shows the plastic deformation of the LWR nozzle at the last converged solution following plastic FEA of the nozzle using the ASME VIII Div 2 stress-strain curve in Figure 18. This agrees with the limit analysis that the inside surface at the corner between the nozzle and vessel on the flat side experiences the greatest plastic strain. However, it proves that the component is capable of withstanding significantly more plastic deformation before failure.

What is immediately clear is that the plastic collapse load calculated using the ASME VIII Div 2 EP method, at $64.45\,MPa$, is considerably greater than that of the limit analysis. This is to be expected, as modelling strain hardening allows the structure to continue carrying additional load until the stresses reach $\sigma_{uts,t}$, as opposed to $1.5S_m$, before the material becomes perfectly plastic.

The main advantage in modelling the strain hardening capability of the material is that the analyst gains a better appreciation of the actual structural response and deformations in the structure at high loads. This is especially useful if there are additional service limits on the maximum permitted deformation.

ASME VIII Div 2 does allow an elastic-perfectly plastic material model to be employed in the plastic analysis but this is effectively a limit analysis with the effects of non-linear geometry considered. There was negligible difference in the plastic collapse load for a limit analysis with large deformation, however, when the ASME VIII Div 2 EP method was applied with small deformation theory assumed, the last converged solution was well in excess of $64.45\,MPa$. Thus highlighting the importance of including the effects of large deformation in the full plastic FEA to ensure any geometric weakening effects are accounted for. Geometric weakening is observed at the nozzle-shell junction for the LWR nozzle and in this case, this means that as the nozzle deforms under the internal pressure load, the load carrying capacity reduces for the deformed shape. This is captured in the elastic-plastic FEA by employing large deformation theory, which allows the stiffness matrix to be updated as the structure deforms.

The design factor specified in ASME VIII Div 2 is 2.4 for the design condition. This guarantees a design margin of 2.4 to the UTS, ensuring that the structure remains safe. Although the design margin in limit analysis is 1.5, this is to the yield strength, or $1.5S_m$. So if the ASME VIII Div 2 EP method is thought of as a limit analysis but with a design margin on the UTS rather than yield, it suggests that modelling the strain hardening could be unnecessary if interest is limited to the plastic collapse load.

Under this assumption, the ASME VIII Div 2 plastic method is simply a limit analysis, with the start of the perfectly plastic material behaviour scaled up by the ratio of the

design margins i.e. 2.4/1.5=1.6. However, this does not take into account the effects of any geometric weakening or strengthening.

Performing the ASME VIII Div 2 plastic method on the tubesheet showed that the collapse load can be predicted very closely. The equivalent plastic strain plot in Figure 61 agrees with the limit analysis that the inner and out row of penetrations experience significant plastic deformation. With the collapse load calculated as only 2.75% less than the average experimental plastic collapse load, this highlights the potential for this method to accurately predict the failure of pressurised components under static loads and demonstrates that there could be scope to include a similar procedure in ASME III for the design of nuclear components.

Formulating the monotonic stress-strain curves for the ASME VIII Div 2 plastic analyses was relatively simple. All the required material data was easily extracted from ASME II and the curve represents the behaviour of carbon steels in an as-fabricated condition [115]. The main issue with implementing the design curve within the elastic-plastic FEA was that the software requires the plastic strain-stress relationship, not the total strain.

The plastic strain portion of the curve is defined as $\gamma_1 + \gamma_2$ from equation (37). This is the true strain in the micro and macro-strain region of the stress-strain curve. To define a multilinear material model in Ansys, the curve must start at zero plastic strain and the corresponding stress. The software then uses Hooks law to define the elastic response at lower stresses. Therefore, the limit of proportionality had to be identified. In ASME PTB-1, the authors suggest that the proportional limit is set to approximately $R\sigma_Y$, where $R = \sigma_Y/\sigma_{uts}$ [115]. It was assumed that the plastic strain is zero for a stress corresponding to a very small value of plastic strain (approx. 1e-5) and for SA508 Gr3 Cl1, this equates to a stress value slightly lower than $R\sigma_Y$. Applying the material model in this way prevents convergence issues that may occur for a sharper transition from fully elastic to plastic behaviour.

Figure 62 displays how accurate the FEA simulated the structural response of the tubesheet with the ASME VIII Div 2 stress-strain curve clearly modelling the material behaviour very effectively. The normalised load-deflection curve from the non-linear FEA follows an almost identical path to that of the test data and highlights how

effective the material model can be. Furthermore, by proving that the material model used in the non-linear FEA accurately reflects the actual response of the structure, it removes an area of uncertainty when investigating the plastic collapse DBA methods i.e. the investigation can focus on determining the accuracy of the actual design methods, not how well the material behaviour is modelled.

Plastic collapse loads when utilising the TES method are calculated in section 5.2.2. One difficulty with the TES method is selecting the correct deformation parameter. ASME III recommends using the maximum principal total strain so plastic collapse loads were calculated based on both the maximum principal total strain and maximum deformation to investigate if there was any significant difference. The intersection points of the characteristic curves gave plastic collapse loads of $33.78\ MPa$ and $36.73\ MPa$ respectively. The curve for maximum principal total strain is shown in Figure 63 for the LWR nozzle.

There was a difference of $2.95\ MPa$ between the two results, with the use of maximum principal total strain as the deformation parameter being more conservative. It is immediately clear from the contour plots in Figure 64 that the choice of deformation parameter is important, as the maximum principal total strain and maximum deformation are located in different regions. The maximum principal total strain is at the inside surface on the corner of the junction between the nozzle and the straight section of the cylindrical vessel, whereas maximum deflection occurs away from the nozzle junction, in the curved section of the cylindrical vessel. These are labelled as location 1 and 2 in Table 23, where collapse loads are presented at each location using both deformation parameters.

The results in Table 23 highlight the issue with the TES as the collapse load is sensitive to the deformation parameter but also the location. Using deflection at the location of maximum principal total strain (Location 1), gives a collapse load only slightly higher than that at location 2, where maximum deflection actually occurs. This, however, is not true for the reverse case where maximum principal total strain is taken at location 2. The load vs deformation curve did not allow a clear tangent to be drawn in the elastic region, making it difficult to determine a collapse load.

Similar observations were made for the tubesheet. The more conservative collapse load was calculated using maximum principal total strain using Figure 65. Once again, the maximum strain did not coincide with the location of maximum deflection. The maximum principal total strain shown in Figure 66 occurred at the inside surface of one of the inner penetrations, whereas the maximum deflection was at the centre of the inner hub. The ASME VIII Div 2 plastic method already proved that the tubesheet fails at the inner row of penetrations. In this case, deflection of the central hub causes the tubesheet to fail in this manner, as it acts like a rigid body, transferring the load to the much thinner penetrated plate.

As with the LWR nozzle, both deformation parameters were investigated at both locations shown in Figure 67. Table 24 shows a 10.04 MPa difference in $P_{L,TES}$ between locations 1 and 2 when deflection is used as the deformation parameter with maximum principal total strain at location 1 still giving the most conservative result. No collapse load could be obtained using the TES method with maximum principal total strain at location 2 as the elastic tangent did not intersect the curve. The solution experienced loss of convergence before reaching strain levels high enough. This reinforces the limitations of the TES method and makes it an inefficient method to apply in industry if multiple load parameters and response curves have to be analysed before the analyst can have confidence in the result.

It is notable that the LWR nozzle TES allowable pressure load is less than the limit analysis result. The main reason for this could be explained by the compatibility of the TES method and use of the ASME VIII Div 2 material model in FEA. The TES in ASME III was originally intended as a method to determine the collapse load from experimental test data, with the linear regression line defined as a line of best fit in the "linear elastic region"[7]. The load vs deformation curve generated using FEA is very smooth and in the definition of the ASME VIII Div 2 material model, the limit of proportionality is defined at a very low strain level. This means that the curve starts to become very slightly non-linear at low loads. Defining the TES then becomes more difficult, as the analyst must decide where to calculate the gradient from.

The proportional limit for the LWR nozzle material model is taken at $140.5\ MPa$, so the FE model begins to experience plastic strain when the stress exceeds this.

However, the magnitude is minimal (<1e-5) and highly localised, so the structure is still predominantly undergoing elastic deformation. This means that defining the TES collapse line using the stress range between zero and 140.5 MPa is not particularly realistic, as the gradient is very steep and so the TES will also be steep, resulting in an under prediction of the plastic collapse load.

This issue was not evident when analysing the tubesheet. The same process was employed but the TES collapse load was comparable to that of the other plastic methods and greater than the limit analysis load. The only differences were in the elastic properties used to define the material model and the number of load increments simulated.

For the TI method, the collapse loads were much higher. Maximum principal total strain was used as the deformation parameter once again for the LWR nozzle in Figure 68. For the tubesheet however, transverse deflection of the inner hub gave a slightly more conservative collapse load. Therefore, the TI method was applied to the load vs deflection plot in Figure 69. Again, the point of failure was easily obtained as the point of intersection between the elastic and plastic tangent lines.

Once again, load vs deformation curves were created for both load deformation parameters and at both locations to determine the sensitivity of each variable. Collapse loads using the TI method for each component are presented in Table 25 and Table 26. As with the TES method, the TI method could not be applied due to the shape of the load vs maximum principal total strain curve at location 2 on the LWR nozzle. The TI method could be applied in all four cases for the tubesheet but again, the results are variable. In this case, the collapse loads calculated using deflection envelope those calculated using maximum principal total strain, again highlighting that the calculated collapse load is sensitive to the judgement of the analyst in deciding on the load parameter and assessment location.

Unlike with the TES method, the collapse load was less sensitive to the slope of the elastic tangent as the slope of the plastic tangent is more dominant. The software assumes perfectly plastic material behaviour at stresses greater than $\sigma_{uts,t}$. As no more strain hardening occurs beyond this point, the strain increases excessively for very small increments of load, meaning that the load vs strain plot becomes flat. This is a

problem because the plastic tangent line would therefore be horizontal. Therefore, the load vs strain and deformation curves do not include FEA results in the perfectly plastic regime for the TI method.

The load vs max principal total strain plot in Figure 68 displays the TI method for the LWR nozzle. It includes the strain up to a maximum internal pressure of $60\ MPa$. The structure enters the perfect plasticity phase of the material model at loads greater than $60\ MPa$. The effect that including these strains has on the TI method is demonstrated using Figure 86, where plastic tangent lines have been drawn based on the maximum principal total strain at $60\ MPa$ and at the converged solution at $64.45\ MPa$. It is clear that the plastic collapse load would be much greater and not representative of the TI method. The elastic tangent becomes redundant as the plastic tangent is almost horizontal. Therefore, it is important for the analyst to be aware that the FE software may assume a perfect plasticity response at stresses and strains greater than those defined in the multilinear model as the plastic tangent must be drawn from the section of the curve where strain hardening still occurs.

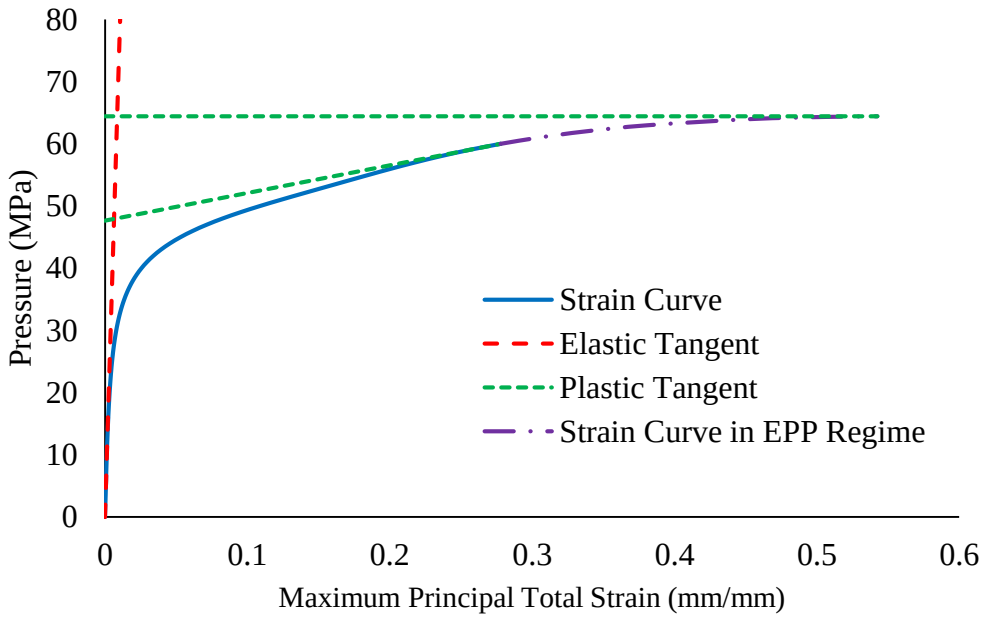

Figure 86: TI method comparison

One advantage of the PW method is that it eliminates the debate over the choice of deformation and load parameters. For both the LWR nozzle and tubesheet, the plot of plastic work vs internal pressure produces a smooth curve as indicated in Figure 70 and Figure 71. A tangent can be drawn from the straight part of the curve and the plastic collapse load is simply defined by the point of intersection between the tangent and the vertical axis.

The PW method was also slightly simpler than the TI, as only a single tangent was needed and as the collapse load depends only on the slope of the curve in the plastic regime, the method is not affected by the elastic response and so the issues experienced with calculating the TES collapse line were eliminated. Again, the LWR nozzle curve demonstrates the plastic work up to a load of $60\,MPa$. Both the load and PW are normalised by their respective maximum values.

By reviewing how the curvature of the plastic work develops, the formation and evolution of plastic deformation at that point is identifiable. There are different ways to calculate the curvature. Fitting a cubic spline to the data and using equation (32) produced a smooth curve with a defined peak for the LWR nozzle, as shown in Figure 72. This method can, however, result in multiple peaks in the curvature and make it difficult to identify a definite limit. This was the case for the tubesheet, with the normalised curvature plot in Figure 75 displaying three peaks and rendering the result invalid. Due to this inconsistency and unreliability, a more robust way of calculating the curvature is required.

Using the curve fitting method [66] to calculate the curvature produced a smooth normalised load vs curvature plot with a distinct peak for both the LWR nozzle and tubesheet. With normalised load on the horizontal axis and normalised plastic work on the vertical axis, Figure 73 shows the curve fitted to the FEA results for the LWR nozzle. The curve fits the data closely with the sum of the square of the difference $R^2 = 99.84\%$. The normalised plastic work curvature plot in Figure 74 could then be used to identify the load corresponding to the maximum curvature.

The same could be said for the tubesheet analysis, with $R^2 = 99.3\%$ the fit in Figure 76 was good but was not as accurate as the fit observed for the LWR nozzle. Also,

with one clear peak in the curvature, the plastic collapse load could be identified from Figure 77.

Determining the plastic collapse load from the local maximum of the normalised curvature plot will not actually be representative of the actual point of failure. It does prevent a non-conservative approximation of the collapse load since the maximum curvature actually indicates maximum stress redistribution. This means that at the peak, further stress redistribution is still possible and plastic collapse will not occur until the curvature of plastic work returns to zero or near zero [61]. For the LWR nozzle using the curve fit method it can be seen in Figure 74 that after the curvature peaks, the magnitude does reduce to a local minimum which equates to a collapse load of $58.42\ MPa$. This is 43 % greater than the plastic load taken from the peak curvature but is still below the ASME VIII Div 2 plastic method collapse load, suggesting that using the maximum curvature is far too conservative.

The main issue is that this point can be difficult to identify accurately and this is shown in Figure 77 for the tubesheet, where the magnitude of normalised curvature decreases steadily towards the maximum applied load. From the published test results it is known that the maximum load does not actually exceed the maximum collapse load, so the collapse load could be defined in this case at the maximum load. If the material model was defined to continue past the true ultimate tensile strength, the curvature should converge on a constant minimum. However, without the validation of test data, it may just be safer to define the collapse criteria conservatively using the maximum curvature. This also allows the process to be automated more easily, especially in the case of the curve-fit method where there is a single distinct peak in the plastic work curvature.

The most problematic aspect of the PWC curve-fit method is determining the optimised curvature parameters in Table 27 and Table 28. Being able to define the curve as a function is definitely advantageous when it comes to calculating the curvature but actually finding the coefficients can be time-consuming. As the plastic collapse load is directly dependent on the shape of the curve, it is of vital importance that the fitted curve is representative. An accurate fit was achieved for the examples

investigated in this study but for this method to be robust this would need to be the case for all problems.

Table 29 summarises the LWR nozzle plastic collapse and allowable load results for each plastic DBA method. It would be expected that the limit analysis gives the lowest plastic collapse load, as no strain hardening is included in the material model. As previously mentioned however, the TES predicts plastic collapse at an even lower load, which is clear from Figure 78. The allowable load was actually calculated as $2.18\ MPa$ less. The PW method gave the least pessimistic allowable load of $33.49\ MPa$, which was $8.79\ MPa$ (or 35.59%) more than that of the limit analysis.

The PW method was also the least conservative for the tubesheet as shown in Figure 79. There was a considerably greater spread in the allowable load results though, with an 85.86% difference between the allowable limit analysis load and PW load.

It is clear from Figure 79 that each DBA method gives a conservative plastic collapse load with respect to the test data. Therefore, the additional load that the PW method would allow is still safe, as it still under predicts the load-carrying capacity of the tubesheet. The PW collapse load was 14.24% less than the actual collapse load, so once the design margin of 1.5 is applied the allowable load still has a design margin of 1.7 to failure.

Again, Figure 79 highlights just how close the ASME VIII Div 2 plastic DBA method predicted the plastic collapse load of the tubesheet. However, it is immediately clear that the advantage gained in determining the actual point of structural instability due to modelling this additional load carrying capacity is negated by the application of the design factor. This was the case for both structures.

Despite demonstrating that structural instability does not occur in the LWR nozzle until the internal pressure reaches $64.45\ MPa$, the ASME VIII Div 2 plastic method allowable design pressure is only $26.85\ MPa$, a mere $2.15\ MPa$ (8.7%) greater than the limit analysis result. While the ASME VIII Div 2 plastic DBA method offers a greater advantage for the tubesheet, with a 31.7% increase over limit analysis, the allowable load is still less than each of the other methods. There is a difference of $47.33\ MPa$ between the PW and ASME VIII Div 2 plastic DBA allowable loads,

which equates to 41.09%. This is a significant difference and raises the question of whether the design margin of 1.7 achieved by the PW method is too low or the design margin of 2.4 in ASME VIII Div 2 is too large. Despite this, use of the ASME VIII Div 2 material model in the FEA provides a far better representation and understanding of the structural response and allows the analyst to reduce some conservatism in the design.

Figure 78 and Figure 79 show that a similar trend exists for both components in the conservatism of the allowable loads. Ranked from least to most conservative: limit analysis, ASME VIII Div 2 plastic DBA, PWC-Curve Fit, TI and PW. The TES was the anomaly, the reasons for which have been discussed detail and the PWC-Cubic Spline results have been omitted as they are not reliable.

The TI and PW methods rely on determining the plastic collapse load by finding tangents based on plastic portions of the load vs deformation curves and as such give comparative results and, without much additional effort, remove some of the pessimism of limit analysis. The main issue with the PWC curve fitting method is that optimised curve parameters need to be found. The fitted curve represents the FE data well for these examples; however other components and loading conditions would need to be investigated to identify if this can be achieved consistently, as the accuracy of the plastic collapse load is directly related to the accuracy of the fitted curve.

The ASME VIII Div 2 plastic method provides an exact solution and does not rely on load and deformation parameters or a graphical representation. It shows that by considering the effects of strain hardening, the plastic instability load is far greater than the limit analysis predicts. The main issue is the requirement of large design margins to satisfy ASME VIII Div 2.

Section 5.4 presents the cycle-by-cycle FEA results for the oblique nozzles. To prove elastic shakedown occurs at the loads calculated using the elastic DBA LMs, elastic-plastic FEA simulating 10 full pressure cycles of the thick nozzle 5 and thinner nozzle 6 was carried out. When subject to the highest allowable cyclic pressures determined from the elastic analysis, Table 31 shows that elastic shakedown was observed, providing further confirmation that each LM under predicted the cyclic pressure to cause alternating plasticity.

The cyclic pressure was then raised to $5MPa$ (i.e. well beyond the elastic shakedown limit pressure) and the plastic strain history for nozzle 6 was plotted in Figure 80. The plastic strain magnitude (PEMAG) and equivalent plastic strain (PEEQ) history outputs from Abaqus show that the plastic strain does fluctuate over each cycle. So it is immediately clear that the structure has not shaken down to fully elastic action.

After the first cycle, the maximum amount of plastic strain over a specific cycle does not increase, indicating an alternating plasticity mechanism, as opposed to ratcheting. This is clear from the plot of PEMAG vs pressure in Figure 80. The plastic strain never goes beyond 0.684%, instead cycling in a stabilised state between 0.578% and 0.684% over future cycles.

Using PEEQ, it is not immediately clear if the cyclic behaviour is alternating plasticity or ratcheting as PEEQ continuously increases over the 10 cycles. The increment by which PEEQ increases during each cycle becomes constant at 0.108%, thus indicating alternating plasticity. If PEEQ increased by a greater increment each time, then the component would be ratcheting.

The reason PEEQ always increases but PEMAG alternates is due to how each plastic strain measure is calculated. Both strain measures are scalar quantities of the total plastic strain and are calculated using the von Mises failure criterion as per equations (60) and (61) [72].

$$PEEQ = \overline{\varepsilon}^{pl}\big|_0 + \int_0^t \dot{\overline{\varepsilon}}^{pl}\, dt \tag{60}$$

$$PEMAG = \sqrt{\frac{2}{3}\varepsilon_{ij}^{pl}\varepsilon_{ij}^{pl}} \tag{61}$$

Where $\overline{\varepsilon}^{pl}\big|_0$ is the initial equivalent plastic strain, $\dot{\overline{\varepsilon}}^{pl}$ is the plastic strain rate and ε_{ij}^{pl} is the plastic strain field.

For proportional loading, $PEEQ = PEMAG$ and this is shown in Figure 80, as the pressure is initially ramped up from zero to P_i in the first cycle. However, as the

pressure is reduced back to zero, PEEQ continues to increase and PEMAG decreases. This is due to the load reversal over the cycle. If the plastic strain does not remain constant during this load reversal, then PEEQ will continue to increase. PEMAG however, takes into account the sign as it is a measure of the plastic strain in the structure at that specific moment in time.

Over the 10 cycles, although the plastic strain alternates, it returns to the original value at the end of the cycle when the load is reversed. This indicates alternating plasticity as the maximum PEMAG would continue to increase if the net plastic strain increased with each cycle. Therefore, although the PEMAG plot gives, at least initially, a clearer indication than PEEQ that alternating plasticity occurs, both are useful in determining the structural response.

The individual plastic strain components can also be inspected over each cycle to help determine if the structure has shaken down to elastic action. The individual plastic strain components can be inspected for nozzle 6 in Figure 81 to help determine that the cyclic load has exceeded the elastic shakedown limit. It is shown that the hoop strain, PE33, is the dominant component leading to alternating plasticity for nozzle 6.

The contour plot of PEEQ in Figure 82 shows that alternating plasticity develops on the inside surface of nozzle 6. It is clearly highly localised and so determining the exact location is crucial. It formed in a similar position for nozzle 5. This also validates the SCL placement for the elastic DBA. SCL 1 in Figure 45 does not capture the stresses leading to alternating plasticity. It does confirm that SCL 2 was in a more appropriate location and correctly deemed to be the critical location in the elastic analysis.

Figure 83 displays the residual plastic strain magnitude for the thermal-shock nozzle and shows that it is severe at the inside surface of the nozzle near the corner. This is remote from SCL 1 and in the region of SCL 2 and 3, indicating that SCL 1 is not positioned effectively to capture the stresses leading to alternating plasticity.

Figure 84 shows that cycle-by-cycle analysis at $P_i = 8\,MPa$ and $T_c = 41.47\,℃$ predicts an alternating plasticity mechanism to form at the inside surface of the nozzle, hence providing further evidence that the results at SCL 1 should not be used. Despite LM 2 and LM 3 giving stricter limits at SCL 1, cycle-by-cycle analysis when $T_c =$

64 ℃ also resulted in alternating plasticity. This shows that the allowable thermal shock load from the most conservative linearisation method at SCL 1 actually leads to alternating plasticity when cycle-by-cycle analysis is performed.

Cycle-by-cycle analysis at the SCL 2 limit of $T_C = 76.01$ ℃ did, however, result in elastic shakedown. This is clear from Figure 84, as PEMAG becomes constant with time. Therefore, the T_c limit for LM 1 at SCL 3 must be safe as it is slightly less severe at $T_c = 79.06$℃. This also proves that the other methods are overly conservative.

To demonstrate ratcheting in the component, a more extreme thermal shock of $T_c = 20$℃ was combined with a higher cyclic pressure of $P_i = 16\ MPa$. It is clear from Figure 83 that plastic deformation occurs through the entire thickness of the structure near the nozzle-vessel junction. The presence of an elastic core can be used to signify whether the component will shakedown, and as there is not one under these conditions in Figure 83, the component is likely to experience ratcheting. The plastic strain history plot in Figure 84 confirms that ratcheting occurs over the first 10 cycles and the magnitude of plastic strain is much greater. More cycles would need to be simulated in order to determine if the component will eventually shakedown or if it will continue to ratchet for these loading conditions.

Rauscher [112] highlighted that an area of significant plastic straining occurs on the inside surface at the junction between the nozzle and connecting pipe. Alternating plasticity actually occurs at this location as well and so this location would be of importance in the fatigue design check. It can be seen in Figure 83 however, that a plastic core exists in this region and the residual plastic strain does not spread through the thickness of the pipe. Therefore, while this location experiences alternating plasticity at lower thermal shock loads, it continues to behave in this manner for more extreme conditions, when other parts of the component are actually ratcheting.

Some of the biggest challenges surrounding elastic-plastic cycle-by-cycle analysis are computation time and interpretation of the results. The computation time for the cyclic analysis considered in this study was not particularly long, with the oblique nozzle 5 analysis taking the longest at 200 minutes for 25 cycles. This is due to the complexity of the geometry and the use of 3D solid continuum FEA, as the loading conditions and material model were simple. The thermal-shock nozzle analysis involved the use of

temperature dependent material properties and a more complex combined thermal-mechanical load transient. Taking advantage of the axisymmetric geometry to simplify the model, the computation time was approximately 60 minutes for 10 cycles.

The solution time obviously depends on the number of cycles and the hardware. What is not so obvious is just how many cycles need to be simulated. Figure 80 shows that the response stabilises after only 2 cycles for the oblique nozzles. Also, elastic shakedown occurs almost instantly in Figure 84 for a thermal shock of 76.01℃. It could then be argued that simulating 25 or even 10 cycles is excessive. However, if too few cycles are simulated, there is a risk that the behaviour will appear to stabilise when, in reality, it has not.

For the examples considered in this study it was fairly clear when elastic shakedown ceased and alternating plasticity began. This is not always the case, so although cycle-by-cycle analysis provides the actual structural response to the loading conditions, it is not always easy to interpret the results. It is particularly difficult to determine the failure mechanism when the response to the applied cyclic load is close to the shakedown and ratchet boundary. When a high degree of accuracy is required in such cases, direct methods such as the LMM are advantageous.

Chapter 7 Conclusion

Design by analysis is the method of choice for the design of Class 1 nuclear pressure vessels. With greater accessibility to increased computing power, analysts are able to take advantage of more detailed analysis methods to reduce the pessimism in the design of complex nuclear components.

A key issue faced by the stress analysis community within the nuclear industry is the apparent lack of cohesion between the use of modern FEA and the ASME III BPVC. Stress linearisation was introduced in an attempt to solve this but with the more recent emergence of non-linear DBA methods, research into elastic methods diminished, leaving many unresolved problems. The main practical problem is that the elastic route is still often used in industry to satisfy Code requirements to the satisfaction of nuclear regulatory bodies. As such, one focus of this thesis was to investigate different linearisation processes, to aid the analyst and provide more clarity when working to ASME III.

The thesis also considered how more advanced DBA methods can be used in the design of pressurised nuclear components. Alternative methods from the literature and other design Codes were investigated to determine their applicability. There was an emphasis on the practicality of such methods for use in industry and a particular focus on nozzle-vessel structures.

Where possible, elastic and elastic-plastic results were validated against published test data. The availability of such data is a noticeable gap in the literature, with computational methods frequently only being compared against each other. This is due to the lack of published test data, especially for realistic loading conditions on actual components. As such, considerable effort was made when reviewing the literature to identify experimental test results for typical nuclear components to validate the DBA methods for static and cyclic loading.

It should be noted that experimental and numerical results will never match exactly. Numerical methods rely on idealisations, assumptions and mathematical models to determine an approximate result. Test data also has limitations. Test results can be sensitive to practical issues such as measurement accuracy, material quality and number of test samples. It is therefore unrealistic to expect to match test results exactly.

Chapter 4 presented the linear elastic DBA results. The investigation into the use of stress linearisation and the individual stress components used in the linearised membrane and membrane plus bending stress tensors was required as much of the literature presents results for linearised stress without going into detail about the process used. This is an important step, as different design Codes prescribe different procedures and simply using built in stress linearisation tools in commercial FE software may actually violate the Code requirements. The methods employed also differ between different FEA programs. Therefore, one aim was to identify why different design Codes were not always in agreement and what exactly sets each linearisation method apart.

This research showed that following the ASME VIII Div 2 stress linearisation procedure can result in non-conservative membrane stress results. This was addressed by relating the linearised elastic stress distributions to limit state boundary conditions of a cylinder under internal pressure, as proposed by Li [114]. However, these results were overly conservative and it was concluded that the ASME VIII Div 2 recommendation on the use of plastic analysis for thick walled structures ($r/t < 4$) is appropriate and that ASME III could benefit from more guidance on when to use elastic or plastic analysis.

For the LWR nozzle, the allowable pressure is determined from the membrane stress only. This meant LM 2 was the only method to give a different result and this proved to be the least accurate. A more thorough investigation was therefore required to make any meaningful recommendations. It was also shown that the ASME VIII Div 2 linearisation method under-estimated the non-linear component of bending in the membrane plus bending tensor for the cylinder analysis. LM 1, 2 and 3 addressed this by including the radial bending component in the membrane plus bending tensor.

Results from elastic DBA of the tubesheet were more informative. Due to the presence of primary bending stress and the complexity of the geometry, there was a spread in the collapse loads. The failure mechanism is driven by a shear load and contradictory to the results of the LWR nozzle, LM 2 gave the least pessimistic collapse load by some margin, whilst still being safe. Including the shear stress in the linearised M+B stress tensor in this case was overly conservative. LM 2 takes the parabolic distribution

of the shear stress into account and by doing so, does not over predict the surface stresses in this case. This is a significant finding, highlighting that LM 2 is particularly effective when analysing thick components subject to high shear loads. This is an area that could be investigated further to determine the reliability of this method. The observations of the primary stress assessment prompted the investigation into the influence of the linearisation methods on the primary plus secondary stress check.

For cyclic pressure loading only, the elastic DBA results were benchmarked against published test data for the onset of alternating plasticity in oblique nozzles. This allowed the research to show that elastic shakedown does occur at the calculated elastic shakedown limit pressures, indicating that all linearisation methods maintained conservatism.

In the cyclic thermal analysis of the cylinder, there was an indication to suggest that the linearisation methods would diverge with increased severity of the thermal load. This was evident when analysing the nozzle with a thermal shock. The allowable thermal shock load did vary, with LM 1 allowing the most severe and ASME VIII Div 2 the least. Plotting the results on a Bree diagram allowed a visualisation of which cyclic response would be expected for each method at each thermal shock load. It was clear that the ASME VIII Div 2 method would predict ratcheting much sooner than the other three methods. In fact, at $T = 550°C$, the ASME VIII Div 2 method predicts ratcheting where LM 1, LM 2 and LM 3 all predict alternating plasticity. This analysis provides a significant contribution into the practical use of elastic DBA. Including a more complex transient combining cyclic thermal and mechanical loading brings together the findings from the previous studies, where cyclic pressure and cyclic thermal loads were considered separately, showing that the linearisation method does impact the primary plus secondary stress range.

Most of the literature on stress linearisation considers 2D axisymmetric models. One significant finding for 3D models, where the SCL is not necessarily defined by an axisymmetric plane, was that the ASME VIII Div 2 procedure is far more sensitive to SCL placement than LM 1. This was evident in the analysis of the oblique nozzles and thermal shock nozzle. The ASME VIII Div 2 method did not accurately calculate $\Delta(P + Q)$, being overly conservative at SCLs in the transition region but satisfying

$3S_m$ for a SCL at the juncture under loading conditions where alternating plasticity was observed in the plastic analysis. For the other linearisation methods however, the results were less sensitive to SCL placement. This is a desirable characteristic because as this thesis shows, effective placement of SCLs remains problematic.

This study on elastic DBA provided a detailed insight into the use of various stress linearisation methods for several different conditions, highlighting the positives of elastic DBA and identifying issues which have yet to be resolved. The main conclusion of this part of the study was that LM 1 proved to be the most consistent and is the recommended method of stress linearisation. It is simple to implement, as all the stress components are linearised, the membrane stress calculation is less conservative than that of LM 2 (and valid so long as $r/t > 4$) and resulted in less pessimistic primary plus secondary stress ranges than the ASME VIII Div 2 method. Further, LM 1 maintained conservatism when assessed against cycle-by-cycle analysis and published test results used to benchmark the elastic shakedown loads.

The non-linear DBA investigation complemented that of the linear elastic methods. Limit analysis of the LWR nozzle allowed the linearised results to be benchmarked whilst also allowing areas of development to be investigated. These findings agree with the literature in that the ability to identify the plastic collapse failure load and location, without complex material modelling or tedious post-processing, makes limit analysis especially useful. There could, however, be more guidance on its application in the context of ASME III. The use of the von Mises failure criterion in the plastic solver of commercial FE software should be specified to prevent any ambiguity. It was shown that applying a factor to shrink the yield surface to satisfy the Tresca criterion is unnecessary conservatism.

Plastic analysis of the tubesheet showed the ASME VIII Div 2 material model is accurate for low alloy steel, with the load vs deformation curve closely matching the published test data. The collapse load determined using the ASME VIII Div 2 plastic method was only slightly lower than the average test collapse load. By comparing the FE results to published tests data of an actual tubesheet, this part of the research provided evidence that the ASME VIII Div 2 material model and plastic analysis method could be adopted by ASME III for the analysis of nuclear pressurised

components. However, the LWR nozzle analysis particularly highlighted that the advantage over limit analysis is greatly reduced by the specified 2.4 design margin.

Application of the twice elastic slope method in conjunction with the ASME VIII Div 2 material model has previously been considered in the literature [116]. The results in this thesis expand on that work, showing that, as the plastic collapse load is dependent on the elastic response for the TES method, care is needed when defining the limit of proportionality in the material model and when defining the elastic region of the load-deformation results curve. This suggests that more guidance is required on defining the ASME VIII Div 2 stress-strain curve in commercial FE software and that other methods, which are not so heavily influenced by the elastic response should be used.

Comparing the various plastic collapse loads showed that the Plastic Work method is the least conservative and maintains an appropriate safety margin against the tubesheet test collapse load. This research confirmed that the Plastic Work method is a simple and straightforward way to determine the collapse load of 3D nuclear structures.

The cyclic structural response of the oblique nozzles, pressurised cylinder and thermal-shock nozzle was found by performing full cycle-by-cycle FEA of each component under their respective loading conditions. It was relatively simple to determine if elastic shakedown had occurred in these cases and this study helped highlight how different plastic strain measures should be interpreted. As shown in the literature other issues such as accounting for numerical error [117] and deciding on the number of cycles to simulate still exist, however, elastic-plastic cycle-by-cycle analysis gives a detailed insight into the cyclic structural behaviour.

The work carried out in this thesis lays the foundations for more research into the use of advanced linear and non-linear DBA methods in the nuclear industry. The elastic DBA study could be expanded to look at a wider range of examples. The sensitivity of each linearisation method to different loading conditions and different components could be considered and extended to consider other design checks, such as the fatigue check.

The ASME VIII Div 2 plastic method could also be investigated on a greater number of structures. Different geometries and materials, such as stainless steels, could be

analysed to provide further evidence for the use of the monotonic stress-strain curve in ASME VIII Div 2.

For the cyclic analysis, elastic-perfectly plastic material properties were assumed. This is required for the shakedown check in ASME VIII Div 2 but not specified in ASME III. As such, there is scope to reduce the conservatism by considering a more complex kinematic hardening material model in the cyclic analysis. Therefore, other material models could be applied to the examples in this thesis to determine how much the shakedown and ratchet boundary moves.

Direct shakedown and ratchet techniques were mentioned in section 2.7 but not considered in the analysis. To provide further justification for their use to satisfy ASME III, further work looking at complex components and loading conditions should be carried out.

One of the biggest issues with developing DBA methods is determining their accuracy. To justify their use, the methods must be validated. Therefore, more experimental results, especially on structures representative of actual nuclear components, would provide invaluable data to benchmark DBA results.

Chapter 8 References

[1] International Atomic Energy Agency (IAEA), Safety of Nuclear Power Plants: Design, IAEA, Vienna, 2016.

[2] Office for Nuclear Regulation (ONR), Pressure Systems Safety, 2017.

[3] D.P. Jones, J.L. Gordon, Comparison of Limit Load Solutions with Results of Collapse Tests of Perforated Plates with a Triangular Penetration Pattern, in: PVP2002-1302, ASME Press. Vessel. Pip. Conf., ASME, 2002. doi:10.1115/PVP2002-1302.

[4] E. Procter, R.F. Flinders, Shakedown investigations on partial penetration welded nozzles in a spherical shell, Nucl. Eng. Des. 8 (1968) 171–185. doi:10.1016/0029-5493(68)90025-3.

[5] D. Moss, Pressure Vessel Design Manual, 3rd ed., Gulf Professional Publishing, 2004.

[6] J. Bree, Elastic-plastic behaviour of thin tubes subjected to internal pressure and intermittent high-heat fluxes with application to fast-nuclear-reactor fuel elements, J. Strain Anal. 2 (1967) 226–238. doi:10.1243/03093247v023226.

[7] ASME Boiler and Pressure Vessel Code Section III Rules for Construction of Nuclear Facility Components, ASME, New York, 2017.

[8] J. Lubliner, Plasticity Theory, Macmillan Publishing Company, New York, 1990.

[9] M. Yu, J. Li, G. Ma, Theorems of Limit Analysis, in: Struct. Plast., Springer, Berlin, 2009: pp. 64–73.

[10] E.G. Berak, J.C. Gerdeen, A Finite-Element Technique for Limit Analysis Of Structures, J. Press. Vessel Technol. 112 (1990) 138–144. doi:Doi 10.1115/1.2928599.

[11] D.C. Drucker, W. Prager, H.J. Greenberg, Extended limit design theorems for continuous media, Q. Appl. Math. 9 (1952) 381–389. doi:10.1090/qam/45573.

[12] R. Adibi-Asl, R. Seshadri, Variational Method in Limit Load Analysis—A

Review, J. Press. Vessel Technol. 140 (2018) 050804. doi:10.1115/1.4041058.

[13] M. Muscat, D. MacKenzie, Elastic shakedown analysis of axisymmetric nozzles, J. Press. Vessel Technol. 125 (2003) 365–370. doi:10.3390/en8031716.

[14] EPERC, The Design-by-Analysis Manual, European Commission, 1999.

[15] M. Muscat, R. Hamilton, Elastic Shakedown in Pressure Vessel Components Under Non-Proportional Loading, in: PVP2002-1522, ASME Press. Vessel. Pip. Conf., 2002.

[16] W. Reinhardt, Distinguishing Ratcheting and Shakedown Conditions in Pressure Vessels, in: PVP2003-1885, ASME Press. Vessel. Pip. Conf., ASME, 2003.

[17] P.T. Phạm, Upper bound limit and shakedown analysis of elastic-plastic bounded linearly kinematic hardening structures, 2011. doi:10.1007/978-94-007-5425-6_4.

[18] J. Ure, An Advanced Lower and Upper Bound Shakedown Analysis Method to Enhance the R5 HIgh Temperature Assessment Procedure, 2013.

[19] A. Jappy, A Constitutively Consistent Lower Bound , Direct Shakedown and Ratchet Method, 2014.

[20] J. Hechmer, G. Hollinger, The ASME Code and 3D Stress Evaluation, J. Press. Vessel Technol. 113 (1991) 481–487. doi:10.1115/1.2928784.

[21] J. Hechmer, G. Hollinger, 3D Stress Criteria Guidelines for Application, Welding Research Council Bulletin No. 429, 1998.

[22] G. Hollinger, J. Hechmer, Three-Dimensional Stress Criteria—Summary of the PVRC Project, J. Press. Vessel Technol. 122 (2000) 105–109. doi:10.1115/1.556157.

[23] ASME Boiler and Pressure Vessel Code Section VIII Division 2 Alternative Design Rules, ASME, New York, 2017.

[24] R. Adibi-Asl, W. Reinhardt, Shakedown And Ratcheting In ASME B&PV

Code, PVP2015-45824, ASME Press. Vessel. Pip. Conf. (2015). doi:10.1115/PVP2015-45824.

[25] D.P. Jones, C. Basavaraju, Subsection NB—Class 1 Components, in: Companion Guid. to ASME Boil. Press. Vessel Code, 4th ed., ASME, Three Park Avenue New York, NY 10016-5990, 2012: pp. 6-1-6–46. doi:10.1115/1.859865.ch6.

[26] O.H. Basquin, The Exponential Law of Endurance Tests, Proc. ASTM. 10 (1910) 625–630.

[27] S.S. Manson, Behavior Of Materials Under Conditions Of Thermal Stress, NACA Rep. 1170. (1954).

[28] L.F. Coffin, A Study of the Effects of Cyclic Thermal Stresses on a Ductile Metal, Trans. ASME. 76 (1954) 931–949. doi:10.1115/1.4015020.

[29] Tavernelli J. F., Experimental Support for Generalized Equation Predicting Low Cycle Fatigue, ASME J. Basic Eng. 84 (1962). doi:10.1016/j.ajem.2007.08.014.

[30] S.S. Manson, Fatigue: A Complex Subject—Some Simple Approximations, NASA TM X-52084. (1964).

[31] D.M. Clarkson, Fatigue Design Criteria for Austenitic Stainless Steels Based on Simplified Elastic-Plastic Analysis, University of Strathclyde, 2020.

[32] A. Kalnins, Stress Classification Lines Straight Through Singularities, in: PVP2008-61746, ASME Press. Vessel. Pip. Conf., ASME, 2008: pp. 317–326. doi:10.1115/PVP2008-61746.

[33] A.T. Strzelczyk, M. Stojakovic, Simplified Stress Linearization Method, Maintaining Accuracy, in: PVP2012-78521, ASME Press. Vessel. Pip. Conf., ASME, 2012. doi:10.1115/1.4024453.

[34] A.T. Strzelczyk, S.S. Ho, Evaluation of “Linearized” Stresses Without Linearization, in: PVP2007-26357, ASME Press. Vessel. Pip. Conf., ASME, 2007: pp. 493–498. doi:10.1115/PVP2007-26357.

[35] M. Lu, Y. Chen, J.-G. Li, Two-Step Approach of Stress Classification and Primary Structure Method, J. Press. Vessel Technol. 122 (2000) 2–8. doi:10.1115/1.556139.

[36] A. Bhattacharya, H. Patel, S. Patel, S. Bapat, An Application Of Two Step Stress Classification Approach (Primary Structure Method) For Stress Classification At Cylindrical Shell- Nozzle Intersections Subjected To Internal Pressure, Radial Load And In-And Out- Of Plane Bending Moments, in: PVP2015-45533, ASME Press. Vessel. Pip. Conf., ASME, 2015. doi:10.1115/PVP2015-45533.

[37] A. Bhattacharya, S. Patel, S. Bapat, M.P. Cross, H. Patel, Stress Classification at Cylindrical Intersections Using Primary Structure Method: A Parametric Study Using Finite Element Method, in: PVP2016-63154 ASME Press. Vessel. Pip. Conf., ASME, 2016. doi:10.1115/PVP2016-63154.

[38] C. Duan, L. Ding, M. Lu, Discussion on the Implementation of the Primary Structure Method in Design by Analysis, Appl. Mech. Mater. 853 (2016) 341–345. doi:10.4028/www.scientific.net/AMM.853.341.

[39] C. Duan, X. Wei, J. Huang, M. Lu, Construction of 3D Primary Structure and Stress Classification of Cylindrical Shell with Nozzle, in: PVP2018-84391, ASME Press. Vessel. Pip. Conf., ASME, 2018. https://asmedigitalcollection.asme.org.

[40] B. Gao, X. Shi, H. Liu, J. Li, Separation of Primary Stress in Finite Element Analysis of Pressure Vessel with the Principle of Superposition, Key Eng. Mater. 353–358 (2007) 373–376. doi:10.4028/www.scientific.net/KEM.353-358.373.

[41] B. Gao, X. Chen, X. Shi, J. Dong, An Approach to Derive Primary Bending Stress From Finite Element Analysis for Pressure Vessels and Applications in Structural Design, J. Press. Vessel Technol. 132 (2010) 061101. doi:10.1115/1.4001656.

[42] D. Mackenzie, Stress Linearization Concepts and Restrictions in Elastic Design by Analysis, in: PVP2017-65678, ASME Press. Vessel. Pip. Conf., ASME,

2017. doi:10.1115/PVP2017-65678.

[43] H. Li, X. Huang, H. Yang, Extending stress linearization procedures for direct method design in pressure vessel design, in: Proc. Int. Conf. Adv. Mater. Struct. Mech. Eng., 2016.

[44] H. Li, X. Huang, P. Yang, H. Yang, A new pressure vessel design by analysis method avoiding stress categorization, Int. J. Press. Vessel. Pip. 152 (2017) 38–45. doi:10.1016/j.ijpvp.2017.05.003.

[45] X. Ren, H. Li, X. Huang, Assessment of DBA-L Pressure Vessel Design Method by a Cylindrical Vessel with Hemispherical Ends, in: 5th Int. Conf. Mechatronics Mech. Eng. (ICMME 2018), 2019.

[46] S. McKillop, W. Reinhardt, V. Reddy, W. Koski, Validation of Thermal Stress Ratcheting Criteria, in: PVP2014-28820, ASME Press. Vessel. Pip. Conf., ASME, 2014. doi:PVP2014-28820.

[47] A.K. Dhalla, Verification of an Elastic Procedure to Estimate Elastic Follow-Up, J. Press. Vessel Technol. 108 (1986) 461–469. doi:10.1115/1.3264813.

[48] R. Seshadri, C.P. Fernando, Limit loads of mechanical components and structures using the GLOSS r-node method, J. Press. Vessel Technol. 114 (1992) 201–208. doi:10.1115/1.2929030.

[49] R. Seshadri, Robust Stress-Classification of Pressure Components Using the GLOSS and GLOSS R-Node Methods, J. Press. Vessel Technol. 118 (1996) 208–215. doi:10.1115/1.2842183.

[50] I.F.Z. Fanous, R. Seshadri, Stress Classification Using the r-Node Method, J. Press. Vessel Technol. 129 (2007) 676–682. doi:10.1115/1.2767357.

[51] D. Mackenzie, J.T. Boyle, A Computational Procedure for Calculating Primary Stress for the ASME B&PV Code, J. Press. Vessel Technol. 116 (1994) 339–344. doi:10.1115/1.2929599.

[52] D. Mackenzie, J.T. Boyle, R. Hamilton, The elastic compensation method for limit and shakedown analysis: a review, J. Strain Anal. Eng. Des. 35 (2005)

171–188. doi:10.1243/0309324001514332.

[53] M. Martin, L. Rawson, D. Rice, A hierarchical finite element framework for the assessment of pressure vessels to the ASME III code, in: PVP2010-25097, ASME Press. Vessel. Pip. Conf., ASME, New York, 2010: pp. 125–135. doi:10.1115/PVP2010-25097.

[54] M. Martin, C. Watson, K. Wright, Review of ASME III code case for the application of finite element based limit load analysis, in: PVP2011-57138, ASME Press. Vessel. Pip. Conf., 2011: pp. 513–518. doi:10.1115/PVP2011-57138.

[55] A. Towse, M. Martin, P. Hurrell, R. Philipson, A. Allen, C. Andrews, Application of limit load analysis to complex structures, in: PVP2012-78040, ASME Press. Vessel. Pip. Conf., 2012: pp. 807–812. doi:10.1115/PVP2012-78040.

[56] R.C. Biel, C. Alexander, Applications of Limit Load Analyses to Assess the Structural Integrity of Pressure Vessels, in: PVP2005-71724, ASME Press. Vessel. Pip. Conf., ASME, 2005. doi:10.1115/PVP2005-71724.

[57] WNA, Non-Linear Analysis Design Rules Part 1: Code Comparison Cooperation in Reactor Design Evaluation and Licensing – Mechanical Codes and Standards Task Force, WNA, 2017.

[58] C.H.A. Townley, G.E. Findlay, A.M. Goodman, P. Stanley, Elastic-Plastic Computations as a Basis for Design Charts for Torispherical Pressure Vessel Ends, Proc. Inst. Mech. Eng. 185 (1970) 869–877.

[59] M. Muscat, D. Mackenzie, R. Hamilton, A work criterion for plastic collapse, Int. J. Press. Vessel. Pip. 80 (2003) 49–58. doi:10.1016/S0308-0161(02)00105-9.

[60] H. Li, D. Mackenzie, Characterising gross plastic deformation in design by analysis, Int. J. Press. Vessel. Pip. 82 (2005) 777–786. doi:10.1016/j.ijpvp.2005.06.003.

[61] D. Camilleri, D. Mackenzie, R. Hamilton, Evaluating Plastic Loads in

Torispherical Heads Using a New Criterion of Collapse, J. Press. Vessel Technol. 130 (2008) 011202. doi:10.1115/1.2826427.

[62] T. Naruse, D. Mackenzie, D. Camilleri, Gross Plastic Deformation of a Hemispherical Head with Cylindrical Nozzle: A Comparative Study, in: PVP2007-26298, ASME Press. Vessel. Pip. Conf., ASME, 2007. doi:10.1115/PVP2007-26298.

[63] V.N. Skopinsky, N.A. Berkov, New Criterion for the Definition of Plastic Limit Load in Nozzle Connections of Pressure Vessels, J. Press. Vessel Technol. 135 (2013) 021206. doi:10.1115/1.4007188.

[64] V.N. Skopinsky, N.A. Berkov, R.A. Vozhov, Effect of Pad Reinforcement on the Plastic Limit Load for Nozzle Connection of Cylindrical Vessel, J. Press. Vessel Technol. 137 (2015) 021207. doi:10.1115/1.4028301.

[65] D.G. Moffat, M.F. Hsieh, M. Lynch, An assessment of ASME III and CEN TC54 methods of determining plastic and limit loads for pressure system components, J. Strain Anal. Eng. Des. 36 (2001) 301–312. doi:10.1243/0309324011514485.

[66] C.K. Seal, R.A. Ainsworth, J.-J. Han, Comparison Of Plastic Work Curvature Methods For Assessing The Collapse Load Of A Structure, in: PVP2015-45544, ASME Press. Vessel. Pip. Conf., ASME, 2015. doi:10.1115/PVP2015-45544.

[67] C.K. Seal, J.J. Han, R.A. Ainsworth, A comparison of various plastic work curvature methods, Int. J. Press. Vessel. Pip. 135–136 (2015) 26–35. doi:10.1016/j.ijpvp.2015.10.001.

[68] J.H. Ricketts, G.A. Head, A five-parameter logistic equation for investigating asymmetry of curvature in baroreflex studies, Am. J. Physiol. - Regul. Integr. Comp. Physiol. 277 (1999) 441–454. doi:10.1152/ajpregu.1999.277.2.r441.

[69] D.P. Molitoris, J. V. Gregg, E.E. Heald, D.H. Roarty, B.E. Heald, Elastic-Plastic Shakedown Evaluation Using Asme Code Section III and Section VIII Methods, in: PVP2010-25669, ASME Press. Vessel. Pip. Conf., ASME, 2016. doi:10.1115/PVP2010-25669.

[70] T.M.L. Nguyen-Tajan, B. Pommier, H. Maitournam, M. Houari, L. Verger, Z.Z. Du, M. Snyman, Determination of the stabilized response of a structure undergoing cyclic thermal-mechanical loads by a direct cyclic method, in: Abaqus Users' Conf., 2003.

[71] M. Martin, Application of direct cyclic analysis to the prediction of plastic shakedown of nuclear power plant components, in: PVP2008-61067, ASME Press. Vessel. Pip. Div. Conf., ASME, 2008: pp. 265–275. doi:10.1115/PVP2008-61067.

[72] Dassault Systemes, SIMULIA User Assistance, (2017).

[73] M. Muscat, D. Mackenzie, R. Hamilton, Evaluating shakedown under proportional loading by non-linear static analysis, Comput. Struct. 81 (2003) 1727–1737. doi:10.1016/S0045-7949(03)00181-0.

[74] A.K. Bakry, C.A. Saleh, M.M. Megahed, Shakedown Limits for Hillside Nozzles in Cylindrical Vessels, J. Press. Vessel Technol. 140 (2018) 031601. doi:10.1115/1.4039503.

[75] H.F. Abdalla, M.M. Megahed, Validation of the Nonlinear Superposition Method (NSM) for elastic shakedown limit pressures via comparison with experimental test results of spherical vessels with radial and oblique nozzles, Int. J. Press. Vessel. Pip. 162 (2018) 19–29. doi:10.1016/j.ijpvp.2018.02.008.

[76] H.F. Abdalla, M.M. Megahed, M.Y.A. Younan, A simplified technique for shakedown limit load determination, Nucl. Eng. Des. 237 (2007) 1231–1240. doi:10.1016/j.nucengdes.2006.09.033.

[77] H.F. Abdalla, Shakedown boundary determination of a 90° back-to-back pipe bend subjected to steady internal pressures and cyclic in-plane bending moments, Int. J. Press. Vessel. Pip. 116 (2014). doi:10.1016/j.ijpvp.2014.01.001.

[78] W. Reinhardt, A Noncyclic Method for Plastic Shakedown Analysis, J. Press. Vessel Technol. 130 (2008). doi:10.1115/1.2937760.

[79] R. Adibi-Asl, W. Reinhardt, Non-Cyclic Shakedown-Ratcheting Boundary

Determination: Analytical Examples, in: PVP2010-25911, ASME Press. Vessel. Pip. Conf., ASME, 2010. doi:10.1115/PVP2010-25911.

[80] R. Adibi-Asl, W. Reinhardt, Ratchet Boundary Determination Using a Noncyclic Method, J. Press. Vessel Technol. 132 (2010) 021201. doi:10.1115/1.4000506.

[81] R. Adibi-Asl, W. Reinhardt, Non-cyclic shakedown/ratcheting boundary determination - Part 1: Analytical approach, Int. J. Press. Vessel. Pip. 88 (2011) 311–320. doi:10.1016/j.ijpvp.2011.06.006.

[82] R. Adibi-Asl, W. Reinhardt, Non-cyclic shakedown/ratcheting boundary determination - Part 2: Numerical implementation, Int. J. Press. Vessel. Pip. 88 (2011) 321–329. doi:10.1016/j.ijpvp.2011.06.007.

[83] W. Reinhardt, R. Adibi-Asl, The Elastic Modulus Adjustment Procedure (EMAP) for Shakedown, in: PVP2008-61641, ASME Press. Vessel. Pip. Div. Conf., ASME, 2008.

[84] R. Adibi-Asl, W. Reinhardt, Ratchet Limit Solution of a Beam With Arbitrary Cross Section, J. Press. Vessel Technol. 137 (2015) 031004. doi:10.1115/1.4028514.

[85] R. Adibi-Asl, W. Reinhardt, Ratcheting with no thermal bending and membrane stress, in: PVP2016-63773, ASME Press. Vessel. Pip. Conf., ASME, 2016. doi:10.1115/PVP2016-63773.

[86] M. Martin, D. Rice, A hybrid procedure for ratchet boundary prediction, in: PVP2009-77474, Press. Vessel. Pip. Div. Conf., ASME, New York, 2010: pp. 81–88. doi:10.1115/PVP2009-77474.

[87] J. Abou-Hanna, T.E. McGreevy, A simplified ratcheting limit method based on limit analysis using modified yield surface, Int. J. Press. Vessel. Pip. 88 (2011) 11–18. doi:10.1016/j.ijpvp.2010.12.001.

[88] J. Abou-Hanna, M. Paluszkiewicz, Finite Element Based Automated Analysis for Determining Ratchet, Shakedown and Elastic Limits, in: PVP2011-57041, ASME Press. Vessel. Pip. Conf., ASME, 2011.

https://asmedigitalcollection.asme.org/.

[89] A.R.S. Ponter, K.F. Carter, Shakedown state simulation techniques based on linear elastic solutions, Comput. Methods Appl. Mech. Eng. 140 (1997) 259–279. doi:10.1016/S0045-7825(96)01105-X.

[90] H. Chen, Lower and Upper Bound Shakedown Analysis of Structures with Temperature-Dependent Yield Stress, J. Press. Vessel Technol. 132 (2010). doi:10.1115/1.4000369.

[91] H. Chen, A.R.S. Ponter, A Direct Method on the Evaluation of Ratchet Limit, J. Press. Vessel Technol. 132 (2010) 041202. doi:10.1115/1.4001524.

[92] N.-K. Cho, H. Chen, Cyclic Plasticity Behavior of 90 degrees Back-to-Back Pipe Bends Under Cyclic Bending and Steady Pressure, in: ICONE26-82386, Int. Conf. Nucl. Eng., ASME, 2018.

[93] D. Barbera, H. Chen, Y. Liu, F. Xuan, Recent Developments of the Linear Matching Method Framework for Structural Integrity Assessment, J. Press. Vessel Technol. 139 (2017) 051101. doi:10.1115/1.4036919.

[94] J. Ure, H. Chen, D. Tipping, Integrated Structural Analysis Tool using the Linear Matching Method Part 1 - Software Development, Int. J. Press. Vessel. Pip. 120–121 (2014) 141–151. doi:10.1016/j.ijpvp.2014.05.005.

[95] H. Chen, J. Ure, D. Tipping, Integrated Structural Analysis Tool using the Linear Matching Method Part 2 - Application and Verification, Int. J. Press. Vessel. Pip. 120–121 (2014) 152–161. doi:10.1016/j.ijpvp.2014.05.005.

[96] H. Chen, A.R.S. Ponter, A Direct Method on the Evaluation of Ratchet Limit, J. Press. Vessel Technol. 132 (2010). doi:10.1115/1.4001524.

[97] M. Lytwyn, H. Chen, A.R.S. Ponter, A generalised method for ratchet analysis of structures undergoing arbitrary thermo-mechanical load histories, Int. J. Numer. Methods Eng. 104 (2015) 104–124. doi:10.1002/nme.4924.

[98] M. Lytwyn, H. Chen, M. Martin, Ratchet analysis of structures under a generalised cyclic load history, in: PVP2014-28326, ASME Press. Vessel. Pip.

Conf., ASME, 2014. doi:10.1115/PVP2014-28326.

[99] M. Lytwyn, H. Chen, M. Martin, Comparison of the Linear Matching Method to Rolls-Royce's Hierarchical Finite Element Framework for ratchet limit analysis, Int. J. Press. Vessel. Pip. 125 (2015) 13–22. doi:10.1016/j.ijpvp.2014.11.001.

[100] Z. Ma, H. Chen, Y. Liu, F.-Z. Xuan, A direct approach to the evaluation of structural shakedown limit considering limited kinematic hardening and non-isothermal effect, Eur. J. Mech. - A/Solids. 79 (2020). doi:10.1016/j.euromechsol.2019.103877.

[101] J. Shen, Z. Ma, H. Chen, Shakedown and ratcheting analysis of Printed Circuit Heat Exchangers under multiple cyclic mechanical and thermal loads, Int. J. Press. Vessel. Pip. 199 (2022). doi:10.1016/j.ijpvp.2022.104723.

[102] Z. Ma, X. Wang, H. Chen, F.-Z. Xuan, Y. Liu, A unified direct method for ratchet and fatigue analysis of structures subjected to arbitrary cyclic thermal-mechanical load histories, Int. J. Mech. Sci. 194 (2021). doi:10.1016/j.ijmecsci.2020.106190.

[103] X. Wang, Z. Ma, H. Chen, W. Luan, Direct Method-Based Probabilistic Structural Integrity Assessment for High-Temperature Components Considering Uncertain Load Conditions, PVP2022-84423, ASME Press. Vessel. Pip. Conf. (2022). doi:10.1115/PVP2022-84423.

[104] X. Wang, H. Chen, F. Xuan, Direct method-based probabilistic shakedown analysis for the structure under multiple uncertain design conditions, Ocean Eng. 280 (2023). doi:10.1016/j.oceaneng.2023.114653.

[105] X. Wang, J. Yang, H. Chen, F. Xuan, Physics-based probabilistic assessment of creep-fatigue failure for pressurized components, Int. J. Mech. Sci. 250 (2023). doi:10.1016/j.ijmecsci.2023.108314.

[106] X. Wang, H. Chen, F. Xuan, Physics-based neural network for probabilistic low cycle fatigue and ratcheting assessments of pressurized elbow pipe component, Int. J. Fatigue. 172 (2023). doi:10.1016/j.ijfatigue.2023.107598.

[107] WNA, Non-Linear Analysis Design Rules Part 2a: Specification of Benchmarks on Nozzles Under Pressure, Thermal and Piping Loads, WNA, 2019.

[108] M. Chen, W. Yu, J. Shi, F. Lv, Nonlinear finite element analysis of class 1 pressure vessels, in: ICONE25-66910 Int. Conf. Nucl. Eng., ASME, New York, 2017. doi:10.1115/ICONE25-66910.

[109] ASME Boiler and Pressure Vessel Code Section II Materials, ASME, New York, 2017.

[110] E. Procter, R.F. Flinders, Experimental elastic stress analysis of partial penetration welded nozzles in a spherical shell, Nucl. Eng. Des. 7 (1968) 73–86. doi:10.1016/0029-5493(68)90128-3.

[111] J. Ure, H. Chen, D. Tipping, Verification of the Linear Matching Method for Limit and Shakedown Analysis by Comparison With Experiments, J. Press. Vessel Technol. 137 (2015). doi:10.1115/1.4028760.

[112] F. Rauscher, Design by Analysis: Direct Route for Cases with Pressure and Thermal Action, J. Press. Vessel Technol. 130 (2006) 011201. doi:10.1115/1.2826407.

[113] D. Gilmartin, D. Mackenzie, C.D. Bell, Limitations of Stress Linearisation in Elastic Design by Analysis of Thick Walled Components, in: ICONE27-1814, 2019.

[114] H. Li, Q. Ding, X. Huang, A New Method of Stress Linearization for Design by Analysis in Pressure Vessel Design, Appl. Mech. Mater. 598 (2014) 194–197. doi:10.4028/www.scientific.net/AMM.598.194.

[115] D. Osage, J. Sowinski, PTB-1-2014: ASME Section VIII-Division 2 Criteria and Commentary, ASME, New York, 2014.

[116] P.E. Prueter, R.G. Brown, A Comparison Of Design By Analysis Techniques For Evaluating Nozzle-To-Shell Junctions Per ASME Section VIII Division 2, in: PVP2015-45408, ASME Press. Vessel. Pip. Conf., ASME, 2015. doi:10.1115/PVP2015-45408.

[117] M.C. Messner, T.L. Sham, Detection of Ratcheting in Finite Element Calculations, in: PVP2018-84102, ASME Press. Vessel. Pip. Conf., ASME, 2018. http://proceedings.asmedigitalcollection.asme.org.